International Atomic Energy Agency

INDC(NDS)-152/L

INDC INTERNATIONAL NUCLEAR DATA COMMITTEE

NUCLEAR DATA FOR STRUCTURAL MATERIALS

Proceedings of the IAEA Consultants' Meeting
held at IAEA Headquarter in Vienna, Austria,
2-4 November, 1983

Edited by Dermott E. Cullen
Nuclear Data Section
International Atomic Energy Agency

October 1984

IAEA NUCLEAR DATA SECTION, WAGRAMERSTRASSE 5, A-1400 VIENNA

INDC(NDS)-152/L

NUCLEAR DATA FOR STRUCTURAL MATERIALS

Proceedings of the IAEA Consultants' Meeting
held at IAEA Headquarter in Vienna, Austria,
2-4 November, 1983

Edited by Dermott E. Cullen
Nuclear Data Section
International Atomic Energy Agency

October 1984

Reproduced by the IAEA in Austria

October 1984

Table of Contents

Programme

of

the Consultants' Mee

Nuclear Data for Structur

Vienna, Austri
2 - 4 November 1

Organization

This Consultants' Meeting was sponso
Section under the auspices of the IAE
Committee (INDC). Based on INDC recon
Organizing Committee for this meeting was composed of

D. Cullen, IAEA/NDS (Scientific Secretary of Meeting)
H. Derrien, Cadarache, France
F. Fröhner, Karlsruhe, Federal Republic of Germany
R.J. Howerton, Livermore, USA
S. Igarasi, JAERI, Japan
V. Konshin, Minsk, USSR
E. Menapace, Bologna, Italy
J. Rowlands, Winfrith, UK
D. Seeliger, Dresden, German Democratic Republic

Scope

The scope of the meeting included discussions of important areas of data discrepancies. The paper presentations focussed particularly on recent improvements in experimental data and calculational models which can be used to improve the quality and reliability of evaluated data for structural materials. The primary scope of the meeting included the important structural materials Fe, Ni and Cr; some other structural materials with similar general properties and problems were also considered, e.g. Ti, V, Mn, Co, Cu, Zr, Nb and Mo.

Objectives

The meeting had the following four main objectives:

(1) to identify the current accuracy requirements for structural material evaluated data (i.e. what is required);

(2) to assess the accuracy of currently available evaluated data as well as assess the accuracy of currently available experimental data and nuclear model codes (i.e. what is currently available);

(3) to formulate a proposed plan of action in order to improve existing evaluations to meet requirements (i.e. what must be done in the future);

(4) to formulate the objective and scope of a proposed IAEA-sponsored Coordinated Research Programme (CRP) on "Methods for the Calculation of Fast Neutron Nuclear Data for Structural Materials".

The first three of these objectives were met by the presentation of invited papers and the fourth objective was met by working group discussions and recommendations.

Format

This three day meeting was attended by 19 scientists from nine countries and two international organizations. The first one and a half days were devoted to presentation of invited papers. The last one and a half days were devoted to working group sessions with the task to review the proposed IAEA CRP and make recommendations concerning its objective and scope.

Programme of Invited Papers

Working Groups

Following the presentation of invited papers the meeting was divided into two working groups to consider the resonance and fast energy ranges. Each Working Group was to consider the proposed IAEA CRP on structural materials and to make recommendations concerning the scope and content of this CRP.

II. List of Participants

E.D. Arthur (Chairman)	Los Alamos National Laboratory P.O. Box 1663 Los Alamos, New Mexico 87545 U.S.A.
T. Asami	Japan Atomic Energy Research Institute (JAERI) Tokai-mura, Naka-gun Ibaraki-ken 319-11 Japan
A.I. Blokhin	Fiziko-Energeticheskij Institut Obninsk, Kaluga Region U. S. S. R.
D.E. Cullen	International Atomic Energy Agency Wagramerstrasse 5 P.O. Box 100 A-1400 Vienna Austria
F. Corvi	Central Bureau of Nuclear Measurements Steenweg naar Retie B-2440 Geel Belgium
F. Fröhner	Institut für Neutronenphysik und Reaktortechnik Kernforschungszentrum Karlsruhe Postfach 3640 D-7500 Karlsruhe Federal Rebuplic of Germany
H. Gruppelaar	Department of Physics Netherlands Energy Research Foundation (ECN) P.O. Box 1, 3 Westernduinweg NL-1755 ZG Petten The Netherlands
V.A. Konshin	Institute of Nuclear Engineering of the BSSR Academy of Sciences 223061 Minsk, Sosny U. S. S. R.

H.D. Lemmel

International Atomic Energy Agency
Wagramerstrasse 5
P.O. Box 100
A-1400 Vienna
Austria

E. Menapace

Centro di Calcolo del
E.N.E.A.
Via Mazzini 2
I-40138 Bologna
Italy

M. Moxon

U.K. Atomic Energy Authority
Atomic Energy Research
Establishemt (AERE)
Harwell, Didcot, OXON. OX11 ORA
U. K.

F.G.J. Perey

Neutron Physics Division
Oak Ridge National Laboratory
P.O. Box X
Oak Ridge, Tennessee 37830
U. S. A.

V.G. Pronyaev

International Atomic Energy Agency
Wagramerstrasse 5
P.O. Box 100
A-1400 Vienna
Austria

G. Reffo

Centro di Calcolo del
E.N.E.A.
Via Mazzini 2
I-40138 Bologna
Italy

B.V. Robouch

ENEA-FAL
C.P. 65
I-00044 Frascati (Rome)
Italy

J.J. Schmidt

International Atomic Energy Agency
Wagramerstrasse 5
P.O. Box 100
A-1400 Vienna
Austria

N.G. Sjöstrand

Department of Reactor Physics
Chalmers Tekniska Hoegskola
Fack
S-402 20 Göteborg 5
Sweden

B. Strohmaier

Institut für Radiumforschung
und Kernphysik
Boltzmanngasse 3
A-1090 Vienna
Austria

K. Wisshak

Institut für Angewandte
Kernphysik II
Kernforschungszentrum Karlsruhe
Postfach 3640
D-7500 Karlsruhe
Federal Rebuplic of Germany

III. Combined Recommendations of the two Working Groups on the proposed IAEA Coordinated Research Programme (CRP) "Methods for the Calculation of Fast Neutron Nuclear Data for Structural Materials"

Introduction

The Nuclear Data Section of the IAEA has proposed that a CRP on "Methods for the Calculation of Fast Neutron Nuclear Data for Structural Materials" be started in 1984. This proposal was reviewed by the International Nuclear Data Committee (INDC) at its 13th Meeting in Rio de Janeiro, Brazil, May 1983. The Committee approved the proposal in principle, subject to the definition of its scope and objectives by this consultants meeting.

Recommendations

The Consultants Meeting on Nuclear Data for Structural Materials recommends to the INDC that it approves the proposed IAEA CRP on "Methods for the Calculation of Fast Neutron Nuclear Data for Structural Materials". Regarding the scope of the CRP it is further recommended that this CRP only consider the fast neutron energy range, i.e. the range above the resolved resonance region.

For the fast energy region there is significant potential for this CRP to contribute towards the development and improvement of calculational methods, particularly for the determination of correlated energy-angle nuclear data. Of great interest are efforts aimed at the formulation of unified reaction theories.

For the resonance region the theory is well defined and experimental measurements and analysis are complicated and expensive. Therefore it was felt that work in this energy range is not appropriate for inclusion within the scope of the CRP. The consultants felt that work within the resonance energy range would be more appropriate to be performed at advanced laboratories where physicists from developing countries could participate with support by the IAEA fellowship programme.

Although the consultants felt that this CRP should not deal with the resolved resonance region they felt that the CRP could contribute toward eliminating problems which concern the matching of resolved resonance data to unresolved data and the handling of intermediate structure.

The continued development of current nuclear models should be pursued within the scope of the CRP with particular emphasis on the improvement of unified reaction models and their implementation into data evaluation. Results from comparisons of nuclear model calculations such as those recently sponsored by the NEA should be used to provide guidance in the assessment of the status and applicability of currently used nuclear models and the identification of areas needing further improvement.

Improved calculational models developed under the CRP should be adequately documented and when applicable, the resulting computer codes and documentation should be made available by the IAEA to the NEA Data Bank for distribution.

In parallel to, but outside of the scope of the CRP, developed countries should host scientists from developing countries to train them in the application of improved calculational methods for evaluation.

Revised CRP Proposal

In hight of the above recommendations, the consultants recommend to revise the CRP proposal as follows.

Revised Proposal for a Co-ordinated Research Programme (CRP) on "Methods for the Calculation of Fast Neutron Nuclear Data for Structural Materials"

1. Background

Fast neutron reaction data for structural materials (Fe, Ni, Cr and some others) including the energy and angular distributions of secondary emitted neutrons, charged particles and gamma-rays are of high importance in neutron economy and shielding calculations and for the assessment of nuclear safety and radiation damage in fission as well as fusion reactors.

With regard to structural materials, apart from improvements in evaluated data for a few selected reactions in special purpose files, the internationally available, more comprehensive evaluated neutron data files used in fission and fusion neutronics calculations are quite old and generally no longer reflect the present state of knowledge. Many of these evaluations, at least partially, date back as far as 1970; since then many new experimental data have become available, as illustrated e.g. by the new results reported at the NEANDC Specialists' Meeting on Fast Neutron Capture Cross Sections held at Argonne National Laboratory in April 1982. Also in the field of nuclear models and computer codes, significant improvements have been made in recent years in the prediction and interpretation of non-compound contributions in fast neutron-nucleus reactions as reflected e.g. in the remarkable improvements achieved in recent years in the description of the energy and angular distributions of secondary emitted particles including consideration of compound, direct and pre-compound emissions.

These new developments have led to the necessity to improve the existing evaluations and perform re-evaluations with due consideration of more recent experimental data and nuclear model descriptions. As a consequence, new evaluations have been started or are planned in several countries, and, as part of this overall effort, a co-ordination of the current development and use of calculational methods for the computation of fast neutron cross sections appears to be timely and desirable.

2. Scientific Scope and Proposed Programme Goals

The materials to be covered by this CRP should be the structural elements and isotopes (Fe, Cr, Ni) most important for fission and fusion reactors. Although not structural materials, but because of their importance in fusion applications, it was felt that the CRP should also include Li, Be and Pb. Incident energies should include the range from the upper energy limit of the resolved resonances to 20 MeV; all neutron reactions should be dealt with, with an emphasis on neutron elastic and inelastic scattering, partial reaction cross sections, gamma-ray production spectra and cross sections, as well as secondary particle energy and angular distributions.

The objectives of the CRP are suggested to be as follows:

- Discussion and intercomparison of the various calculational methods used and/or developed by the CRP participants in dealing with the problem areas mentioned below;

- Summary of the results of these intercomparisons and, if possible, identification of the most appropriate methods recommended for use in calculations of neutron cross sections and an assessment of the reliability of such calculations for the structural materials considered under this CRP, (final goal).

Although the CRP will only deal with the calculations, experimental measurements are also mentioned below. All such measurements are of interest in order to verify methods, but should be performed outside of the scope of the CRP.

The CRP should deal with the following topics:

- Comparison of secondary particle energy - angle distributions. Models that allow realistic calculations of these data are being developed at a rapid rate. Such models should be considered within the scope of the CRP, particularly those aimed at unification of Hauser-Feshbach and pre-equilibrium theories. The above mentioned models should be used to produce complete energy-angle data sets suitable for inclusion in evaluations in the ENDF/B File VI format. Realistic error estimates should also be prepared.

  To aid in development and verification of such methods, a few experimental measurements should be made of angular distribution of emitted particles induced by neutrons with incident energies between 8 and 14 MeV. Materials to be investigated should include Fe, Pb, and Li.

- Two step and multi-step reactions. Modern combined Hauser-Feshbach/pre-equilibrium calculations treat such reactions consistently and can allow separation of spectra from processes such as (n,np) and (n,pn). Such separations could be important for recoil energy calculations.

- Small yield cross sections (n,d), (n,t), (n, ^{3}He). Systematics should be investigated further and combined with simplified reaction models to provide the required quality of evaluated data.

- Consistency of discrete and continuum level description. Continuum level densities of residual nuclei used in Hauser-Feshbach calculations are currently normalized to discrete level densities at low energies. Often there are inconsistencies between the level densities used in Hauser-Feshbach and pre-equilibrium model calculations which should be corrected.

- The role of nuclear structure theories. Methods of calculation of direct reaction contributions based on spectroscopical information obtained from experiments, as well as from nuclear structure calculations, should be implemented.

- Consistency between evaluated neutron and gamma-ray data files. Comprehensive nuclear models can provide an accurate prediction of the total energy release and give a realistic framework for the evaluation of experimental data on the energy release for a variety of partial reaction channels. Such techniques can produce improved gamma-ray heating and KERMA values.

  Additional gamma-ray production data measurements are needed to verify such calculations.

Several areas exist where calculational models should be improved.

a) Pre-equilibrium and unified reaction models - improved description of exciton-dependent state/level densities, along with incorporation of $J\pi$ effects. Additionally transition matrix element descriptions should be improved.

b) Optical Model (OM) calculations. For phenomenological optical models this could include the implementation, in chi square search routines, of the constrained least squares method that uses prior information as well as input parameter uncertainties . A parallel area of OM improvement would be the implementation of the microscopic methods as developed by Satchler, Vinh Mao, Lev and Beres or of the folding models of Jeukenne, Lejeune, and Mahaux, and of Brieva and Rook.

c) Improved methods for the description of collective effects in nuclear level densities. Some examples are: development and application of asymetric rotator models; investigations of the energy dependence of level density enhancements for deformed nuclei.

d) Development and application of microscopic nuclear level density calculation methods, including those which take into account short-range pairing correlations and long-range residual forces, and more advanced shell model approaches such as the moments method.

3. Benefits

Participation in this CRP and exchange of experience and results under this CRP will be of benefit to

- developed countries, since it will assist in the development of improved evaluated neutron data files for structural materials needed for their nuclear power programmes; and to

- developing countries, since it will provide an opportunity for training and gaining experience in methods of nuclear cross-section calculations and interpretation of experimental results and thus help in the development of scientific infrastructure for nuclear technology.

4. Connection with other programmes

The proposed CRP will partly complement, partly have a natural connection with other IAEA/NDS and national programmes, for the

experimental and theoretical determination of fast neutron cross sections, i.e. with

- the Workshop on Nuclear Model Computer Codes organized jointly by IAEA-NDS and the International Centre for Theoretical Physics in Trieste in January/February 1984;

- the ongoing CRP on the measurement and analysis of 14 MeV neutron nuclear data needed for fission and fusion reactor technology;

- the development and intercomparison of neutron cross section files for radiation damage computation;

- the activities in the field of nuclear level densities following the IAEA Advisory Group Meeting on Basic and Applied Problems of Nuclear Level Densities held at Brookhaven in April 1983.

5. Participation

Many laboratories from different parts of the world are or may be interested to participate in the proposed CRP:

Several U.S. and U.S.S.R. Laboratories, e.g. LANL (Los Alamos), ORNL (Oak Ridge), FEI (Obninsk), INE (Minsk);
TUD (Dresden), GDR;
KFK (Karlsruhe) Jülich, FRG;
ENEA (Bologna), Italy;
CEN (Saclay, Cadarache, Bruyéres-le-Châtel), France;
IRK (Vienna), Austria;
ANEB (Sofia), Bulgaria;
PFU (Bratislava), Czechoslovakia;
BARC (Bombay), India;
JAERI (Tokyo), Japan;
ECN (Petten), Netherlands
IBJ (Warsaw), Poland
IFIN and IRNE (Bucharest), Romania
AERE (Harwell), United Kingdom
CTA/IEA Nuclear Data Centre, Sao José dos Campos, Brazil.
BCMN (Geel), CEC, Belgium

This is not an exhaustive list. Of course, in view of budgetary limitations, only a limited, carefully selected number of institutes could participate in the CRP.

6. CRP start and duration

Subject to INDC and internal IAEA approval, the CRP could be started in the course of 1984 by concluding research agreements or contracts with several institutes for the first year of the CRP with the possibility of renewal after the first year. In order to accomplish the goals of this CRP as tentatively outlined under point 2 above, a total duration of at least three years, in line with the normal duration of IAEA CRPs, is deemed necessary. The funds will be provided from the NDS' part of the Agency's Research Contract Programme Budget.

IV. Invited Papers

The invited papers are presented here in the order in which they are described in the programme (see p.6).

Neutron Resolution Functions

by

M. Moxon

AERE Harwell, United Kingdom

Paper was not sumitted for publication by author.

Measurement and Analysis of Neutron Spectrum in Structural Materials for Reactors
- Iron, Nickel and Chromium -

S.A. Hayashi, I. Kimura, K. Kobayashi, S. Yamamoto

Research Reactor Institute, Kyoto University
Kumatori-cho, Sennan-gun, Osaka 590-04, Japan

Hiroshi Nishihara, Satoshi Kanazawa

Department of Nuclear Engineering, Kyoto University
Yoshidahonmachi, Sakyo-ku, Kyoto 606, Japan

T. Mori and M. Nakagawa

Reactor System Laboratory, Japan Atomic Energy Research Institute
Tokai-mura, Naka-gun, Ibaraki 319-11, Japan

ABSTRACT

In order to assess neutron cross section data and group constants for the main constituent elements of stainless steel, the energy spectra of the neutrons from about 1 keV to a few MeV in sample piles of iron, nickel and chromium have been measured by the linac time-of-flight methood.

We used spherical vessels in which powder of each sample element was packed. Each pile had a lead target at the center. To verify the spherical symmetry of neutron transport in the pile, the spatial and angular distributions of $^{58}Ni(n,p)^{58}Co$ and $^{197}Au(n,\gamma)^{196}Au$ reactions were measured for each pile.

Group constants were produced by SUPERTOG-JR3 from the two nuclear data files, JENDL-2 and ENDF/B-IV, and the the one-dimensional neutron transport calculation was carried out by DTF-IV or ANISN. A continuous energy neutronics and photon transport code, VIM, was used for checking of calculational method, and the result was compared with that by DTF-IV. There is little difference between the results of these two methods. General shape of the experimental spectra agrees with the calculated for all cases. But in detail the C/E agreement is rather poor in the energy just below big resonances, i.e. around the 27 keV resonance for iron, around the 15, 35 and 75 keV resonances for nickel and around the 4 to 8 keV resonances for chromium. The calculated spectrum for iron with JENDL-2 in the energy less than the 27 keV resonance region is better than that with ENDF/B-IV. For nickel the calculated spectra with JENDL-2 and ENDF/B-IV agree each other, which is supposed to be caused by almost the same values of the group constants. In the case of chromium the C/E agreement in the energy less than about 100 keV region is rather worse with both nuclear data files.

(Neutron spectrum, time-of-flight method, neutron cross sections, group constants, integral check, structural materials, iron, nickel, chromium, stainless steel, transport calculations, Monte Carlo method, spatial and angular distributions, electron linear accelerator)

INTRODUCTION

For the purpose of safe and economical design of reactors, the neutron cross section data for structural materials are required with the accuracy of a few % to a few ten % in relevant energy region[1].

At several nuclear data centers in the world the neutron cross section data for important rector materials are collected and evaluated systematically, and thereby large scale evaluated nuclear files or libraries are prepared for reactor design.

However, there frequently exist considerable large discripancies among different evaluated nuclear data files. Even though the values in a few data files seem to agree satisfactorily each other, the accuracy of these values may be beyond the requested value.

There are several methods for the integral check of evaluated nuclear data files. For the purpose of checking nuclear data for such as inelastic scattering cross section for structural materials, measurement of the energy spectrum of neutrons in a sample pile is superior to the method of a critical experiment with its sample, because this method has less ambiguity because of its simple geometry and by its homogeneous single constituent. The experimental success of this method is mainly due to the development of electron linear accelerators as a powerful tool of an intense pulsed neutron source for the neutron time-of-flight spectroscopy (linac TOF method). Several groups applied this method to the intermediate and fast neutron regions, and tried to assess nuclear data of reactor materials in these region[2~7]. Present authors started the measurement and analysis of neutron spectrum in reactor materials more than 16 years ago and have investigated more than 20 samples[8~12].

In this paper, the outline of our works on the linac TOF method is presented and some newer results of neutron spectra in main constituent elements of stainless steel, such as iron, nickel and chromium, are mainly presented for the integral check of neutron cross section data for these elements.

EXPERIMENTAL ARRANGEMENT AND PROCEDURE

Sample Piles

As the samples, we have mainly chosen structural materials of fission reactors and fusion reactors. The sample piles which we have experimentally and theoretically studied at the Research Reactor Institute, Kyoto University (KURRI), are listed in Table 1. The purity of samples and the shape, and the size of samples are tabulated in this table.

The borated graphite pile was used as the standard neutron field of intermediate neutron energy spectrum in order to calibrate efficiencies of neutron TOF detectors[13].
Among a large number of the sample piles, we have recently finished the measurement and the analysis of the neutron spectra in three main constituents of stainless steel, Fe, Ni and Cr, in almost the same conditions.

Each powder sample was packed in a spherical steel vessel 60 mm in inner diameter. Recently the hydrogen contents in these powder samples were measured by gas chromatography and the results were 4.73 ppm, 32.8 ppm and 88.5 ppm, for iron, nickel and chromium, respectively. The hydrogen content for the iron sample seems to be negligible, but those for nickel and chromium are fairly high.

Each pile had a cylindrical or cubic lead target at the center and a reentrant hole from which the neutron beam with certain position and direction (r= 15 cm, μ=0) was extracted to the neutron flight path. When we measured the background counts, a plug in the bottom of the reentrant hole was removed and then the hole became through. In order to measure angular and spatial distribution of neutrons around the photoneutron target, we set radially activation nickel wires and gold foils from the side of the target.

Pulse Neutron Source

Fast neutron pulses were generated with the electron linear accelerator (linac) of the KURRI. The typical operating conditions of the linac were as follows:

electron energy	:	about 30 MeV
repetition rate	:	167 or 250 pps
pulse width	:	22, 30, 33, 47 or 100 nsec
target current	:	about 300 or 700 mA at peak

The spectrum of the neutrons directly emitted from the lead target was measured by the linac time-of-flight method and the result is shown in elsewhere[14]. The angular distribution of

the photoneutrons was measured by making use of the $^{27}Al(n,\alpha)^{24}Na$ reaction and was seen to be isotropic as shown before [14].

Collimators and Flight Tube

The general configuration of the collimators and the flight tube was almost the same as earlier works of ours and is depicted in Fig. 1. The total flight path between the electron beam center and the front face of the ^{6}Li glass scintillator or ^{10}B-vaseline-NaI(Tl) detector was about 22 m or 24 m, respectively. A natural uranium plate of 2 cm thick and a cadmium plate of 0.5 cm thick were set into the neutron flight path to suppress gamma flash and slow neutron backgrounds.

Neutron Detector and Electronics

As the neutron detector, we used a bank of three ^{6}Li glass scintillation counters (NE-912, in 12.7 cm in diameter and 1.27 cm thick) and a ^{10}B-vaseline-NaI(Tl) counter. The structure and characteristics of these detectors were given elsewhere [13]. The significance of using these two detectors is to avoid a systematic error which may be caused by the detector system.

The relative detection efficiencies of the both detectors along with some correction factors such as the transmission function through the flight tube, were experimentally determined by making use of the standard neutron pile of borated graphite [15]. Recently we encased this pile in a steel frame and recalibrated the efficiencies of both detectors. A ^{235}U fission chamber and a BF_3 counter are used for neutron monitoring.

The electronic circuits and the computer system for the measurement and the data analysis are shown in Fig. 2. The neutron signals are stored in a multi-channel analyzer, CANBERRA Series 88/MP, through a time analyzer unit, Oken S-1218. The obtained data is processed with the PDP-11/34 computer.

Measurement of Spatial Distributions of Neutrons

Nickel wire of 1 mm in diameter and gold foils of 3 mm in diameter or 5 mm square and 0.05 mm thick were used for the measurement of spatial distribution of neutrons around the photoneutron target by the $^{58}Ni(n,p)^{58}Co$ and $^{197}Au(n,\gamma)^{198}Au$ reactions. The induced activities of both ^{58}Co and ^{198}Au were measured with a Ge(Li) detector and spatial distributions of neutrons are always determined in all of the sample piles by this activation method.

THEORETICAL CALCULATION OF NEUTRON SPECTRUM

Computer Codes and Calculational Models

Main calculation have been performed by DTF-IV [15] or ANISN [16] for all of the piles. In this calculation each pile is assumed to be a spherically symmetric geometry with an homogeneous isotroic neutron source in the central region.

In the typical calculation, space mesh and number of angular quadrature points are taken to be 1 cm and, 8 or 16, respectively. The scattering anisotropy of the elastic scattering kernel was obtained by P_8 approximation. The neutron spectrum in the lead target was taken from Ref. 14.

For the calculation of neutron distribution by the Monte Carlo method, a continuous energy neutronics and photon transport code, VIM was used [17]. In this calculation the neutron flux was obtained by a method of track length estimators in a homogeneous medium of piles.

Cross Section Libraries and Group Constants

As shown in Fig. 3, 100 group constants were produced by the SUPERTOG-JR3 code [18] from two evaluated nuclear data files ENDF/B-IV [19] and JENDL-2 [20] for DTF-IV or ANISN. In this calculation we assumed the weighting spectrum having the 1/E type below 100 keV and the fission neutron spectrum above 100 keV. The material numbers in these libraries which we used in this work are tabulated in Table 2. The obtained group constants for iron, nickel and chromium are shown in Figs. 4, 5 and 6, respectively.

On the other hand the self-shielding factors for elastic scattering, absorption and removal cross sections were calculated by the RIFF-H code[21], which had been prepared by one of the authors. In this calculation, ultra fine mesh (0.0021 lethargy width) was taken. Multiplying the above group constants by these self-shielding factors, we obtained the self-shielded group constants for computer input.

As the group constants for the calculation of the reaction rate in activation foils, we took the data from the ENDF/B-IV dosimetry file.

Unlike the earlier results which were presented at the Antwerp Conference[12], we took into account the hydrogen contents of the sample powders in the calculation. The spectrum was softened in lower energy region in all cases, comparing with that of the Antwerp Conference, but it is more noticeable for the chromium pile than the others.

Cross section library in VIM code was obtained from ENDF/B-IV file and has about 10,000 pointwise cross sections in each partial reaction for the energy region of 10^{-5} eV to 20 MeV. Angular distribution of scattered neutrons are tabulated as probabilities in center of mass system for 20 angular intervals.

RESULTS AND DISCUSSION

The neutron spectra in the three main constituent elements of stainless steel were measured with almost the same experimental conditions.

Iron

The experimentally obtained angular neutron spectrum at r=15 cm and μ=0.0 for the iron pile with the calculated values by ANISN is shown in Fig. 7. The normalization between the measured spectrum and the calculated one was performed by the average flux in the region of 300 keV to 1 MeV. In this figure, the ratio of the theoretically calulated spectrum to the experimentally obtained (C/E ratio) is also depicted below. In this case, we took the data with the ^{6}Li glass scintillation counter bank to calculate the above ratio, because the these data agree with those with the ^{10}B-vaseline-NaI(Tl) counter and have less statistical uncertainty.

For the spectrum in the iron pile, it can be seen that: (1) The experimentally obtained spectrum with the ^{6}Li glass scintillation counter bank or the ^{10}B-vaseline-NaI(Tl) counter comparatively agree with the calculated in general from 1 keV to 2 MeV. (2) The C/E ratio for JENDL-2 is flatter than that for ENDF/B-IV in the energy less than 10 keV region. (3) Most of the measured data are larger than the calculated ones below a few 100 keV, except around the region of a 27 keV resonance peak. (4) As comparing with the neutron spectra in the large rectangular parallelpiped pile which had been obtained by the present authors before[9], the similar tendency of the general spectrum shape can be seen in the experimental and the calculated ones.

Figure 8 shows the total fluxes calculated by VIM and by DTF-IV codes with the same nuclear data file, ENDF/B-IV. In this figure, the spectral shape of total fluxes is almost the same each other. This fact verifies that the difference between the experimental and calculated values in Fig. 7 is not caused by the difference of the calculational methods.

Nickel

The experimental angular neutron spectrum in the nickel pile is shown in Fig. 9, together with the calculated values by ANISN at r=15 cm and μ=0.0. The normalization procedure was the same as the iron pile. In the same figure, the C/E ratio is also depicted below. Figure 10 shows the total fluxes calculated by VIM and DTF-IV codes with ENDF/B-IV file.

For the spectra in the nickel pile, it can be seen that: (1) The agreement between the experimental and the calculated spectra is good in general shapes. (2) The experimental values slightly exceed the calculational values around the resonances

of 15 keV, 35 keV and 75 keV. (3) The two spectra calculated with the ENDF/B-IV and JENDL-2 agree with each other better than the cases for iron and chromium. This is due to the fact that both group constants for nickel agree with each other in the relevant energy region, as seen in Fig. 5. (4) The spectral shape of total fluxes with VIM and DTF-IV codes are almost the same each other. This means also that the differences between the calculated spectra with different nuclear data files were caused by the use of the difference of nuclear data themselves but not by the use of different codes.

Chromium

The experimental angular neutron spectrum for the chromium pile is shown in Fig. 11, together with the calculated values of ANISN at r=15 cm and μ=0.0. The normalization procedure was the same as the others. In the same figure, the C/E ratio is also depicted below. Figure 12 shows the total fluxes calculated by VIM and DTF-IV with ENDF/B-IV file.

As the hydrogen content in the sample powder was considerd in the present calculation, the calculated spectrum was increased in lower energy part of less than 150 keV and considerably approached to the experimental one.

From Figs. 11 and 12 for the chromium spectra, it can be seen that: (1) A satisfactory agreement between the experimental and calculated spectra can be seen in general, but in the resonances from 4 keV to 8 keV the experimental values still exceed the calculated ones noticeably. (2) The spectrum calculated with ENDF/B-IV is about 30 % to 50 % higher than that with JENDL-2 in the energy less than 40 keV and moreover it is more close to the experimental values than that with JENDL-2. (3) The calculated total fluxes with VIM and DTF-IV give almost the same shape.

The precise cross section data for these three elements in the energy less than 100 keV, especially around the 4 keV to 8 keV resonances region for chromium are required to solve the above problems in future. Moreover not only precise cross section data but also those with higher resolution must be obtained for the purpose of precise prediction of neutron spectrum in nuclear reactors, especially in fast reactors.

ACKNOWLEDGMENT

This work has been supported by the Grant in Aid for Fundamental Research of the Ministry of Education, Science and Culture of Japan, by the Visiting Researchers Program of Research Reactor Institute, Kyoto University and by the Cooperative Research Program with JAERI.

The authors wish to express their sincere thanks to the staff of the Nuclear Data Center of JAERI and to the members of the Japanese Nuclear Data Committee, especially Drs. S. Igarashi, T. Asami, Y. Kikuchi and S. Iijima for the valuable discussion on the cross section data and for the presentation of this report. They would like to acknowledge the cooperation and the fruitful discussion of Mr. Y. Fujita of KURRI and Mr. W. Sato of Japan Information Service.

REFERENCES

1. D. W. Muir(ed.), World Request List for Nuclear Data, INDC(SEC)-73/URSF, IAEA(1979).
2. M. S. Coates, et al., AERE-R 5364 (1968).
3. A. E. Profio, et al., Nucl. Sci. Eng., 35, 91 (1969).
4. R. C. Cerbone, GA-9149, Vol.1 (1969).
5. B. K. Malaviya, et al., Nucl. Sci. Eng., 47, 329 (1972).
6. N. N. Kaushal, et al., ibid., 49, 330 (1972).
7. A. J. H. Goddard, et al., Annals of Nucl. Sci. Eng., 1, 139 (1974).
8. I. Kimura, et al., NBS Sp. Publ. 425, Vol.1, p.184 (1977).

9. Hiroshi Nishihara, et al., J. Nucl. Sci. Technol., 14, 426 (1977).
10. I. Kimura, et al., ibid., 15, 183 (1978).
11. I. Kimura, et al., NBS Sp. Publ. 598, p.265 (1980).
12. I. Kimura, et al., "Nuclear Data for Science and Technology" p.98 (1983).
13. I. Kimura, et al., Nucl. Instr. Meth., 137, 85 (1976).
14. S. A. Hayashi, et al., Annu. Rep. Res. Reactor Inst. Kyoto Univ., 13, 23 (1980).
15. K. D. Lathrop, LA-3373 (1965).
16. W. W. Engle, Jr., K-1693 (1967).
17. R. N. Blomquist, et al., ORNL/RSIC-44 (1980).
18. K. Koyama, et al., JAERI M 7155 (1977).
19. National Neutron Cross Section Center, BNL "Evaluated Nuclear Data File IV" (data tape).
20. Nuclear Data Center, JAERI "Japanese Evaluated Nuclear Data Library" (data tape).
21. M. Nakagawa, unpublished.

Table 1 Sample piles for experimental study

Pile	Purity	Shape and size
Borated graphite	2.5% B in C	Rectangular parallelepiped 70 cm x 70 cm x 70 cm
Iron	Soft steel, SS-41	Rectangular parallelepiped 100 cm x 90 cm x 90 cm
Iron sphere with lead reflector	Soft steel, SS-41 99.9% Pb	Iron: simulated sphere 35 cm in diameter lead: cube, 76 cm cube
Stainless steel	SUS-304	Cube, 76 cm cubic
Aluminum	99.5% Al (A 1050 P)	Cube, 70 cm cubic
Lithium	99.8% Li	Rectangular parallelepiped 60 cm x 50 cm x 40 cm
Barytes concrete	Barytes and portland cement	Cube, 50 cm cubic
Lead	99% Pb	Cube, 70 cm cubic
Iron oxide	99.2% Fe_2O_3	Powder packed into a spherical vessel of 60 cm in diameter
Iron	99.87% Fe	Same above
Nickel	99.7% Ni	Same above
Chromium	99.8% Cr	Same above
Molybdenum	99.9% Mo	Same above
Zirconium	99.6% Zr	Same above
Alumina	99.5% Al_2O_3	Same above
Thoria	99.9% ThO_2	Same above
Lithium fluoride	98.1% LiF	Same above
Copper	99.993% Cu	Same above
Manganese	99.95% Mn	Same above
Titanium	99.4% Ti	14-hedron, in which a sphere 104 cm in diameter inscribes
Polytetrafluoro-ethylene	99.9% $(CF_2)_n$	14-hedron, in which a sphere 90 cm in diameter inscribes
Niobium	99.8% Nb	Powder packed into a spherical vessel of 28 cm in diameter
Niobium sphere with lead reflector	99.8% Nb 99.9% Pb	Niobium: same above lead: cube, 50 cm cubic

Table 2 List of material numbers used in files

Element	JENDL-2	ENDF/B-IV
Fe	2260	1192
Ni	2280	1190
Cr	2240	1191

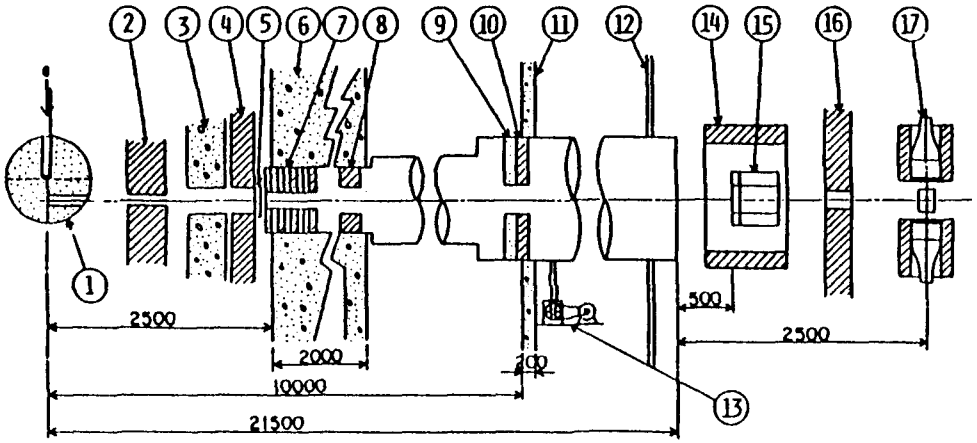

Fig. 1 Experimental arrangement of TOF experiment.
(1) Sample pile, (2) Pb pre-collimator(22 mm in diameter, 400 mm thick), (3) heavy concrete shield(400 mm thick), (4) Pb collimator(50 mm in diameter, 200 mm thick), (5) U filter(2 mm thick), (6) concrete wall, (7) Pb and B_4C collimators((47 mm Pb and 47 mm B C)x4, 50 mm in diameter), (8) Pb collimator(100 mm in diameter, 200 mm thick), (9) B_4C collimator(160 mm in diameter,80 mm thick), (10) Pb collimator (160 mm in diameter,60 mm thick), (11) concrete wall, (12) wall of hut, (13) rotery pump, (14) Pb shield for ^{6}Li glass scintillators, (15) ^{6}Li glass scintillation counter bank being removed when a ^{10}B-vaseline-NaI(Tl) counter is used, (16) Pb shield (150 mm thick), (17) ^{10}B-vaseline-NaI(Tl) counter.

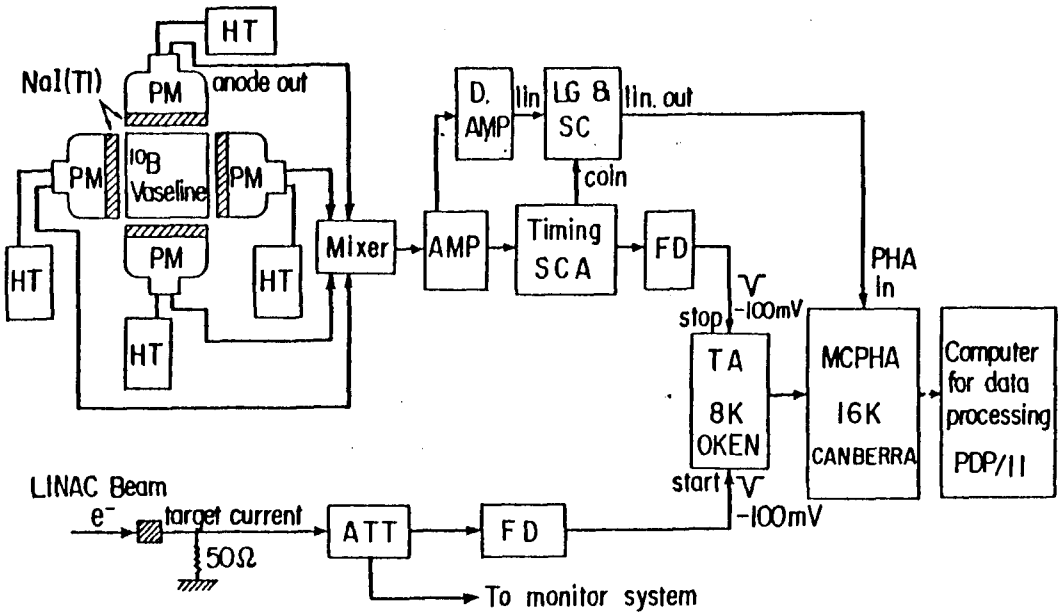

Fig. 2 Block diagram of electronic circuits and computer system for TOF measurement: ^{10}B-vaseline-NaI(Tl) counter system.

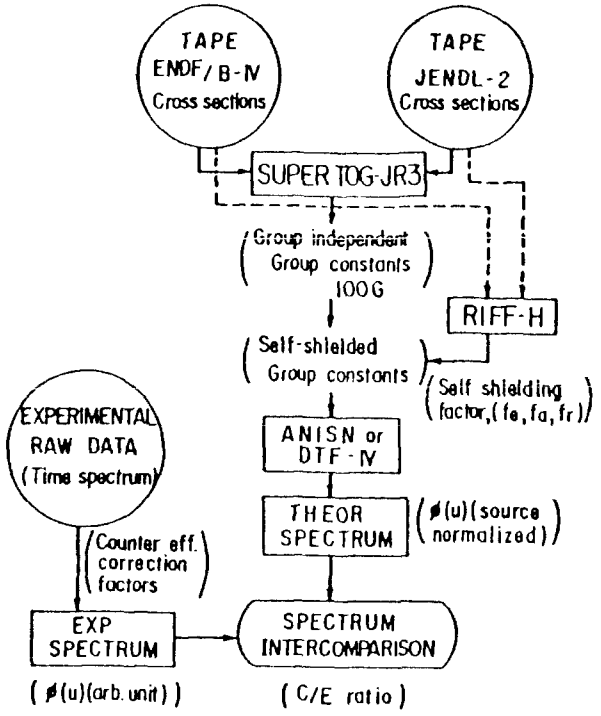

Fig. 3 Flow chart of neutron spectrum calculation: production of self-shielded group constants from evaluated nuclear data files and neutron transport calculation.

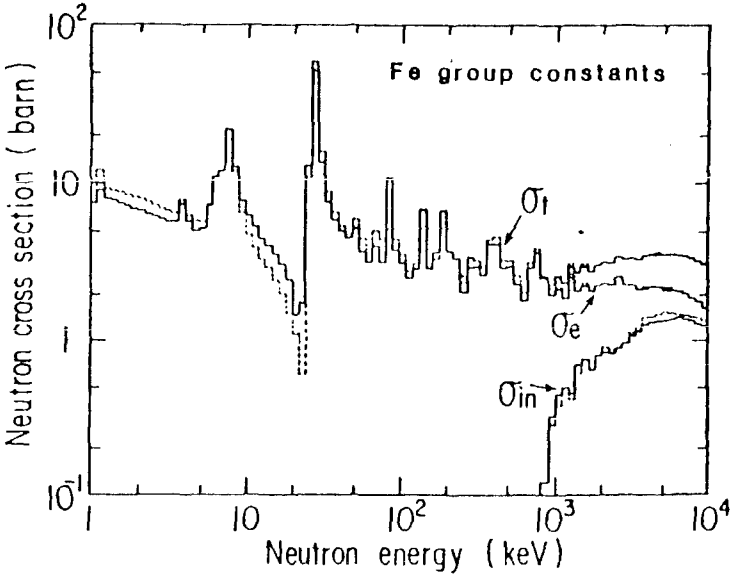

Fig. 4 Comparison of the group constants for iron produced by SUPERTOG-JR3. —— JENDL-2, ····· ENDF/B-IV.
σ_t : total cross section, σ_e : elastic scattering cross section, σ_{in} : inelastic scattering cross section, σ_γ : capture cross section.

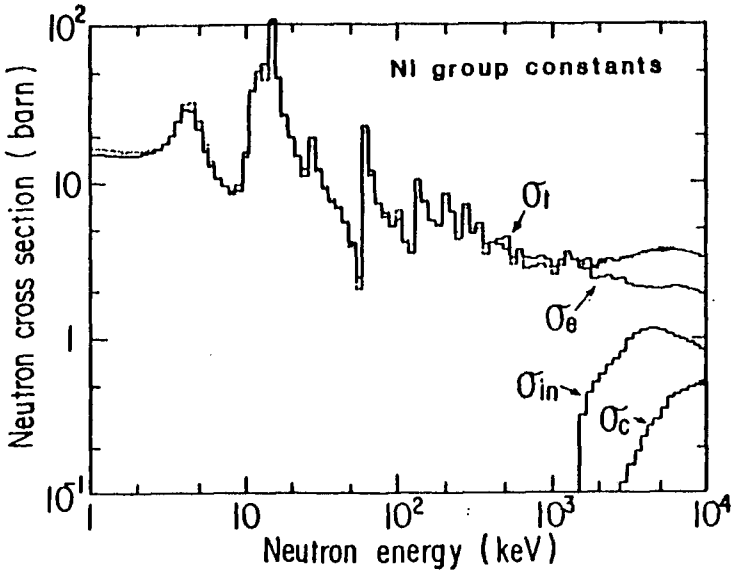

Fig. 5 Comparison of the group constants for nickel produced by SUPERTOG-JR3. All symbols are the same as in Fig. 4.

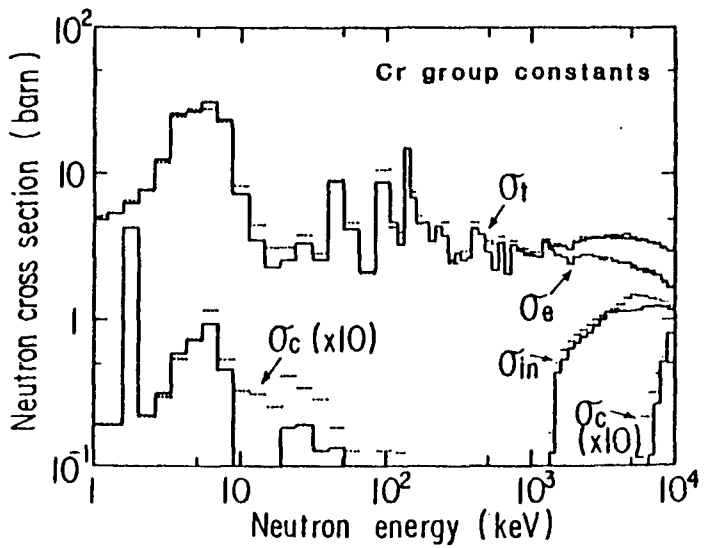

Fig. 6 Comparison of the group constants for chromium produced by SUPERTOG-JR3. All symbols are the same as in Fig. 4.

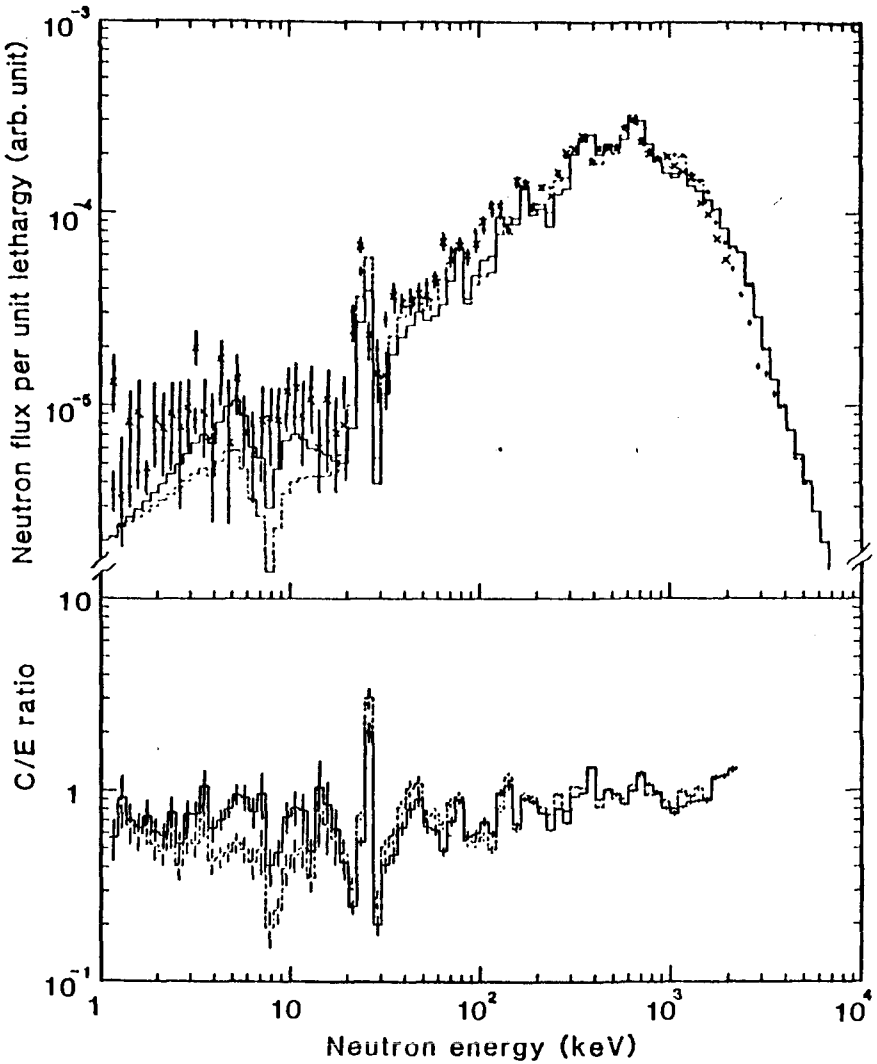

Fig. 7 Angular neutron spectrum at r= 15 cm and μ= 0.0 in the iron pile: top.
Ratio of the calculated to the experimental result (^{6}Li glass): bottom.
•.• measured (^{6}Li glass), ×.× measured (^{10}B-V-NaI), —— JENDL-2, ---- ENDF/B-IV.

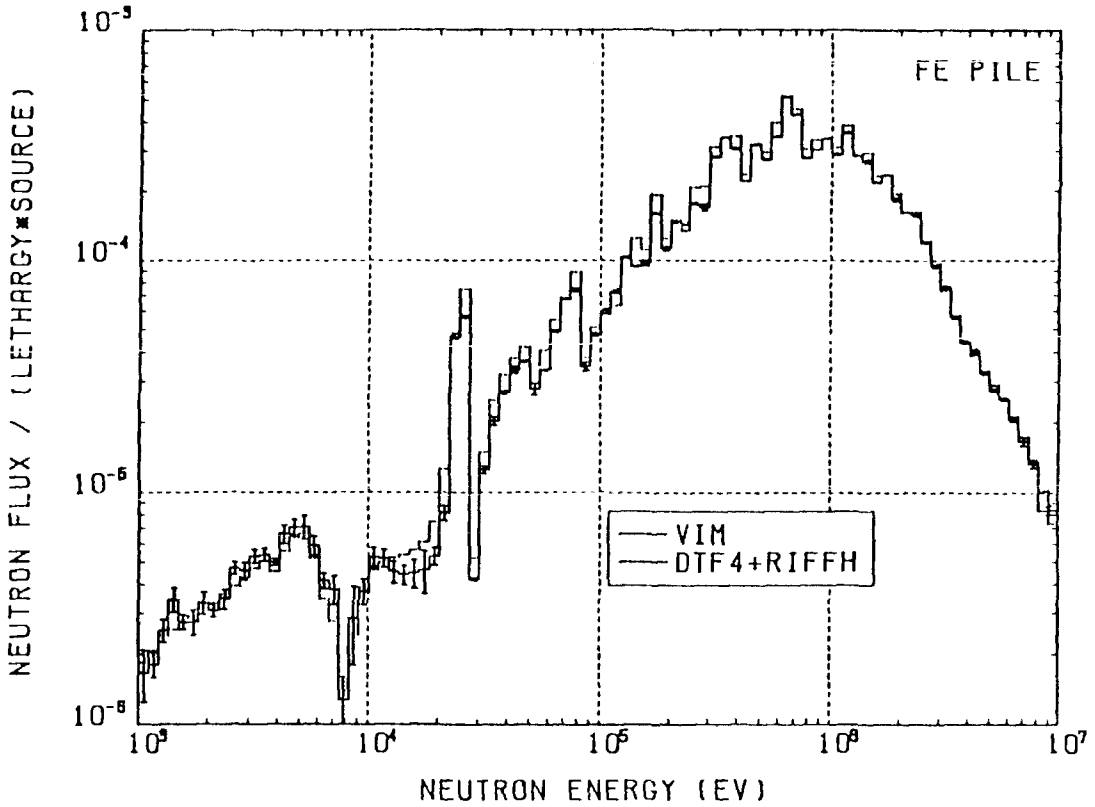

Fig. 8 Total neutron fluxes calculated by VIM and DTF-IV with ENDF/B-IV.
—— VIM, ·-·-· DTF-IV

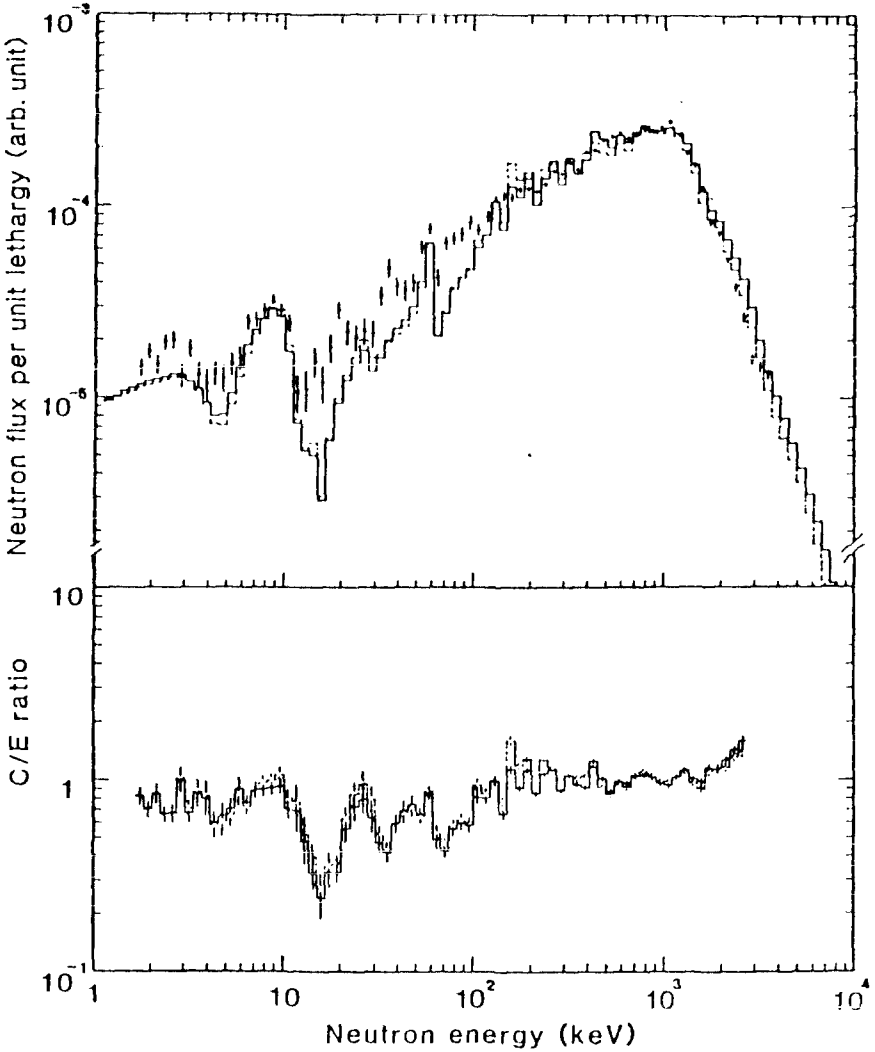

Fig. 9 **Angular neutron spectrum at r= 15 cm and μ= 0.0 in the nickel pile: top.**
Ratio of the calculated to the experimental result (^{6}Li glass): bottom.
All symbols are the same as in Fig. 7.

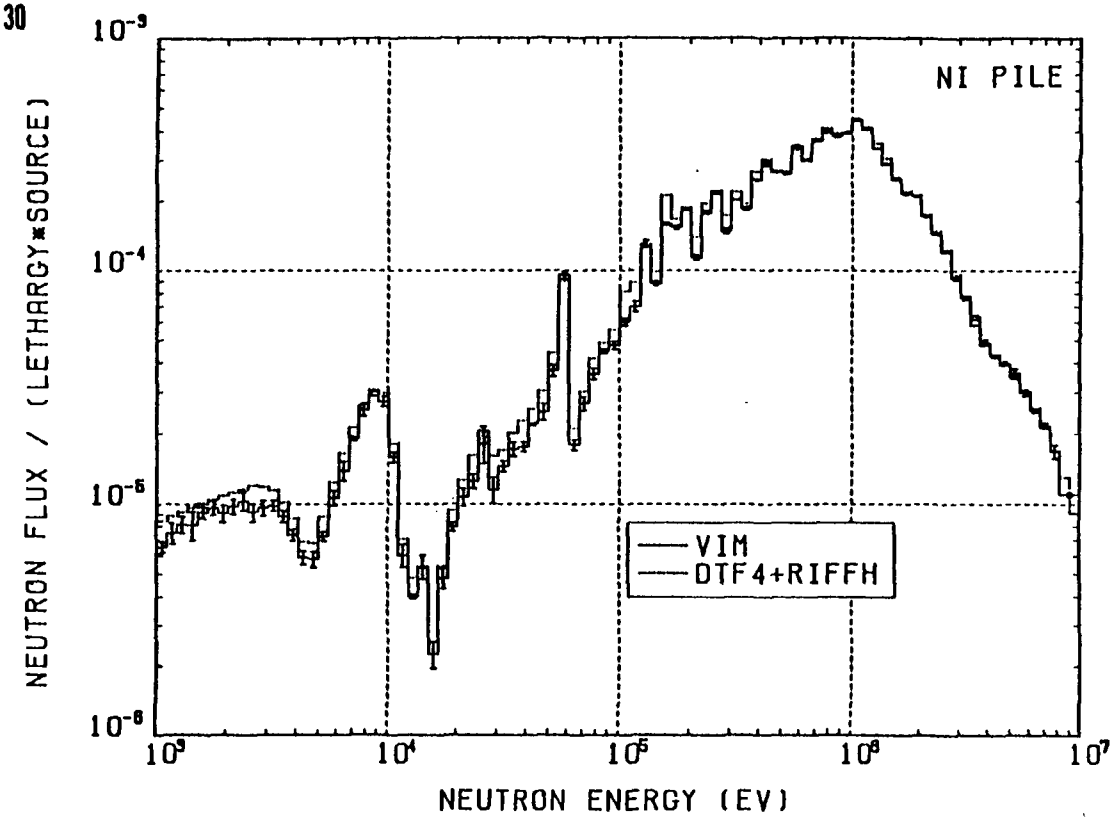

Fig.10 Total neutron fluxes calculated by VIM and DTF-IV with ENDF/B-IV.
All symbols are the same as in Fig. 8.

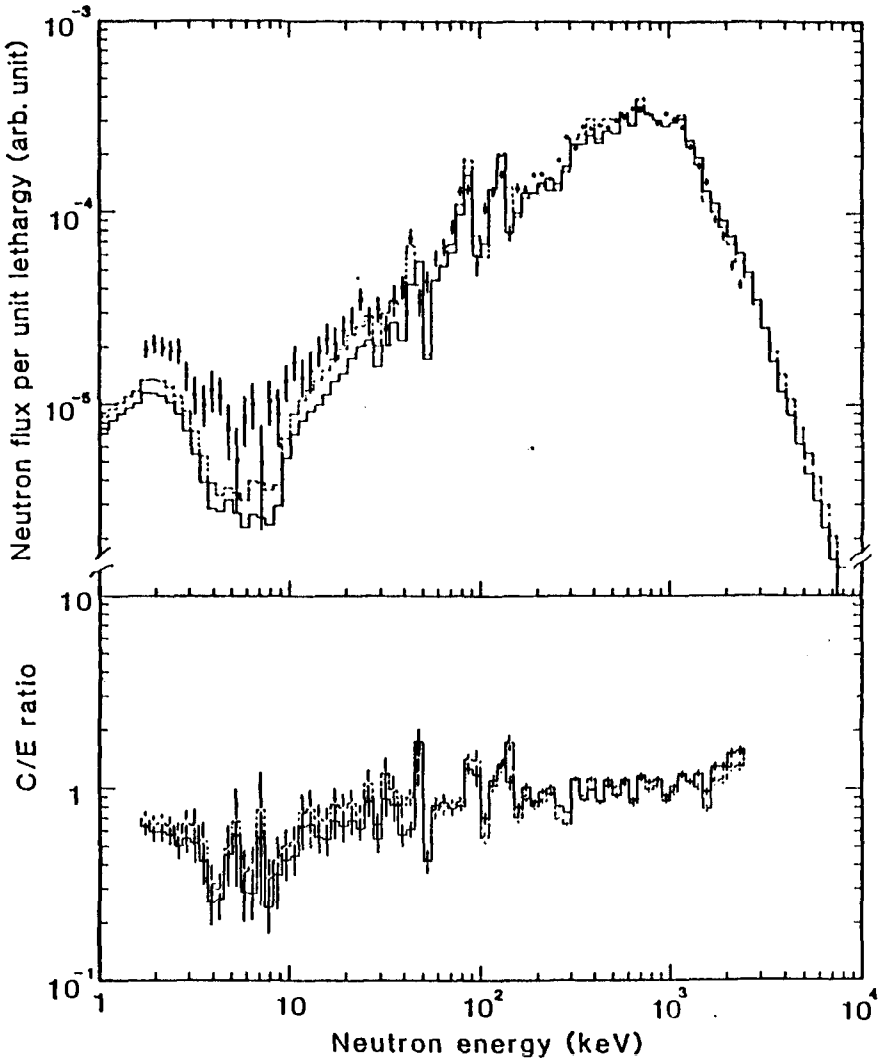

Fig.11 Angular neutron spectrum at r= 15 cm and μ= 0.0 in the chromium pile: top.
Ratio of the calculated to the experimental result (^{6}Li glass): bottom.
All symbols are the same as in Fig. 7.

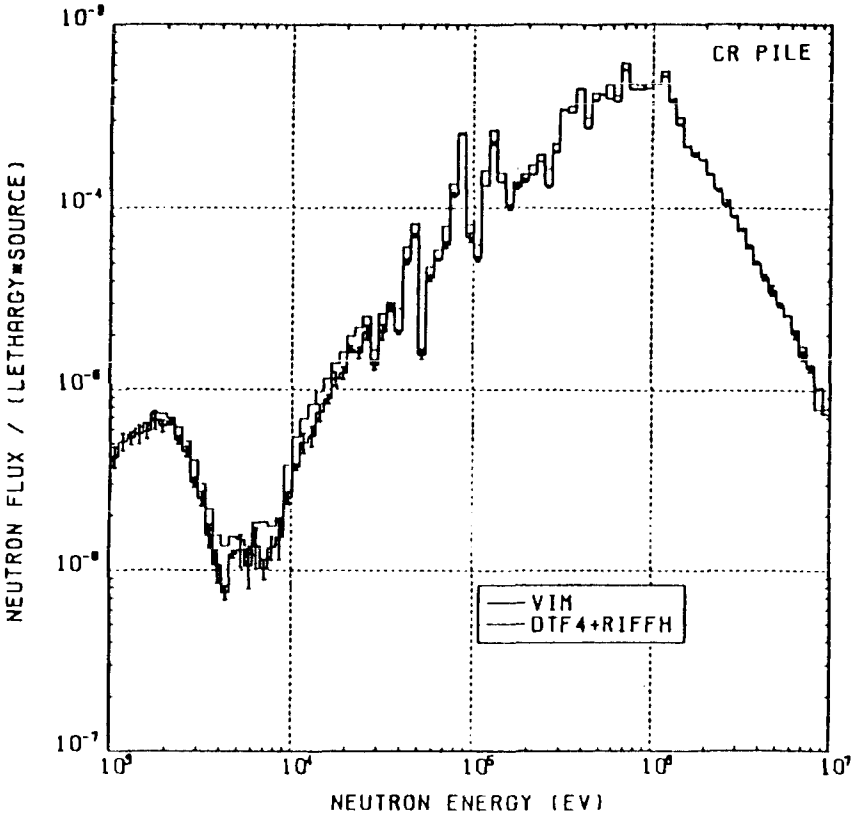

Fig.12 Total neutron fluxes calculated by VIM and DTF-IV with ENDF/B-IV.
All symbols are the same as in Fig. 8.

THE NEUTRON CAPTURE CROSS SECTION OF ^{56}Fe FROM 1 TO 350 keV

F. Corvi, A. Brusegan, R. Buyl, G. Rohr
CEC-JRC, Central Bureau for Nuclear Measurements, B-2440 Geel, Belgium

1. Introduction

Being the major constituent of stainless steel alloys, iron, and in particular its most abundant isotope ^{56}Fe plays a key role with regards to structural materials present in fast breeder reactors. Therefore it is no wonder that its fast capture cross section, in the range 100 eV to 1 MeV neutron energy, is required with 5 to 10% precision in the High Priority List issued by NEANDC-NEACRP [1]. Capture cross sections of Cr, Fe and Ni have also received special attention from the Discrepancies Subcommittee of NEANDC, due to large differences in resonance parameters and normalization procedures. To help solve this last point, NEANDC has set up, in September 1982, an international Task Force charged to solve the discrepancy of the parameters of the most important 1.15 keV resonance in ^{56}Fe. This Task Force, which is chaired by Dr. Francis Perey and to which participate the laboratories of Oak Ridge, Harwell, Geel and JAERI, has already produced some results.

This paper is divided into three parts :

a) Presentation of the final Geel data. Previous ^{56}Fe capture data have been reported by us at the Knoxville Conference [2] (Run 1, range 1 to 100 keV) and at the Antwerp Conference [3] (Run 2, range 1 to 255 keV). The results reported here have been obtained from a careful re-analysis of the Run 2 experimental data using improved versions of the FANAC and TACASI programmes. Moreover the analysed energy range was extended up to 350 keV for a total of 115 resonances. Also, a new measurement of the scattered neutron sensitivity as a function of neutron energy helped to improve the knowledge of the contribution which such an effect has on the areas of s-wave resonances. For all these reasons, the present results supersede those of ref.[3] and can be considered final as far as the Run 2 measurements campaign is concerned.

b) Comparison of the present results to previous data sets. First of all, these results are compared to Run 1 data in an effort to understand the reason for the systematic shift between the two sets of results. Secondly, the data are compared to previous data sets, with special emphasis put on the most recent works and on those performed with comparable resolution. Conclusions about the level of agreement of the data are drawn.

c) Discussion of the normalization problems for neutron capture in structural materials. This problem, which is the very subject of the mentioned Task Force, is related to the discrepancy between the resonance parameters (in particular Γ_n) of the 1.15 keV resonance derived from transmission measurements and those derived from normalizing the Fe capture data to saturated Ag or Au resonances. No convincing explanation of such a discrepancy has yet been found. Some original pieces of information relevant to this problem are presented here together with some considerations on the results obtained so far by the Task Force. In line with the scope of such a meeting, we try in particular to assess quantitatively the systematic errors in the final data brought about by such a discrepancy.

2. The Geel Data

After a short description of the experimental set up, the attention is focused on some special topics such as the determination of the neutron flux and of the scattered neutron sensitivity, and on the improvements made in the data analysis procedure since our last paper [3]. Finally, the table of resonance parameters is introduced and various average values are calculated.

2.1. Experimental Method

The measurements were performed at the 150 MeV Geel Electron Linear Accelerator (GELINA), at a flight distance of 58 m. The linac was operated to provide 4.4 ns wide bursts of electrons of 100 MeV energy with a repetition frequency of 800 Hz. Since the peak current was 10 A, the average beam power was about 3.6 kWatt. Neutrons impinging on the sample were only those coming from the 4 cm thick polyethilene moderator, while neutrons and gammas coming directly from the uranium target were blocked by a copper and lead shadow bar. The sample, on loan from ORNL, consisted of iron oxide enriched to 99.93% ^{56}Fe, packed in a thin aluminium container of 8 cm diameter. The sample thickness was 0.015 atoms/barn. The detectors were two C_6D_6 liquid scintillators encapsulated in thin aluminium containers of 10.2 cm diameter and 7.6 cm height. Events were weighted according to their amplitude information in order to achieve a detector efficiency proportional only to the total γ-ray energy emitted in the capture process. The weighted counting rate was sorted out as an 8K time-of-flight spectrum with 4 ns minimum channel width, covering the energy range from 1 keV to about 600 keV.

2.2. Measurement of the Relative Neutron Flux

When measuring capture over such a large energy range the determination of the relative neutron flux is a problem. In fact, we don't know of any neutron detector based on a reaction which is standard over the whole energy range under consideration here. Similar to what is done in other laboratories, the problem was circumvented by measuring the flux below 100 keV with a ^6Li-glass scintillator 0.5 mm thick and above 100 keV with a multi-plate ^{235}U fission-chamber. A description of this chamber can be found in ref. [4]. After correcting for the transmission of the ^{10}B anti-overlapping filter, of thickness 0.0129 at/b, the relative neutron flux ϕ_T (expressed in neutrons per time-of-flight unit) measured with the ^6Li-glass was fitted from a few eV to 100 keV with the following expression :

$$\phi_T(E) = E^{\alpha(E)}$$

were $\alpha(E) = 0.58154 + 0.43276\cdot10^{-3}\cdot\sqrt{E} - 0.50107\cdot10^{-6}\cdot E$, with E given in eV.

The relative flux from the fission chamber was fitted with a polynomial in a log-log plane in the region from 60 to 400 keV. After normalization to the above expression in the overlapping zone from 60 to 100 keV, the expression for the flux above 100 keV was :

$$\ell n\,\phi_T = 40.798 - 11.374\cdot\ell nE + 1.1564\cdot(\ell nE)^2 - 0.036346\cdot(\ell nE)^3.$$

The ENDF/B-V values of the standard cross sections were used in the calculations for both ^6Li and ^{235}U. In the fission chamber case, a possible systematic error can be originated by a variation of the detection efficiency following a change with energy of the fission fragments anisotropy. In fact, fragments emitted at grazing angles are largely absorbed in the rather thick ($\bar{t}$ = 1.18 mg/cm^2) deposits of U_3O_8 . We have evaluated such an effect considering that the change in the ratio $W(0°)/W(+90°)$ of the angular distributions at 0° and 90° degrees is at most 10% in the present energy range [5]. To such a change corresponds a variation of the efficiency equal to 1.1% or less.

It is important here to note that the same two flux runs just considered have been used in ref. [4] to derive average $\bar{\sigma}_F$ values of ^{235}U in the range 100 eV to 100 keV. The values so determined all lie within $\pm$ 2.5% of the corresponding averages given by Bhat [6] in his evaluation for ENDF/B-V. This can be seen in Fig. 1, where the ratios of the two data sets are plotted. This fact is therefore an important check of the neutron flux measured with a ^6Li-glass scintillator below 100 keV.

If we normalize the neutron flux at a fixed value at 1 keV, then its relative error is estimated to increase from 0 at 1 keV to 5% at 100 keV and then to stay at a constant value of 5% above.

2.3. Determination of the Scattered Neutron Sensitivity

One type of background which is very difficult to evaluate, is that originated by the prompt detection of scattered neutrons. For its very nature, this background is indistinguishable from the actual capture events since it contributes directly

to the resonance areas. Although this effect is usually very small compared to capture detection efficiency, it acquires importance in the case of s-waves of structural materials where the ratio Γ_n/Γ_γ ranges typically from 10^3 to 10^4. We define here scattered neutron sensitivity $\epsilon_n/\epsilon_\gamma$ the ratio between the prompt detection efficiency of a scattered neutron and that of a capture event. In ref.[3] a value $\epsilon_n/\epsilon_\gamma = (1.5 \pm 0.75)\cdot 10^{-4}$ was measured for 100 keV neutrons : because of lack of information at other neutron energies, this value was considered to hold over the whole energy range of interest. This is certainly a poor approximation since all determinations of scattered neutron sensitivity indicate a decrease of $\epsilon_n/\epsilon_\gamma$ with energy. To improve such a situation, we have recently repeated this measurement in a more accurate way. The counting rate of a 7 mm thick graphite sample, which scatttera about 27% of the neutrons, was compared to that of a 0.5 mm thick gold sample. "Black resonance" filters of S and Na were continuously kept in the beam in order to monitor the background around 102 keV and 2.85 keV. In the graphite sample run, a sizeable dip was apparent at about 102 keV, corresponding to a signal-to-background ratio of 1 : 1, while practically no dip was visible at 2.85 keV. Additionally, an "open beam" run was performed, always with the same filters in place : the TOF spectrum from such a run was then taken as a background for the other runs after having normalized it to the same counting rate at 102 keV. The results, listed in Table I for a number of energy intervals between 6 and 350 keV, are plotted in Fig. 2. In this figure are also drawn the results of other detector set-ups, taken from ref. [7] : the present data follow a trend with energy similar to that of the C_6F_6 detectors of Oak Ridge but they are a factor 2 to 6 lower. This is probably due to the absence of fluorine in the scintillators and of any massive material in the vicinity except for a light aluminium support. The peaks below 10 keV and around 40 keV should be due to aluminium, which is also present in the sample holders and in the detectors canning. In view of the uncertainties inherent in the background subtraction, a relative error of $\pm$ 50% in the values of $\epsilon_n/\epsilon_\gamma$ is still considered appropriate.

In order to correct the capture widths of s-wave resonances for such an effect, the data of Table I were first divided by the constant 1.17, corresponding to the ratio between ^{56}Fe and Au binding energies. Secondly, the shape analysis programme FANAC was modified in order to subtract from the normalized capture yield an energy variable background equal to $\epsilon_n/\epsilon_\gamma$ times the scattered neutron probability.

2.4. Data Analysis and Results

In order to evaluate the background, the total spectrum was divided into three energy regions : 1 to 35 keV, 35 to 100 keV and 100 to 350 keV. For each of these regions, a number of energy zones in between the resonances were chosen. The counting rate in these zones was then fitted with an expression of the type $F(T) = A + B \cdot T^C$, where T is the time of flight and A, B, C are constants. While this procedure is satisfactory at low energy, e.g. below 100 keV, it becomes rather doubtful at higher energies because of the increasing difficulty in finding intervals far enough from nearby resonances. Moreover, these intervals, even when available, are usually not free from multiple scattering effects, due to the large energy range accessible after one neutron scattering in such an oxide sample. Because of these reasons, a relative error of 5% was associated to the measured background. After background subtraction and correction for the neutron flux the data were normalized to the capture area of the 1.15 keV ^{56}Fe resonance. In contrast to our previous papers [2,3], we took for this resonance the parameters very recently determined in Oak Ridge [8] from a set of transmission measurements performed at both room and liquid nitrogen temperatures. These parameters are : $\Gamma_n = 61.7 \pm 0.9$ meV and $\Gamma_\gamma = 574 \pm 40$ meV. We believe that this new determination is more accurate than pour previous value of $\Gamma_n = 58 \pm 3$ meV which was based essentially on one measurement only. In practice, the adoption of these new normalization parameters is equivalent to an increase of 3.8% in the capture kernels $g\Gamma_n\Gamma_\gamma/\Gamma$ of all ^{56}Fe resonances. After normalization, the weighted counting rate could be reduced to capture cross section. This is shown in figs. 3a and 3b, where $\sigma(n,\gamma)$ for ^{56}Fe is plotted va neutron energy in the range from 85 to 265 keV. It should be noted that the plotted $\sigma(n,\gamma)$ is still Doppler and resolution broadened and it is not corrected for multiple scattering and prompt background contributions. The data were analysed with the R-matrix shape fitting program FANAC. Two important operational improvements were introduced in it since our last paper : firstly, the number of mesh points used to describe the energy region under consideration was increased up to a maximum of 4100. This allowed a more detailed description of resonance shapes, particularly at higher energy. Secondly , the option allowing the use of an asymmetric resolution function was implemented. In this option, already present in the original FANAC version, the resolution is described by a χ^2-function. We found empirically that resonance profiles were fitted best by a χ^2-distribution with $\upsilon = 24$ degrees of freedom. This has to be compared with a value of $\upsilon = 17$ obtained by Bignami et al.[9] in a simulation of the resolution spread produced by the Geel moderator. While the shape of the resolution was kept

fixed throughout the whole energy range its standard deviation was systematically increased with energy as a result of empirically fitting the resonance shapes. One example of fit is reported in Fig. 4 for the doublet at 102.8 - 103.2 KeV. After such improvements the data of Run 2 were completely re-analysed. Practically the same results were obtained for resonances below 100 keV, while capture areas at higher energy experienced some changes, usually of only a few percent, as compared to the results of ref.[3]. As a check, isolated p- or d-wave resonances were also analysed with the area code TACASI ; 25 resonances above 100 keV were so compared. The agreement was found to be good, the TACASI capture areas being, on average, only 3% larger than the FANAC ones. For such resonances then the mean of the two results was adopted.

The results obtained are listed in Table 2 : the columns from left to right report for each resonance the energy in keV, the neutron width Γ_n and its error, the capture width Γ_γ and its error, the values of 2J and ℓ and the kernel $(g\,\Gamma_n\,\Gamma_\gamma/\Gamma)$ and its error. The last two columns give, for sake of comparison, the kernel taken from the evaluation of F. Perey[10] and based essentially on the ORNL capture data of Allen et al.[11], and the ratio of this kernel to the present one. All widths and kernels are given in units of eV.

It should be stressed that all values of widths listed with zero errors in Table 2 are not a result of the present work but were taken from ref.[10] and used as fixed input parameters in the FANAC or TACASI codes. The only exceptions are the resonances at 341.05 and 341.98 keV whose widths and spin were taken from ref.[13]. It was necessary to introduce fixed parameters, at least for p- and d-waves, since the resolution width is normally considerably larger than the width of the Doppler broadened resonances and therefore even the shape program FANAC provides information about the capture areas only. The usual procedure was to fix the larger of the two widths Γ_n or Γ_γ since that is the parameter to which the capture area is less sensitive. When Γ_γ had to be fixed we conformed to the prescription of F. Perey[10] who assumed Γ_γ = 0.84 eV for d-waves and Γ_γ = 0.54 eV for p-waves. As we will see later, these values are in good agreement with the averages derived from our data. In the case of the s-waves, which have widths usually larger than the resolution width, the FANAC fit was performed in both ways either by letting both Γ_n and Γ_γ varying or by fixing Γ_n to the value of ref.[10]. The result was practically the same as far as the derived value of Γ_γ was concerned. As to the value of Γ_n obtained from the fit, we estimate that the quality of the data is not good enough (because of statistics, multiple scattering, prompt and delayed neutron background) to allow a precise determination of the neutron width. Therefore these Γ_n values are ignored and only the values of ref.[10] are listed in Table 2. A last remark concerning s-waves : the resonance at 317 keV with Γ_n = 6500 eV was not analysed by us because it was practically indistinguishable from the background. It is however mentioned in Table 2 for sake of completeness. The errors on the data were calculated by combining quadratically the statistical error, a 5% error on the background line and the error on the relative neutron flux. For s-wave resonances we considered also a 50% uncertainty in the correction for scattered neutron sensitivity. On the contrary, the uncertainties related to the following effects were not included:

i) data normalization. Taking into account the thickness of the sample used, the normalization uncertainty associated to the errors in the 1.15 keV resonance parameters given in ref.[8], is not larger than 1%;

ii) anisotropy of the capture γ-ray angular distribution for resonances with J = 3/2, 5/2. This effect is not negligible in the present experimental set-up since we observe only γ-rays emitted at angles centered around 90° with respect to the neutron direction. No attempt was made to estimate such uncertainty. It should however be noted that such an effect may influence the capture areas of individual resonances but becomes negligible when averaging over many levels because different spins and parities of initial and final states tend to compensate each other ;

iii) differences in spectrum shape of individual resonances : this point is treated in Section 5. All values of J and ℓ listed in Table 2 are taken from ref.[10] : most but not all of these values were determined from a measurement of the angular distribution of scattered neutrons performed in Oak Ridge. Since the values of Γ_γ or Γ_n derived from the capture kernels depend critically on the spin J, they should be taken with some caution particularly when the J value proposed in ref.[10] is not based on experimental data. The present values of Γ_γ and their errors are plotted vs neutron energy in Fig. 5 and 6 for p-waves and d-waves, respectively. One may notice that the spread of values is real since it is considerably larger than many of the errors given. Averages and standard deviations of Γ_γ are given in Table 3 for s-, p- and d-waves together with the number of degrees of freedom υ_{eff} of the corresponding χ^2 distribution. This parameter is in keeping with the number of available primary transitions known from the ^{56}Fe level scheme.

In view of the interest in stellar nucleo synthesis, we give in Table 4 the capture cross sections averaged over a Maxwellian distribution centered at thermal energies between 20 and 40 keV. These values are very similar to those reported in ref.[12].

Finally, in order to investigate whether the valence neutron reaction plays a role in ^{56}Fe neutron capture, the parameters of the 11 measured s-wave resonances were taken and the correlation coefficient $\rho(\Gamma_n^\circ, \Gamma_\gamma)$ between the reduced neutron widths

and the corresponding capture widths was calculated. It was found $\rho = 0.013 \pm 0.34$ where the standard deviations were obtained from Fisher's transformation. We can then conclude that there is no evidence of valence neutron capture in ^{56}Fe.

3. Comparison of the present results to other data sets

3.1. Run 1 - Run 2 Inter-comparison

When applying the same normalization, the present capture kernels for non s-wave resonances below 100 keV are systematically larger than the corresponding ones of Run 1 by an average amount which varies from 5% to 9%, depending whether we consider all resonances or only the most intense ones. In connection also with the normalization problems treated in Section 4, it is a useful exercise to try to find the reason for such a shift.

The improvements in Run 2 experimental procedure as compared to Run 1 are listed in the introduction of raf.[3]. The most important is probably the reduction of the amplitude threshold from 300 keV electron energy to 150 keV. However, this difference can't produce any sizeable effect since the contribution of the 150-300 keV energy window to the weighted counting rate of the ^{56}Fe capture spectrum is typically 2%.

A more direct inter-comparison between the two data sets can be obtained by looking, rather than at the kernels, at the integrals Y of the weighted counts for each resonance corrected only for background and for the difference in the relative neutron flux. This is possible because the two runs were performed in very similar experimental conditions, i.e. with same sample, detectors and flight path length. Also, the same "old" weighting function referred to in ref.[2] was used for both runs. The results are quite surprising : when plotting, as in Fig.7, the relative difference $|Y(2)-Y(1)|/Y(1)$ between Run 2 and Run 1, normalized to zero at 1.15 keV, vs the average weight $\bar{w}$ (taken from Table III of ref.[2]), we notice that the two quantities are negatively correlated. In particular, a linear fit through the data points gives ~ 15% difference between the resonance with the hardest spectrum and that with the softest one !

To investigate further this effect, we have plotted in Fig.8 the high energy end of the cumulative pulse height spectra of Run 1 and Run 2 together with the calculated shape of the ^{56}Fe thermal spectrum. How this was obtained, is explained in detail in Section 4. The Compton shoulder visible in the spectra is related to the doublet at 7.643 - 7.629 MeV, which dominates the high energy part of the spectrum. From Fig.8 one can see that the 1/2 MAX point of the Compton shoulder of Run 1 is 725 keV too low while that of Run 2 is only 225 keV too high as compared to the calculated value. Moreover the resolution of the Run 1 spectrum is worse, which indicates a shift of the photo-multipliers gain during the measurement. There is therefore, on average, an error of 10% in the amplitude calibration of Run 1. The influence which such an error can have on resonance parameters was studied for a similar situation by Käppeler et al.[12]: they found that for a gain change of 1 MeV at 10 MeV, the variation of the relative capture areas is at most 2%. Therefore this effect can only explain part of the discrepancy. However, in view of this considerable error in amplitude calibration, Run 1 should be considered with some suspicion and the related data should be given less weight in any evaluation.

3.2. Inter-comparison of s-wave resonances

When comparing results, it is useful to consider s-waves separately from the rest because their capture areas depend critically on the correct evaluation of such effects as the multiple scattering inside the sample and the prompt detection of scattered neutrons. In Table 5 are listed the capture widths Γ_γ for the eleven s-wave resonances measured in the present work together with the corresponding values of Allen et al.[22], Fröhner[14] and Käppeler et al.[12]. The widths of ref.[22] were obtained from a re-analysis of the original Oak Ridge data[11] using Monte Carlo methods to account for prompt background due to scattered neutrons. It is explicitly stated in the paper that for s-waves these results supersede the old ones for which only crude corrections were made. The inter-comparison of Table 5 does not pretend to be complete: only relatively recent works providing data at least up to 100 keV have been selected. In particular, for the important 27.7 keV resonance, for which many more experimental determinations exist, we refer the reader to the evaluation paper of Allen[15] and to the recent work of Wisshak et al.[16]. One may notice from Table 5 that the ORNL widths are on average about 60% larger than our values, the ratio between the two data sets fluctuating widely. This is in keeping with the data of Fig.2, discussed in sect. 2.3., pointing to a larger scattered neutron sensitivity of the Oak Ridge experimental set up. When looking at the average widths $\bar{\Gamma}_\gamma$ given in Table 3 for both data sets, we notice that the Geel $\bar{\Gamma}_\gamma$ values for s- and d-waves are similar while the ORNL ones differ greatly. Now we can't think of any reason for such a large difference unless one assumes a very strong valence contribution which is neither theoretically expected for ^{56}Fe nor experimentally verified. Also, all recent measurements of the 27 keV resonance[15,16]

give Γ_γ values around 1 eV or lower, indicating, over the past few years, a trend towards lower Γ_γ values for s-wave resonances as a result of more careful measurements and more precise evaluation of the backgrounds involved. For all these reasons there is little doubt that the results of the present work provide a more faithful representation of s-wave capture than those of refs. [10,11,22].

3.3. Intercomparison of p- and d-wave resonances

The ratios $r = A_\gamma$ (ORNL)/A_γ (GEEL) between the ORNL capture kernels and the present ones are plotted vs resonance energy in Fig. 9 for p- and d-waves. All resonances have been considered except for the partially unresolved multiplets at 96, 122, 173, 209 and 306 keV where the single kernels have been replaced by their sum. This was done in order to avoid systematic errors due to insufficient resolution. The average values of the ratios in 50 keV intervals are also plotted as histogram in Fig. 9 and listed, together with their standard deviations, in Table 6. The larger spread in data points above 150 keV is an indication of the increasing difficulty in obtaining precise values of the capture areas at high energy because of lower signal-to-background ratios, uncertainty in background determination and lack of resolution. The average ratio values, however, lie within a few percent of unity except for a peak in the region 150-250 keV. A possible reason for such a peak might be an incorrect determination of the relative neutron flux in one of the two measurements. In this respect we notice that this region corresponds approximately to the 250 keV ^{6}Li resonance and that Allen et al.[11] have measured the neutron flux with the ^{6}Li-glass all the way up to 400 keV. It is possible that the neutron efficiency is not so precisely determined around the resonance peak. The average of the ratios over the whole energy range is 1.039 showing an excellent overall agreement. The situation has even improved since our last paper [3] as a result of the normalization of our data to the new 1.15 keV resonance parameters. The comparison of our data with the recent Karlsruhe [12] results obtained with C_6D_6 detectors is also very encouraging: the widths of the individual resonances are in good agreement and the average ratio of the KFK capture kernels to the Geel ones for 17 p- or d-wave resonances or multiplets below 115 keV is $\bar{r} = 0.99 \pm 0.09$.

4. Data Normalization and the Weighting Method

The nice agreement found in Sect. 3.3 between the present results and those of Oak Ridge [10] and Karlsruhe [12] for p- and d-waves is unfortunately undermined by normalization problems. In fact, while the present data are normalized to the capture kernel of the 1.15 keV resonance derived from transmission measurements, the other two data sets are referred to Au neutron capture, either in the 4.9 eV saturated resonance [10] or in the average keV region [12]. It is now well known that there are important discrepancies between the two methods [3,18]. The situation up to date is summarized in the following. In Table 7 are listed the results of the transmission measurements performed in Geel and Oak Ridge. These last ones have been promoted by the Task Force and have only very recently been completed. The results agree within the errors and, as already stated in Sect. 2.4., the ORNL value has been chosen as our new reference because of its higher precision. The results of capture normalization of the 1.15 keV resonance to Ag or Au resonances are reported in the first three rows of Table 8 for two Geel and one recent Oak Ridge measurement : the quantity N is here representing the capture kernel A_γ obtained from the normalization while R is the reference value from transmission. The ratio $\epsilon = N/R$, quoted in the last column is a measure of the discrepancy. It is extremely important to observe that the ORNL capture result is also about 20% larger than the transmission value, completely confirming the experimental evidence accumulated in Geel in these last years. The last three rows of Table 8 concern thermal normalization: here N and R are the thermal Fe capture cross sections from the normalization and from the literature [20], respectively. These thermal measurements, which were already reported in Table 1 of ref.[3], have recently been re-analysed with an improved background determination. The new values (which therefore supersede those of ref.[3]) show that the discrepancy observed at 1.15 keV is also reproduced at thermal energy both in sign and magnitude. This is in keeping with the thermal calibration of the 1.15 keV resonance [3] which yields a value $\Gamma_n = 56 \pm 6$ meV, which agrees with the transmission data. The obvious conclusion to be drawn from Table 8 is that normalization problems are not only limited to the 1.15 keV resonance alone but are characteristic of ^{56}Fe capture in general. It should however be noted that the shape of the thermal capture γ-ray spectrum is very similar to that at 1.15 keV [21]: in fact, it is not known whether the values of ϵ given in Table 8 apply also to resonances with much softer spectra. It is only natural at this point to look whether the weighting method can provide an explanation for such a discrepancy. In Fig. 10 are plotted three weighting functions, the OLD WF, NEW WF and EMP WF. The first two have already been discussed in the past [2,18], in particular the NEW WF is the one presently in use. It was obtained by introducing in the Monte Carlo based simulation programme of the detection process [18] an increased (as compared to OLD WF) energy loss of electrons in the scintillator employing newly evaluated data from Atomic Data.

The EMP WF is the one which is necessary to introduce in order to derive from the Ag, Au normalization values 18% lower, i.e. in agreement with the transmission data at 1.15 keV or with the known thermal cross section $\sigma(n_{th},\gamma)$ at 0.025 eV. It should be stressed that EMP WF has no physical meaning since it is impossible to produce such a drastic change in the shape of the weighting function without substantially modifying the interaction laws of electromagnetic radiation and/or electrons with matter.

In order to check the programme used for deriving the weighting function, we have calculated the $^{56}Fe(n_{th},\gamma)$ γ-ray spectrum exploiting the fact that practically all transitions in such a nucleus are known and can be found in Nuclear Data Tables. We have grouped such transitions around 16 average energies and we have calculated the corrasponding response functions. We have then summed them up after having multiplied by their relative intensities, and finally convoluted with the amplitude resolution function. The obtained spectrum, weighted over the energy for better representation, is compared in Fig. 11 with the experimental one : the agreement between the two curves is not too bad as can be seen also by the $\bar{w}$ values which differ only by 9%. At least one thing can be learned from such a comparison : the peak around 7.5 MeV is not underestimated in the calculations. Only an underestimation of the high energy part of the spectrum could give rise to a weighting function increasing too steeply at high energy.

The conclusion to be drawn from such tests is that, at the present moment, we can't find anything wrong with the weighting method which could explain the observed discrepancy. We believe however that more checks of this type should be carried out in order to gain a deeper insight into the general valididty of the method.

The implications of this 18-20% normalization difference with regard to the reliability of the data sets presented in Section 3 are quite serious: if two data sets agree in spite of the fact that they are normalized in a different way, this can only mean that there are systematic errors in one or both measurements which compensate for such a discrepancy. Therefore the consistent data sets of Sect. 3.3. can be shifted upwards or downwards by as much as 20% depending on which normalization is chosen and which measurement is considered correct. Fortunately, the situation is not as bad as it appears: a transmission measurement of the 22.8 keV resonance recently performed in Oak Ridge [8] gives a kernel $g\Gamma_n\Gamma_\gamma/\Gamma$ = 0.161 eV, in agreement with all three data sets of sect. 3.3.

In order to get an idea of the systematic errors connected with such normalization, we have calculated the relative change $\Delta A_\gamma / A_\gamma$ of the kernels when using EMP WF instead of NEW WF while normalizing always to unity at E_o = 1.15 keV. The results are plotted vs $\bar{w}$ in Fig. 12, together with a linear fit, for 17 p- and d-wave resonances below 100 keV. The change goes from + 9.7% to - 4.1% for the two extremes and the average is + 3.2%. This means that even in the extreme scenario of the EMP WF the increase in the average ^{56}Fe capture is very small. Lacking for the moment any convincing explanation of the normalization discrepancy, we should take this finding as a reassuring temporary conclusion: even if, for reasons which we ignore, extreme weighting functions such as EMP WF should be applied to the ^{56}Fe data, the net capture effect would be almost negligible as long as the data are normalized to the 1.15 keV resonance. We believe therefore that the present data set can be used with a certain confidence.

References

1. J.L. Rowlands, NEACRP-A-568/NEANDC-A-180 (1983)

2. Brusegan, F. Corvi, G. Rohr, R. Shelley, T. van der Veen, Proc. Int. Conf. on Neutron Cross Sections for Technology, Knoxville, 1979, NBS-SP. 594, p.163

3. F. Corvi, A. Brusegan, R. Buyl, G. Rohr, R. Shelley, T. van der Veen, Proc. Int. Conf. on Nucl. Data, Antwerp, 1982, p. 131

4. F. Corvi et al., Proc. NEANDC/NEACRP Spec.Meeting on Fast Neutron Capture Cross Sections, Argonne, 1982, ANL-83-4, p.347

5. J.W. Meadows, C. Budtz-Jørgensen, Proc. Int. Conf. on Nucl. Data, Antwerp, 1982, p. 740

6. M.R. Bhat, Rep. BNL-NCS-51184 (1980)

7. D.B. Gayther, R.B. Thom, Rep. ANL-83-4 (1982), p.205

8. F.G. Perey, Private Communication and Proc. of this Meeting

9. A. Bignami, C. Coceva, R. Signorini, Rep. EUR 5157e (1974)

10. F.G. Perey, G.T. Chapman, W.E. Kinney, C.M. Perey, Neutron Data of Structural Materials for Fast Reactors, Geel 1977, Pergamon Press, p.530

11. B.J. Allen, A.R. de L. Musgrove, J.W. Boldeman, M.J. Kenny, R.L. Macklin, Nucl. Phys. A269 (1976) 408

12. F. Käppeler, K. Wisshak, L.D. Hong, Rep. KFK 3412 (1982)

13. F. Poortmans, Private Communication

14. F. Fröhner, Neutron Data of Structural Materials for Fast Reactors, Geel 1977, Pergamon Press, p.138

15. B. Allen, Proc. NEANDC/NEACRP Spec. Meeting on Fast Neutron Capture Cross Sections, Argonne, 1982, ANL-83-4, p.431

16. K. Wisshak, F. Käppeler, G. Reffo, F. Fabbri, Rep. KFK 3516 (1983)

17. A. Brusegan, Private Communication

18. G. Rohr, Rep. ANL-83-4, p. 394 (1982)

19. R.L. Macklin, Nucl. Sci. Eng. 83 (1983) 309

20. S.F. Mughabghab, M. Divadeenam, N.E. Holden, Neutron Cross Sections, Vol. 1, Part. A, Academic Press, 1981

21. R.E. Chrien, M.R. Bhat, O.A. Wasson, Phys. Rev. C1 (1970) 973

22. B.J. Allen and A.R. de L. Musgrove, Neutron Data of Structural Materials for Fast Reactors, Geel 1977, Pergamon Press, p. 447

TABLE 1 : Measured values of the scattered neutron sensitivity relative to gold neutron capture $\epsilon_n/\epsilon_\gamma$ in the range from 6keV to 350 keV.

En.Interval (keV)	$\epsilon_n/\epsilon_\gamma$ (10^{-4})	En. Interval (keV)	$\epsilon_n/\epsilon_\gamma$ (10^{-4})
6 - 7	7.6	40 - 50	2.54
7 - 8	9.0	50 - 60	1.80
8 - 10	3.85	60 - 70	1.23
10 - 12.5	2.00	70 - 80	1.00
12.5 - 15	1.52	80 - 90	0.83
15 - 20	1.39	120 - 150	1.07
20 - 25	1.43	150 - 200	0.64
25 - 30	1.34	200 - 250	0.56
30 - 35	2.12	250 - 300	0.38
35 - 40	2.53	300 - 350	0.35

TABLE 2. RESONANCE PARAMETERS OF ^{56}Fe IN THE RANGE 1 TO 350 keV FROM THE PRESENT WORK

N	ENERGY (keV)	GN	ΔGN (eV)	GG	ΔGG (eV)	2J	L	KERNEL	ΔK (eV)	K.ORML	RAT
1	1.15	61.7E-3	.00	.60	.04	1	1	55.7E-3	.00	55.E-3	1.00
2	2.35	.21E-3	.05E-3	.84	.00	3	2	.42E-3	.08E-3	.40E-3	.96
3	12.46	2.9E-3	.7E-3	.54	.00	1	1	2.8E-3	.7E-3	2.3E-3	.81
4	17.77	14.8E-3	1.6E-3	.54	.00	1	1	14.4E-3	1.6E-3	19.E-3	1.32
5	20.19	4.2E-3	.8E-3	.84	.00	3	2	8.3E-3	1.8E-3	9.4E-3	1.13
6	22.82	.251	.017	.54	.00	1	1	.171	.008	.18	1.05
7	27.74	1520.00	.00	.95	.13	1	0	.95	.13	1.40	1.47
8	34.26	.79	.00	.49	.01	3	1	.61	.03	.64	1.05
9	36.75	.101	.006	.84	.00	5	2	.271	.015	.28	1.03
10	38.45	.267	.020	.54	.00	3	1	.357	.019	.40	1.12
11	46.09	10.00	.00	.57	.03	1	1	.54	.03	.50	.93
12	52.18	12.00	.00	.40	.02	3	1	.77	.04	.81	1.05
13	53.60	1.00	.00	.61	.05	1	1	.38	.02	.40	1.05
14	53.72	.037	.009	.54	.00	1	1	.034	.008	.00	.00
15	59.28	4.00	.00	.46	.03	3	1	.82	.05	.87	1.06
16	63.52	.80	.00	.55	.05	3	1	.65	.04	.65	1.00
17	73.05	20.00	.00	.75	.05	1	1	.73	.05	.70	.97
18	74.07	535.00	.00	.51	.08	1	0	.51	.08	.73	1.43
19	77.14	3.60	.00	.30	.03	1	1	.28	.02	.30	1.08
20	80.91	7.00	.00	.77	.04	5	2	2.07	.11	2.04	.98

Table 2 continued

N	ENERGY (keV)	GN	ΔGN (eV)	GG	ΔGG (eV)	2J	L	KERNEL	ΔK (eV)	K.ORNL	RAT
21	83.63	1250.00	.00	.50	.08	1	0	.50	.08	1.28	2.56
22	90.42	14.00	.00	.43	.03	3	1	.83	.05	.89	1.07
23	92.76	1.60	.00	.79	.07	3	2	1.06	.06	.93	.88
24	92.98	.58	.08	.54	.00	3	1	.56	.04	.53	.95
25	96.27	.18	.04	.84	.00	5	2	.44	.08	1.26	2.88
26	96.44	1.10	.00	.99	.17	1	1	.56	.06	.30	.53
27	96.69	2.50	.00	.90	.10	3	1	1.33	.12	.70	.53
28	102.78	21.00	.00	.33	.03	3	1	.65	.06	.71	1.10
29	103.17	.76	.00	.74	.09	3	2	.75	.06	.80	1.07
30	106.03	2.80	.00	.88	.06	3	2	1.34	.09	1.55	1.16
31	112.81	5.50	.00	.56	.04	3	2	1.02	.07	1.17	1.14
32	121.12	.034	.028	.54	.00	1	1	.032	.027	.03	.93
33	122.70	.071	.025	.54	.00	3	1	.126	.044	.15	1.19
34	122.92	46.00	.00	.30	.03	3	1	.59	.07	.54	.91
35	124.29	7.50	.00	.64	.06	1	1	.59	.05	.63	1.07
36	125.28	10.00	.00	.62	.04	3	2	1.16	.08	1.27	1.10
37	130.11	500.00	.00	.54	.08	1	0	.54	.08	1.10	2.04
38	130.38	.79	.11	.84	.00	3	2	.82	.12	.79	.97
39	140.37	2700.00	.00	1.38	.24	1	0	1.38	.24	2.19	1.59
40	141.38	.57	.00	.86	.20	3	2	.70	.17	.68	.97
41	142.56	.56	.00	.65	.11	3	1	.60	.11	.55	.92
42	150.01	.11	.02	.54	.00	3	1	.21	.03	.29	1.39
43	154.09	.43	.05	.84	.00	3	2	.56	.05	.56	.99
44	161.92	6.50	.00	.62	.05	3	2	1.13	.09	1.14	1.01
45	169.28	6.00	.00	.97	.15	3	2	1.67	.25	2.00	1.20
46	169.35	1000.00	.00	0.92	.14	1	0	0.92	.14	1.10	1.20
47	173.30	.14	.03	.54	.00	3	1	.22	.05	.56	2.55
48	173.82	42.00	.00	.24	.03	3	1	.48	.07	.36	.74
49	175.94	.07	.03	.54	.00	3	1	.13	.05	.00	.00
50	179.92	13.00	.00	.51	.07	1	1	.49	.07	.53	1.08
51	181.34	17.00	.00	1.01	.09	5	2	2.86	.25	3.21	1.12
52	187.26	1.70	.00	.32	.08	3	2	.54	.13	.60	1.11
53	187.56	3600.00	.00	.82	.25	1	0	.82	.25	2.98	3.63
54	188.14	.066	.03	.54	.00	3	1	.096	.053	.00	.00
55	190.15	15.00	.00	.46	.05	3	2	.88	.10	1.04	1.18
56	193.17	20.00	.00	.59	.05	3	2	1.15	.10	1.13	.98
57	195.95	66.00	.00	.54	.08	1	1	.54	.07	.69	1.28
58	201.76	24.00	.00	.84	.07	3	2	1.61	.14	1.95	1.20
59	203.91	.041	.019	.84	.00	3	2	.079	.033	.00	.00
60	206.14	1.14	.00	.51	.06	5	2	1.05	.10	1.45	1.38
61	208.20	22.00	.00	.70	.09	1	1	.68	.08	1.19	1.75
62	209.12	.14	.04	.54	.00	3	1	.22	.07	.27	1.23
63	210.03	.06	.02	.84	.00	3	2	.11	.04	.39	3.55
64	210.90	9.00	.00	.62	.07	3	2	1.16	.12	1.33	1.15
65	216.04	.82	.11	.54	.00	1	1	.33	.06	.40	1.23
66	220.82	1150.00	.00	1.59	.21	1	0	1.59	.21	2.16	1.36
67	222.10	8.00	.00	.21	.04	3	1	.41	.09	.64	1.56
68	223.88	10.00	.00	.53	.06	3	1	1.02	.10	1.32	1.30
69	226.07	28.00	.00	.45	.06	3	1	.89	.11	1.00	1.12
70	230.13	7.50	.00	.28	.04	3	1	.54	.08	.62	1.15

Table 2 continued

N	ENERGY (keV)	GN	ΔGN (eV)	GG	ΔGG (eV)	2J	L	KERNEL	ΔK (eV)	K.ORNL	RAT
71	232.77	20.00	.00	1.18	.10	3	2	2.22	.19	2.67	1.20
72	235.09	20.00	.00	.83	.06	5	2	2.38	.18	2.51	1.05
73	241.86	10.00	.00	1.30	.10	5	2	3.46	.26	3.84	1.11
74	243.63	.10	.04	.54	.00	3	1	.17	.06	.14	.83
75	245.21	435.00	.00	.57	.10	1	0	.57	.10	.80	1.40
76	246.54	.14	.09	.54	.00	1	1	.11	.07	.00	.00
77	252.70	.09	.05	.54	.00	3	1	.16	.08	.24	1.51
78	253.83	28.00	.00	.59	.06	5	2	1.74	.19	1.53	.88
79	256.41	6.00	.00	.60	.07	3	1	1.08	.12	1.08	1.00
80	260.18	29.00	.00	.70	.10	1	1	.68	.10	.54	.79
81	261.14	.09	.04	.84	.00	3	2	.16	.07	.00	.00
82	264.02	140.00	.00	.56	.11	1	1	.56	.11	.68	1.21
83	264.71	.20	.08	.54	.00	3	1	.29	.12	.26	.89
84	267.31	55.00	.00	.33	.06	5	2	.98	.19	1.00	1.02
85	267.89	.72	.27	.84	.00	3	2	.77	.30	.58	.75
86	270.16	144.00	.00	.41	.11	1	1	.41	.11	.30	.73
87	275.06	.48	.25	.54	.00	1	1	.25	.14	.20	.79
88	276.52	85.00	.00	.26	.06	3	1	.52	.11	.32	.62
89	278.24	4000.00	.00	.63	.19	1	0	.63	.19	1.01	1.60
90	281.32	8.00	.00	.95	.10	3	2	1.70	.19	1.69	1.00
91	283.62	.77	.37	.54	.00	3	1	.64	.32	.47	.74
92	284.37	12.00	.00	.74	.10	3	2	1.40	.19	1.54	1.10
93	285.83	15.00	.00	1.16	.11	3	2	2.15	.21	1.79	.83
94	288.99	12.00	.00	.73	.09	3	2	1.38	.17	1.86	1.35
95	290.86	13.00	.00	.82	.09	3	1	1.55	.17	1.32	.85
96	293.54	130.00	.00	.69	.11	1	1	.69	.11	.60	.87
97	296.07	.29	.10	.54	.00	3	1	.38	.11	.42	1.12
98	300.28	23.00	.00	.78	.09	3	2	1.51	.18	1.46	.97
99	303.31	.14	.07	.54	.00	3	1	.22	.11	.30	1.36
100	304.77	19.00	.00	.41	.07	3	1	.81	.14	.65	.81
101	306.70	.28	.19	.54	.00	1	1	.19	.12	.30	1.61
102	307.33	1.04	.42	.54	.00	3	1	.71	.30	.40	.56
103	311.39	38.00	.00	.60	.08	3	2	1.18	.16	.85	.72
104	313.28	.27	.08	.84	.00	3	2	.41	.13	.00	.00
105	315.07	28.00	.00	1.17	.10	5	2	3.36	.29	2.60	.77
106	317.00	5500.00	.00	.00	.00	1	0	.00	.00	1.70	.00
107	321.99	2.50	.00	.82	.15	3	2	1.23	.22	1.26	1.02
108	324.38	.23	.11	.54	.00	3	1	.32	.16	.37	1.14
109	331.82	320.00	.00	1.44	.20	1	0	1.44	.20	1.27	.88
110	334.83	1.70	.00	.90	.15	5	2	1.77	.20	1.68	.95
111	341.05	110.00	.00	.93	.14	3	1	1.85	.27	2.68	1.45
112	341.98	27.00	.00	.61	.11	3	1	1.24	.22	.00	.00
113	345.18	47.00	.00	.81	.11	3	1	1.63	.22	1.12	.69
114	349.12	120.00	.00	.62	.09	3	1	1.23	.19	1.18	.96
115	350.67	27.00	.00	.67	.09	5	2	1.96	.25	1.45	.74

TABLE 3 : Average values $\bar{\Gamma}_\gamma$ and standard deviations $\delta\Gamma_\gamma$ calculated from the present data for s-, p- and d-wave resonances. The corresponding number of degrees of freedom υ_{eff} was calculated from the expression $2/\upsilon_{eff} = (\delta\Gamma_\gamma / \bar{\Gamma}_\gamma)^2$. In the last column the $\bar{\Gamma}_\gamma$ values from ref.[10] are listed for comparison.

ℓ	sample population	$\bar{\Gamma}_\gamma$ (eV)	$\delta\Gamma_\gamma$ (eV)	υ_{eff}	$\bar{\Gamma}_\gamma$(ORNL) (eV)
0	11	0.895	0.404	9.8	1.46
1	35	0.552	0.203	14.8	0.54
2	31	0.768	0.238	20.9	0.84

TABLE 4 : Capture cross sections averaged over a Maxwellian distribution for different thermal temperatures

$\bar{E}_{th}$ (keV)	σ_γ (mb)
20	13.9
25	14.0
30	13.8
35	13.4
40	13.0

TABLE 5 : Comparison of the s-wave capture widths from the present work with those from some recent data sets.

E_o (keV)	Γ_γ (eV)			
	Present work	Allen et al.[22) (1977)	Fröhner et al.[17) (1977)	Käppeler et al.[12) (1982)
27.74	0.95 ± .13	1.6 ± .4 a)	1.25 ± .20	1.04 ± .08
74.06	0.51 ± .08	0.8 ± .1	0.75 ± .15	0.86 ± .08
83.64	0.50 ± .08	0.9 ± .2	0.58 ± .22	0.54 ± .09
129.90	0.54 ± .08	0.8 ± .2	1.30 ± .40 b)	
140.30	1.38 ± .24	2.4 ± .3	1.48 ± .31 b)	
169.26	0.92 ± .14	0.6 ± .3		
187.56	0.82 ± .22	2.8 ± .6		
220.80	1.59 ± .21	2.8 ± .3		
245.14	0.57 ± .10	0.9 ± .2		
277.88	0.63 ± .19	1.3 ± .4		
331.80	1.44 ± .20	1.3 ± .1		

a) uncertain analysis

b) incompletely resolved

TABLE 6 : Average values and standard deviations of the ratio

$r = \frac{A_\gamma(ORNL)}{A_{\gamma(GEEL)}}$ between the Oak Ridge and Geel capture kernels calculated over 50 keV intervals for p- and d-wave resonances.

Energy Interval (keV)	$r = \frac{A_\gamma(ORNL)}{A_\gamma(GEEL)}$
0 - 50	1.04 ± .14
50 - 100	1.00 ± .06
100 - 150	1.07 ± .13
150 - 200	1.13 ± .12
200 - 250	1.21 ± .19
250 - 300	0.95 ± .23
300 - 350	0.95 ± .24
0 - 350	1.039

TABLE 7 : Summary of the results of transmission measurements of the 1.15 keV ^{56}Fe resonance performed in the last years in Geel and Oak Ridge.

Lab.	Year	Ref.	Thickness (mm)	Γ_n (meV)	Γ_γ (meV)	$g\Gamma_n\Gamma_\gamma/\Gamma$ (meV)
Geel	1979	2	2	58 ± 4	610 ± 60	53 ± 3
Geel	1982	17	1	61 ± 3	680 ± 140	56 ± 3
Oak Ridge	1983	8	1.5 - 25	61.7 ± 0.9	574 ± 40	55.7 ± 0.7

TABLE 8 : Results of normalization of capture in natural and enriched Fe samples relative to capture in Ag and Au at both resonance and thermal energies. The quantity A_γ indicates the capture kernel $g\Gamma_n\Gamma_\gamma/\Gamma$, the quantity $\epsilon = N/R$ in the last column is the ratio between the value obtained from normalization and the reference value. All Geel data have not been corrected for γ-ray absorption in the sample.

Lab. Year	Ref.	Normalization sample Element	Thn. (mm)	Energy	Fe-sample Nucl.	Thickn. (mm)	Energy	Γ_n (meV)	Γ_γ (meV)	N (result of normalization)	R (reference value)	$\epsilon = N/R$
Geel'82	18	Ag	1	16-71 eV	natur.	1.0	1.15 keV	72.8±3.2	610[a]	A_γ = 65 ± 3 meV	A_γ = 55.7 ± 0.7 meV	1.17±.06
Geel'82	3	Ag Au	0.2 0.1	5.2 eV 4.9 eV	^{56}Fe	0.5	1.15 keV	74.3±3	610[a]	A_γ = 66.2 ± 2.8meV	A_γ = 55.7 ± 0.7 meV	1.19±.05
Oak Ridge'82	19	Au		4.9 eV	natur.	0.5	1.15 keV	77.3±1.7	615[a]	A_γ = 68.7 ± 1.5 meV	A_γ = 55.7 ± 0.7 meV	1.23±.03
Geel'82	3	Au	0.1	thermal	natur.	0.5	thermal			σ_{th} = 3.02 ± .09 b	σ_{th} = 2.56 ± .03 b[b]	1.18±.04
Geel'82	3	Au	0.1	thermal	natur.	1.0	thermal			σ_{th} = 2.87 ± .08 b	σ_{th} = 2.56 ± .03 b[b]	1.12±.04
Geel'82	3	Au	0.1	thermal	^{56}Fe	0.5	thermal			σ_{th} = 3.06 ± .08 b	σ_{th} = 2.59 ± .14 b[b]	1.18±.07

a) assumed values

b) values taken from Mughabghab et al.[20]

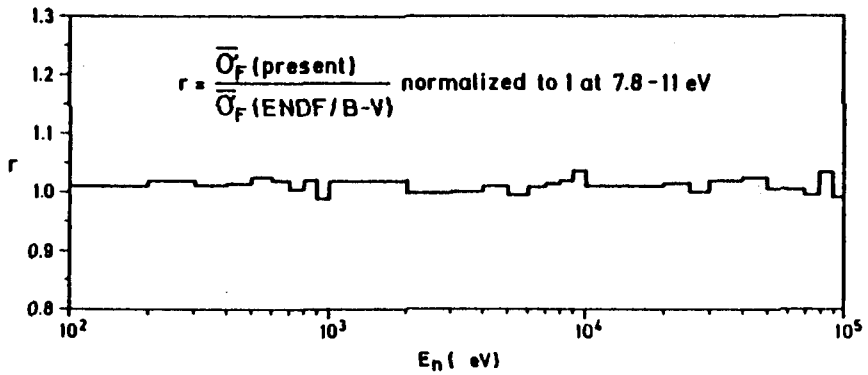

Fig. 1. Average $\bar{\sigma}_F$ values obtained using the neutron flux from the ^{6}Li-glass, compared to ENDF/B-V values [6]. Our data have been normalized to the weighted mean [6] of the low energy fission integral $I_{7.8\ eV}^{11\ eV}$ = 241.2 b·eV.

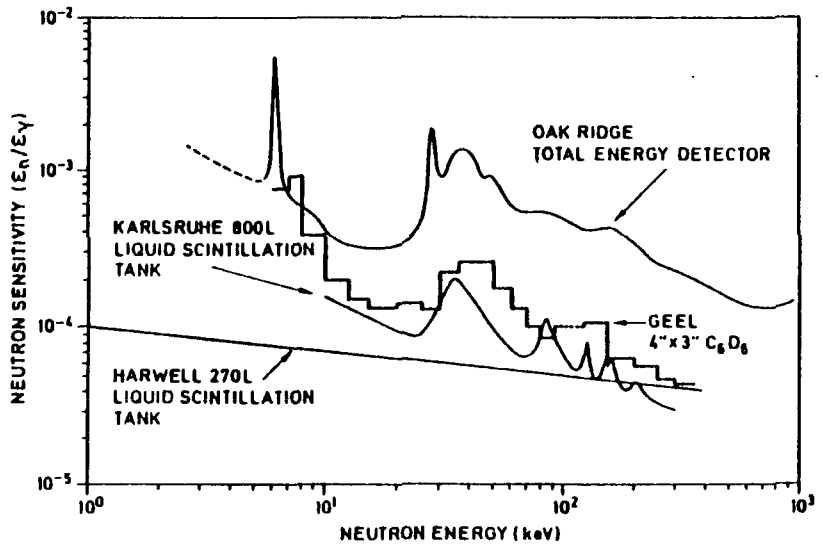

Fig. 2. Scattered neutron sensitivity of the Geel scintillators compared to that of other detector systems.

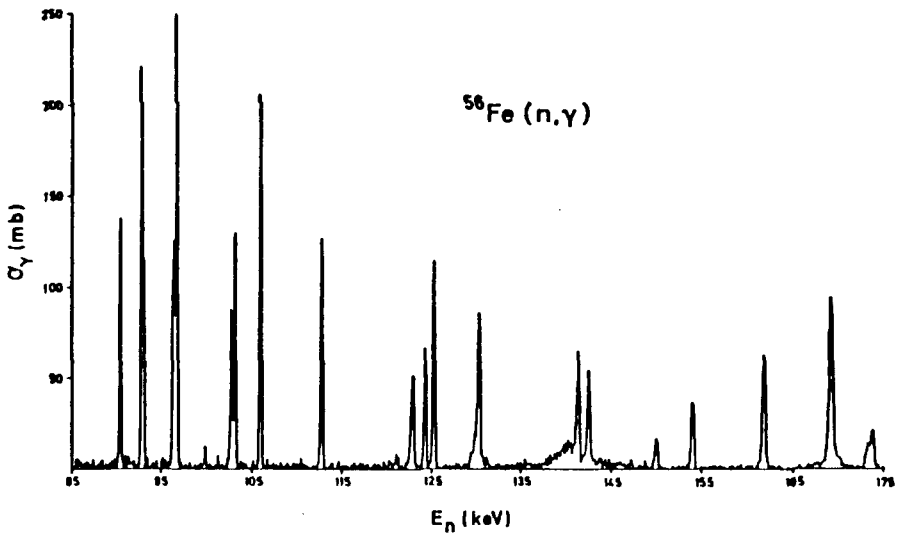

Fig. 3a. The resolution broadened ^{56}Fe capture cross section from 85 to 175 keV.

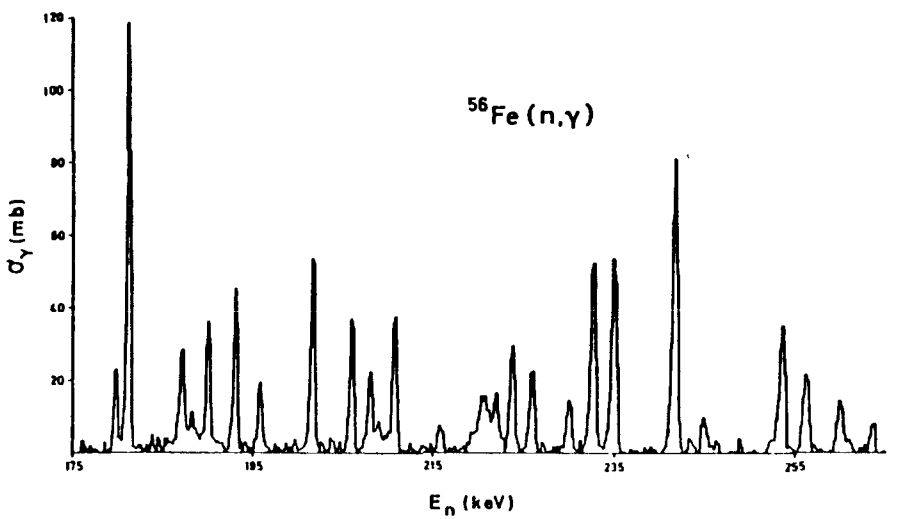

Fig. 3b. The resolution broadened ^{56}Fe capture cross section from 175 to 260 keV.

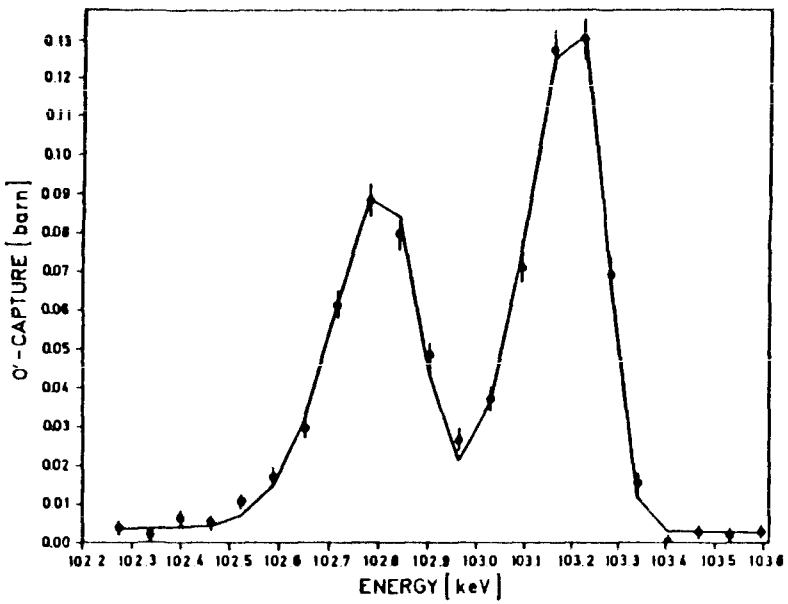

Fig. 4. Example of fit of the 102.8-103.2 keV doublet using an asymmetric resolution function.

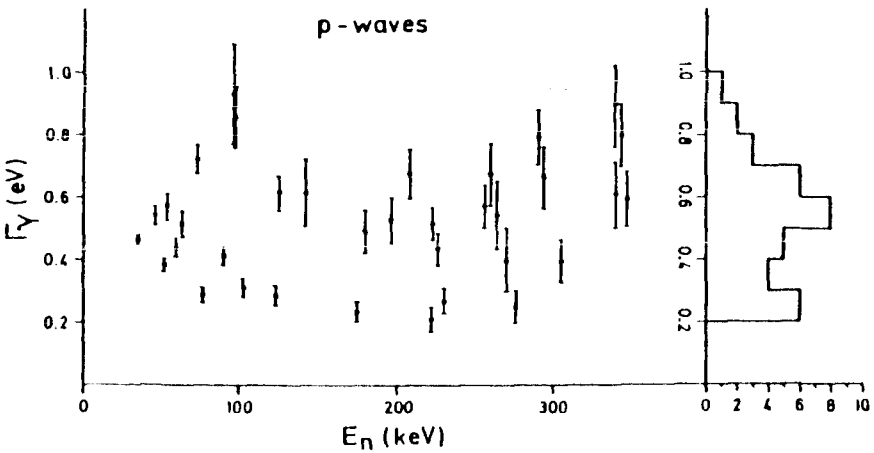

Fig. 5. Plot of Γ_γ values of p-wave resonances vs neutron energy. On the right is plotted the cumulative distribution.

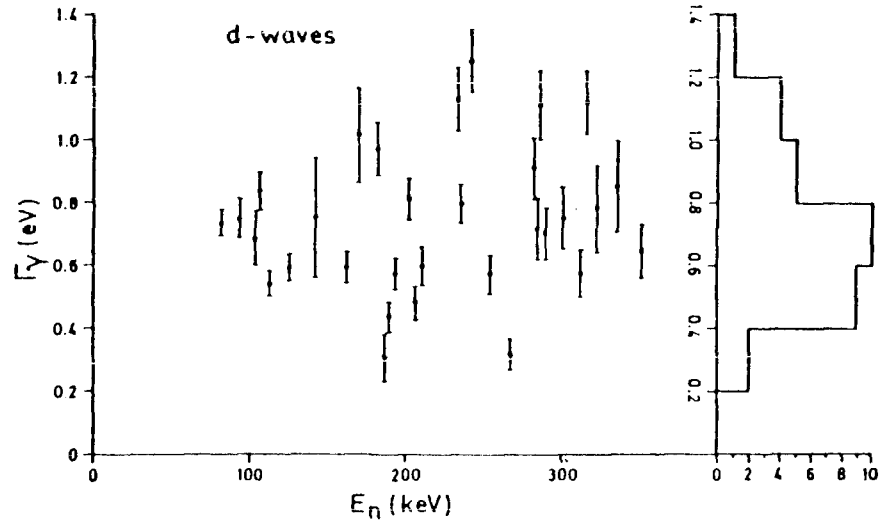

Fig. 6. Plot of Γ_γ values of d-wave resonances vs neutron energy.

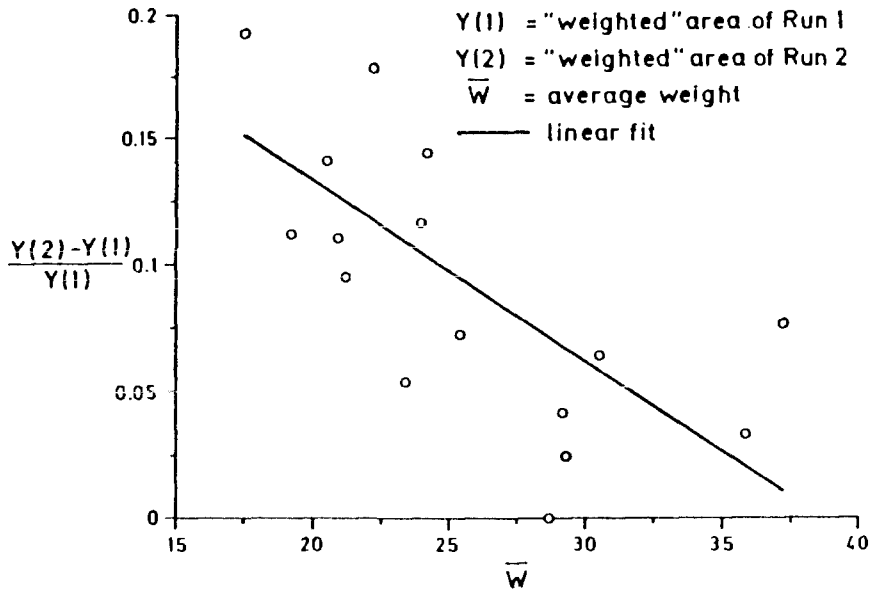

Fig. 7. Relative difference of the resonance yields of Run 2 and Run 1 plotted vs the average weight $\bar{w}$ (old weighting function).

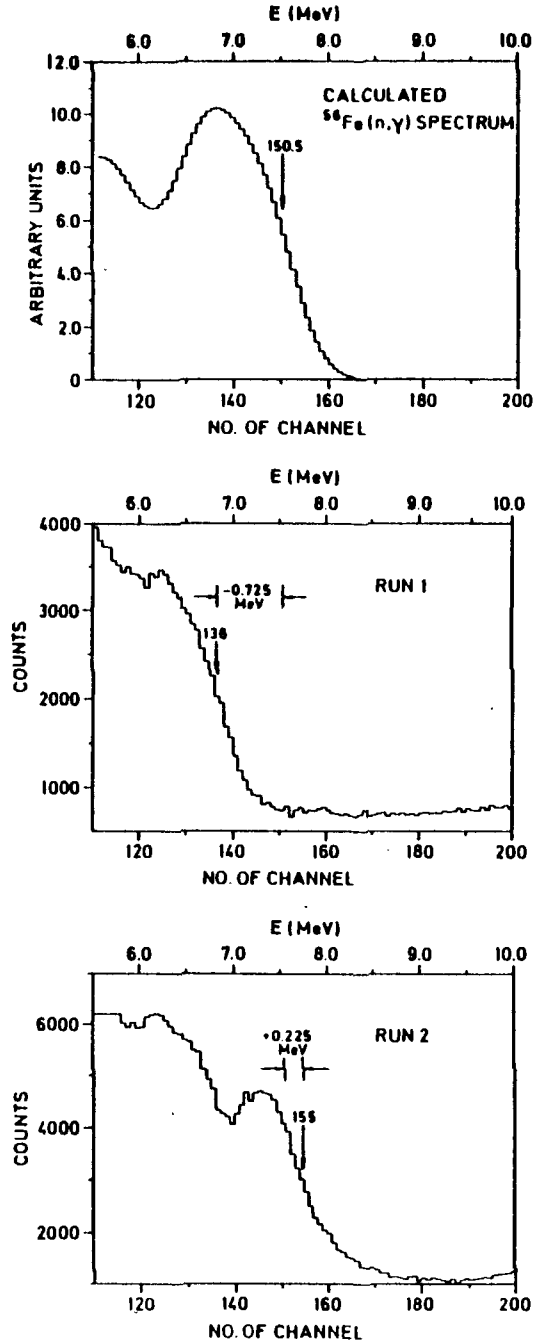

Fig. 8. Comparison of the high energy part of the amplitude spectra of Run 1 and Run 2 with the calculated spectrum.

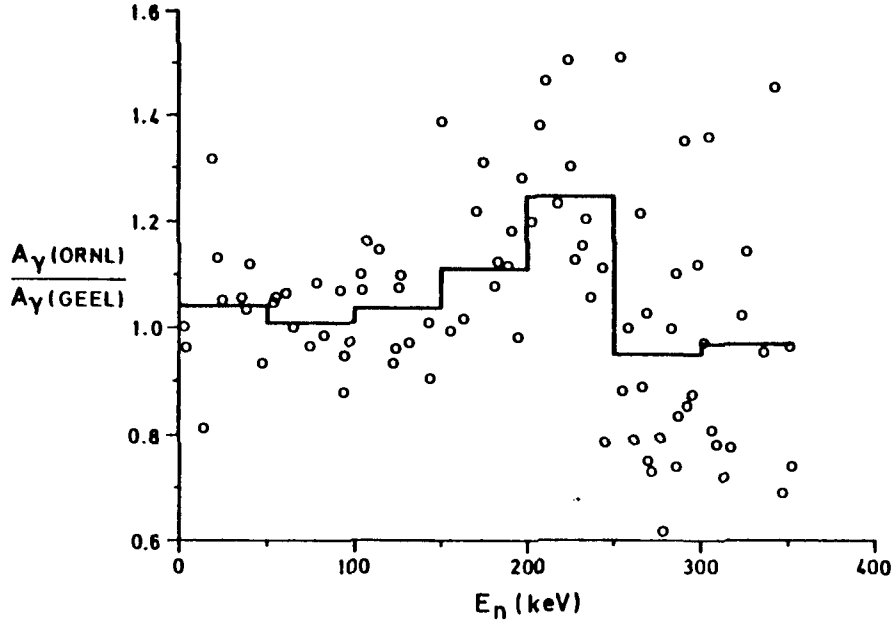

Fig. 9. Ratio of the capture kernels of ORNL and Geel plotted vs energy for p- and d-waves only. The histogram indicates the averages over 50 keV intervals.

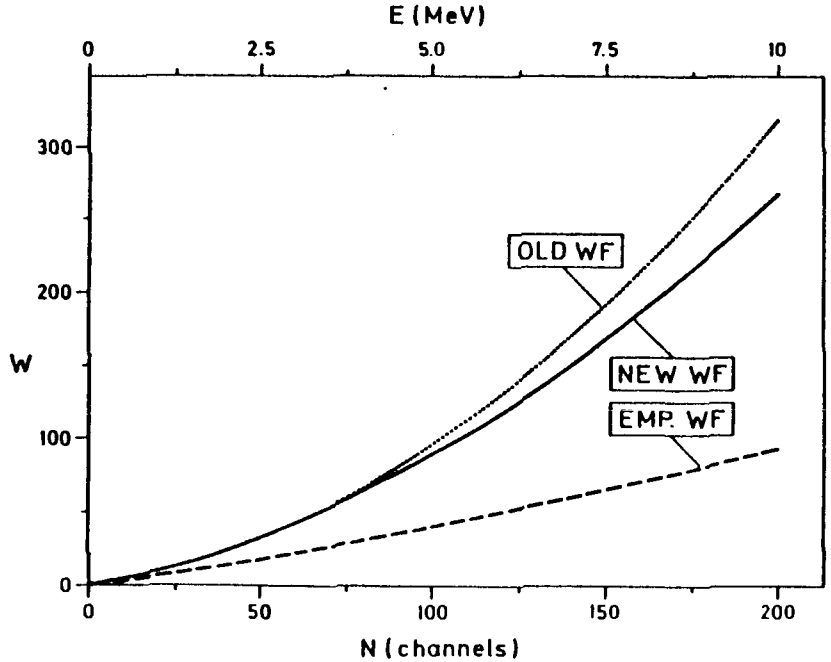

Fig. 10. Plot of three different weighting functions. The energy scale corresponds to 50 keV/channel.

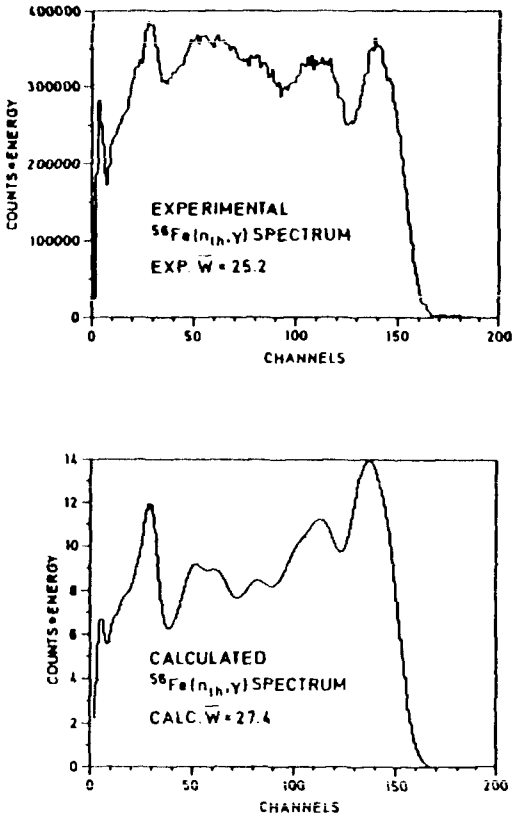

Fig. 11. Comparison of one experimental thermal capture γ-ray spectrum of ^{56}Fe with the calculated one.

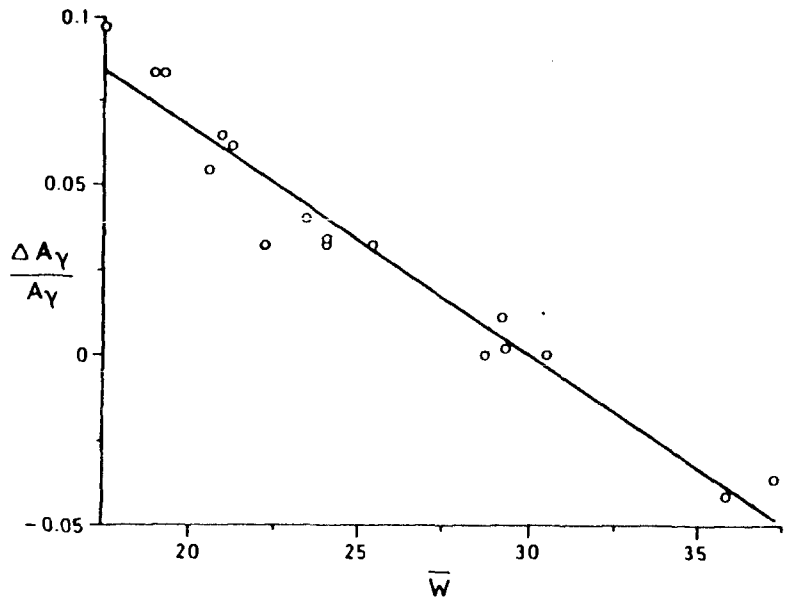

Fig. 12. Relative difference between the kernels obtained using the EMP WF and those obtained with the NEW WF, plotted vs $\bar{w}$.

The 1.15 keV ^{56}Fe Resonance

by

F. G. J. Perey

Oak Ridge National Laboratory, U. S. A.

Paper was not submitted for publication by author.

Neutron Capture in s-Wave Resonances of ^{56}Fe and ^{58,60,64}Ni

K. Wisshak and F. Käppeler

Kernforschungszentrum Karlsruhe, Institut für Kernphysik III

P.O.B. 3640, D-7500 Karlsruhe, Federal Republic of Germany

ABSTRACT

The neutron capture widths of s-wave resonances in ^{56}Fe (27.7 keV), ^{58}Ni (15.4 keV), ^{60}Ni (12.5 keV) and ^{64}Ni (13.9, 33.8 keV), have been determined using a setup completely different from most previous experiments on these isotopes. A pulsed 3-MV Van de Graaff accelerator and a kinematically collimated neutron beam, produced via the ^{7}Li(p,n) reaction, was used in the experiments. Capture gamma-rays were observed by three Moxon-Rae detectors with graphite-, bismuth-graphite-, and bismuth-converters, respectively. The samples were positioned at neutron flight paths of only 6 - 9 cm. Thus events due to capture of resonance scattered neutrons in the detectors or in surrounding materials are completely discriminated by their additional time of flight. The high neutron flux at the sample position allowed the use of very thin samples (0.15 - 0.45 mm), avoiding large multiple scattering corrections. The data obtained with the individual detectors were corrected for the efficiency of the respective converter materials. For that purpose, detailed theoretical calculations of the capture gamma-ray spectra of the measured isotopes and of gold, which was used as a standard, were performed. The final results are Γ_γ(27.7 keV, ^{56}Fe) = 1.06 $\pm$ 0.05 eV, Γ_γ(15.4 keV, ^{58}Ni) = 1.53 $\pm$ 0.10 eV, Γ_γ(12.5 keV, ^{60}Ni) = 2.92 $\pm$ 0.19 eV, Γ_γ(13.9 keV, ^{64}Ni) = 1.01 $\pm$ 0.07 eV and Γ_γ(33.8 keV, ^{64}Ni) = 1.16 $\pm$ 0.08 eV. The accuracy obtained with the present experimental method represents an improvement of a factor 3 - 6 compared to previous experiments. The investigated s-wave resonances contribute 10 - 50 % to the total capture rate of the respective isotopes in a typical fast reactor.

I. INTRODUCTION

The exact determination of the capture widths of broad s-wave resonances in structural materials is an important problem in fast reactor physics because of two reasons: (i) By their large capture area, these resonances contribute significantly to the capture cross section averaged over the reactor spectrum. (ii) In previous measurements their large ratio $\Gamma_n/\Gamma_\gamma \sim 10^3$-$10^4$ caused severe systematic uncertainties due to capture of resonance scattered neutrons. These difficulties are strikingly illustrated at the example of Γ_γ for the 27.7 keV resonance in ^{56}Fe where the published values vary by a factor of two[1]. Recently, a careful reevaluation of the Oak Ridge data [2,3] for ^{58,60}Ni showed that the present accuracy for strong s-wave resonances around $\sim$ 10 keV is limited to $\sim$ 30 % for resonances with $\Gamma_n/\Gamma_\gamma \sim 10^3$. These uncertainties do not meet the requests formulated for capture cross sections of structural materials [4].

Part of the experimental difficulties have been overcome in LINAC experiments by the use of arrangements with very low neutron sensitivity [5,6]. In the present work, which was performed at a Van de Graaff accelerator, a completely different approach was made to solve the problems. Events due to capture of resonance scattered neutrons are discriminated compietely by time-of-flight (TOF). This was possible using an experimental setup where the primary flight path of the neutrons is shorter than the distance from sample to detector. This approach has the additional advantage of a very high neutron flux at the sample position thus allowing for thinner samples than were used in any other capture measurement. In this way sample related uncertainties were greatly reduced, e.g. due to large multiple scattering corrections.

In the present experiment, data were taken simultaneously with three Moxon-Rae detectors which were equipped with graphite, bismuth-graphite and bismuth converters, respectively. The capture width as determined with each of the three detectors was corrected for the efficiency of the respective converter. For this purpose detailed theoretical calculations were performed in the framework of the statistical and spherical optical model to determine the shape of the capture gamma-ray spectra for the investigated isotopes and for gold, which was used as a standard. These spectra together with the shape of the detector efficiencies (evaluated from literature) allowed for a correction of the results which were obtained with the individual detectors. The final values for Γ_γ agreed within the remaining total systematic uncertainty of 5 - 6 %.

We measured the s-wave resonance at 27.7 keV in ^{56}Fe and the resonances at 15.4 and 12.5 keV in ^{58}Ni and ^{60}Ni, respectively. For each isotope three samples were used (0.15, 0.3 and 0.45 mm). It has to be noted that the 0.15 mm sample is nearly a factor of three thinner than the thinnest sample used up to now. The final data have a total uncertainty of 5 - 7 % thus satisfying the current requests [4].

To test the potential of this experimental method we measured the capture widths of two s-wave resonances in ^{64}Ni at 13.9 and 33.8 keV. The final results showed that they have Γ_n/Γ_γ ratios of 2900 and 7700, respectively. For such resonances accurate data can hardly be obtained at a LINAC. But in turn, accurate capture widths of such resonances can be used to check and to improve the neutron sensitivity correction of LINAC experiments. This might help to clarify existing discrepancies for resonances with $\Gamma_n/\Gamma_\gamma \sim 1000$. Due to their large neutron widths (8.9 keV for the resonance at 33.8 keV) these resonances are spread over many TOF channels in an actual experiment and, therefore, it is very hard to obtain a reasonable signal to background ratio. With the very short flight path of 6 cm and with an optimization for further background reduction our setup allowed to detect the 33.8 keV resonance with a signal to background ratio of one in spite of its small peak cross section of only 10 mb. Thus, an overall statistical and systematic uncertainty of 7 % was obtained even

for this extreme case. The present results are documented in detail in Refs. 1,7 and 8.

II. EXPERIMENTS

The experiment is an optimized version of a setup proposed by Macklin et al. [9] already in 1963. A schematic drawing is shown in Fig. 1. The measurements were performed at the Karlsruhe 3-MV pulsed Van de Graaff accelerator. A kinematically collimated neutron beam is produced via the $^{7}Li(p,n)$ reaction by adjusting the proton energy just above the reaction threshold. In this case no further collimation is required and the samples can be placed at a flight path as short as 6 - 9 cm. The capture detectors are arranged at backward angles completely outside the neutron cone. The distance from sample to detector is $\sim$ 16 cm. Data were taken simultaneously from three Moxon-Rae detectors with graphite, bismuth-graphite and pure bismuth converters, respectively. Two ^{6}Li-glass detectors are used to ensure that all samples are irradiated by the same neutron fluence. A TOF-spectrum is recorded from a transmission detector located at 0° with respect to the beam axis and a pulse height spectrum is taken from a neutron monitor at 20°.

In each run: data were taken from the structural material under investigation, from a gold sample as a cross section standard, from a graphite sample as a pure scatterer and from an empty position in the sample changer frame for background determination. Details of the experimental methods, data evaluation and systematic uncertainties are given in Refs. 1, 7 and 8.

The main advantages of this setup are the following:

1.) The distance between samples and detectors is a factor of two larger than the flight path of the primary neutrons. Thus, events due to capture of scattered neutrons in the detector or in surrounding materials are completely discriminated by the additional TOF.

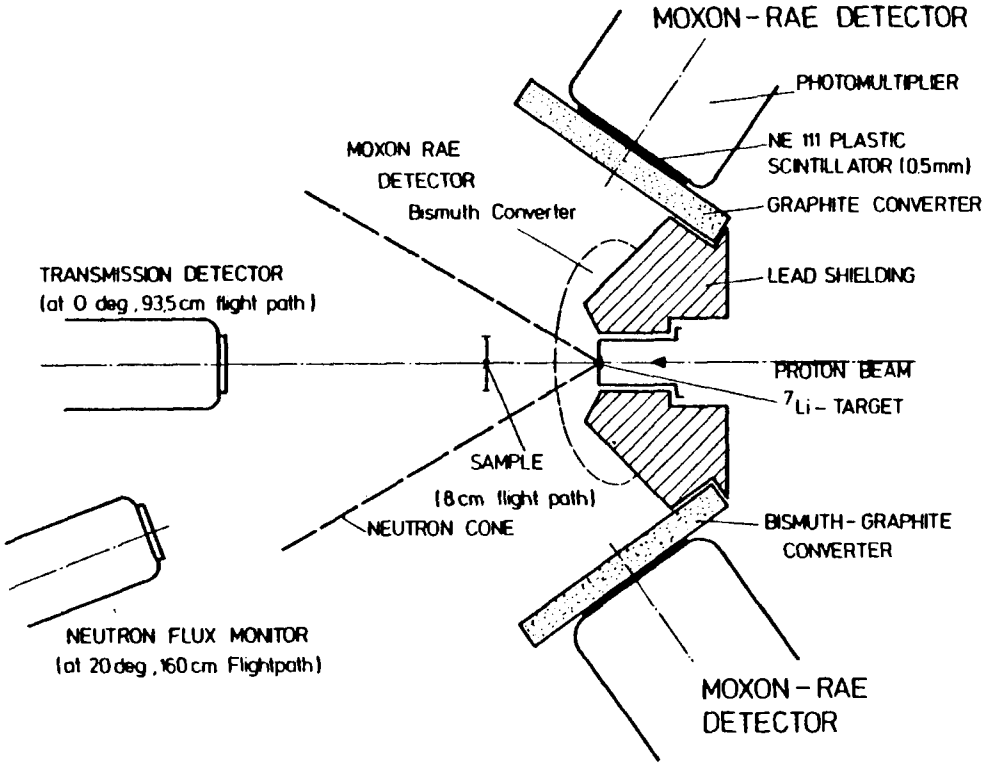

Fig. 1 Schematic view of the experimental setup to measure the capture widths of s-wave resonances in structural materials.

2.) The high neutron flux at the sample position allowed the use of very thin samples (0.15 mm for $^{58,60}Ni$ and ^{56}Fe and 0.5 mm for ^{64}Ni).

3.) The very short flight path of 6 cm allowed for a signal-to-background ratio of $\sim$ 1 even for the very broad resonance at 33.8 keV in ^{64}Ni ($\Gamma_n/E_{res} = 0.26$).

4.) The limited energy range of the neutron spectrum from 10 to 60 keV avoids unwanted background from scattering resonances at higher energies.

5.) The total time resolution of 1.2 ns is sufficient to separate the s-waves from neighbouring p-wave resonances (except for ^{60}Ni).

In order to study the individual systematic uncertainties in detail several runs were made with modified experimental conditions. This is possible only, because the high neutron flux at the sample position reduces significantly the measuring time compared to previous experiments.

The proton energy was adjusted at three different energies (20 keV, 13 keV and 6 keV) above the reaction threshold of the ^{7}Li(p,n) reaction. In this way continuous neutron spectra in the energy range 5 to 90 keV, 7 to 75 keV and 10 to 60 keV were obtained, respectively. The higher proton energy offers a higher neutron flux at the resonance energy but on the dispense of a reduced signal to background ratio.

For each isotope except ^{64}Ni three samples were used with thickness between 0.15 and 0.60 mm. Thus the correction for multiple scattering in the investigated s-wave resonances vary by a factor of three. For ^{56}Fe as an additional check a 2 mm thick sample was used, to demonstrate that the multiple scattering correction of the present analysis works correctly even in such extreme cases. This point was mainly motivated by the experiment of Allen et al. [10] where a similar technique was used but where a discrepant result was obtained with a sample of 2.4 mm thickness. To demonstrate the effect-to-background ratio Fig. 2 shows the TOF spectra measured with the graphite converter and ^{58,60}Ni samples of 0.3 mm thickness. In Fig. 3 the respective spectra as measured with the ^{64}Ni sample of 0.46 mm thickness are shown.

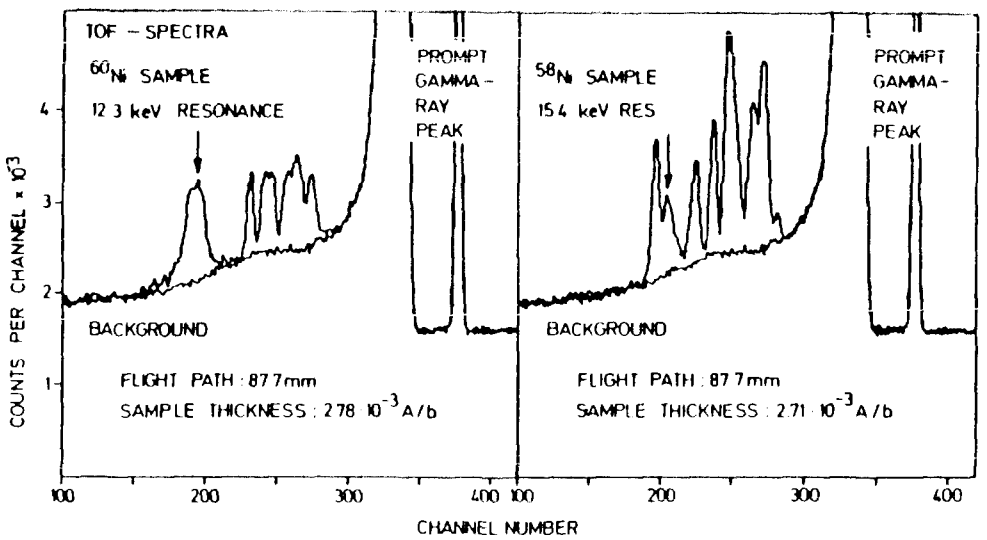

Fig. 2 TOF spectra of ^{58,60}Ni samples and the corresponding background as measured with the Moxon Rae detector with graphite converter (sample thickness 0.3 mm, flight path 87.8 mm).

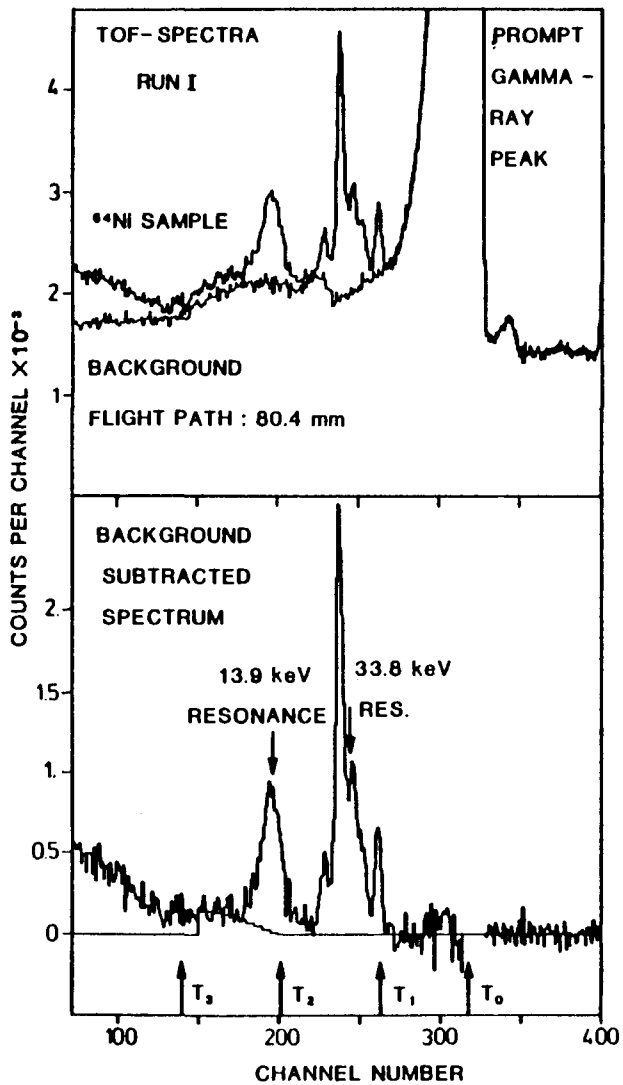

Fig. 3 Experimental TOF spectra measured with the ^{64}Ni sample and with an empty position in the sample changer frame (background). The background subtracted spectrum shows the residual background due to capture of scattered neutrons caused by the resonance at 33.8 keV (Γ_n/Γ_γ = 7700). This component was subtracted in the region of the 13.9 keV resonance as indicated by the histogramm (lower part). Four time marks are given which illustrate the TOF discrimination of events due to capture of scattered neutrons.

T_o: Position of prompt gamma-ray peak, which corresponds to the zero point of the TOF scale.

T_1: First neutrons are scattered in the 33.8 keV resonance.

$T_2 = 2 \times T_1$: First of these scattered neutrons reach again the neutron target.

T_3: First of these scattered neutrons reach the detectors or the sample changer frame.

III. DATA ANALYSIS

The data analysis is described in detail in Refs. 1,7 and 8, therefore we enumerate only briefly the individual steps performed.

III.A Evaluation of the Capture Yield

The capture yield was evaluated from the measured TOF spectra in the following way:

a) Transformation of the individual TOF spectra of each sample (measuring time ∿ 10 min) to a common position of the prompt gamma ray peak.

b) Transformation of the summed TOF spectra of sample and reference sample to a common average flight path.

c) Normalization to equal neutron fluence per sample.

d) Subtraction of time dependent and time independent background.

e) Correction for multiple scattering and self-shielding in the gold reference sample.

f) Correction for gamma ray self-absorption in sample and reference sample.

g) Multiplication with the gold standard cross section.

III.B Determination of the Capture Widths

To determine the capture widths of s-wave resonances the capture yield was analyzed using the FANAC code of Fröhner[11]. The data measured with three different converter materials were analyzed separately. The parameters of the p-wave resonances as well as the resonance parameters of isotopic impurities were taken as fixed input from literature. The analysis was performed twice, taking Γ_n of the investigated s-wave resonances as free or as fixed parameter. Fig. 4 shows as an example the Fanac fits to the capture yield of ^{58,60,64}Ni as evaluated from the spectra given in Figs. 2 and 3.

III C Correction for Detector Efficiency

The main systematic uncertainty in our measurements on structural material isotopes relative to a gold standard is caused by the efficiency of the Moxon-Rae detectors. It deviates from the ideal shape, which is linearly increasing with gamma-ray energy. Neutron capture in structural materials is characterized by a low multiplicity of the associated gamma-ray cascades. Consequently, the capture gamma-ray spectrum is dominated by a hard component caused by transitions to the ground state or the first excited levels and by a soft component from the ground state decay of these low lying states. On the other hand, the high level density in gold yields a higher multiplicity of the cascades and thus a softer spectrum. This difference leads to a systematic uncertainty in the measured cross section ratio. In the present experiment data were taken with three different converter materials and the correction was applied for each detector separately. In this way we tried to overcome the uncertainty which is caused by the fact that the efficiency of the individual converter materials is not known with good accuracy.

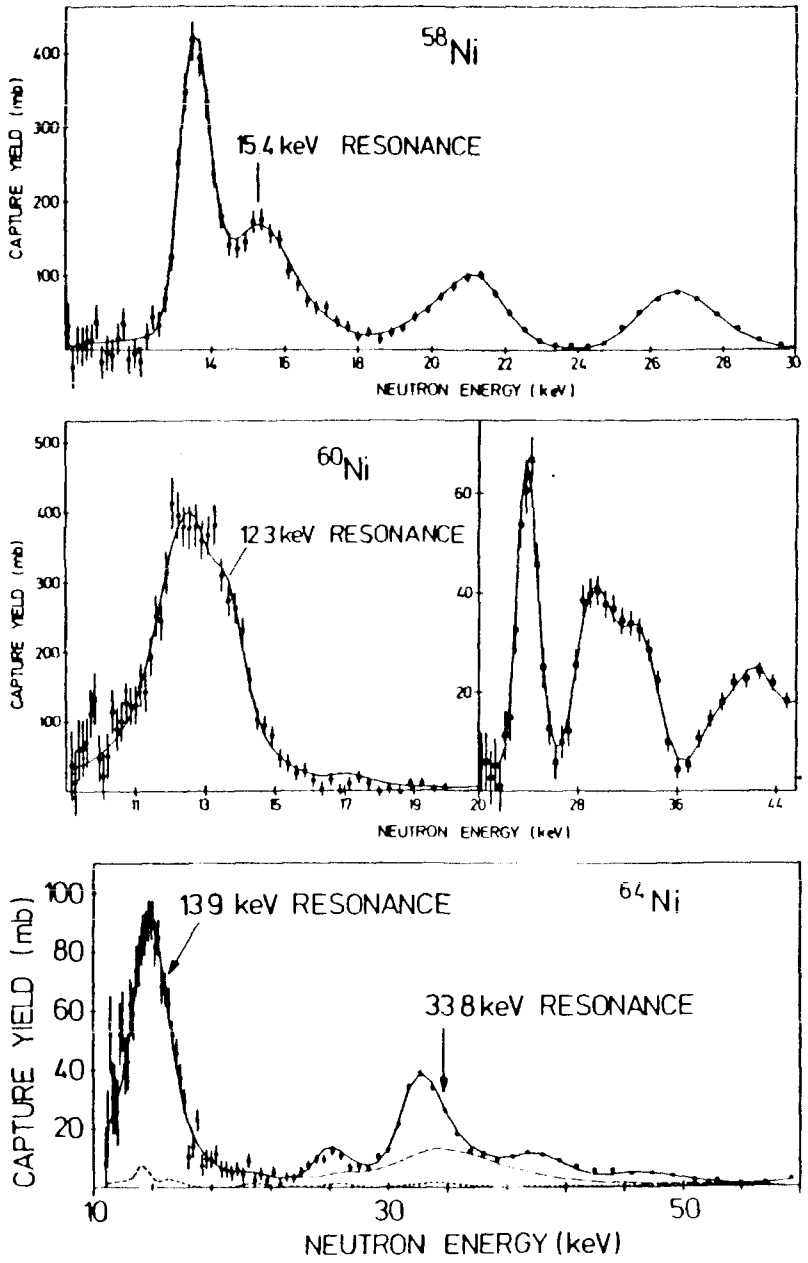

Fig. 4 Fanac fits to the capture yield of ^{58}Ni, ^{60}Ni and ^{64}Ni as evaluated from the TOF spectra shown in Figs. 2 and 3.

The evaluation of the efficiency correction, is described in detail in Ref. 12. Two pieces of information are required: the relative shape of the detector efficiency $\varepsilon(E_\gamma)$ and the relative shape of the capture gamma-ray spectrum $I(E_\gamma)$.

In Fig. 5 the efficiency of the individual converter materials is displayed. Two possible shapes for the graphite converter were used, one as evaluated from experimental data in Ref. 1 and the other as calculated by Malik and Majkrzak [13]. The efficiency of the bismuth-graphite detector was taken from Ref. 9. For the bismuth converter we used the average of the calculation in Ref. 13 and the Monte Carlo simulation by Iyengar et al.[14].

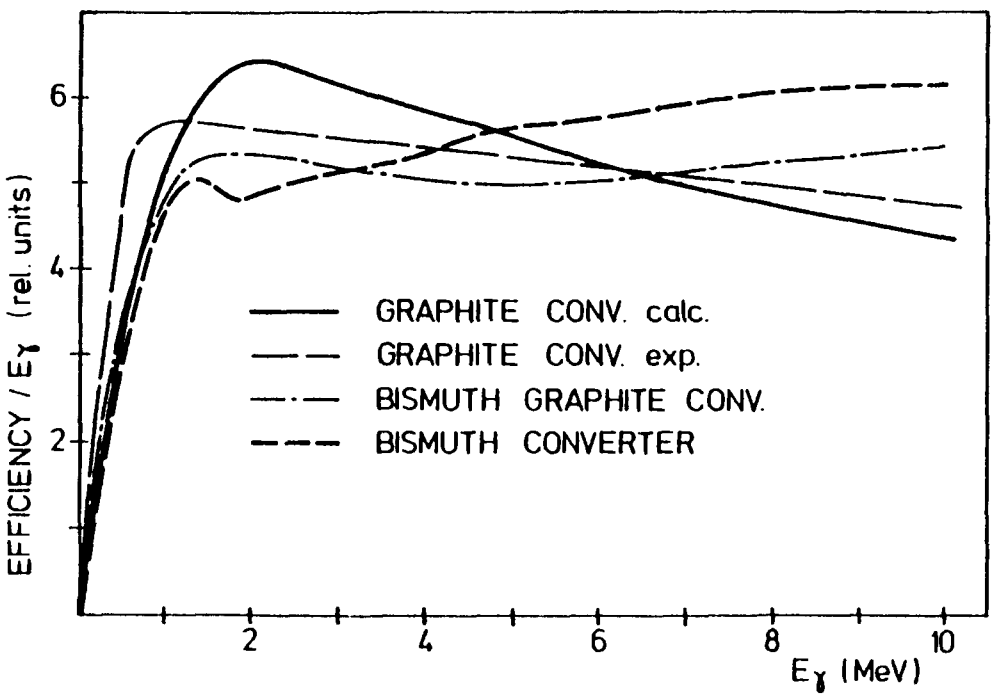

Fig. 5 The shape of the detector efficiency of Moxon Rae detectors with different converter materials.

The capture gamma-ray spectra were calculated in the framework of the statistical model and the spherical optical model. The method is described in Ref. 15 where the results for gold are already published. Details of the calculations for the structural materials are given in Refs. 7, 8 and 16. These calculations have been performed for s-, p- and d-wave resonances and for all possible spin values, separately. As for the narrow p- and d-wave resonances in many cases the spin and even the parity is unknown and as for a given orbital angular momentum the correction factors are not strongly spin-dependent, only averaged values for p- and d-wave resonances have been used for correction. The correction is $\sim$ 5 % for measurements on ^{56}Fe and ^{64}Ni while they increase up to 10 % for measurements on ^{58}Ni and ^{60}Ni.

IV RESULTS

The individual results for the capture widths of s-wave resonances in ^{56}Fe and ^{58,60,64}Ni as obtained from different experimental runs, sample thickness, converter materials and evaluation methods are compiled in full detail in Refs.7 and 8. The fact that no systematic differences are observed in the results of one detector in the individual runs confirms that the effects of sample thickness and neutron spectrum are accounted for correctly. Therefore, in further evaluation averages over all runs are used.

In Table I the final data are given. The correction for detector efficiency strongly reduced the spread in the data obtained with different detectors which now agree within their remaining statistical and systematic uncertainty. There is an indication that the data obtained with the bismuth graphite converter are systematically higher than the results of the two other detectors. The most probable explanation is the uncertainty in the shape of the efficiency curve for this detector. However, these differences can be tolerated in view of the systematic uncertainty of the efficiency correction.

In the last columns of Table I the final values for the capture widths of the investigated s-wave resonances are given together with their statistical and systematic uncertainties. These values are obtained as an average of the results from the individual detectors. In case of ^{60}Ni the contribution of the two p-wave resonances at 12.2 and 13.6 keV is subtracted because it could not be separated in the fits. The individual systematic uncertainties are discussed in detail in Refs. 7 and 8. For completeness we include in Table I the result for ^{56}Fe obtained in our first experiment where we used three different sample thicknesses but only one Moxon-Rae detector (with graphite converter, Ref. 1). In Ref. 1 a correction for detector efficiency was not applied as no reliable capture gamma-ray spectra were available at that time. The value given in Table I is now corrected and thus supersedes the earlier results.

^{58}Ni: The final value Γ_γ = 1.53 eV ± 6.6 % for the s-wave resonance at 15.35 keV is in good agreement with the data of Fröhner[17] and with the KEDAK-3 evaluation[18] but is lower by ∿ 35 % than the data given in Refs.19 and 20. However, the results of Ref. 20 were not yet properly corrected for neutron sensitivity. A re-evaluation of these data at Oak Ridge [3] yielded a preliminary value of Γ_γ = 1.3 ± 0.4 eV in agreement with our value. But it has to be pointed out that the neutron sensitivity of the respective

Table I Final Results for the s-Wave Resonances in ^{58,60,64}Ni and ^{56}Fe

Isotope	Resonance Energy	Graphite Converter	Bismuth-Graphite Converter	Bismuth Converter	Average	Uncertainty (%)		
		Γ_γ(eV)	Γ_γ(eV)	Γ_γ(eV)	Γ_γ(eV)	statistical	systematic	total
^{58}Ni	15.35	1.41	1.63	1.56	1.53	1.9	6.3	6.6
^{60}Ni[a]	12.5	2.88	3.07	2.88	2.92	3.5	5.6	6.6
^{64}Ni	13.9	0.97	1.01	1.01	1.01	3.7	5.7	6.8
	33.8	1.24	1.18	1.06	1.16	3.4	6.2	7.1
^{56}Fe	27.7	1.07	1.14	1.06	1.09	2.1	4.6	5.1
corrected results form Ref. 1:								
^{56}Fe	27.7	1.05			1.05	1.3	4.7	4.9
averaged value form Ref. 1 and present work								
^{56}Fe	27.7				1.06	1.1	4.7	4.8

a) a value $g\Gamma_\gamma\Gamma_n/\Gamma$ = 0.56 has been subtracted from the fitted resonance area to account for the unresolved p-wave resonances at 12.2 and 13.6 keV

experimental setup limits the accuracy of this resonance parameter to ∿ 15 % in the tank measurement performed at KfK (Ref. 17) and to ∿ 30 % in the measurement with the C_6F_6 detector at Oak Ridge (Refs. 3 and 20). Compared to that the present method provides a significant improvement.

^{60}Ni: For this isotope the two weak p-wave resonances at 12.2 and 13.6 keV could not be resolved from the area of the s-wave resonance. Therefore, always the sum of the three resonances was analyzed. To obtain the final value for the capture width of the s-wave resonance the value $g\Gamma_\gamma\Gamma_n/\Gamma$ = 0.56 eV of Ref.17 was subtracted from the observed area. This value is in very good agreement with the recent results of Perey et al.[2] who quote $g\Gamma_\gamma\Gamma_n/\Gamma$ = 0.554 eV. Our final value for the s-wave resonance Γ_γ = 2.92 eV ± 6.6 % is in good agreement with data of Fröhner[17], with the KEDAK-3 evaluation [18] and with the new results from Oak Ridge [2]. But, again, these data carry uncertainties of 18 % and 34 %, respectively. The value in Ref. 19 which is based on the work of Stieglitz et al. [21] is ∿ 15 % larger than the present value.

^{64}Ni: The final values are: Γ_γ = 1.01 ± 0.07 eV for the resonance at 13.9 keV and Γ_γ = 1.16 ± 0.08 eV for the resonance at 33.8 keV. If we compare the present results to the data of Beer and Spencer [22] one has to keep in mind that these data were not corrected for the neutron sensitivity of the liquid scitillator tank. This correction can be applied according to Ref. 17 yielding Γ_γ = 1.6 eV for both resonances which is still significantly larger than the present values. The difference may be accounted for by the 20 % uncertainty quoted by Beer and Spencer[22] to which an additional uncertainty of the neutron sensitivity correction has to be added. Preliminary results from a measurement performed at Oak Ridge at a 20 m flight path yielded even higher values for these radiative widths[23]. This suggests that the neutron sensitivity corrections were underestimated in both cases. The present results yield new values Γ_n/Γ_γ of 2900 and 7740 for the resonances at 13.9 and 33.8 keV, respectively. This means that this ratio is nearly one order of magnitude larger for the resonance at 33.8 keV than for the investigated s-wave resonances in ^{56}Fe and ^{58,60}Ni.

^{56}Fe: Even with the limited resolution of the present experiment, this resonance is undisturbed by any p-wave contribution. The final result for the 27.7 keV s-wave resonance (see Table I) agrees very well with our extensive measurements published already in Ref. 1, if properly corrected for the detector efficiency. Thus our measurements with Moxon Rae detectors yielded a consistent final value of Γ_γ = 1.06 ± 0.05 eV for this resonance using samples which differ by more than a factor of 10 in thickness. This is an impressive confirmation of the multiple scattering correction of the FANAC code. There is also excellent agreement with the value Γ_γ = 1.04 ± 0.08 eV obtained recently at Karlsruhe [24] in a measurement using C_6D_6 detectors and a flight path of 60 cm. The present value is significantly lower than all results published before 1980 (Refs. 25 to 27), except the results of Fröhner [17] (Γ_γ = 1.25 ± 0.2 eV) and Gayther et al. [5,28] (Γ_γ = 0.89 eV). We also agree with the result from a measurement at Geel [6], which was analysed by Moxon using the REFIT code [29] (Γ_γ = 1.0). Recently, a new measurement was published [30] which yielded a significantly lower value Γ_γ = 0.82. This result is correlated with a surprisingly low value for the neutron width of this resonance (Γ_n = 1.15 keV). Low values for Γ_γ are also reported by Allen et al. [10] (Γ_γ = 0.82 ± 0.11 eV).

VI FAST REACTOR SPECTRUM AVERAGED CROSS SECTIONS

To study the influence and importance of the present results for an actual reactor we chose the core design studies for the SNR-2 power reactor by Kiefhaber [31]. For the purpose of the intended comparison a one dimensional representation seemed sufficient, assuming a constant neutron flux for the whole core, grouped into 26 energy bins. About 12 % of the total capture rate is due to capture in structural materials. The bulk of this

rate is due to capture in iron (50 %) and nickel (22 %), while the rest is caused by chromium, molybdenum and niobium. In all involved materials neutron capture proceeds via the (n,γ)-reaction with the exception of nickel where one third of the capture events is attributed to the (n,p) reaction because of the low threshold energy.

In each energy group an average capture cross section was determined by lumping together the resonance areas of the individual resonances: Here we used the data from KEDAK 3 (Ref. 18) for ^{56}Fe and ^{58}Ni, from Ref. 2 for ^{60}Ni and from Ref. 32 for ^{64}Ni and our own values for the s-wave resonances. Above 200 keV smoothed cross sections were taken from Ref. 33. These cross sections were weighted with the neutron flux of the respective group. This procedure was performed twice, with and without the measured s-wave resonance. The resulting contributions of the s-wave resonances to the local capture rate of the respective isotopes are given in Table II in comparison to the values obtained with the s-wave resonance parameters quoted by Mughabghab et al. (Ref. 19). From this Table the following conclusions can be drawn:

1.) About 9 % of the total capture rate in structural materials is caused by the three investigated resonances.

2.) Using the present data the capture rate in structural materials is reduced by more than 2 %.

3.) With the improved accuracy of ∿ 5 - 6 % of the present experiment the uncertainty in capture rate of structural materials is not longer dominated by the uncertainty of the s-wave resonances. The main uncertainty is now determined by the 1.15 keV resonance in ^{56}Fe, which contributes ∿ 35 % to the capture rate in ^{56}Fe.

4.) Finally, one has to keep in mind that all other s-wave resonances as measured in previous experiments have been overestimated, too. If this is corrected a further reduction of the capture rate in structural materials is expected.

Table II Contribution of the Investigated s-Wave Resonances to Fast Reactor Averaged Neutron Capture Cross Sections

Resonance	Relative Contribution to Total Capture Rate of the Respective Isotope (%)		Relative Contribution to Total Capture Rate of All Structural Materials (%)	
	Γ_γ taken from Ref. 19	Γ_γ from present results	Γ_γ taken from Ref. 19	Γ_γ from present results
^{56}Fe (27.7 keV)	11	8	5.1	3.7
^{58}Ni (15.4 keV)	20	16	2.0	1.6
^{60}Ni (12.5 keV)	46	37	1.8	1.4
^{64}Ni (13.9 and 33.8 keV)	70	52	-	-

REFERENCES

1.) K. WISSHAK and F. KÄPPELER, Nucl. Sci. Eng. 77, 58 (1981)

2.) C.M. PEREY, J.A. HARVEY, R.L. MACKLIN, R. R. WINTERS, and F.G. PEREY, Phys. Rev. C 27, 2556 (1983)

3.) C. M. PEREY, Private Communications 1982

4.) N. DAYDAY, Ed. "World Request List for Nuclear Data", INDC (SEC) - 78 / URSF International Atomic Energy Agency, Vienna 1981

5.) D.B. GAYTHER, B.W. THOMAS, B. THOM, and M.C. MOXON, Proc. Specialists' Meeting Neutron Data of Structural Materials for Fast Reactors, Geel, Belgium, December 5-8, 1977, Pergamon Press, Oxford (1979) p. 547

6.) A. BRUSEGAN, F.CORVI, G. ROHR, R. SHELLY, and T. VAN DER VEEN, Proc. Conf. Nuclear Cross Sections and Technology, Knoxville, Tenn., October 22-26, 1979, NBS Spec. Publ. 594, National Bureau of Standards.

7.) K. WISSHAK, F. KÄPPELER, G. REFFO, and F. FABBRI "Neutron Capture in s-Wave Resonances of ^{56}Fe, ^{58}Ni and ^{60}Ni", KfK 3516, Kernforschungszentrum Karlsruhe and accepted for publication in Nucl. Sci. Eng.

8.) K. WISSHAK, F. KÄPPELER, R.L. MACKLIN, G. REFFO, F. FABBRI, "Neutorn Capture in s-Wave Resonances of ^{64}Ni", KfK 3582, Kernforschungszentrum Karlsruhe and submitted for publication to Nucl. Sci. Eng.

9.) R.L. MACKLIN, J.H. GIBBONS, and T. INADA Nucl. Phys. 43, 353 (1963)

10.) B.J. ALLEN, D.D. COHEN, and F.Z. COMPANY, J. Physics G: Nucl. Phys. 6, 1173 (1980)

11.) F.H. FRÖHNER, "FANAC - A Shape Analysis Program for Resonance Parameter Extraction from Neutron Capture Data for Light- and Medium Weight Nuclei", KfK-2145, Kernforschungszentrum Karlsruhe (1977)

12.) G. REFFO, F. FABBRI, K. WISSHAK, and F. KÄPPELER Nucl. Sci. Eng. 83, 401 (1983)

13.) S.S. MALIK and C. F. MAJKRZAK, Nucl. Instr. Methods 130, 443 (1975)

14.) K.V.K. IYENGAR, B.LAL and M.L. JHINGAN Nucl. Instr. and Methods 121, 33 (1974)

15.) G. REFFO, F. FABBRI, K. WISSHAK, and F. KÄPPELER, Nucl. Sci. Eng. 80 630 (1982)

16.) G. REFFO contribution to this meeting

17.) F.H. FRÖHNER, Proc. of a Specialists Meeting on Neutron Data of Structural Materials for Fast Reactors, Geel 5-8 December 1977, Pergamon Press Oxford (1979) p. 138

18.) F.H. FRÖHNER, KEDAK - 3 evaluation 1977-79, unpublished

19.) S.F. MUGHABGHAB, M. DIVADEENAM, and N.E. HOLDEN, Neutron Cross Sections Vol. I Neutron Resonance Parameters and Thermal Cross Sections Part A, Academic Press New York 1981

20.) F.G. PEREY, G.T. CHAPMAN, W.E. KINNEY and C.M. PEREY, Proc. of a Specialists Meeting on Neutron Data of Structural Materials for Fast Reactors, Geel 5-8 December 1977, Pergamon Press Oxford (1979) p. 530

21.) R.G. STIEGLITZ, R.W. HOCKENBURY and R.C. BLOCK, Nucl. Phys. A163, 592 (1971)

22.) H. BEER and R.R. SPENCER, Nucl. Phys. A 240, 29 (1975)

23.) R.L. MACKLIN, private communication

24.) F. KÄPPELER, K. WISSHAK, and L.D. HONG, Nucl. Sci. Eng. 84, 234 (1983)

25.) R.L. MACKLIN, P.J. PASMA, and J.H. GIBBONS, Phys. Rev. 136, 695 (1964)

26.) R.W. HOCKENBURY, Z.M. BARTOLOME, J.R. TATARCZUK, W.R. MOYER, and R.C. BLOCK, Phys. Rev. 178, 1746 (1969)

27.) B.J. ALLEN, A.R. de L. MUSGROVE, J.W. BOLDEMAN, and M.J. KENNY, Nucl. Phys. A 269, 408 (1976).

28.) D.B. GAYTHER, M.C. MOXON, R.B. THOM, and J.E. JOLLY, "U.K. Nuclear Data Progress Report 1979", UKNDC (80), P. 96, NEANDC (E) 212, Vol. 8, United Kingdom Atomic Energy Authority Harwell 1980

29.) M.C. MOXON, "Nuclear Physics Division Progress Report 1980", AERE-PR/NP 28 United Kingdom Atomic Energy Authority Harwell 1981

30.) F. CORVI, A. BRUSEGAN, R. BUYL, G. ROHR, R. SHELLEY and T. VAN DER VEEN, Proc. Int. Conf. on Nuclear Data for Science and Technology, Antwerp 6-10 September 1982

31.) E. KIEFHABER, private communications 1983

32.) R.R. SPENCER and R.L. MACKLIN, private communications 1982

33.) C.LE. RIGOLEUR, A. ARNAUD, and J. TASTE, Mesures en Valeur Absolue des Sections Efficases de Capture Radiative des Neutrons par le ^{23}Na, Cr, ^{55}Mn,Fe,Ni, ^{103}Rh, Ta, ^{197}Au, ^{238}U dans le Domaine de 10 à 600 keV", CEA-R-4782 Commissariat à l'Energie Atomique 1976

MODEL CALCULATIONS OF DOUBLE-DIFFERENTIAL CROSS SECTIONS

H. Gruppelaar

Netherlands Energy Research Foundation ECN, P.O.Box 1,
1755 ZG Petten, The Netherlands

ABSTRACT

A survey is given of recent developments in the calculation of angular distributions based upon the generalized master-equation approach of the exciton model. Some comments are also made on the relation between the exciton model and the Hauser-Feshbach model.

INTRODUCTION

The underlying naive picture of the model that is used to calculate double-differential cross sections of (n,n') or (n,p) reactions at energies from about 10 to 50 MeV is as follows. A neutron enters the nucleus with a probability predicted by the reaction cross section of the optical model. After a refraction at the nuclear surface it may collide with a target nucleon. The initial neutron generally looses energy which is transferred to the target nucleon. Next, one of the collission partners may be emitted or further collissions may take place until eventually a particle is emitted. It is assumed that before emission a refraction at the nuclear surface has occured. Secondary emission of a particle is described by following the collissions inside the nucleus also after the first emission.

In three cases this picture leads to simple models:
(a) equilibrium limit, (b) precompound emission after the first internal collission, (c) "leading particle" model.

In the well-known *equilibrium limit* it is supposed that no particle is emitted before a large number of collissions has occurred and the initial energy of the projectile has been exchanged with most of the target nucleons. The decay of this "compound state" is described by a statistical model. The Hauser-Feshbach (HF) model is usually employed, although at high energies it could be approximated by the much simpler Weiskopf-Ewing (WE) model, where a summation over spins and parities has been made. Some inconsistency problems between HF and WE models have been discussed in Refs. [1,2]. We note that the HF model also predicts angular distributions, although for continuum emission usually isotropy in the center-of-mass system is assumed. A useful approximation to estimate the (symmetric) angular distribution of continuum reactions has been given by Ericson and Strutinsky [3]. The complete expression is found in Ref. [4].

When emission occurs *after the first collission*, it is still relatively simple to describe the angle and energy distributions of the emitted particle, assuming geometrical optics for the refraction processes and the Kikuchi-Kawai (KK) expression for the scattering of two

nucleons inside nuclear matter [5]. Since an important fraction of the precompound emission originates from a single collission in the nucleus, this description could be quite useful. It is the basis of a model recently developed at our laboratory [6]. There is a distinct forward-peaked angular distribution and there is a strong coupling between energy and angle of the emitted particles, cf. Sect. 2.

In the *"leading particle"* model, developed by Mantzouranis et al. [7] there is one "fast" particle (the projectile) that is followed on its way through the nucleus. After each collission the direction of the followed particle is changed according to the angular distribution of the free nucleon-nucleon scattering cross section that is assumed to be isotropic in the center-of-mass system of the two colliding particles. This assumption leads to the so-called "generalized" master equation, that is solved most easily by the method of Akkermans [8,9]. We note that in this model the angular distribution of the emitted particle after n collissions is independent of its energy. Recently, this model has been refined by various authors [10,11] and a combination with the above-mentioned model to describe the emission after the first internal collission has been made [6], cf. Sect. 3.

The remaining problem is to assure that the equilibrium limit of the above-mentioned exciton model (EM) agrees with the HF model, both with regard to the angular distribution (cf. Sect. 4) and the angle-integrated cross section (cf. Sect. 5). This problem has also been discussed in Ref. [2].

2. PRECOMPOUND EMISSION AFTER FIRST COLLISSION

When a nucleon is emitted after the first intra-nuclear collission, its angular distribution will be a folding of three angular distribution functions corresponding with incident refraction, intra-nuclear scattering and outgoing refraction. This "folding" is most easily performed with the mathematical description of Akkermans et al. [8,9], where the angular distribution is represented by Legendre polynomial coefficients. It follows from Ref. [6] that

$$\left(\frac{d^2\sigma(a,b)}{d\varepsilon d\Omega}\right)_{n_o} = \sigma_a\, w_b(n_o,\varepsilon)\tau(n_o) \sum_\ell \frac{2\ell+1}{4\pi}\, \rho_\ell(E)\mu_\ell^{KK}(\varepsilon)\rho_\ell(\varepsilon)P_\ell(\cos\theta), \qquad (1)$$

where ρ_ℓ are eigenvalues of the refraction operator (based upon geometrical optics) and μ_ℓ^{KK} are eigenvalues of the scattering operator (based upon the KK expression). For $\ell=0$ the eigenvalues are equal to unity and the expression reduces to the well-known angle-integrated cross section of the exciton model for emission from the initial exciton state ($n_o=3$), divided by a factor 4π. In Eq. (1) the emission rate for emission of a particle b from $n=n_o$ to $n=n_o-n_b$ is indicated by $w_b(n_o,\varepsilon)$; the *mean life time* $\tau(n_o)$ equals in this case the reciprocal value of the total emission $W(n_o)$.

From Eq. (1) it follows that the model is free from fit parameters and that there is a strong correlation between the angle- and energy distributions. It is illustrative to note that in most earlier work, corresponding to the concept of Mantzouranis et al. [7] the coefficients ρ_ℓ were not used ($\rho_\ell=1$), and the scattering kernel was taken from free nucleon-nucleon scattering: μ_ℓ^F, independent of ε. In a previous analysis of 14-MeV data we have assumed (in Ref. [9]) a *maximum* refraction index of the incident beam (i.e. $\rho_\ell(E)=\mu_\ell^F$), together with the free scattering coefficient μ_ℓ^F. In addition, a fit parameter c_ℓ was used to obtain optimal agreement with the measured data [9,12].

More recently, Sun Ziyang et al. [10] have adopted a Kikuchi-Kawai kernel, averaged over all possible scattering energies: $\bar{\mu}_\ell^{KK}$, i.e. independent of ε. In a very recent paper Iwamoto et al. [11] have used an expression, similar to Eq. (1), neglecting refraction, cf. Sect. 3.

Without considering the contributions from further internal collissions, Eq. (1) already describes the main features of the angular distribution of emitted nucleons at the highest outgoing energies, say at $\varepsilon=E-1$ MeV. In Fig. 1 we show the results of calculations of the reduced Legendre coefficients for the ^{93}Nb(n,n') reaction, using Eq. (1). These results compare quite well with the systematics of Kalbach and Mann [13] and with averaged experimental data, extrapolated to the energy $\varepsilon=E-1$ MeV (cf. Figs. 2,3). The deviating experimental value of f_2 at 14.6 MeV is quite uncertain, see also the discussion in Sect. 3. We note that in the early model of Mantzouranis et al. [7] there is no energy dependence at all in Fig. 1 ($f_1=2/3$, $f_2=1/4$, $f_3=0$). In the more recent model of Sun Ziyang et al. [10] the energy dependence is too weak. Furthermore, in the recent model of Iwamoto et al. [11] refraction has been neglected. It turns out that refraction effects are quite important in neutron scattering at low energies. So far, reflection effects have been neglected in our model.

3. RELAXATION TOWARDS ISOTROPY

In the previous section internal transitions after the first collission were not considered. In the exciton model the probability for such a transition is given by:

$$\lambda(n\to m) = \frac{2\pi}{\hbar}\,\overline{|M(n)|^2}\;\omega_f(m), \qquad (2)$$

where ω_f is the density of accessible final states and $\overline{|M(n)|^2}$ is the transition matrix element, averaged over all possible internal transitions $n\to m$. Therefore, the mean life time in Eq. (1) has to be replaced by

$$\tau'(n_o) = \frac{1}{\sum_m \lambda(n_o\to m) + W(n_o)} \qquad (3)$$

with $n_o=3$.

In order to find the remaining contributions to the double-differential cross section we should follow each of the collission partners on its way through the nucleus. This is not very practical. Instead, we follow only one "leading" particle, assuming an "average" angular distribution after each collission. In that case the relaxation process of the composite nucleus is described by the generalized master equation [7] for the occupation probability $q(n,\Omega,t)$ of exciton state

n at time t. The solid angle Ω is the direction of the leading particle, that is changed after each collission, according to the adopted scattering kernel with eigenvalues μ_ℓ [9]. In the model of Mantzouranis et al. the free nucleon-nucleon scattering values were adopted for μ_ℓ. In our model we have followed the description of Sun Ziyang et al. [10], who adopted an *average* Kikuchi-Kawai scattering kernel. Denoting the energy-dependent eigenvalues of the KK angular distribution by

$$\mu_\ell^{KK}(\varepsilon',\varepsilon), \tag{4}$$

where ε' and ε are the energies before and after scattering, respectively, we may write for the average coefficients:

$$\mu_\ell^{KK}(\langle\varepsilon'\rangle_n,\langle\varepsilon\rangle_n). \tag{5}$$

For the averaging procedure we refer to Ref. [10].
In our model we have used

$$\bar{\mu}_\ell^{KK} = \mu_\ell^{KK}(E,\langle\varepsilon\rangle), \tag{6}$$

after a check [6] that there was not much difference in the angular distributions of neutron emission spectra calculated with (5) and (6). Consequently, the solution of the generalized master equation is as simple as in the case of the model of Mantzouranis et al., and we find very easily the time integrals over the occupation probabilities $\tau(n,\Omega)$ as a sum over Legendre polynomial terms $\zeta_\ell(n)P_\ell(\cos\theta)$. Writing $\zeta_\ell(n) = \xi_\ell(n)\,\tau(n)$, where $\tau(n)$ is the mean life time of the angle-integrated exciton model and including reflection, we find

$$\frac{d^2\sigma(a,b)}{d\varepsilon d\Omega} = \sigma_a \sum_n w_b(n,\varepsilon,\tau(n) \sum_\ell \frac{2\ell+1}{4\pi} P_\ell(\Omega)\,\xi_\ell(n)\,\rho_\ell(\varepsilon)\,P_\ell(\cos\theta)\,(n>n_o). \tag{7}$$

For the initial n_o-contribution we adopt Eq. (1) with $\tau(n_o)$ according to the solution of the full master equation. Actually, the n_o-contribution should be divided into a part Eq. (1) with Eq. (3) and a part Eq. (7) with $\tau(n_o) = \tau(n_o) - \tau'(n_o)$, because a (small) fraction of the emission from $n = n_o$ results from more than one collission.

Independently of the work performed at our institute, but still based upon the *same mathematical description* of Akkermans et al. [8], the JAERI group [11] has developed a more general approach to account for the angle-energy correlations, without restricting these to the first collission. Iwamoto et al. have introduced the full KK expression into the scattering kernel. This leads to a further generalized occupation probability $q(n,\Omega,\varepsilon,t)$, where ε is the energy at which the leading particle will be emitted when no further collissions occur. In the solution of their generalized master equation energy-dependent eigenvalues (4) occur. In our model this energy dependence was taken into account only for the first collission ($\varepsilon' = E$), that gives the main contribution to the angular distribution. From the argument that the results of using (5) or (6) are almost the same [6] we expect that the improvement of Iwamoto et al. is not very large.

Another interesting aspect of the Japanese work is their effort to relax the assumption of the "leading" fast particle by admitting collissions (changing the exciton number) that leave the angular direction Ω unaffected. The result of these calculations is that the angular distribution becomes slightly more forward-peaked, due to the slowing down of the relaxation towards isotropy.

Finally, we present in this section some results of calculations with our own model, based upon the work of Costa et al. [6], see Figs. 2,3. The calculated data are compared to systematics [13] and experimental data [14,15]. No fit parameters were used in the calculations, as far as the angular distribution is concerned. The overall results are quite acceptable except for f_2 at 14.6 MeV. This could be due to the neglect of a symmetric component (included in the systematics), as will be discussed in the next section.

4. SYMMETRIC COMPONENT

The model discussed in the previous sections leads to isotropy in the equilibrium limit. This is correct when it is assumed in the HF model that the spin distribution of the levels in the continuum is proportional to 2J+1, where J denotes the spin of the levels [1]. For the more realistic spin distribution

$$R(J) = \frac{2J+1}{2\sigma^2}\exp[-\frac{(J+\frac{1}{2})^2}{2\sigma^2}] \tag{8}$$

with a finite value of the spin cut-off parameter σ, the HF model for continuum emission [4] predicts a symmetric angular distribution. This is a consequence of the conservation of angular momentum: the incoming angular momentum is absorbed by the compound nucleus, leading to a rotation *around an axis perpendicular to the incoming direction*. Emission from the compound nucleus then leads to an anisotropic distribution, symmetric around 90^o [3].

In the model that we have used there is angular-momentum conservation (in a classical sense) only for the component of emission at the first collission. After the first collission only the "leading" fast particle is followed that collides with target nucleons which are supposed to be at rest. In each collission a recoil nucleus absorbs part of the energy and angular momentum. After a long lapse of time all incoming angular momentum has been absorbed by the nucleus and a symmetric angular distribution should result. However, also at an earlier stage, when most of the incoming angular momentum has been exchanged, but still the energy is not yet equilibrated, a symmetric component has to be added. It was shown by Akkermans and Gruppelaar [16] that indeed the characteristic times for these processes are different.
Consequently one might expect that emission from already relatively low exciton numbers should have a symmetric component, in addition to the forward peaked-angular distribution.

In order to estimate the symmetric component one could start from a spin-dependent exciton model or "unified" model, using the random-

phase approximation for the (pre-)compound contributions. The resulting expression for the double-differential cross section has been given by Plyuĭko [17] and Fu [18]. In the weak-coupling limit this expression can be reduced to [19]:

$$\left(\frac{d^2(a,b)}{d\varepsilon d\Omega}\right)_{sym} = \sigma_a \sum_n w_b(n,\varepsilon)\tau(n)\frac{1}{4\pi}\left[1+\frac{\langle \ell_a^2\rangle\langle \ell_b^2\rangle}{12\sigma^4(n-n_b)} P_2(\cos\theta)\right], \qquad (9)$$

where $\langle \ell^2\rangle$ is the average value of the angular momentum of the incoming or outgoing particle (denoted by a and b respectively), weighted with the corresponding transmission coefficients:

$$\langle \ell^2\rangle = \sum_\ell \ell^3 T_\ell(E) / \sum_\ell \ell T_\ell(E). \qquad (10)$$

In the equilibrium limit Eq. (9) reduces to the expression of Ericson and Strutinsky [3]. Therefore it seems clear that for high values of n where $\xi_\ell(n) \approx 0$ Eq. (9) should be inserted.

For low values of n there is a problem of how to determine the fraction of $\tau(n)$ that contributes to the symmetric component. Denoting this fraction by r we could use for the double-differential cross section the expression:

$$\frac{d^2\sigma(a,b)}{d\varepsilon d\Omega} = \sigma_a w_b(n,\varepsilon)\tau(n)\sum_\ell \frac{2\ell+1}{4\pi} f_\ell(n) P_\ell(\cos\theta) \qquad (11)$$

with

$$\begin{aligned} &f_0(n) = 1, \\ &f_\ell(n) = [1-r(n)]\rho_\ell(E)\xi_\ell(n)\rho_\ell(\varepsilon) + r(n)\frac{\langle \ell_a^2\rangle\langle \ell_b^2\rangle}{60\,\sigma^4(n-n_b)}\delta_{\ell 2}, \\ &\xi_\ell(n_0) = \mu_\ell^{KK}(\varepsilon). \end{aligned} \qquad (12)$$

Quantitatively we may say that r(n) will be large when the number of collissions is large. Therefore r(n) could be equated with:

$$r(n) \approx 1 - \tau'(n)/\tau(n), \qquad (13)$$

where $\tau'(n)$ is the mean life time corresponding to the "never-come-back" assumption in the formulation of the random-walk model:

$$\tau'(n) = \tau'(n-2)\frac{\lambda(n-2\to n)}{\sum_m \lambda(n\to m) + W(n)} \qquad (14)$$

with $\tau'(n_0)$ given by Eq. (3).
This gives values of r(n) equal to 8.1%, 39%, 67% and 96% for n= 3, 5, 7 and 9, respectively, in the case of ^{93}Nb+n at 14.6 MeV. However, due to the fact that σ^4 is proportional to $(n-n_b)^2$ the symmetric component of f_2 is rather small at high exciton numbers. We expect that the main result of adopting Eq. (3) will be a decrease of f_1 at low values of outgoing energies, where in addition f_2 will be somewhat increased.

Another possibility to estimate the fraction of symmetric emission comes from the work of Feshbach et al. [20], who introduced the distinction between *multi-step-direct* (MSD) and *multi-step-compound* processes (MSC). It was postulated that these processes proceed through unbound and bound states, respectively. For the MSC reaction mechanism the random-phase approximation was assumed to be valid, leading to a symmetric angular distribution; for the MSD reaction mechanism a distinct forward-peaked angular distribution was predicted. It was assumed that the MSD and MSC branches are independent of each other.

Kalbach [21] has introduced some of these ideas in the exciton model by defining internal transition rates from unbound to unbound, bound to bound, unbound to bound and bound to unbound states and by limiting the emission to unbound states only. In Kalbach's model the MSC definition of emission is based upon the processes that have passed through at least one bound state and eventually through one unbound state. This refinement was made since in the exciton model emission from a bound state requires first at least one collission to free a particle. Kalbach has confirmed that the MSC and MSD mechanisms are almost uncorrelated.

In the *systematics* of Kalbach and Mann [13] the fraction of (symmetric) MSC emission is used as follows:

$$\begin{aligned} f_\ell(\varepsilon) &= [1 - r_{MSC}(\varepsilon)]\, f_\ell^{syst}(\varepsilon) \quad \text{(odd } \ell\text{)}, \\ f_\ell(\varepsilon) &= f_\ell^{syst}(\varepsilon) \quad \text{(even } \ell\text{)}, \end{aligned} \qquad (15)$$

where $f_\ell^{syst}(\varepsilon)$ has been obtained from experimental data of reactions predominated by the MSD process (cf. Figs. 1-3). At high outgoing energies ε the fraction r_{MSC} is usually small, even at E = 14.6 MeV (about 3% in the case of ^{93}Nb+n); at lower outgoing energies this fraction increases.

A rough estimate of r_{MSC} could be made by equating it with the fraction of bound states in the composite nucleus [19,21]:

$$r_{bound}(p,h) = 1 - p\left(1 - \frac{B}{E+B}\right)^{p+h-1}, \qquad (16)$$

where B is the binding energy. This gives values of 10%, 40%, 64% and 80%, for n = 3, 5, 7 and 9, respectively, in the case of ^{93}Nb+n at 14.6 MeV. We recall that in the model of Kalbach [21] MSC emission is only possible after the particle has made at least one additional collission to free the particle. This leads to smaller fractions of MSC *emission* than indicated by Eq. (16). In particular MSC emission from the initial state $n_0 = 3$ is strongly reduced.

In Fig. 4 an estimate of the symmetric component in the case of the ^{93}Nb+n reaction at 14.6 MeV was made by combining Eq. (9) and Eq. (16). The average fraction of symmetric emission is about 25% for the outgoing energies at 6 to 11 MeV. This reduces the f_1 component by the same amount. The symmetric angular distribution coefficient was estimated to be $f_2^{sym} = 0.06$. It is noted that the improvement observed in Fig. 4 is mainly due to the reduction of f_1.

In conclusion we may say that a symmetric component is needed to describe precompound emission at low (outgoing) energies. The fraction of symmetric emission depends upon the number of internal collisions before emission. The fact that from the closed configurations no emission is possible needs to be accounted for. More study is required to find a reliable estimate of symmetric emission in the framework of the exciton model. This may help to remove at least part of the discrepancy between theoretical and experimental values of f_2 at low incident energies (see Fig. 2).

5. CONSISTENT MODELS

The exciton model describes in principle both the pre-equilibrium and equilibrium parts of the decay process, at least when the full master equation is solved. An important condition for the use of this simple description of the complete de-excitation process is that the sum over all particle-hole state densities equals the total state density, that in turn should agree with the measured level density. In the work performed at our institute we have followed this prescription by renormalizing the exciton state densities to the back-shifted Fermi gas formula [22], at least in an approximate way [23]. Of course, this procedure does not change the ratios between the various particle-hole state densities. In future calculations these quantities should be related to results from microscopic calculations.
A drawback of the use of the above-mentioned *"combined preequilibrium/equilibrium model"* (EM) is that no spin-parity conservation is considered nor discrete level excitation. At high incident energies this might not be too serious, in particular when one is not interested in multi-particle emission. However, in many applications one would like to combine the benefits of the preequilibrium exciton model with those of the HF model.

The most simple way to obtain this *"modified HF model"* (MHF) is to replace the level density in the HF model by

$$\rho(E',I',\Pi') \rightarrow \sum_n \frac{\omega(n-1,E')\ Q(n)\ \tau(n)}{\omega_c(n,E)}\ f(I',\Pi',E') \qquad (17)$$

where $\omega(n-1,E')$ and $\omega_c(n,E)$ refer to the state density in the final and composite nucleus, respectively. $Q(n)$ is a factor to enhance emission of the projectile at low values of n and $f(I',\Pi')$ is the spin-parity distribution factor that is supposed to be the same as that of $\rho(E',I',\Pi')$. In most codes Eq. (17) is divided into a preequilibrium part (the summation is limited to $n=\bar{n}$) and an equilibrium part, proportional to $\rho(E',I',\Pi')$. It is of interest to investigate whether this model is consistent with the combined preequilibrium/equilibrium model. This appears to be true under the same conditions that lead to consistency between HF and WE models [11], e.g. a spin-parity distribution $f(I',\Pi',E')$ that is proportional to $2I'+1$ (without a spin cut-off factor). However, these assumptions are usually not made in HF models. In Ref. [2] we have pointed out that in general the following approximate relation exists between the two models:

$$\left(\frac{d\sigma}{d\varepsilon}\right)_{MHF} = \frac{f(I,\pi,E')}{f_c(I,\pi,E)}\left(\frac{d\sigma}{d\varepsilon}\right)_{EM}, \qquad (18)$$

The ratio between the spin-parity distribution factors of the final and composite nuclides for the target spin and parity in Eq. (18) is different from unity when the spin cut-off parameters $\sigma^2(E')$ and $\sigma^2(E)$ are not the same. We mention that the same discrepancy is in fact also found between the HF and WE model [2]; only in the latter case it is usually less important.

In the *"unified model"* (UM) the exciton model is reformulated by including spin- and parity conservation in a consistent way. Straightforward generalization of the exciton model then leads to a set of master equations (one for each J and Π) in which all quantities depend upon spin and parity [2,17,24]. The solutions of these master equations lead to mean life times $\tau^{J\Pi}(n)$. Formally, the following substitution could be made in the HF model to obtain the unified model:

$$\frac{\rho(E',J',\Pi')}{\rho_c(E,J,\Pi)} \rightarrow \sum_n \frac{\rho(n,E',J',\Pi')}{\rho_c(n,E,J,\Pi)}\ Q(n)\ \tau^{J\Pi}(n). \qquad (19)$$

The important quantities occurring in the master equations are: the initial condition,

$$q^{J\Pi}_{t=0}(n) = \frac{\sigma_a^{J\Pi}}{\sigma_a}\ \delta_{nn_o}, \qquad (20)$$

the total emission rates $W^{J\Pi}(n)$ and the internal transition rates $\lambda^{J\Pi}(n\rightarrow m)$. The total emission rates are easily calculated; it turns out that there is some limitation to small spins at low n-values [2]:

$$W^{J\Pi}(n) = \frac{f(n-1,J)}{f_c(n,J)}\ W(n). \qquad (21)$$

Assuming that $\sigma^2(n) = cn$ we may approximate Eq. (21) by

$$W^{J\Pi}(n) = \left(\frac{n}{n-1}\right)^{3/2} \exp\left[-\frac{(J+\tfrac{1}{2})^2}{2cn^2}\right]\ W(n). \qquad (22)$$

It is more difficult to evaluate the internal transition rates. Assuming that the spin distribution of the level density is proportional to $2J+1$ we find from the argument that there should be consistency between the UM and EM that $\lambda^{J\Pi}(n\rightarrow m) = \lambda(n\rightarrow m)$, i.e. independent from J and Π. The same holds approximately when f is assumed to be independent from n. Therefore, it seems that the spin-parity dependence of the average matrix element in the expression

$$\lambda^{J\Pi}(n\rightarrow m) = \frac{2\pi}{\hbar}\ \overline{|M^{J\Pi}(n)|^2}\ \rho_c^{\,f}(m,J,\pi) \qquad (23)$$

at least partly cancels against that of the level density of the final state. In Ref. [25] it is clearly atated that $|M^{J\pi}(n)|^2$ is a "suitable average over the possible final states", indicating that a $(2J+1)^{-1}$ dependence of this matrix element is possible. There is an other argument that $\lambda^{J\pi}$ cannot have a sharp spin cut-off: there is no emission possible from high-spin states at low values of n[Eq. (22)]; first the exciton number of high-spin states should increase by internal transitions. Consequently, also $\tau^{J\pi}(n)$ cannot have a sharp spin cut-off. Assuming spin independence of λ and W we find [2]:

$$\tau^{J\pi}(n) = \frac{\sigma_a^{J\pi}}{\sigma_a}\,\tau(n), \qquad (24)$$

where the spin-parity population is constant† and determined by the formation of the composite state. This assumption leads to consistency with the HF model when emission is allowed only from equilibrium. On the other hand, complete consistency with the spin-independent exciton model is *not* obtained:

$$\left(\frac{d\sigma_n}{d\epsilon}\right)_{UM} \simeq \frac{f(n-1,I)}{f_c(n,I)}\left(\frac{d\sigma_n}{d\epsilon}\right)_{EM}. \qquad (25)$$

However, as noted before [cf. Eq. (18)], a similar discrepancy is observed between the HF and WE models. These discrepancies suggest modifications in the EM and WE models, depending upon the assumptions made for the spin distribution of the level density and the spin population of the exciton states during equilibration [2].

The above-mentioned "unified model" could be used to calculate angular distributions, in the same way as the (continuum) HF model. This leads to the symmetric component [17-19], discussed in Sect. 3. Asymmetry in the angular distribution is obtained when the random-phase approximation is rejected [17,18]. However, it is not known to which extend these assumptions are valid. Therefore the semi-classical leading-particle model could be used to determine the angular distribution in the precompound phase, supplemented with a fraction of symmetric emission as discussed in Sect. 3.

6. CONCLUSION

In this paper some recent improvements of the exciton model in its master-equation formulation have been discussed. With regard to the description of the angular distributions of emitted particles the "leading particle" concept of Mantzouranis et al. [7], combined with the mathematical work of Akkermans [8,9] has shown to be a fruitful base for further developments. In recent work [6,10,11] the Kikuchi-Kawai expressions are employed for the angular distribution of the intra-nuclear scattering. In particular for the first collission it is important to include the full angle-energy correlation of that distribution [6].

† Fu [24] assumes a different spin-parity population, proportional to $f_c(n,J)$.

At lower incident energies it was shown that refraction effects are significant [6]. Furthermore, an additional symmetric component [17-19] might be needed to account for angular-momentum effects in "multi-step-compound" reaction mechanisms. Here the fraction of symmetric emission [cf. Eqs.(11,12)] is a quantity that is related to the number of collission [Eq. (13)]or could be inferred from the distinction between multi-step-direct and multi-step-compound reaction mechanisms [20,21]. Further work is needed to find a reliable estimate of symmetric emission in the framework of the exciton model. This could help to remove at least part of the discrepancy between theoretical and experimental values of the second-order Legendre coefficient of the angular distribution at low incident energies.

Part of the above-mentioned problems are due to the neglect of angular-momentum conservation after the first collission and the semi-classical description of the system of target+projectile. Therefore, it is of interest to follow the development of the spin-parity dependent "unified" exciton model [2,17,24]. In this paper we have restricted ourselves to some remarks on the consistency between the unified exciton model, the Hauser-Feshbach model, the spin-independent exciton model and the Weisskopf-Ewing model. The requirements of consistency are easily met when the spin distribution is proportional to 2J+1 (without a spin cut-off factor) [1,2,19]. When the spin cut-off factor is a function of exciton number and/or energy, discrepancies are observed between the various spin-dependent and spin-independent models. Assuming a constant spin population during equilibration, the discrepancies between UM and EM are similar to those between HF and WE. More study with regard to the spin distributions and populations is required to establish the unified model. This holds in particular for the spin-dependence of the internal transition rate.

REFERENCES

[1] H. Goldstein in: Fast Neutron Physics, vol. II, edited by J.B. Marion and J.L. Fowler, Interscience, New York (1963) p. 1525.

[2] H. Gruppelaar, Level density in unified preequilibrium and equilibrium models, Contr. to the IAEA Advisory Group Meeting on Basic and Applied Problems of Nuclear Level Densities, Brookhaven National Laboratory, April, 1983.

[3] T. Ericson and V. Strutinski, Nucl. Phys. 8 (1958) p. 284.

[4] C.C. Lu, L.C. Vaz and J.R. Huizenga, Nucl. Phys. A190 (1972) p. 229.

[5] K. Kikuchi and M. Kawai, Nuclear Matter and Nuclear Reactions, North Holland, Amsterdam (1968).

[6] C. Costa, H. Gruppelaar and J.M. Akkermans, Phys. Rev. C28 (1983) p. 587.

[7] G. Mantzouranis, D. Agassi and H.A. Weidenmüller, Phys. Lett. 57B (1975) p. 220.

[8] J.M. Akkermans, Phys. Lett. 82B (1979) p. 20.

[9] J.M. Akkermans, H. Gruppelaar and G. Reffo, Phys. Rev. C22 (1980) p. 73.

[10] Sun Ziyang, Wang Shunsan, Zhang Jingshang and Zhuo Yizhong, Z. Phys. A305 (1982) p. 61.

[11] A. Iwamoto and K. Harada, Extension of generalized exciton model and calculation of (p,p') angular distribution, Contr. to Int. Symp. on Light Ion Reaction Mechanisms, Osaka (1983).

[12] H. Gruppelaar and J.M. Akkermans, Comparison of experimental and calculated neutron emission spectra and angular distributions, ECN-84 (1980), Netherlands Energy Research Foundation.

[13] C. Kalbach and F.M. Mann, Phys. Rev. C23 (1981) p. 112.

[14] D. Hermsdorf et al., Differentielle Neutron n-emissionsquerschnitte $\sigma_{nM}(E_o,E,\theta)$ bei 14.6 MeV Einschussenergie für die Elemente Be,....., Bi, ZfK-277 (1974) Zentralinstitut für Kernforschung, Rossendorf; J.L. Kammerdiener, Report UCRL-51232 (1972), California Univ., LLL.

[15] A. Marcinkowski et al. Nucl. Sci. Eng. 83 (1983) p. 13.

[16] J.M. Akkermans and H. Gruppelaar, Z. Phys. A300 (1981) p. 345 and J.M. Akkermans, Z. Phys. A313 (1983) p. 83.

[17] V.A. Plyuĭko, Sov. J. Nucl. Phys. 27 (1978) p. 625.

[18] C.Y. Fu, Development and applications of multi-step Hauser-Feshbach pre-equilibrium model theory, Symp. on Neutron Cross Sections from 10 to 50 MeV Brookhaven, 1980. BNL(USA)-84/L (1980) p. 675.

[19] A.V. Ignatyuk, V.P. Lunev and V.G. Pronyaev, Izv. Akad. Nauk. SSSR, Ser. Fiz. 39 (1975) p. 2144.

[20] H. Feshbach, A. Kerman and S. Koonin, Annals of Phys. 125 (1980) p. 429.

[21] C. Kalbach, Phys. Rev. C25 (1981), p. 112, p. 124, p. 2798; Phys. Rev. C24 (1981) p. 819.

[22] W. Dilg, W. Schantl, H. Vonach and M. Uhl, Nucl. Phys. A217 (1973) p. 269.

[23] H. Gruppelaar, C. Costa, D. Nierop and J.M. Akkermans, Calculation and processing of continuum particle-emission spectra and angular distributions, Proc. Int. Conf. on Nuclear Data for Science and Technology, Antwerp (1982), D. Reidel Publ. Co., Dordrecht, Holland (1983), p. 537.

[24] C.Y. Fu, A consistent nuclear model for compound and precompound reactions with conservation of angular momentum. Proc. Int. Conf. on Neutron Cross Sections for Technology, Knoxville, 1979, N.B.S., Sp. 594 (1980) p. 757.

[25] E. Fermi, Nuclear Physics, The University of Chicago Press, revised edition 1951, p. 142, 214.

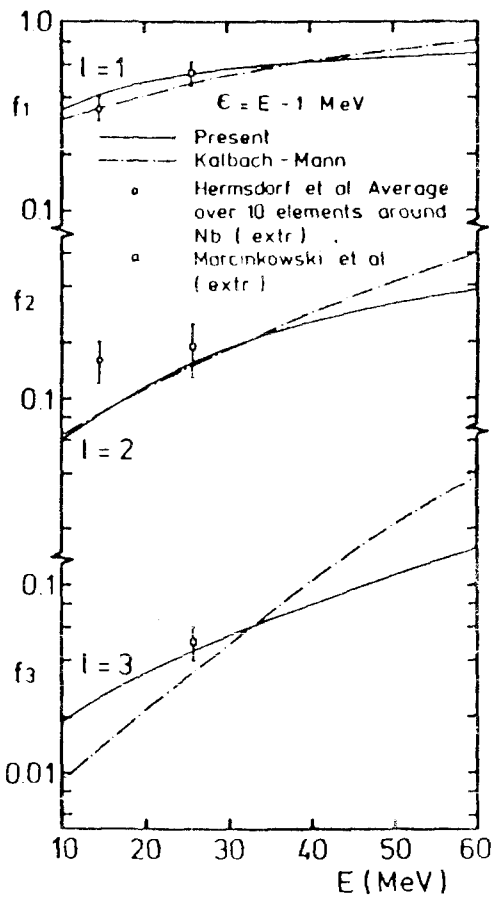

Fig. 1. Reduced Legendre coefficients for inelastic neutron scattering at ^{93}Nb as a function of incident energy E at high emission energies (ε = E-1 MeV). The theoretical curve (full line) is based upon the angular distribution of Eq. (1). The dashed-dotted curve represents the systematics of Kalbach and Mann [13]. The points have been obtained from the graphs given in Figs. 2 and 3, by extrapolation.

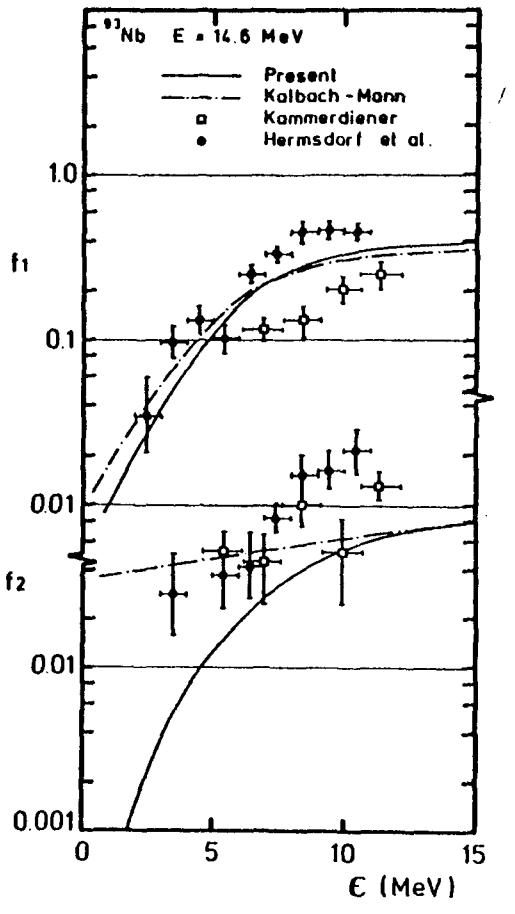

Fig. 2. Reduced Legendre coefficients for neutron emission from the reaction ^{93}Nb+n at incident energy E = 14.6 MeV, as a function of emission energy ε. The full curve has been calculated by Costa et al. [6], Eqs. (1,7); the dashed curve represents the systematics of Kalbach and Mann [13]. The experimental points are from Hermsdorf et al. and Kammerdiener [14].

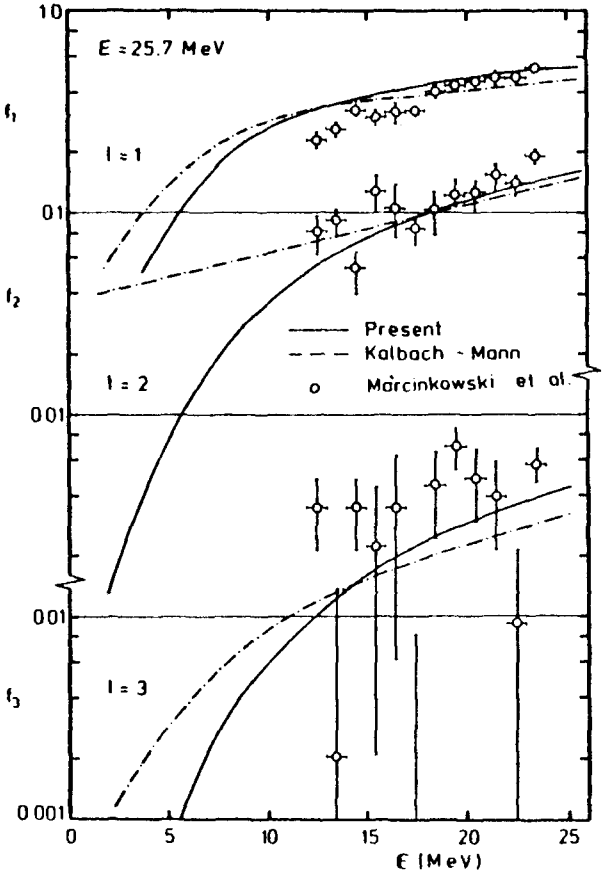

Fig. 3. Reduced Legendre coefficients for neutron emission from the reaction ^{93}Nb+n at incident energy E = 25.7 MeV. See further caption of Fig. 2. The experimental data are from Marcinkowski et al. [15].

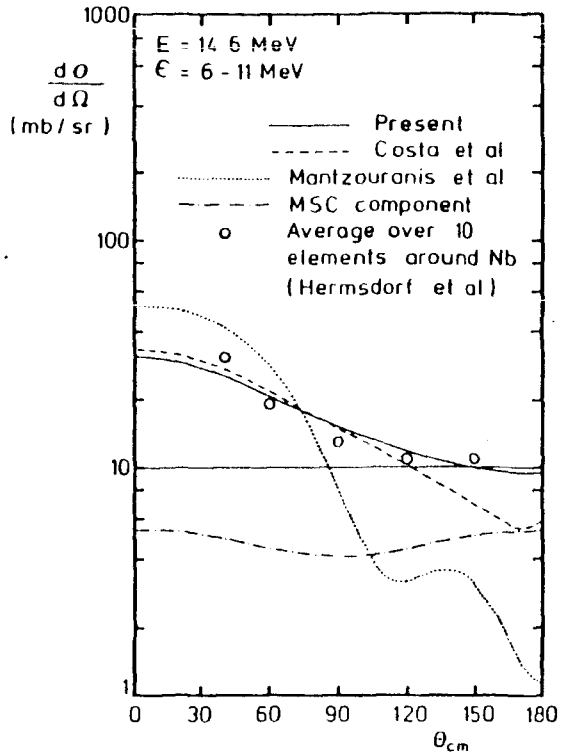

Fig. 4. Angular distribution of neutrons emitted from inelastic neutron scattering at ^{93}Nb with incident energy E = 14.6 MeV. The experimental data of Hermsdorf et al. [14] have been averaged over ten elements around Nb. The dotted and dashed curves correspond to calculations according to the models of Mantzouranis et al. [7] and Costa et al. [6], respectively. The full curve has been obtained by replacing 25% of the cross section by a symmetric angular distribution (dashed-dotted curve).

CALCULATIONAL METHODS FOR STRUCTURAL MATERIALS NUCLEAR DATA

E. D. Arthur

Theoretical Division
Los Alamos National Laboratory
Los Alamos, New Mexico 87545

ABSTRACT

The nuclear models applicable to the evaluation of neutron cross sections for structural materials are briefly reviewed. Recent efforts to improve data models are discussed, particularly regarding techniques used to produce realistic input parameters. Examples of current calculations using such models for provision of structural materials nuclear data are given. In this context, emphasis is placed on the use of nuclear model calculations to correct certain fundamental problems occurring in evaluated data files. Finally, new areas of effort involving more basic nuclear models are described that may impact future applied theoretical calculations.

I. INTRODUCTION

The use of theoretical nuclear models in the provision of evaluated nuclear data for structural materials has increased significantly over recent years. Several reasons can be cited for this trend, some being the projected need for nuclear data at higher energies (E_n > 20 MeV), the availability of new experimental results for reaction types where measurements were previously nonexistent or sparse, and the realization that a careful application of such models can provide a framework for the consistent analysis of data from a variety of experimental sources. In this paper we will discuss the principal theoretical models used to provide data for energy regions above where resonance effects are minimal. For structural materials, this generally means incident energies greater than 1 MeV where the applicable models are the Hauser-Feshbach statistical model, along with direct-reaction and preequilibrium models. We will also implicitly include discussions of the optical model because it is used to produce theoretical predictions for quantitites such as total cross sections as well as to provide input quantities for use in the other mentioned models.

The format of the paper will be a short overview of each model with examples of its application to the calculation of nuclear data for structural materials. Emphasis will be placed on energy regions or reaction types in which the use of a given model is necessary to describe experimental data or in which a marked improvement in agreement to such data occurs. Underlying the success that such nuclear models have enjoyed recently is a significant improvement in parametera determined for use in them. Such advances will be discussed and examples provided in which improved models or techniques have occurred. Also, examples of recent applications of such models in the calculation of nuclear data will be provided. Particular emphasis will be placed on instances where nuclear models are used to correct certain fundamental problems in evaluated nuclear data files. Finally, selected areas will be illustrated in which more basic theoretical nuclear models can be expected to yield satisfactory results.

II. THEORETICAL MODELS

A. Hauser-Feshbach Statistical Model.

Calculations using the Hauser-Feshbach statistical model generally employ the following expression [1,2]

$$\bar{\sigma}^{J\pi}_{cc'} = \left\langle \frac{\Gamma^{J\pi}_c \Gamma^{J\pi}_{c'}}{\Gamma^{J\pi}} \right\rangle = \frac{\langle \Gamma^{J\pi}_c \rangle \langle \Gamma^{J\pi}_{c'} \rangle}{\langle \Gamma^{J\pi} \rangle} W^{J\pi}_{cc'} , \qquad (1)$$

where c and c' represent the entrance and exit channels respectively and $J\pi$ refers to the spin and parity of a given compound-nucleus state. The widths, $\langle\Gamma\rangle$, are generally calculated using transmission coefficients (particle or gamma-ray) produced from other models. In particular, for particles, such transmission coefficients can be obtained from diagonal elements of the S-matrix resulting from optical model calculations if direct-reaction effects are neglected.

Expression (1) is a generalization of the original Wolfenstein, Hauser, and Feshbach expression [3] to the more universal case where the spacing of levels in a compound nucleus is much larger than their widths. In this circumstance, width fluctuation and correlation corrections (represented by $W^{J\pi}_{cc'}$) must be applied, the general result being a significant enhancement in the compound elastic cross section. This enhancement (represented by w_c) can be on the order of 2-3. To evaluate $W^{J\pi}_{cc'}$, two methods are principally used today. The first, due to Tepel, Hoffmann, and Wiedenmüller [4] employs a form (dropping the explicit notation for J and π):

$$W_{cc'} = \frac{V_c V_{c'}}{T_c T_{c'}} \frac{T}{V} [1 + \delta_{cc'} \cdot (w_c - 1)] \qquad (2)$$

where V is related to the transmission coefficient T through an expression based on the unitary nature of the S-matrix

$$T_c = V_c + \frac{V_c^2}{V} (w_c - 1) . \qquad (3)$$

The expressions for determination of $W_{cc'}$ originating from this approach have an advantage in terms of computational speed and simplicity.

An alternative form for $W_{cc'}$ has been formulated by Moldauer [1,5] and involves a more rigorous and complicated expression:

$$W_{cc'} = \int_0^\infty dt\, e^{-t\Gamma_\gamma/\langle\Gamma\rangle} \prod_i \left(1 + 2/\nu_i \frac{\langle\Gamma_i\rangle}{\langle\Gamma\rangle} t\right)^{-\left(\frac{1}{2}\nu_i + \delta_{ci} + \delta_{c'i}\right)} \left(1 + \frac{2\delta_{cc'}}{\nu_{c'}}\right) . \qquad (4)$$

The quantity ν appearing in Expression (4) and throughout both the Tepel et al. and Moldauer formalisms represents the degree of freedom associated with an χ^2 distribution assumed for the partial widths occurring in the compound nucleus. It can be related to the enhancement factor w_c by

$$\nu_c \cong \frac{2}{w_c - 1} \quad \text{and is often assumed to have the form } 1 + \sqrt{T} \quad [5].$$

The increased complexity of the Moldauer expression is actually not a significant hinderance to its use, particularly when Gaussian quadrature integration techniques are used [6]. The form for $W_{cc'}$ appearing in Expression (4)

has fewer restrictions on its use (it can be used at lower energies) and generally offers a better reproduction of simulation experiments aimed at examination of the behavior of the S matrix [7].

Figure 1 illustrates the necessity for including such $W_{cc'}$ corrections in Hauser-Feshbach calculations for structural materials. The data are those of Smith et al.[8] for neutron scattering from the 0.846-MeV level in ^{56}Fe. The solid curve represents the calculated compound nucleus cross section obtained, incorporating such corrections [Eq. (4)], while the dashed curve results when width fluctuation/correlation effects are ignored. Since these curves represent only compound nucleus contributions, an even greater overprediction would occur in the case of the dashed curve when direct-reaction cross sections (see following section) are included. The resulting overprediction of the inelastic scattering excitation function principally results because of lack of enhancement in the calculated compound-elastic cross section. This enhancement is illustrated in Fig. 2 and is significant in this example (and for other similar structural materials) for energies up to several MeV.

B. Direct Reaction Models

Above several MeV, neutron inelastic scattering from collective states in structural materials is dominated by direct-reaction effects. Such contributions are generally calculated using the vibrational or rotational form of the coupled-channel (CC) model or the Distorted Wave Born Approximation (DWBA). Recent CC calculations have been made by Delaroche for ^{54,56}Fe [9], by Guenther for natural chromium [10], and by Korzh et al. [11] for ^{52}Cr in the analysis of neutron scattering from low-lying collective states. Figure 3 illustrates such results (along with compound nucleus calculations) from the analysis of Korzh and illustrates the necessity for inclusion of direct-reaction contributions at energies above 3-4 MeV.

Both direct-reaction models, CC and DWBA, offer certain advantages (as well as disadvantages) when applied to structural materials. Coupled-channel calculations involve the coupling of several states and can represent multiple phonon excitations. DWBA theory, on the other hand, generally involves first-order collective form factors [12] and cannot provide a physically accurate description of scattering from states involving higher order phonon effects. Such problems not withstanding, DWBA calculations can be used reasonably well for the determination of direct inelastic scattering contributions assuming β_ℓ values from charged-particle reactions are available. Figure 4 compares a DWBA calculation using realistic spherical optical model parameters [13] to a CC calculation [9] made for 14-MeV neutron scattering from the 0.846-MeV 2^+ state in ^{56}Fe. Reasonable agreement exists between the two calculations.

The Distorted Wave Born Approximation can also be used to determine direct-reaction contributions from higher lying collective states in which application of the CC formalism might be difficult. Figure 5 illustrates several such states for ^{56}Fe where β_ℓ values [12] are displayed at the excitation energy appropriate to the state. Such higher lying collective states have been measured in high resolution neutron emission experiments and must be included in theoretical calculations in order to produce agreement with experimental data. Such an example appears in Figure 6 where forward angle (35°) scattering data for natural iron measured by Kammerdienner [14] are compared to theoretical calculations [13] that included DWBA contributions for states up to E_x = 4.8 MeV.

C. Preequilibrium Models.

The use of preequilibrium models to describe nonstatistical effects in nucleon-induced reactions has been firmly established [15], and preequilibrium corrections are routinely applied in nuclear model calculations at incident energies above about 10 MeV. However, most applications to date for data evaluation have been aimed at preequilibrium effects on integrated cross sections and particle emission spectra. Figure 7 presents a typical illustration of the impact of preequilibrium corrections on the proton emission spectrum calculated for the interaction of 14.6-MeV neutrons on ^{56}Fe. Obviously, such corrections are necessary to produce agreement with the high energy portion of the experimental spectrum [16].

Recent developments in the preequilibrium formalism have concentrated on its generalization to produce angular distribution information. One such effort by Kalbach and Mann [17] relied upon guidance from the multistep reaction theory developed by Feshbach, Kerman, and Koonin [18] to separate the nonstatistical contributions into multistep direct (involving unbound states) and compound (involving bound states) processes. The resulting expression:

$$\frac{d^2\sigma}{d\varepsilon d\Omega} = a_0(\mathrm{MSD}) \sum_{\ell=0}^{8} b_\ell P_\ell(\cos\theta) + a_0(\mathrm{MSC}) \sum_{\substack{\ell=0 \\ \Delta\ell=2}}^{8} b_\ell P_\ell(\cos\theta) , \qquad (5)$$

relied upon parameterizations for the Legendre coefficients, b_ℓ, determined from fits to a variety of particle emission data. Techniques for calculation of multistep direct and compound processes have been formulated by Kalbach [19] and have been embodied in the PRECO-D code [20]. Recently the functional form of the b_ℓ coefficients has been modified by Foster [21] to smoothly extrapolate to a zero value for small secondary energies. Figure 8 compares results from these latter systematics to 14-MeV angular distribution data for nickel.

Angular distributions for emitted particles can also be calculated using a generalized form of the master equations exciton model developed by Mantzouranis et al. [22]:

$$\frac{d}{dt} q(n,\Omega,t) = \sum_m \int d\Omega q(m,\Omega',t) W_{mn}(\Omega',\Omega) - q(n,\Omega,t) \sum_m \int d\Omega' W_{nm}(\Omega,\Omega'). \qquad (6)$$

In this expression, $q(n,\Omega,t)$ represents the probability of finding the system in a state (n,Ω) at time t. $W_{nm}(\Omega,\Omega')$ is the transition rate from state (n,Ω) to (m,Ω') and results from a product of transition rates, λ^+,λ^0, λ^-, and an angle-dependent factor. This factor $G(\Omega,\Omega')$ is then related to the nucleon-nucleon scattering cross section.

Akkermans et al [23] were able to reduce this generalized expression to a form similar to that for the standard master equation [24]. This technique thus allows a simple and fast method for the calculation of double differential cross sections. In Ref. [23] this formalism was applied to the calculation of angular distributions for a variety of nuclei covering a large portion of the periodic table ($9 \leq A \leq 209$). With only two adjustable parameters, satisfactory agreement was achieved with angular distributions measured for 14.6 MeV incident neutrons. For materials in the mass range $40 < A < 100$, Fig. 9 compares calculated and experimentally determined $\ell = 1$ Legendre coefficients for particles having secondary energies, $6 \leq E' \leq 11$ MeV.

In spite of the success of this model as originally developed, there were problems resulting from underprediction of data at backward angles. Such problems have been addressed recently [25] [26] through inclusion of refraction effects and by improved treatments of the scattering kernel occurring in $G(\Omega,\Omega')$. In particular, Fermi motion and Pauli principle effects have been included. Also, the addition of multistep compound processes to this formulation [27] has produced improved agreement to experimental data at back angles.

III. MODEL PARAMETERS

A significant improvement in recent nuclear model calculations for structural materials can be largely attributed to the better determination of input parameters used in them. Increasingly, a trend has developed in which parameters are developed for an extensive incident energy range, but which are valid for a rather restricted mass region. Development of these parameter sets are characterized by the use of a variety of independent data sources including charged-particle reactions, to both determine and verify them. By using techniques that involve a consistent analysis of numerous data types, one can readily confirm the applicability of the models as well as provide a measure of the reliability of the calculated results.

A. Neutron and Charged-Particle Optical Parameters.

Optical model calculations are used to provide transmission coefficients and inverse cross sections in Hauser-Feshbach and preequilibrium calculations. Calculation of the neutron-induced reactions of interest imposes substantial requirements upon the neutron optical parameters to be used. They must reproduce or predict total and shape elastic cross sections. In Hauser-Feshbach calculations they also must produce realistic compound-nucleus-formation cross sections valid over the entire incident energy range of interest. Finally, they should simultaneously produce reasonable low energy transmission coefficients important in processes such as (n,2n) or (n,np) reactions.

To ensure such capabilities, the determination of neutron optical parameters often follows the so-called "SPRT" method utilized at Bruyeres-le-Chatel [28]. In this technique, higher energy data (total, elastic cross sections) are supplemented by fits to average resonance quantities at low incident energies. Further constraints on the determined neutron parameters, as well as development of a consistent set of proton optical parameters can be achieved

through a simultaneous analysis of proton reaction data that employs a Lane-form of the optical potential [29]. However, presently most applied calculations [13],[30] continue to determine neutron parameters separately while relying upon proton parameters originating from global parameter sets [31],[32].

A recent example [13] of an optical-model parameter set for neutron reactions on iron resulted from a simultaneous fit to (a) total cross sections between 2 and 40 MeV; (b) s- and p-wave strength functions, along with values for the potential scattering radius; (c) elastic scattering angular distributions between 6 and 14 MeV; and (d) reaction cross sections between 5 and 30 MeV. Figure 10 compares the total cross section calculated using the resulting parameters (see Ref. [13]) to data available between 2 and 40 MeV. Figure 11 compares total and reaction cross sections calculated with these optical parameters to similar calculations that employ the Wilmore-Hodgson global parameter set [33]. Such global parameters have been routinely used in the past to provide theoretical predictions. However, the figure shows that such sets cannot adequately describe both low- and high-incident energy regions that impact current nuclear model calculations.

The demands placed upon charged-particle transmission coefficients in the calculation of neutron-induced reaction data are generally less than those for neutrons. As previously noted, global parameter sets, perhaps modified for the problem of interest, are generally employed in such calculations. Concurrently, there is an increasing use of charged-particle reaction data, particularly that from (p,xn) and (α,xn) reactions, to verify the behavior and applicability of such charged-particle transmission coefficients. For proton transmission coefficients it is often quite important to verify their low-energy sub-Coulomb barrier behavior for several of the structural materials. For several compound nuclei, the situation exists in which the proton binding energy may be significantly less than that for neutrons. This leads to a so-called "proton window" where only proton and gamma-ray emission are energetically allowed. Under such circumstances, the correct description of proton emission is particularly sensitive to this sub-Coulomb barrier region. This assumes, of course, that gamma-ray transmission coefficients have been determined using realistic strength functions (see Section III.B). To verify this behavior, one can calculate (p,n) cross sections for reactions having very low threshold values. Such an example appears in Fig. 12 where a calculation for ^{45}Sc(p,n) employing a modified form [13] of the Perey proton optical parameters [31] is compared to data [34]. With such agreement in hand, one can proceed to the calculation of proton emission from n+^{46}Ti reactions. For this system, proton emission dominates over neutron-emission principally because of significant (n,np) reactions that populate the ^{45}Sc residual nucleus. Again, this situation arises because the proton binding energy in the ^{46}Ti compound system is 3 MeV less than for neutrons. Figure 13 shows the good agreement obtained with the ^{46}Ti proton emission spectrum measured at 14.6 MeV by Grimes et al.[15].

Comparison with higher energy charged-particle reaction data can also be used to provide parameter verification and other information that may not be available for the neutron system of interest. Additionally, such comparisons can provide data concerning level densities at high excitation energies, above that in which neutron resonance spacing information may be available. Figure 14 shows such verification calculations performed for ^{51}V(p,xn) cross sections by Strohmaier et al.[30] as part of their extensive calculations on ^{52}Cr, ^{55}Mn, ^{56}Fe, and ^{58,60}Ni.

B. Gamma-Ray Strength Functions.

A trend in several recent nuclear model calculations has been use of gamma-ray strength function data or systematics to provide reliable normalizations for gamma-ray transmission coefficients. The gamma-ray strength function can be defined as [36]

$$\frac{\langle\Gamma_\gamma\rangle}{\langle D\rangle} = \int_0^{B_n} [f_{E1}(\varepsilon_\gamma) + f_{M1}(\varepsilon_\gamma)]\, \varepsilon_\gamma^3 \rho(B_n - \varepsilon_\gamma) d\varepsilon_\gamma \,, \qquad (7)$$

where $\langle\Gamma_\gamma\rangle$ and $\langle D\rangle$ are average radiation widths and spacings for s-wave resonances, and ρ is the nuclear level density. Direct use of the strength function defined in Eq. (7) reduces or eliminates many of the problems previously associated with the determination of the magnitude of gamma-ray transmission coefficients. In such instances, such data were normalized at the neutron binding energy to the ratio, $2\pi\langle\Gamma_\gamma\rangle/\langle D\rangle$. Although this procedure is adequate for compound systems having reliable resonance data, the need to extrapolate to less favorable situations generally entails use of $\langle\Gamma_\gamma\rangle$ and $\langle D\rangle$ values deduced

from systematics. In some mass regions, particularly around shell closures, such procedures can be unreliable because of large variations occurring in <D> between nearby nuclei. The determination of strength function systematics and their subsequent use in nuclear model calculations provides a reliable means for gamma-ray transmission coefficient determination appropriate to compound systems lacking the necessary resonance data. This is particularly important for compound nuclei having proton windows where only gamma-ray and proton emission compete. Assumptions made concerning gamma-ray competition also significantly affect calculated (n,2n) cross section shapes, particularly around threshold where its values may rise rapidly.

Gardner et al. [37],[38] have devoted considerable effort to the determination and parameterization of gamma-ray strength functions appropriate to an extensive variety of nuclei, both spherical and deformed. To do so, they have developed an energy-dependent Breit-Wigner form for the E1 strength function.[38] Its form, appropriate to the mass region $40 \leq A \leq 160$, is given by

$$f_{E1}(\varepsilon_\gamma)(\mathrm{MeV})^{-3} = 3.72 \times 10^{-8} A^{4/3} \frac{(1.5-2.8A^{-1/3})}{\varepsilon_\gamma} G_R(\varepsilon_\gamma) , \qquad (8\text{-a})$$

where

$$G_R(\varepsilon_\gamma) = \left[1 + \frac{(5+E_R)^2 (\varepsilon_\gamma - E_R)^2}{(\varepsilon_\gamma \Gamma_R^*)^2} \right]^{-1} \qquad \varepsilon_\gamma < \frac{(E_R+5)}{2} \qquad (8\text{-b})$$

$$= \left[1 + \left(\frac{2}{\Gamma_R^*}\right)^2 (\varepsilon_\gamma - E_R)^2 \right]^{-1} \qquad \frac{(E_R+5)}{2} < \varepsilon_\gamma < E_R \ . \qquad (8\text{-c})$$

In this parameterization the width associated with the giant dipole resonance-like shape is assumed to be energy dependent and is given by

$$\Gamma_R^* = 22.3A^{-1/3} \left(1.052 - 6.E\text{-}5 \frac{\varepsilon_\gamma^4}{E_R}\right) \ . \qquad (8\text{-d})$$

These systematics allow one to parameterize the strength function with confidence even for unstable compound systems. An example of the results obtained from the above expressions is compared in Fig. 15 to f_{E1} values measured for the ^{65}Cu nucleus [39]. The dashed curve shows the results obtained when a Lorentzian line shape was assumed for the gamma-ray transmission coefficients, which was subsequently normalized to $\langle\Gamma_\gamma\rangle$ and <D> values inferred from systematics.

IV. RECENT CALCULATIONAL EXAMPLES

Several recent calculations have been made for structural materials that utilized the models and parameter verification techniques discussed earlier. As noted earlier in Section II-A, Strohmaier et al.[30],[40] have calculated, using the STAPRE code[41], cross sections for the principal isotopes of Cr, Mn, Fe, and Ni. Calculated data included the total and differential elastic cross sections; activation cross sections for specific reaction paths; production spectra for particles and gamma rays; and total hydrogen and helium production cross sections. As a preparatory step to such analyses, a significant effort was directed towards parameter determination and verification, particularly through use of charged-particle reaction data. Figure 16 shows calculated values for the total hydrogen- and helium-production cross section for n+^{58}Ni reactions up to E_n = 30 MeV.

The TNG code, developed at ORNL by Fu[42], has been used to upgrade ENDF/B data for Fe and Cu and is presently being used in new calculations of particle emission for Cr and Ni isotopes. Additionally, an improved unified-reaction model version of this code[43] has been under development for the past several years. Obvious resultant benefits would be incorporation of angular momentum effects in preequilibrium models, so as to obtain consistency with Hauser-Feshbach models used for equilibrium calculations. A substantial part of this effort is directed toward a consistent description of state densities used presently in preequilibrium calculations and the level density (Fermi-gas portion) description employed in Hauser-Feshbach models. Initial applications of this model have been successful, as illustrated in Fig. 17, where a preliminary calculation by Fu[44] is compared with the angular distributions of emitted neutrons resulting from 14-MeV neutron interactions with iron.

The COMNUC-GNASH [45],[46] combination of codes has been applied in several structural materials calculations, some of which are ^{54,56}Fe for $3 \leq E_n \leq 40$ MeV [13], ^{59}Co for neutron energies between 3 and 50 MeV [47], as well as various calculations for V, Ti, Ni, and Cu isotopes [48],[49]. The ^{54,56}Fe calculations placed considerable emphasis on the determination of neutron optical parameters along with verification of these and other parameters through calculation of numerous charged-particle reaction cross sections. Figure 18 provides a measure of the reliablity of such an approach, particularly where cross sections may be predicted for regions lacking experimental data. A comparison is made here with recently measured [50] neutron emission spectra produced by 25.8-MeV neutrons on ^{56}Fe. The calculation shown was made three years prior to publication of these data. Figure 19 illustrates another benefit arising from consistent analyses employing the models and parameter techniques described earlier. In this instance, a GNASH calculation [49] of the minor reaction path, ^{46}Ti(n,2n), is compared with data. Good agreement is obtained without optimization to this particular channel. The agreement shown results from the constraints introduced into the calculation through parameter determinations based on numerous sources of independent data.

Results from GNASH calculations have recently been coupled with a new code, RECOIL, [51] for calculation of recoil energy distributions. The code follows reaction paths in detail and allows one to compute such energy spectra resulting not only from binary but tertiary and higher-order reactions. Such techniques provide a reliable means of producing data necessary for radiation damage calculations. An example of recoil spectra calculated for 14-MeV neutron reactions on ^{56}Fe appears in Fig. 20.

V. IMPROVEMENT OF EVALUATION TECHNIQUES

In the previous sections the improved predictive capability of modern nuclear model calculations has been illustrated, particularly regarding data for minor reactions, energy regions lacking experimental measurements, or isotopes where data may be sparse or nonexistent. There are other evaluation areas in which nuclear model calculations can provide substantial benefits. For example, Hetrick et al. [52] have noted that for numerous ENDF/B materials, 14-MeV neutron emission spectra are deficient, primarily because preequilibrium effects were neglected. Model calculations using the TNG code are under way at Oak Ridge National Laboratory to correct such problems for chromium and nickel isotopes.

A significant evaluation problem is that of energy nonconservation which results in negative gamma ray heating and kerma [53] values. Such effects introduce complications in the calculation of local heating effects and are of particular concern in fusion applications. The primary cause of energy nonconservation in evaluated data files generally stems from inconsistencies between neutron and gamma-ray portions of the evaluation. The use of nuclear model calculations to simultaneously analyze both neutron and gamma-ray data automatically ensures that overall energy conservation will occur. Additionally, such an analysis method provides a framework for the concurrent analysis of data occurring simultaneously in several reaction channels. Often data sets that may be in error because of their inconsistency with other information can be identified.

A partial motivation of the n+^{54,56}Fe calculations [13] discussed previously was the correction of the gamma-ray heating problems occurring in the ENDF/B-V evaluation for iron. Results for the calculated neutron and gamma-ray yield, as well as neutron and gamma-ray average energies have been compared to similar values resulting from the ENDF/B-V evaluation. While the average energies and neutron yields compare well, there are significant differences in the gamma-ray yield, as illustrated in Fig. 21. The cause of the higher ENDF/B-gamma-ray yields arose from the use of gamma-ray production data measured by Chapman et al.[54] However, as shown in Fig. 22-a, calculations that are consistent with neutron reaction data cannot reproduce these results for neutron energies around 14 MeV where largest ENDF heating problems occur. The calculations do agree with the Drake[55] measurements, as indicated in Fig. 22-b. In a recent revision[56] to the ENDF/B-V iron evaluation, the gamma-ray yield values have been lowered to be more consistent with the model calculations, as shown by the squares in Fig. 21. Significant heating problems still remain for several ENDF/B structural material evaluations, most notably those for Cr, Ni, and Mn.

VI. NEW DIRECTIONS IN NUCLEAR MODEL CALCULATIONS

To conclude this review, we discuss briefly some possible future improvements in the nuclear models used for structural materials nuclear data. In particular, such improvements are aimed at replacing phenomenological models used in present calculations with more fundamental microscopic approaches. Two areas in which significant efforts are under way involve microscopic optical model and level density calculations.

Microscopic optical models use nuclear matter calculations employing realistic two-nucleon interactions. These are then applied to a finite nucleus through use of a local density approximation. Nuclear structure information for the target nucleus is required in order to compute neutron and proton density distributions. The principal development of such approaches have centered about the efforts of Jeukenne, Lejeune, and Mahaux (JLM) [57],[58] and the folding model of Brieva and Rook [59],[60]. Recent applications to the analysis of experimental results have been made at Livermore, [61] Ohio University, [62] and Bruyères-le-Châtel. [63]. In particular, a recent measurement of ^{54,56}Fe elastic cross sections in the neutron energy range from 11-26 MeV has been analyzed in terms of both microscopic approaches. Figure 23 compares calculations made with the JLM model with these data, as well as lower energy results from TUNL [64]. The agreement is remarkably good considering the basic nature of the calculations and the local density approximation used for a finite nucleus. Only two adjustable parameters must be applied to the results of this model. These are the normalization parameters λ_V and λ_W, which multiply, respectively, the calculated real and imaginary potentials. In this example, the λ_V parameter varied little over the energy range covered, having values that were consistently near 0.9-1.05. Variations for λ_W were slightly larger, 0.9-1.25, but still were acceptable. The λ_V and λ_W values were very similar to results [65],[66] obtained for a similar analysis of proton reactions on ^{58}Ni. Such studies therefore indicate that microscopic calculations can produce results that compare favorably with phenomenological optical model fits and, in addition, provide an improved physical basis for data prediction.

Microscopic level density models offer the possibility for improved descriptions of the nuclear level density at excitation energies where lack of data may make parameterization of phenomenological models difficult. Application of such models has generally been restricted to consideration of the microscopic Fermi-gas level-density formalism, and data comparisons have generally involved calculation of s-wave neutron resonance spacings [67],[68]. In only a relatively few instances [69],[70],[71] have nuclear model calculations been made that employ microscopic descriptions. In such cases data comparisons impose added constraints in that a range of excitation energies for several residual nuclei must be described simultaneously.

The microscopic Fermi-gas model uses as input realistic single-particle levels [72],[73], coupled with a realistic interaction Hamiltonian, to produce state densities, spin cutoff parameters, and parity ratios as a function of excitation energy. The use of the superconductivity formalism [74] produces a shape having roughly a constant temperature dependence at low excitation energies, while at higher energies, the calculated results become consistent with a Fermi-gas form. A comparison for ^{60}Ni of the predictions from this model [71] with results from two phenomenological formalisms, the Gilbert-Cameron [75] and back-shifted Fermi gas models [76], appears in Fig. 24. Two features are noteworthy. The first is the agreement to the data that results from a model with few adjustable parameters. The second is the differences in shape occurring between this model and the phenomenological ones, particularly the Gilbert-Cameron. Despite the success shown in this comparison, routine application of these models in standard nuclear model calculations is still difficult, partially because the level density for several residual nuclei must be described simultaneously. Additionally, such models exhibit a lack of sensitivity to parameter adjustments that might be employed to optimize agreement to experimental data.

VII. CONCLUSIONS

The basic nuclear models used in calculations of evaluated neutron cross sections for structural materials were developed two or more decades ago. Although they have been regularly employed throughout this period for such applications, it is only relatively recently that they have been utilized in the consistent and universal analyses described in this paper. The success of such calculations stems partially from new theoretical developments, particularly those aimed at improved preequilibrium formalisms and at a unified description of preequilibrium and equilibrium processes. Also important are new techniques developed for parameter determination and verification, as well as improved systematics for extrapolation to unmeasured mass or energy regions. Because of these developments, nuclear model calculations have progressed to the point where they play a basic role in the evaluation process, particularly in instances where they can be used to correct certain fundamental problems occurring in evaluated data files. Finally, the development of more microscopic models offers the promise of improved physical descriptions that can readily be used in theoretical calculations for applied purposes.

VIII. ACKNOWLEDGMENTS

I would like to acknowledge the valuable help provided by P. G. Young in the preparation of this paper. I would also like to thank R. C. Harper and W. K. Matthes for their calculational efforts, as well as S. Mellema and F. Dietrich for providing data prior to publication.

REFERENCES

1. P. A. Moldauer, "Statistical Theory of Neutron Nuclear Reactions," Proc. Course on Nuclear Theory for Applications, Trieste, 1978, IAEA-SMR-43, p. 165 (1980).

2. H. Gruppelaar and G. Reffo, Nucl. Sci. Eng. 62, 756 (1977).

3. L. Wolfenstein, W. Hauser, and H. Feshbach, Phys. Rev. 87, 366 (1952).

4. J. W. Tepel, H. M. Hoffmann, and H. A. Weidenmüller, Phys. Lett. B 49, 1 (1974).

5. P. A. Moldauer, Phys. Rev. C 11, 426 1975.

6. M. Beer, Nucl. Sci. Eng. 50, 171 (1973).

7. P. A. Moldauer, Phys. Rev. C 14, 764 (1976).

8. A. Smith and P. Guenther, Nucl. Sci. Eng. 73, 186 (1980).

9. J. P. Delaroche, S. M. El-Kadi, P. P. Guss, C. E. Floyd, and R. L. Walter, Nucl. Phys. A 390, 541 (1982).

10. P. Guenther, A. B. Smith, and J. F. Whalen, Nucl. Sci. Eng. 82, 408 (1982).

11. I. A. Korzh, V. A. Mishchenko, É. N. Mozhzhukhin, and N. M. Pravdivyi, Sov. J. Nucl. Phys. 35, 641 (1982).

12. G. S. Mani, Nucl. Phys. A165, 225 (1971).

13. E. D. Arthur and P. G. Young, "Evaluated Neutron-Induced Cross Sections for ^{54,56}Fe to 40 MeV," Los Alamos Scientific Laboratory report LA-8626-MS (ENDF 304) (1980).

14. J. L. Kammerdiener, "Neutron Spectra Emitted by ^{239}Pu, ^{238}U, ^{235}U, Pb, Nb, Ni, Al, and C Irradiated by 14-MeV Neutrons," University of California report UCRL-51232 (1972).

15. See, for example, E. Gadioli and E. Gadioli Erba, "Recent Results in the Theoretical Description of Pre-equilibirum Processes," Proc. Interregional Advanced Training Course on Application of Nucl. Theory, Trieste, 1980, IAEA-SMR-68/7, p. 3 (1981), and references contained therein.

16. S. M. Grimes and R. C. Haight, Phys. Rev. C 19, 2127 (1979).

17. C. Kalbach and F. M. Mann, Phys. Rev. C 23, 112 (1981).

18. H. Feshbach, A. Kerman, and S. Koonin, Ann. Phys. (N.Y.) 125, 429 (1981).

19. C. Kalbach, Phys. Rev. C 23, 124 (1981).

20. C. Kalbach, "PRECO-D: Program for Calculating Preequilibirum and Direct Reaction Double Differential Cross Sections," informal report, 1980 (unpublished).

21. D. G. Foster and E. D. Arthur, "Average Neutronic Properties of "Prompt" Fission Products," Los Alamos National Laboratory report, LA-9168-MS (February 1982).

22. G. Mantzouranis, H. A. Weidenmüller, and D. Agassi, Z. fur Physik, A276, 145 (1976).

23. J. M. Akkermans, H. Gruppelaar, and G. Reffo, Phys. Rev. C 22, 73 (1980).

24. C. K. Cline and M. Blann, Nucl. Phys. A 172, 225 (1971).

25. H. Gruppelaar, C. Costa, D. Nierop, and J. M. Akkermans, "Calculation and Processing of Continuum Particle-Emission Spectra and Angular Distributions," Proc. Int. Conf. Nucl. Data Sci. Technol., Antwerp, Belgium, September 1982, p. 537 (1983).

26. Sun Ziyang, Wang Shunman, Zhang Jingshang, and Zhuo Yizhong, Zeits. fur Physik A305, 61 (1982).

27. A. Chatterjee and S. K. Gupta, Zeits. fur Physik A313, 93 (1983).

28. J. P. Delaroche, Ch. Lagrange, and J. Salvy, "The Optical Model with Particular Consideration of the Coupled-Channel Optical Model," IAEA-190, p. 251 (1976).

29. A. M. Lane, Phys. Rev. Lett. 8, 171 (1962).

30. B. Strohmaier and M. Uhl, "Nuclear Model Calculations of Neutron-Induced Cross Sections for ^{52}Cr, ^{55}Mn, ^{56}Fe, and ^{58,60}Ni for Incident Energies up to 30 MeV," Proc. Int. Conf. Nucl. Data Sci. Technol., Antwerp, Belgium, 1982, p. 552 (1983).

31. F. G. Perey, Phys. Rev. 131, 745 (1962).

32. F. D. Bechetti, Jr., and G. W. Greenlees, Phys. Rev. 182 (1969).

33. D. Wilmore and P. E. Hodgson, Nucl. Phys. 55, 673 (1964).

34. K. V. K. Iyengar, S. K. Gupta, K. K. Sekharan, M. K. Mehta, and A. S. Divatia, Nucl. Phys. A 96, 521 (1967).

35. S. Grimes, R. C. Haight, and J. D. Anderson, Nucl. Sci. Eng. 62, 187 (1977).

36. D. G. Gardner and M. A. Gardner, "Gamma-Ray Strength Functions for Medium Weight Nuclei," Proc. Third Int. Symp. Neutron Capture, Brookhaven, 1978, p. 612 (1979).

37. D. G. Gardner and F. S. Dietrich, "A New Paramterization of the E1 Strength Function," Proc. Int. Conf. Nucl. Cross Sections for Technol., Knoxville, Tenn., 1979, NBS Special Publication 594, p. 770 (1980).

38. D. G. Gardner, "Current Status of Fast Neutron Capture Calculations," Proc. NEADC/NEACRP Specialists' Meeting on Fast Neutron Capture Cross Sections, Argonne National Laboratory report ANL-83-4, p. 67 (1983).

39. B. Kerlandsson, K. Nilson, A. Marcinkowski, and J. Piotrowski, Zeits. fur Physik A293, 43 (1979).

40. B. Strohmaier, M. Uhl, and W. Reiter, "Neutron Cross Section Calculations for ^{52}Cr, ^{55}Mn, ^{56}Fe, and ^{58,60}Ni for Incident Energies up to 30 MeV," Proc. Adv. Group Meet. on Nucl. Data for Radiation Damage Assessment, Vienna, 1981, IAEA-7ECDOC-163, p. 135 (1982).

41. B. Strohmaier and M. Uhl, "STAPRE - A Statistical Model Code with Consideration of Preequilibrium Decay," Proc. Course on Nuclear Theory for Applications, Trieste, 1978, IAEA-SMR-43, p. 313 (1980).

42. C. Y. Fu, "A Two-Step Hauser Feshbach Model Code with Precompound Effects and Gamma-Ray Cascades," Proc. Conf. Nucl. Cross Sections and Technology, NBS Special Publication SP-425, Vol. I, p. 328 (1975).

43. C. Y. Fu, "A Consistent Nuclear Model for Compound and Precompound Reaction with Conservation of Angular Momentum," Oak Ridge National Laboratory report ORNL/TM-7042 (1980).

44. C. Y. Fu, Oak Ridge National Laboratory provided this information in September 1983.

45. C. L. Dunford, "A Unified Model for Analysis of Compound Nucleus Ractions," Atomics International report AI-AEC-12931 (1970).

46. P. G. Young and E. D. Arthur, "GNASH: A Preequilibrium Statistical Nuclear Model Code for Calculation of Cross Sections and Emission Spectra," Los Alamos Scientific Laboratory report LA-6947 (1977).

47. E. D. Arthur, P. G. Young, and W. K. Matthes, "Calculation of ^{59}Co Neutron Cross Sections between 3 and 50 MeV," Proc. Symp. Neutron Cross Sections from 10 to 50 MeV, Brookhaven National Laboratory report BNL-NCS-51245, Vol. 2, p. 751 (1980).

48. R. C. Harper and W. L. Alford, J. Phys. G 8, 153 (1982).

49. D. W. Muir and E. D. Arthur, "Improved Activation Cross Sections for Vanadium and Titanium," presented at the Third Topical Meeting on Fusion Reactor Materials, Albuquerque, New Mexico, 1983 (to be published).

50. A. Marcinkowski, R. W. Finlay, G. Randers-Pherson, C. E. Brient, R. Kurup, S. Mellema, A. Meigooni, and R. Tailor, Nucl. Sci., Eng. 83, 13 (1983).

51. R. E. MacFarlane and D. G. Foster, "Advanced Nuclear Data for Radiation Damage Calculations," presented at the Third Topical Meeting on Fusion Reactor Materials, Albuquerque, New Mexico, 1983 (to be published).

52. D. M. Hetrick, D. C. Larson, and C. Y. Fu, "Status of ENDF/B-V Neutron Emission Spectra Induced by 14-MeV Neutrons," Oak Ridge National Laboratory report ORNL/TM 6638 (1979).

53. C. Y. Fu, "Evaluation of Photon Production Data from Neutron-Induced Reactions," Proc. Conf. Nuclear Data Eval. Methods, Brookhaven, 1980, BNL-NCS-51363, Vol. 2, p. 753 (1981).

54. G. T. Chapman, G. L. Morgan, and F. G. Perey, "A Remeasurement of the Neutron-Induced Gamma-Ray Production Cross Sections for Iron," Oak Ridge National Laboratory report ORNL/TM 5416 (1976).

55. D. M. Drake, E. D. Arthur, and M. G. Silbert, Nucl. Sci. Eng. 65, 49 (1978).

56. C. Y. Fu, "Summary of ENDF/B-V Evaluations for C, Ca, Fe, Cu, and Pb and ENDF/B-V Revision 2 for Ca and Fe," Oak Ridge National Laboratory report ORNL/TM-8283 (1982).

57. J. D. Jeukenne, A. Lejeune, and C. Mahaux, Phys. Rev. C 16, 80 (1977).

58. A. Lejeune, Phys. Rev. C 21, 1107 (1980).

59. F. A. Brieva and J. R. Rook, Nucl. Phys. A 291, 317 (1977).

60. F. A. Brieva and J. R. Rook, Nucl. Phys. A 307, 493 (1978).

61. T. W. Phillips and F. S. Dietrich, Bull. Am. Phys. Soc. 28, p. 983 (1983).

62. S. Mellema, R. W. Finlay, F. S. Dietrich, and F. Petrovich, Bull. Am. Phys. Soc. 28, p. 983 (1983).

63. Ch. Lagrange and A. Lejeune, Phys. Rev. C 25, 2278 (1982).

64. S. M. El-Kadi, C. E. Nelson, F. O. Purser, R. L. Walter, A. Beyerle, C. R. Gould, and L. W. Seagondollar, Nucl. Phys. A 390, 509 (1982).

65. A. Lejeune and P. E. Hodgson, Nucl. Phys. A 295, 301 (1978).

66. A. Lejeune, Fizika 9, Supplement 3, 79 (1977).

67. J. R. Huizenga, A. N. Behkami, J. S. Sventek, R. W. Atcher, Nucl. Phys. A 223, 577 (1974).

68. J. R. Huizenga and L. G. Maretto, Ann. Rev. Nucl. Sci. 22, 427 (1972).

69. B. P. Bayhurst, J. S. Gilmore, R. J. Prestwood, J. B. Wilhelmy, N. Jarmie, B. H. Erkkila, and R. A. Hardekopf, Phys. Rev. C 26, 1792 (1977).

70. S. M. Grimes, J. D. Anderson, J. W. McClure, B. A. Pohl, C. Wong, Phys. Rev. C 10, 2373 (1974).

71. E. D. Arthur, "The Impact of Level Density Models on Cross-Section Calculations," presented at the IAEA Advisory Group Meeting on Basic and Applied Nuclear Level Densities, Brookhaven, 1983 (to be published).

72. P. A. Seeger and W. M. Howard, Nucl. Phys. A 238, 491 (1975).

73. P. A. Seeger and R. C. Perischo, "A Model-Based Mass Law and a Table of Binding Energies," Los Alamos Scientific Laboratory report LA-3751 (1967).

74. J. Bardeen, L. N. Cooper, and J. R. Schrieffer, Phys. Rev. 108, 1175 (1957).

75. A. Gilbert and A. G. W. Cameron, Can. J. of Phys. 43, 1446 (1965).

76. W. Dilg., W. Schantl, H. Vonach, and M. Uhl, Nucl. Phys. A 217, 167 (1973).

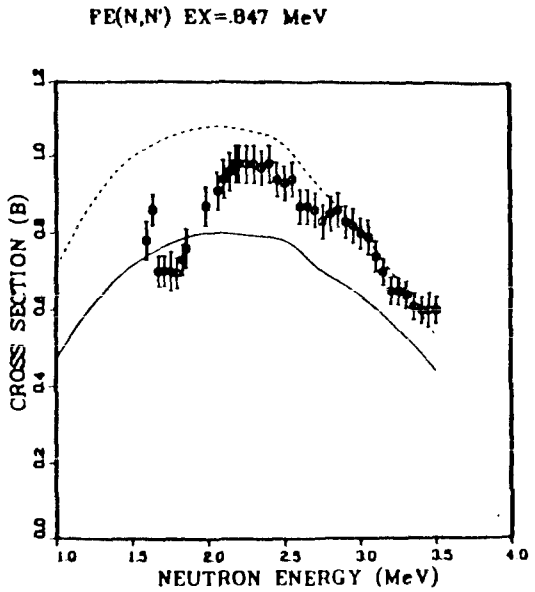

Fig. 1. Compound nucleus calculations of inelastic neutron scattering from the 847-keV state in ^{56}Fe are compared to the data of Smith [8]. The solid curve includes width-fluctuation corrections while the dashed curve does not. No direct-reaction contributions have been included.

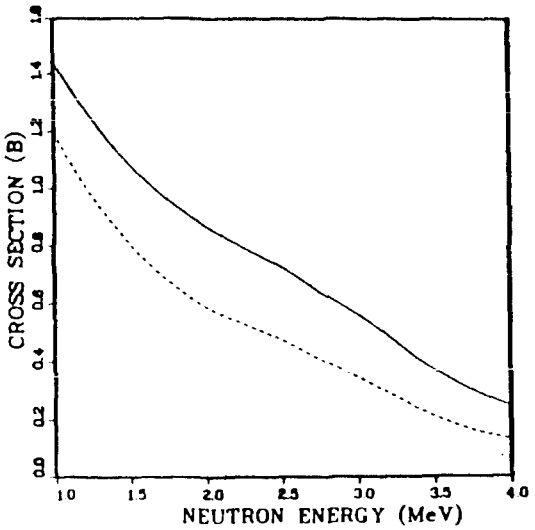

Fig. 2. Compound elastic cross sections calculated for ^{56}Fe with (solid curve) and without (dashed curve) width fluctuation corrections.

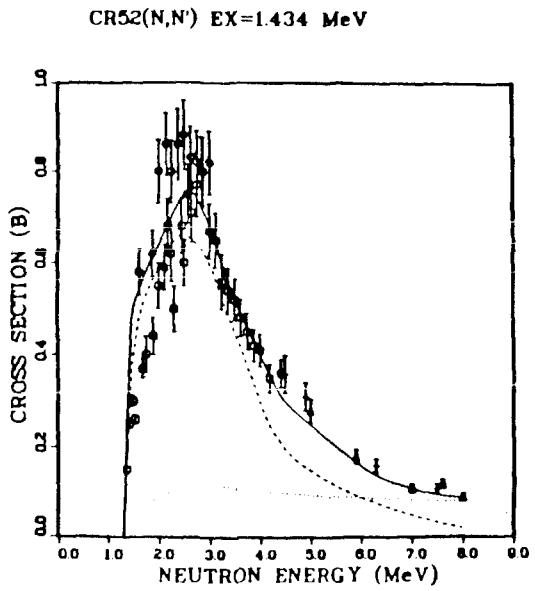

Fig. 3. Calculations by Korzh [11] are compared with data for inelastic scattering on ^{52}Cr. The dashed curve represents width-fluctuation-corrected Hauser-Feshbach results, the dotted curve represents coupled-channel calculations, and the solid curve is the incoherent sum of the two.

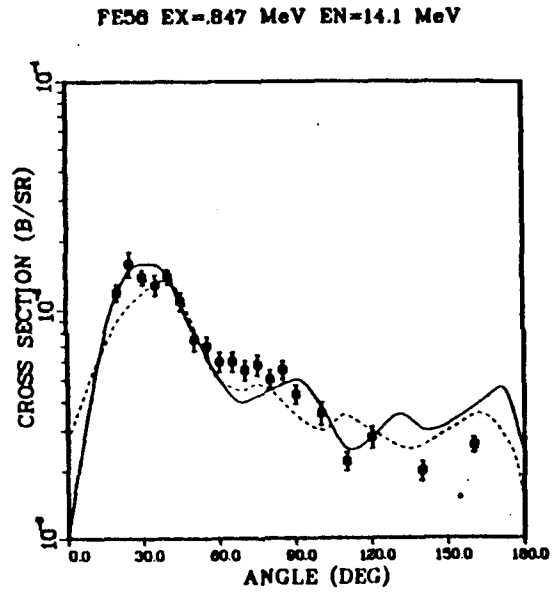

Fig. 4. Calculations of the angular distribution produced by 14.1-MeV inelastic neutron scattering from the 0.847-MeV ^{56}Fe level. The solid curve represents DWBA calculations, while the dashed curve illustrates coupled-channel results.

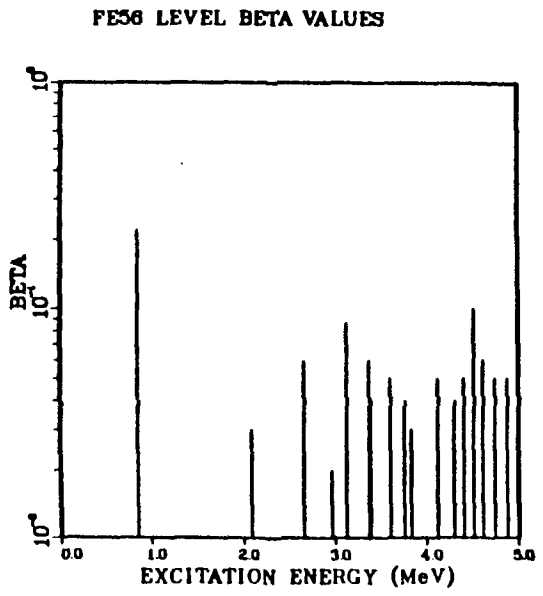

Fig. 5. The distribution of β_ℓ values determined [12] for excited levels of ^{56}Fe.

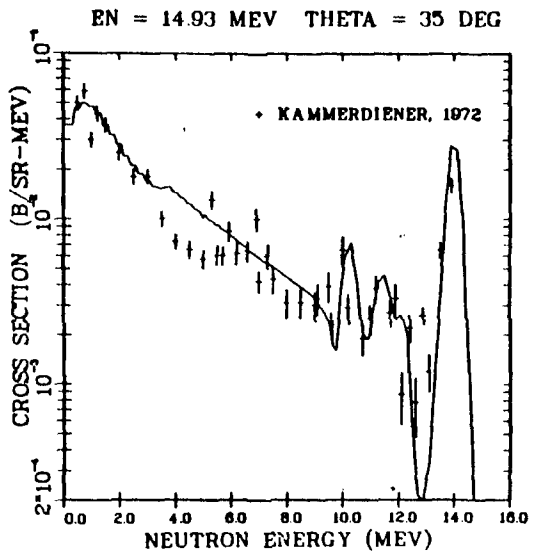

Fig. 6. The calculated [13] neutron emission spectrum produced by 14.9-MeV incident neutrons at an angle of 35° is compared with the Kammerdiener data.

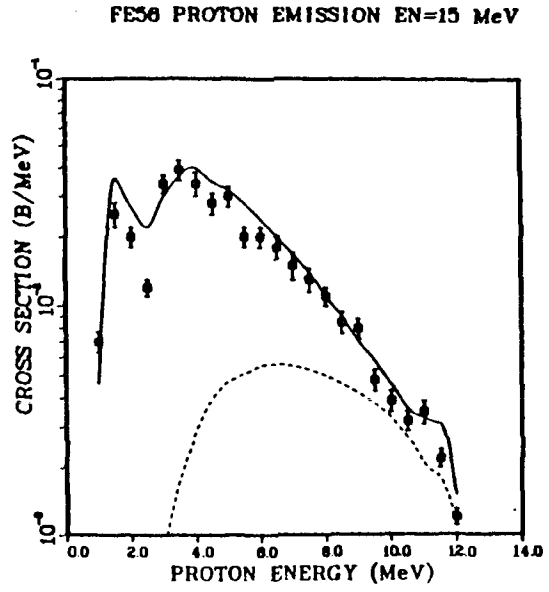

Fig. 7. The calculated proton emission spectrum induced by 15-MeV neutrons on ^{56}Fe is compared with data [16]. The solid curve represents the total emission spectra, while the dashed curve represents preequilibrium contributions.

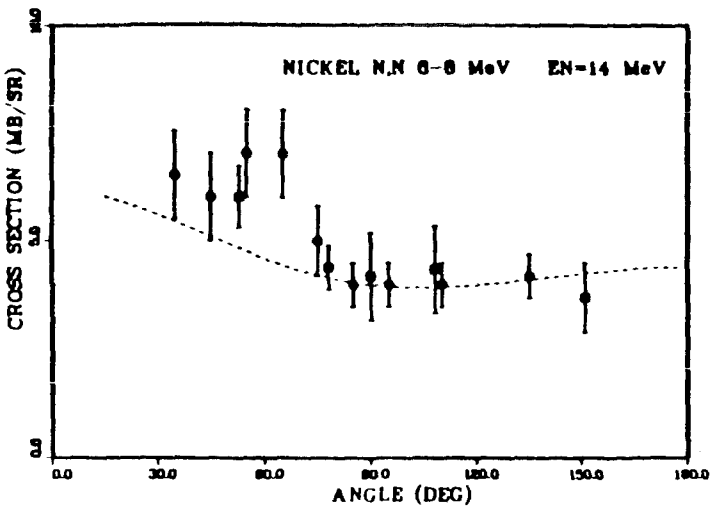

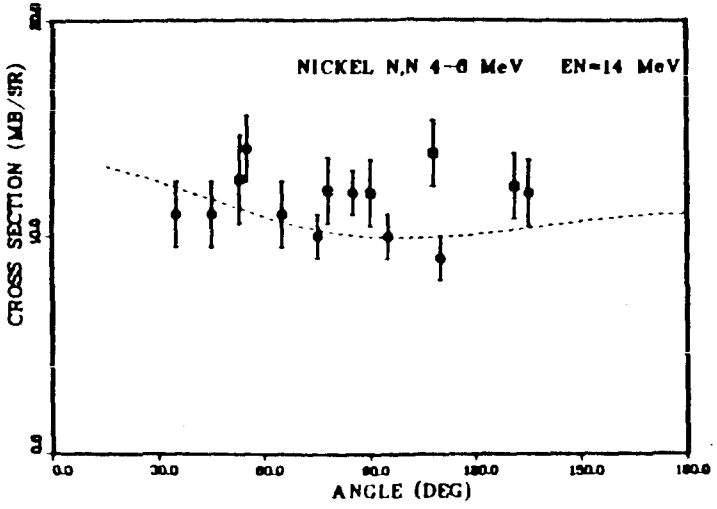

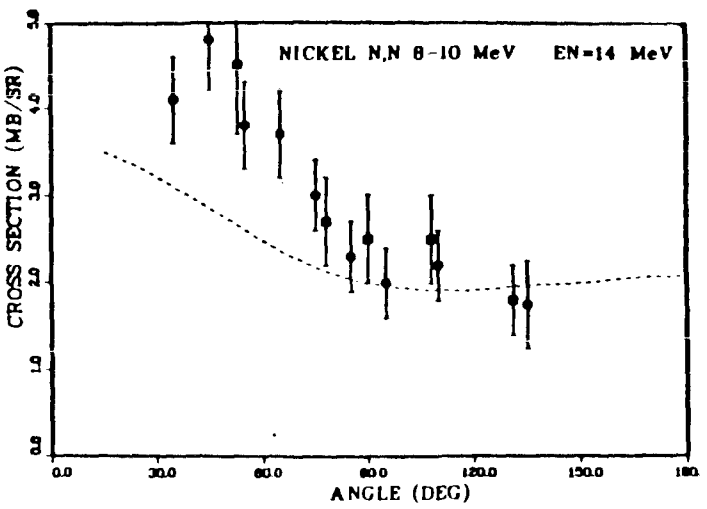

Fig. 8. Angular distributions calculated for three secondary energy groups, using the modified [21] Kalbach-Mann Legendre coefficient expressions are compared with 14-MeV neutron data for natural nickel.

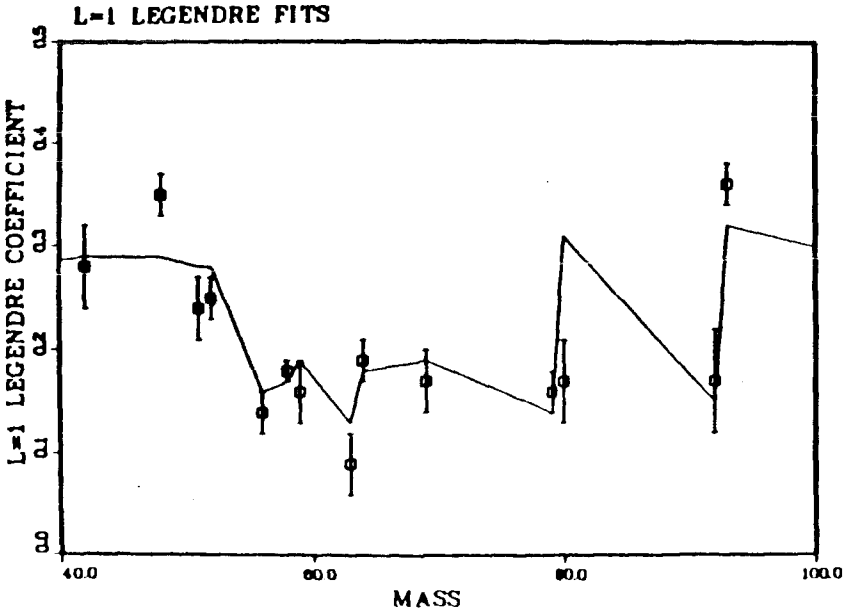

Fig. 9. Values obtained from an analysis by Akkermans et al. [23], using the preequilibrium models described in the text, are compared with $\ell=1$ Legendre coefficient data for 14-MeV neutron reactions.

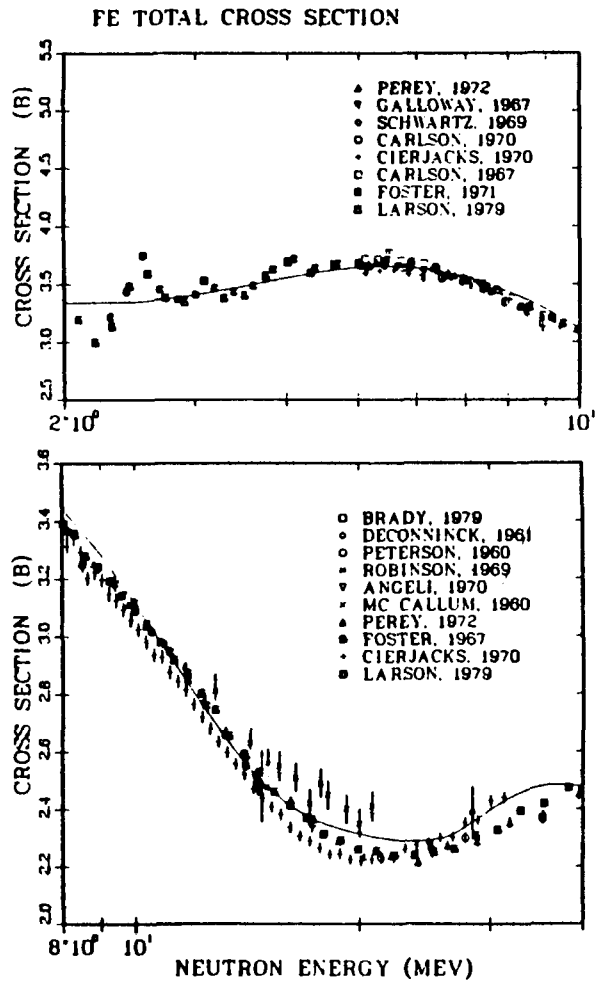

Fig. 10. Total cross sections for iron calculated using the neutron optical parameters of Ref. [13].

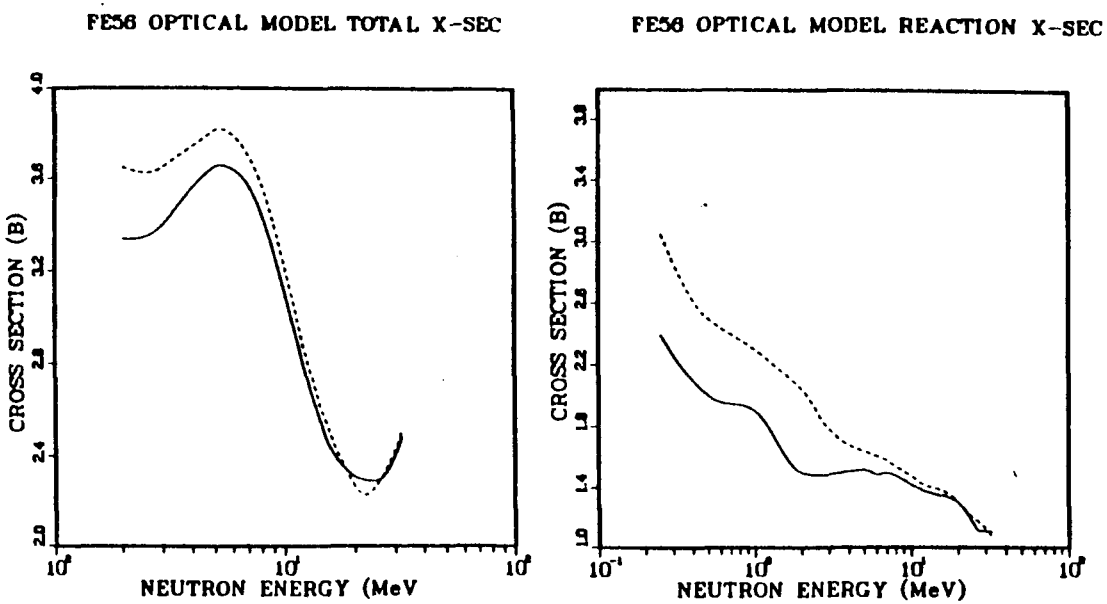

Fig. 11. A comparison of ^{56}Fe total and reaction cross sections calculated using the parameters of Ref. [13] (solid curve) and the Wilmore-Hodgson global optical parameters [33] (dashed curve).

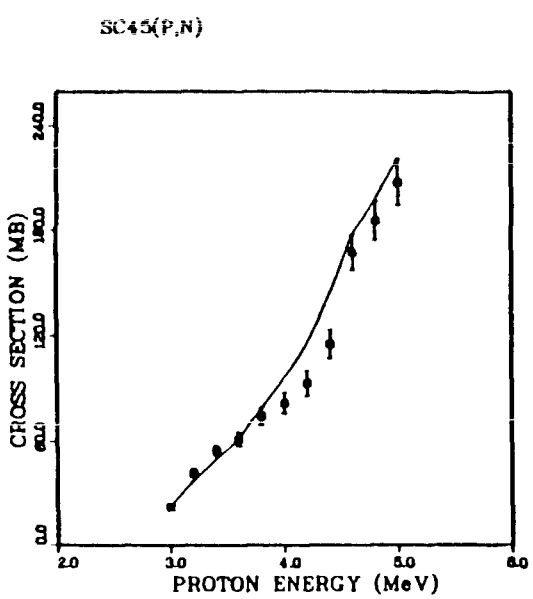

Fig. 12. Verification of the sub-Coulomb behavior of proton optical parameters used in n+^{46}Ti calculations [49] through comparisons with ^{45}Sc(p,n) data [34].

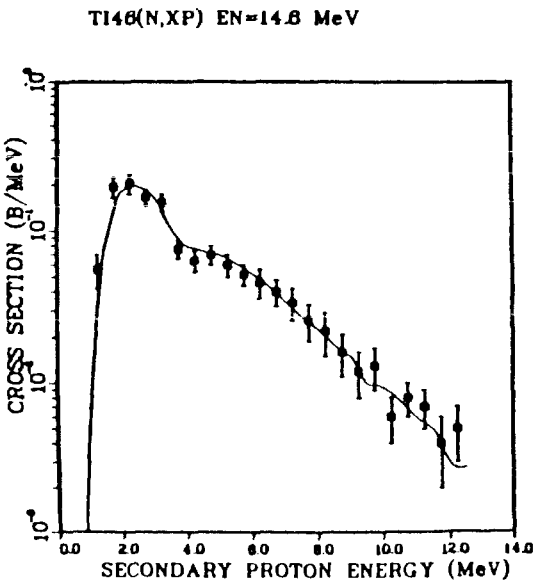

Fig. 13. Comparison of the calculated [49] proton emission spectrum induced by 15-MeV neutrons on ^{46}Ti with data measured by Grimes et al. [35].

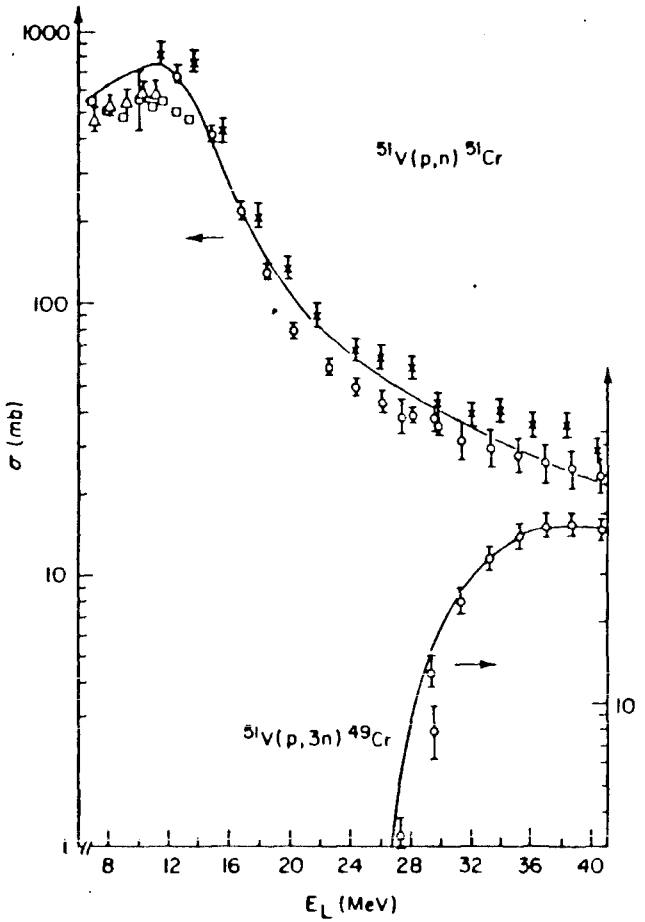

Fig. 14. Calculations of ^{51}V(p,xn) cross sections performed by Strohmaier et al. [30] to verify model parameters used in neutron cross section calculations.

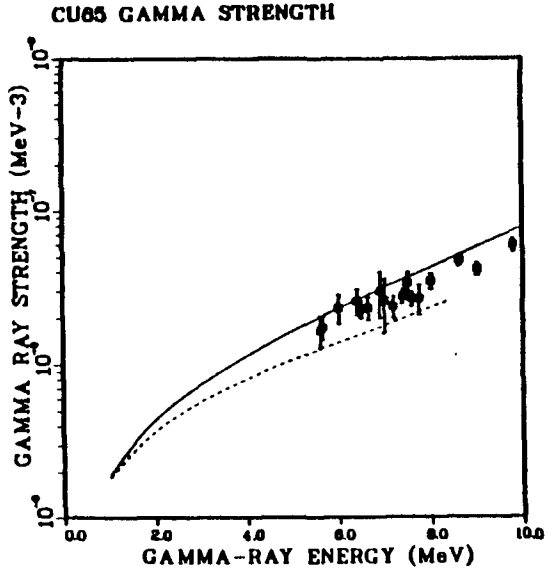

Fig. 15. The gamma-ray strength function (solid curve) calculated using the Gardner energy-dependent Breit-Wigner expressions is compared with measured data [39]. The dashed curve is the strength function normalized to fit a $2\pi \langle\Gamma_\gamma\rangle/\langle D\rangle$ value inferred from systematics.

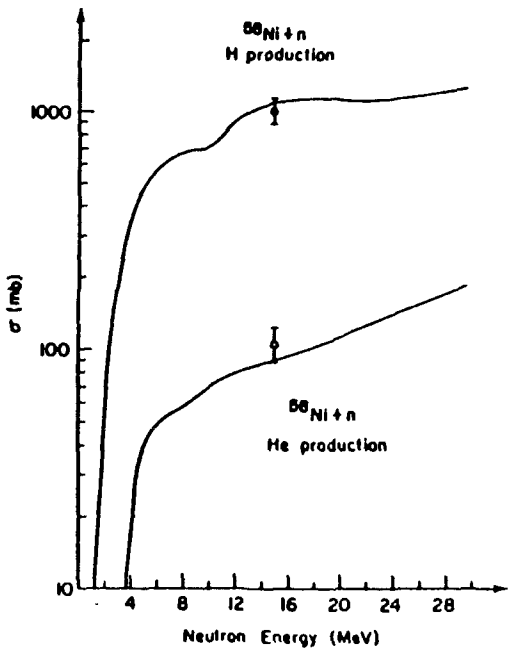

Fig. 16. An example of hydrogen and helium production cross sections calculated by Strohmaier et al. [30] for $n+^{58}Ni$ reactions.

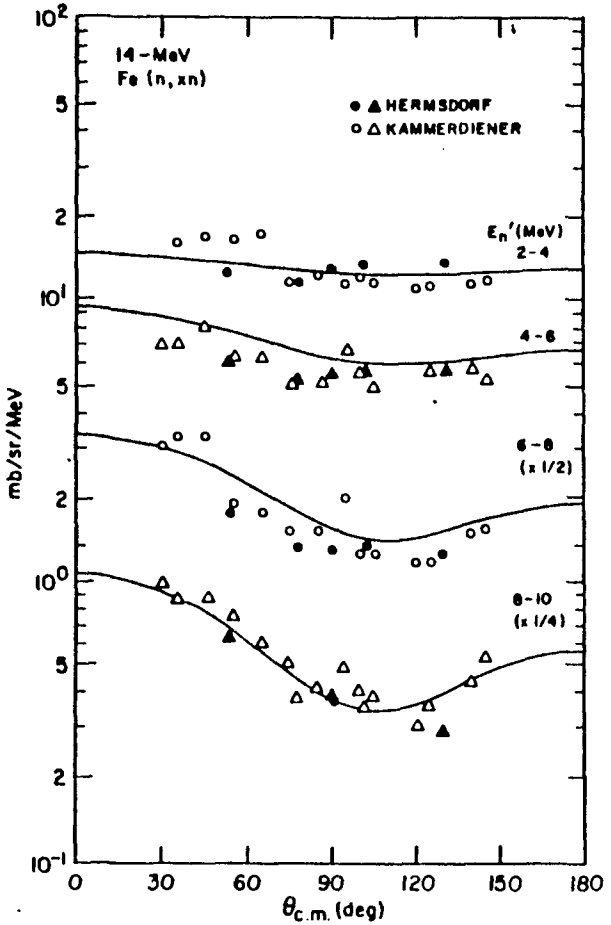

Fig. 17. Angular distributions calculated by Fu using an improved version of the TNG code are compared with data.

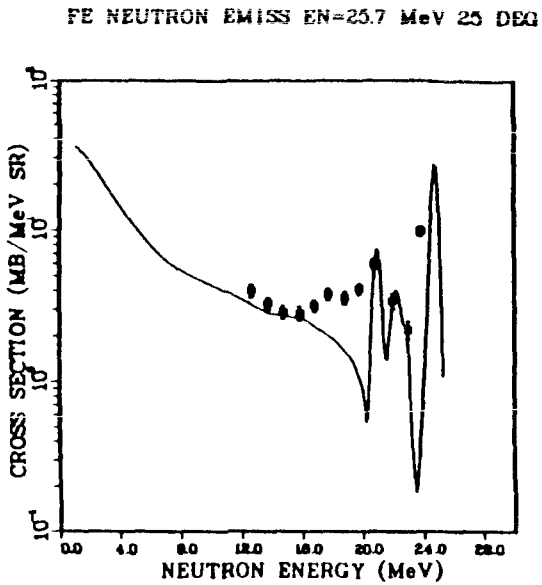

Fig. 18. The calculated 25°-neutron emission spectrum [13] produced by 25.7-MeV neutrons on iron is compared with recent measurements [50].

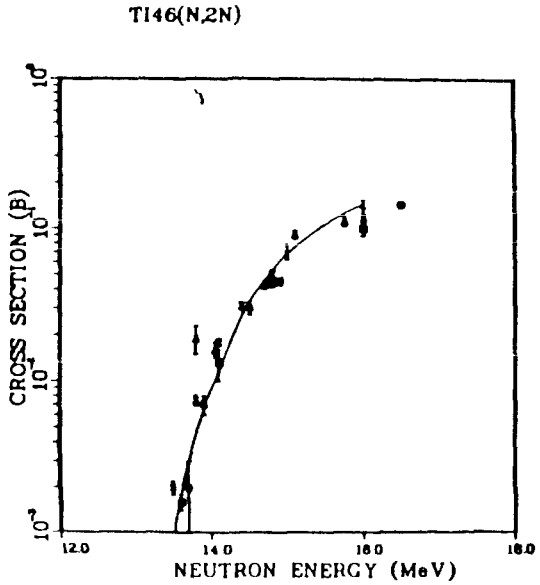

Fig. 19. An example of a GNASH calculation [49] for a minor reaction path, $^{46}Ti(n,2n)$, using the parameter determination and verification techniques described in the text.

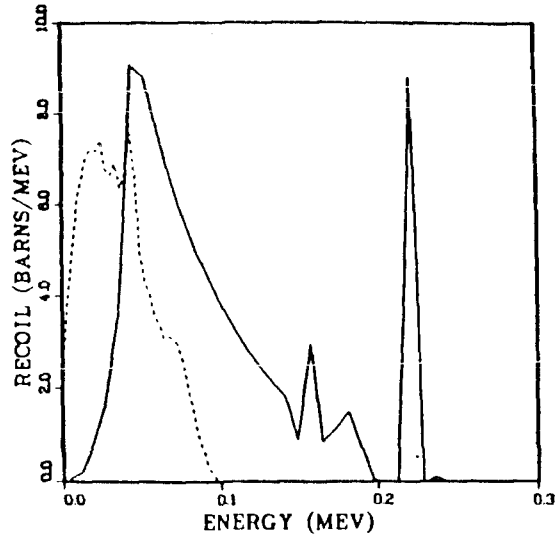

Fig. 20. The recoil energy spectrum calculated for 14-MeV neutrons on iron using the RECOIL code. The solid curve represents elastic and inelastic neutron reactions, while the dashed curve results from the (n,2n) reaction.

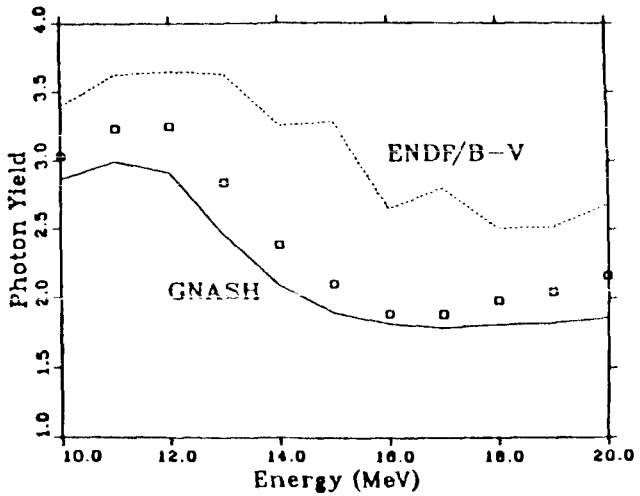

Fig. 21. A comparison of the total gamma-ray yield appearing in the ENDF/B-V evaluation for iron with results calculated in Ref. [13]. The squares indicate yields appearing in Revision 2 of ENDF/B-V [56].

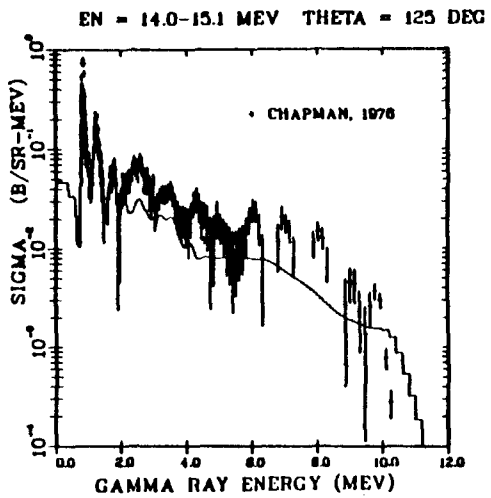

Fig. 22-a. Comparison of the calculated gamma-ray production spectrum induced by 14.5-MeV neutrons on iron with data measured in Ref. [54].

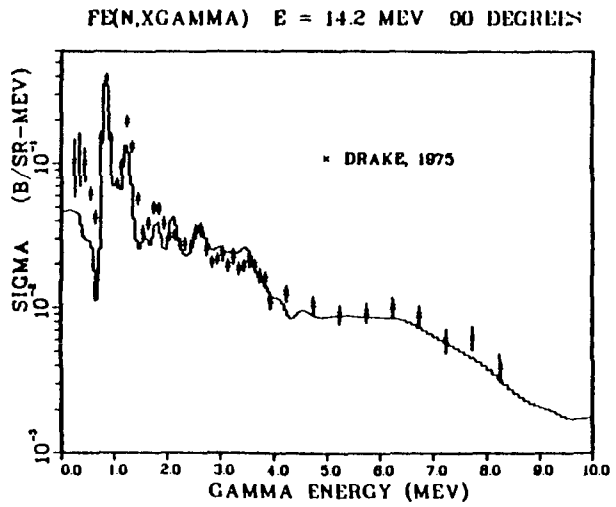

Fig. 22-b. Similar to Fig. 22-a, but here the calculations are compared to data measured by Drake [55].

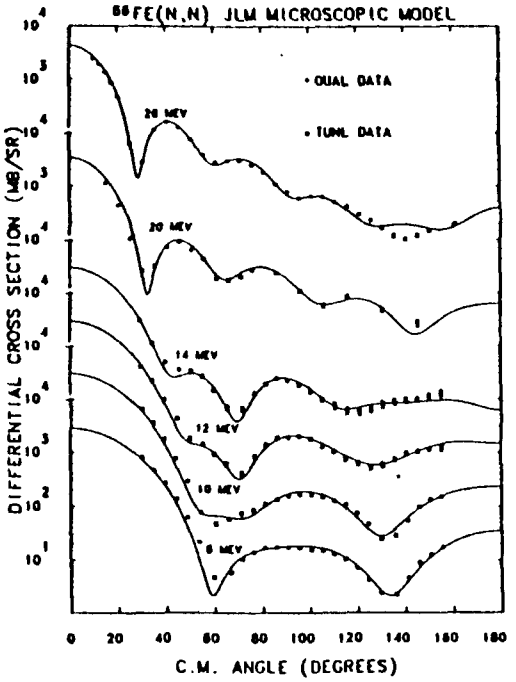

Fig. 23. Comparison of results calculated [62] using the JLM microscopic optical model [57] to data measured at Ohio University [62] and TUNL [64].

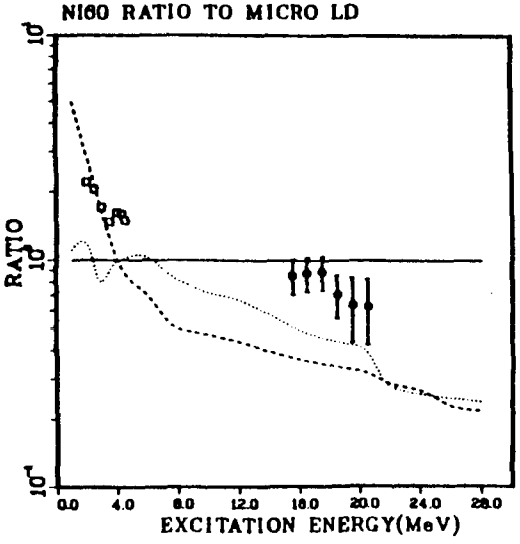

Fig. 24. Level densities calculated with the Gilbert-Cameron (dashed curve) and the back-shifted Fermi gas (dotted curve) phenomenological models are compared to microscopic level density results [71] and data available for ^{60}Ni.

PARTICLE AND γ RAY SPECTRA CALCULATIONS IN STRUCTURAL MATERIAL

G. Reffo

ENEA, CRE "E. Clementel", Bologna, Italy

Abstract

The models, the methods and the results obtained in particle and γ ray spectra calculations for structural material are briefly outlined.

1. γ-ray emission.

1.1. The model and the code

The cascade model adopted has been illustrated in detail in ref. 1,2 and will be described here only briefly. Continuum bands are treated like discrete levels. For each band spin and parity dependent branching ratios are calculated allowing for the competition of E1, M1, E2 transition probabilities which are estimated according to Lorentz curve approximations to the respective giant resonances (GR) and using a Gilbert-Cameron[3] (GC) level density formula, as parameterized in ref. 4.

A split GR model is used for E1 photon absorption, the Lorentzian parameters being taken from the systematics of ref. 4. Parameters for M1 and E2 Lorentz formulae are also taken from systematics[5][6].

The experimental branching ratios are used for discrete levels. Missing ones are estimated assuming single particle state transitions (with E1, M1 transitions dominating) for spherical nuclei and assuming collective transitions (with E2 transitions dominating) for collective nuclei.

These calculations were performed with our modular master code the IDA MODULAR SYSTEM[7]. It is capable of calculating integrated and differential cross sections for all reactions possible up to 50 MeV incident energies including most reaction mechanisms, whatever the projectile. As a particular option γ-ray cascades may be started at any step of the multiple cascading particle emission.

The main effort of the code is on organization. Cascade events are simultaneously ordered in as many different ways as there are purposes of the code i.e. according to a) stories with the same number of steps in the cascade (which allows for calculating cross sections of each γ-ray multiplicity and the corresponding partial spectra); b) cascades feeding levels a priori marked (for calculating excitation cross sections of marked levels, corresponding spectra and isomeric ratios, IR); c) emitted energy bands, where single-step contributions are lumped according to the respective γ-ray energies (for total γ-ray spectra calculations); d) initially a), b), c) are given for any J^{π} couple of the initial decaying level (this can be useful in several investigations e.g. either to isolate a), b), c) for given incident angular

momentum, l, when the initial level is a compound nucleus one; or to estimate a), b), c), for a given Jπ couple; etc.).

1.2. Rôle of relevant parameters

a) Optical model parameters

The optical model affects especially those calculations (like for IR determination) where the population probability of initial levels of given spin plays an important rôle and may be strongly influenced by the relative magnitude of strength functions (see ref. 2).

b) Giant resonance parameters (GRP)

GRP are involved only in the decay of continuum levels, where in most cases only one type (among E1, M1, E2) of transition dominates in each branching ratio. M1 or E2 transitions play their rôle when the other two types are forbidden. As a consequence, Lorentzian curve parameters do not greatly influence these calculations because they all tend to cancel out in the branching ratios, whenever γ-ray energies are smaller than the giant resonance peak energy.

For higher emitted γ-ray energies only peak energy (which is the best known) is expected to affect calculations.

c) Level density parameters

The result of γ-ray cascade calculations greatly depends on the level density and level schemes adopted.

In spite of the encouraging success of recent investigations (especially BCS), the corresponding model parametrizations do not yet offer the same confidence level as the model and the systematics[4] here adopted. The validity of this approach has been recently discussed in ref. 8.

The effect of the spin distribution of level density was tested on ^{241}Am calculations[1], by reduction of the spin cut off factor by a factor of 2. This produced only slight effects with a shift of the spectrum toward the soft part. In addition an increase in IR of 5% was observed.

As far as the low energy region is concerned large difficulties arise where discrete level informations is missing (like energy levels, their quantum characteristics or branching ratios).

In the case of the spectrum for gold we have investigated the impact of the following assumptions: (i) all known levels (28, at all, up to .571 MeV) are neglected, and replaced by the level density treatment; (ii) all discrete levels have been included, but experimental branching ratios are replaced by theoretical estimates according to sec. II.

The resulting spectra, dashed and dotted histograms, respectively, are given in fig. 1 together with the result of the standard calculation, ful line.

As can be observed from the figure, hypothesis i) is much too crude and introduced severe changes in the energy

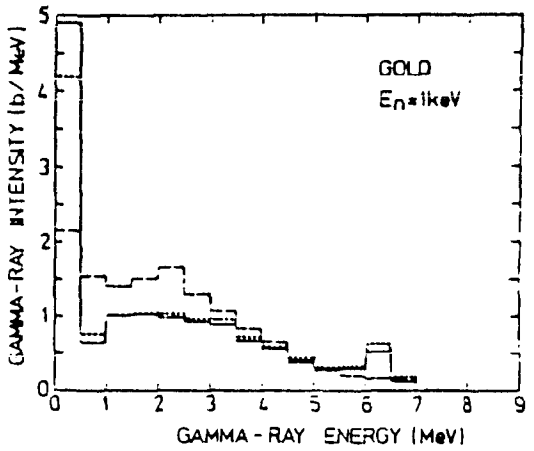

Fig. 1

trend of the spectrum. On the contrary hypothesis ii) does not appreciably influence the final result.

The influence of the discrete level scheme on isomeric ratio calculations (here = $\sigma_g(n,\gamma)/\sigma(n,\gamma)$ has been investigated in ^{241}Am[2] at 30 KeV, where a value IR =.75 is obtained from standard calculations.

Skipping half of the discrete levels we got IR =.69, while, by skipping the complete level scheme we obtained IR=.5.

No significant difference was observed through replacing E2 collective transition probabilities by E1, M1 single particle transition probabilities.

d) Effect of width fluctuations

It was assumed that width fluctuations effects influence only the primary γ-ray spectrum. An investigation of the width flectuation correction on the primary γ-ray spectrum leads to the conclusion that (exception made for very weak transitions, which are strongly enhanced) single transition probabilities are affected by correction factors very close to that of the corresponding integral cross section.

Thus the whole primary spectrum is uniformly shifted by width fluctuation correction factor.

e) Energy dependence of γ-ray intensities

Essentially one has three types of energy dependences for E1 transitions:

i) E_γ^3, according to Blatt-Weisskopf single particle transitions.

ii) E_γ^5, according to Axel.

iii) E_γ^7, according to Dover et al.[9], Arenhovel et al.[10], Gardner et al[11].

Recently McCullagh et al.[12] found experimental evidence for an $E_\gamma^{5.5}$ energy dependence, while Raman[13] verified that the validity of the Brink-Axel hypothesis has only a few exceptions.

The impact of the above three assumptions has been investigated in the total spectrum calculation of gold where measurements are available from ref. (14). To this end fig. 20 of ref. (11) is here reproduced as fig. (2), where we have plotted, for comparison, our results (hystograms).

The data in fig. 2 correspond to the following incident neutron energies: the experimental ones are measured in the interval .2÷6. MeV, the two full line curves have been

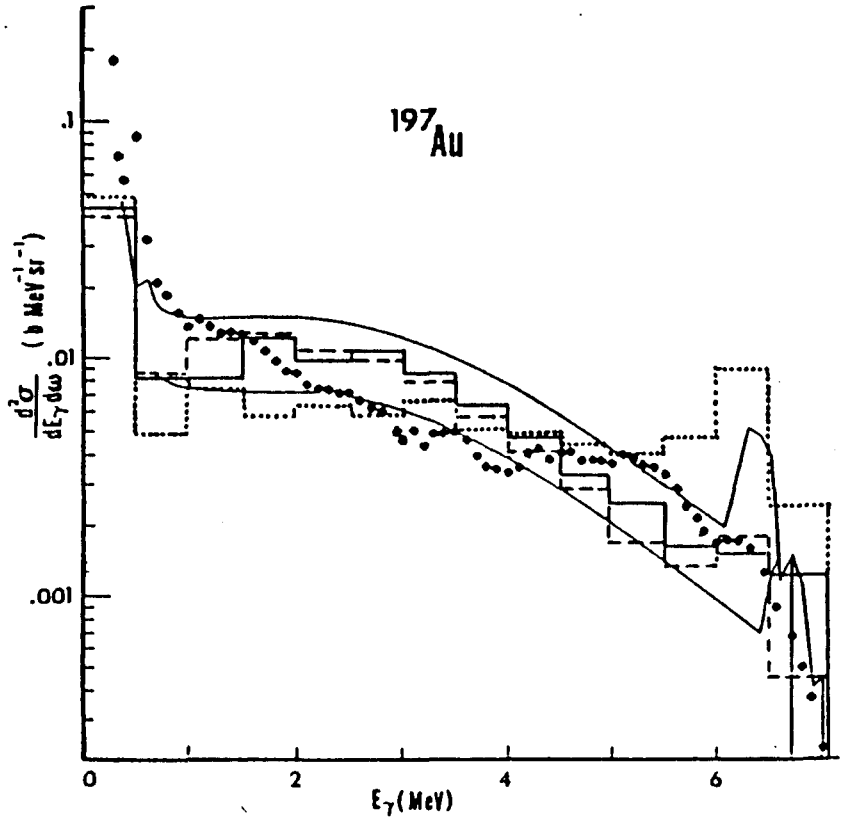

Fig. 2

calculated[11] at .2 and .6 MeV, respectively while the hystograms at .4 MeV. (It should be noted that the spread of neutron energies, ΔE=.4 MeV, may affect the comparison of present calculations especially in the last hystogram step).

One observes that the spectrum from our E_γ^5 -calculation, full line hystogram, well agrees with the Gardner et al[11] spectrum, except for the hard part. This seems in contradiction with the wrong trend of the E_γ^7 - calcolation (dotted hystogram) which clearly favours the hard tail against the soft one, as expected.

Except for the hard tail of the spectrum, no remarkable difference is observed between E_γ^5 - and E_γ^3 - calculations (dashed hystogram).

On the whole, one may conclude on the better results of the E_γ^5 - law, in agreement with the mentioned experimental investigations of refs (12) and (13).

As far as M1 and E2 transitions are concerned, there is not sufficient information for a more than tentative treatment.

Finally, it must be noted that only the Brink-Axel approach allows for absolute calculations of $\Gamma_\gamma(B_n,J,\Pi)$, as shown in refs. (15), (16), provided correct parametrization is adopted for both the level density and Lorentz-curve.

1.3. γ-decay calculations in structural material. The rôle of E1 and M1 transitions and of Valence mechanism

In the literature, in general, one assumes that E1 transitions dominate the γ-ray decay of composite systems. Here we have selected some structural materials of interest in reactor technology, where the necessity of accounting also

for M1 transitions is shown by means of detailed model calculations. The rôle of Valence reaction mechanism in also illustrated by few examples.

We have estimated the E1 and M1 contributions to the total and partial average radiative widths and to the average total γ-ray spectra following s-, p-, d-wave neutron capture in the resonance region of ^{58,60}Ni and ^{56}Fe.

The adopted parameterization is shown in table 1. the level schemes adopted were taken from ref. 17, while missing γ-ray branching ratios of discrete levels were estimated by means of the well known Weisskopf transitions probabilities. Level density parameterization was done according to ref. 3.

M1 transition probabilities were estimated in terms of a giant resonance model the parameterization of which was determined (see table 1) by normalization of the strength to the systematics of ref. 6.

Calculated average total E1 and M1 radiative widths are shown in table 2 for the various ℓJ^{π} quantum numbers involved in the respective resonance regions of ^{58,60}Ni and ^{56}Fe. The effective number of degrees of freedom of the lumped χ^2 distributions are also given in order to quantify the size of the statistical fluctuations characterizing the various calculated as well as measured radiative widths.

table 1

Summary of adopted parameters for the calculation of level densities and radiative widths.

Model param. / Isotope	a MeV^{-1}	U_x MeV	T MeV	B	σ^2	D_{OBS} keV	E_1 MeV	Γ_1 MeV	σ_1 mb	E_2 MeV	Γ_2 MeV	σ_2 mb	E_{M1} MeV	Γ_{M1} MeV	σ_{M1} mb
^{58}Ni	7.32	8.2	1.31	.17	7.3	14.	16.0	3.7	53	18.6	5.1	75	11.8	2.36	10.6
^{60}Ni	8.4	7.3	1.2	.17	4.5	14.	16.0	3.7	55	18.4	5.1	78	11.7	2.34	11.0
^{56}Fe	8.52	6.9	1.14	-.25	5.1	19.	17.5	4.8	77	21.4	4.95	39	12.0	2.4	10.3

table 2

Calculated average E1 and M1 contributions to the total radiative width for s-, p- and d- wave resonances compared to results evaluated from experimental data.

isotope	ℓ	J^{π}	$\bar{\Gamma}_\gamma$(E1)	ν_{eff}	$\bar{\Gamma}_\gamma$(M1)	ν_{eff}	$\bar{\Gamma}_\gamma^{EXP}$	Ref.	ν_{eff}^{EXP}
^{58}Ni	0	$\frac{1}{2}^+$	2200±883	12	113±38	17			
	1	$\frac{1}{2}^-$	766±244	20	456±234	8			
		$\frac{3}{2}^-$	726±230	20	380±153	12			
	2	$\frac{3}{2}^+$	1823±602	18	106±36	18			
		$\frac{5}{2}^+$	1387±444	20	97±32	18			

table 2 continues

Isotope	ℓ	J^π	$\bar{\Gamma}_\gamma$(E1)	ν_{eff}	$\bar{\Gamma}_\gamma$(M1)	ν_{eff}	$\bar{\Gamma}_\gamma^{EXP}$	Ref.	ν_{eff}^{EXP}
^{60}Ni	0	$\frac{1}{2}^+$	1050±420	12	59±21	16	1300±70	[18]	
	1	$\frac{1}{2}^-$	443±148	18	208±98	9	1200	[18]	
		$\frac{3}{2}^-$	401±132	19	190±69	15			
	2	$\frac{3}{2}^+$	1109±353	20	53±18	17			
		$\frac{5}{2}^+$	896±268	22	45±15	18			
^{56}Fe	0	$\frac{1}{2}^+$	1070±428	11	34±12	15	850±410	[19]	9.6
	1	$\frac{1}{2}^-$	246±87	16	203±97	9	500±180	[19]	17.1
		$\frac{3}{2}^-$	231±75	19	162±64	13			
	2	$\frac{3}{2}^+$	900±313	17	32±11	18	730±250	[19]	18.5
		$\frac{5}{2}^+$	652±224	17	25± 8	18			

On the whole a good agreement, within statistical fluctuations, is obtained between the calculated and experimental quantities given in table 2.

In table 3 we quote the calculations for one well known s-wave resonance E_λ for each isotope considered. For each resonance the total as well as the partial radiative width for the transitions to the first two excited level of energy E_μ are given. Γ_γ^0 is the reduced neutron width.

table 3

Calculated partial and total gamma widths for s-wave resonances. Quoted uncertainties are the standard deviation of the respective statistical χ^2 distributions.

Isotope	E_λ (kev)	E_μ (keV)	Γ_λ^o (eV)	$\Gamma_\gamma^{C.N.}$ (meV)	Γ_γ^{VAL} (meV)	Γ_γ^{TOT} (meV)	Γ_γ^{EXP} (meV)	Ref.
^{58}Ni	15.4		9.19	2200±40%	62	1745±50%	1530±7%	[20]
		0		340	35	150	124±17	[21]
		465		305	18	176	110±19	[21]
^{60}Ni	12.3		23.98	1050±40%	127	1670±50%	2920±7%	[20]
		0		178	60	444	514±72	[21]
		283		150	57	380	289±46	[21]
^{56}Fe	27.7		8.72	1070±40%	145	650±50%	1090±5%	[10]
		0		183	12	103	145±25	[21]
		14		182	71	26	35±13	[21]

For the valence mechanism we found a negligible M1 contribution, but an E1 contribution which seems to affect rather significantly the total radiative width Γ^{TOT}, provided an interference term is accounted for

$$(\Gamma_{\gamma_{\lambda\mu}}^{TOT})^{1/2} = (\Gamma_{\gamma_{\lambda\mu}}^{CN})^{1/2} + (\Gamma_{\gamma_{\lambda\mu}}^{VAL})^{1/2}$$

The valence model adopted, namely is the one by Lane-Mughabghab (22) according to the specifications in ref. 23.

Percentual error quoted with calculated quantities are the standard deviations of the corresponding χ^2 lumped distribution.

$$S.D. = \sqrt{2/\nu}\ \langle \Gamma \rangle$$

ν being the effective number of degrees of freedom.

As an example, in fig. 3 , the average compound nucleus total γ-ray spectrum (full line) and separately only the E1 contribution (dashed line) are given for ^{58}Ni in the resonance region.

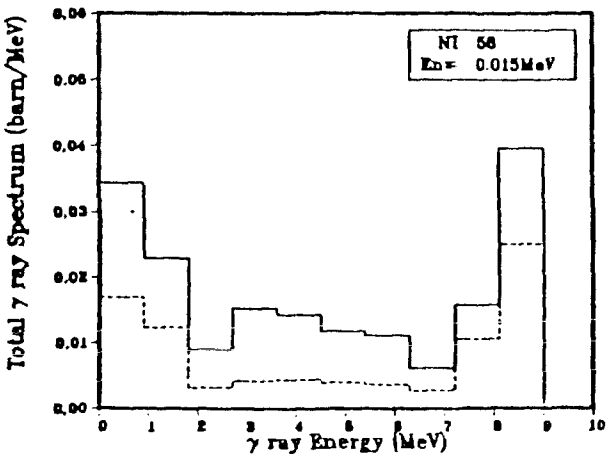

Fig. 3

In fig. 4 again for the same case, the different shapes are shown of the s-(full line) and p-wave spectra (J=1/2, =3/2 dotted and dashed line, respectively). Due to the parity selection rules of γ-ray transitions the s- and d-spectra are dominated by E1 transitions, while the p-spectrum by M1 ones.

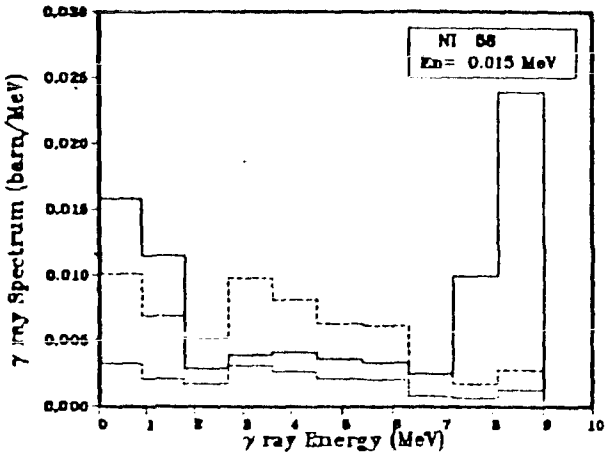

Fig. 4

1.4. Importance of valence mechanism in neutron capture

Becouse valence mechanism mostly affect the resonance region, the effects of valence mechanism in neutron capture are to be considered also dealing with average cross sections.

In order to illustrate the subject, the case of ^{86}Kr has been chosen becouse, differently from the structural materials, for this isotope one has the availability of recent measurements for the average cross section of neutrons with maxwellian energy distributions peaked at 30 KeV:

$\langle \sigma_{n,\gamma} \rangle = (5.6 \pm .7)$ mb [24] ; $\langle \sigma_{n,\gamma} \rangle = (4.6 \pm .7)$ mb [25] ;

$\langle \sigma_{n,\gamma} \rangle = (4.8 \pm .1.2)$ mb [26] .

In addition ^{86}Kr neutron resonance characteristics are also available from ref. 26.

All these experimental information makes possible the study of ^{86}Kr KeV neutron capture to test the validity and

the role played by compound nucleus and valence capture mechanisms.

In Table 4 a selection, out of ref. 26, is reported for the ^{86}Kr neutron resonances of known characteristics.

Table 4. Experimental and calculated neutron resonance characteristics in ^{86}Kr.

E_n	J^π	$g\Gamma_n$	$^{EXP}\Gamma_\gamma^{J\pi}$	$\langle {}^{EXP}\Gamma_\gamma^J \rangle_\ell$	$\langle {}^{STAT}\Gamma_\gamma^J \rangle_\ell \pm S.D.^\nu$ M1,E1	$^{VAL}\Gamma_\gamma^J$ M1,E1	$^{TOT}\Gamma_\gamma^{J\pi}$
36.93	$\frac{1}{2}^+$	53	300±80	250±80	200 ± 80^{10}	40	240±80
42.91	$\frac{1}{2}^-$	125	390±100	360±100	340 ± 200^{6}	20	360±200
49.64	$\frac{1}{2}^+$	42	200±60	250±80	200 ± 80^{10}	15	215±80
54.37	$\frac{3}{2}^-$	402	550±150	550±150	390 ± 200^{8}	210	600±200
28.86	$\frac{1}{2}^-$	95	330±120	360±120	340 ± 200^{6}	15	355±200

In the columns from left to right one has the resonance energies E_n; the quantum characteristics J^π; the neutron widths, $g\Gamma_n$; total measured radiative widths $^{EXP}\Gamma_\gamma^{J\pi}$; average s-and p-wave total experimental radiative widths per spin state $\langle {}^{EXP}\Gamma_\gamma^J \rangle$; average s-and p-wave total radiative widths per spin state $\langle {}^{STAT}\Gamma_\gamma^J \rangle_\ell \pm$ S.D.$^\nu$ calculated in terms of Brink-Axel model for compound nucleus radiative decay[4], inclusive of M1 and E1 transitions, S.D. being the standard deviation of the lumped χ^2 distribution of all partial widths and ν the inherent number of degrees of freedom; total valence contribution as a sum of E1 and M1 contributions $^{VAL}\Gamma_\gamma^J$; total calculated radiative width $^{TOT}\Gamma_\gamma^J$ as a sum of valence and compound nucleus contribution (both E1 and M1 transitions included), without interference effect.

In order to determine the expectation value of the n,γ cross section at 30 KeV the usual Hauser-Feshbach theory with width fluctuation correction has been used. This was parameterized using the mean spacing of s-wave resonances, D_{OBS} = (40±14) KeV, deduced from the complete set of data of ref. 26 and normalizing the calculated $\Gamma_\gamma^{J\pi}$ to the corresponding average values in column 5 (see Table 4). It is important to note here that the adopted values for D_{OBS} is in perfect agreement with the local systematics of the level density parameter "a" deduced for the families of Kr, Se, Br isotopes.

So far the value which can be obtained in terms of statistical model is $\langle \sigma_{n,\gamma}$ (30 KeV)$\rangle$= 20 mb, 4 times greater than experimental ones.

The idea to overcome the discrepancy found by assuming a valence contribution comes from the large value ρ=.94 of the correlation coefficient between the measured values for Γ_n and Γ_γ. In particular, from the comparison of experimental and calculated quantities in table 4 one can

see that the large Γ_γ^{EXP} observed at 54.37 KeV comes from the large E1 valence transitions correlated to the large Γ_n values. Differently, the fluctuations observed for the Γ_γ^{EXP} of the other quoted resonances mostly are denominated by statistical fluctuations according to the very low number of degrees of freedom characterizing the lumped width distribution in all cases, see Column 6. The very good overall agreement between columns 4 and 7 suggets that the appropriate average $\langle \Gamma_\gamma^{J\pi} \rangle$ values to be used in capture calculations are just the Brink-Axel model ones[4] quoted in column 6, without any normalization to the experimental ones.

One finds that at 30 KeV the valence contribution to neutron capture is negligibe because it affects only a few channels feeding the lower lying levels in ^{87}Kr, out of the bulk of all other innumerable statistical channels.

On the contrary the compound nucleus contribution dominates and is so found to be $\langle \sigma_{n,\gamma}$ (30 KeV)$\rangle = (8 \pm 2.7)$ mb, the quoted uncertainty being due to that of D_{OBS}, according to error propagation.

2. NEUTRON EMISSIONS

2.1. The models and the code

Careful studies of the neutron induced reactions at 14-15 MeV on structural material are requested as a part of fusion neutronic. A few model calculations on ^{56}Fe, ^{93}Nb, ^{59}Co performed in this contest, are here presented. The rôle of equilibrium and preequilibrium emissions and the limits and validity of the model are illustrated.

Our results are obtained improving the unified exciton model extensively described in ref. 27,28 by the introduction of the principle of conservation of total angular momentum. This, also, implied the use of a suitable particle-hole spin dependent level density.

Since one can show that the master equations as well as the methods of ref. (27), still apply, then the new occupation probability $q^{J\pi}(n,\Omega,t)$ of the composite nucleus state (n,Ω,J,π) (where n and Ω are the exciton number and the direction of the projectile inside the nucleus, and J and π denote the total angular momentum and parity of the composite nucleus at time t) can be expressed as a Legendre polynomial series:

$$q^{J\pi}(n,\Omega,t) = \sum_\ell \eta_\ell^{J\pi}(n,t) P_\ell(\Omega) \quad .$$

The time-integrated master equation is then given by:

$$-\eta_\ell^{oJ\pi}(n) = \mu_\ell \lambda^+(n-2)\, Z_\ell^{J\pi}(n-2) + \mu_\ell \lambda^-(n+2)\, Z_\ell^{J\pi}(n+2)$$

$$-\left[w^{J\pi}(n) + \lambda^+(n) + \lambda^-(n) + (1-\mu_\ell)\lambda^o(n) \right] Z_\ell^{J\pi}(n)$$

the λ^+, λ^- and λ^o are the intranuclear transition rates and w is the total emission rate.

Here whe assume J-independent transition rates, but this generally adpted assumption must be reconsidered.

The μ_ℓ are the eigenvalues of the intranuclear scattering Kernel, $\eta^0_\ell(n)$ refers to the Legendre coefficients of the initial (t=0) occupation probability, and $Z^{J\Pi}_\ell(n)$ are the Legendre coefficients of the mean lifetime of the nuclear state (n,Ω,J,Π).

The double differential cross section including equilibrium and preequilibrium emission is

$$\frac{\delta^2\sigma(a,b)}{\delta\varepsilon\delta\Omega} = \frac{\lambda^2\Pi}{(2s_a+1)(2I+1)} \sum_{J\Pi j_a \ell_a} (2J+1)\, T_{\ell_a j_a}(\varepsilon_a) \sum_n W^{J\Pi}_b(n,\Omega)\, \tau^{J\Pi}(n,\Omega)$$

where $T_{\ell_a j_a}(\varepsilon_a)$ are the optical model trasmission coefficients J and I denote the composite and target nucleus total angular momentum respectively, ℓ_a, s_a and j_a are the orbital angular momentum, spin and total angular momentum of incident particle, $W^{J\Pi}_b(n, \varepsilon_b)$ is the probability of emission of particle b with energy ε_b from the exciton state (E,n,J,Π) $\tau^{J\Pi}(n,\Omega)$ is the mean lifetime of this state and n run over all possible exciton configurations.

A particular mention must be devoted to the J dependent p-h level density involved in the model.

Namely a Williams' formula[29] was adopted, normalized to reproduce the total level density observed according to ref. 30.

Following ref. (31) the distribution of the p-h states on the spin projection M was assumed to be of a Gaussian type. An exciton dependent spin cut off was found[31], $\sigma_n = .28n\, A^{2/3}$valid through the whole periodic table.

Calculations are performed with the modular master Code IDA above mentioned[7]. Sferical optical model transmission coefficients are used. On option, self consistent calculations in generalized optical model approximation may also be requested. Up to four subsequent particle emissions are allowed followed by a γ-ray cascade of maximum multeplicity 7. Integral or double differential cross sections can be calculated for any single emission process, as well as total spectra and angular distribution for any given emission type; the unified model[27] with conservation of total angular momentum is used for the description both of equilibrium and prequilibrium emissions.

The master code consists of modules, one for each step of the calculation procedure, from neutron resonance statistical analysis and from optical model parameter automatic search to the more sophisticated calculations, like isomeric cross sections in a multiple particle emission reaction and to the data management and graphical display.

The whole calculation is completely automatitized. Where no particular check is necessary against available experimental data, thanks to a shared nuclear data library, only Z,A energy and projectile are sufficient to get the complete information allowed by the system.

Calculations were performed using the neutron optical model of ref. 32.

In the figs.5-10, the contribution of the unified model

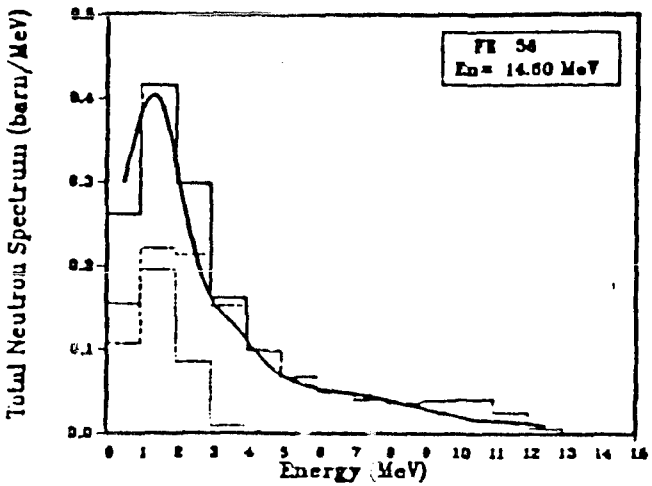

Fig. 5

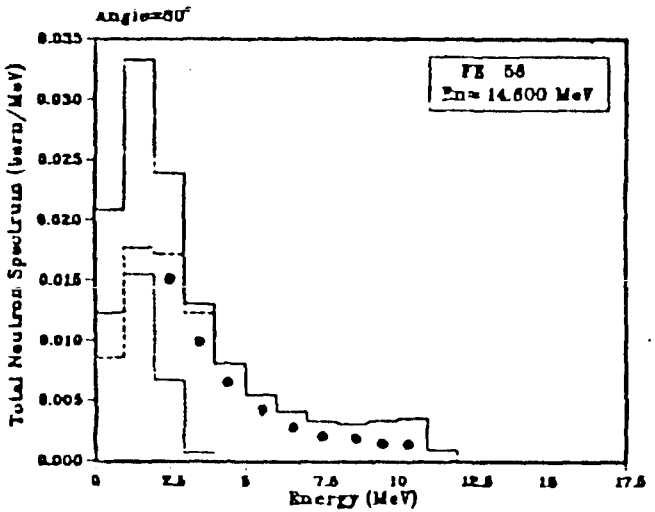

Fig. 7

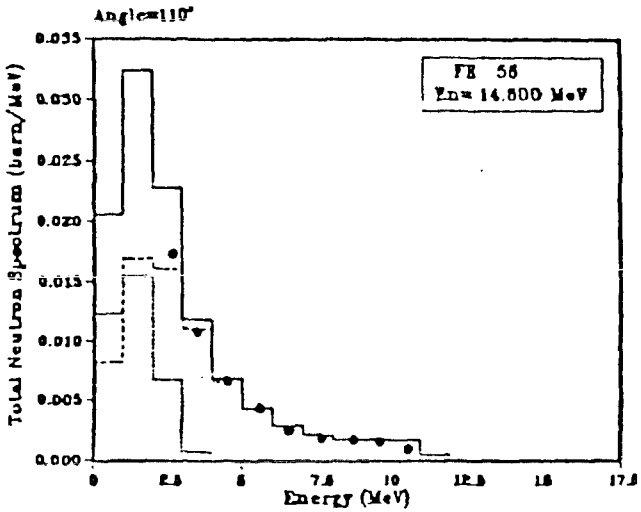

Fig. 9

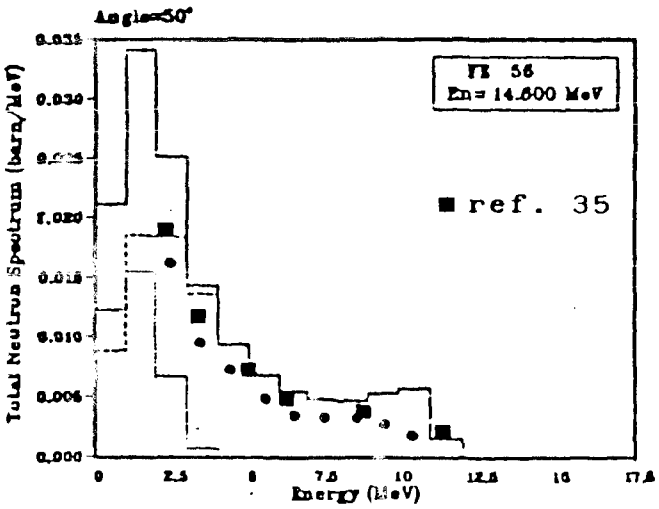

Fig. 6

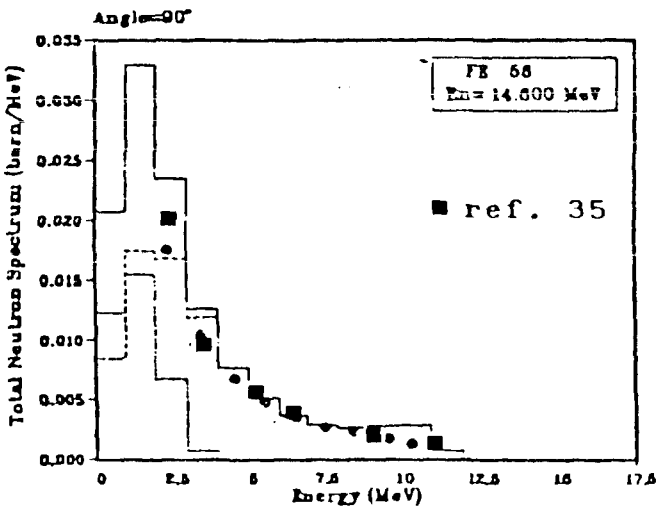

Fig. 8

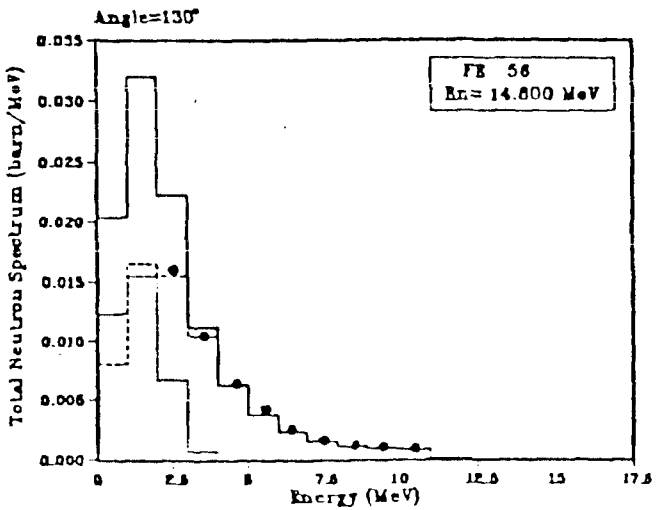

Fig. 10

to equilibrium and preequilibrium emissions (namely the primary emissions) and of all the energetically possible secondary equilibrium emissions according to Hauser-Feshbach theory are the dashed and dotted hystograms respectively. The sum of the two contributions gives the total neutron emission spectrum, full line hystogram.

In fig. 5 the calculated total spectrum is compared to an average spectrum, full line curve, obtained averaging over all experimental data available. Here the model appears to overestimate the hard tail of the spectrum, where lower exciton state emissions are expected to dominate.

In figs.5 to 10 che total spectrum at different angles is given, the dots representing the measurements of ref. 33. In these figures one observes an agreement between the calculated and experimental spectra which is very good at backward angles while worsening at forward angles, again where the lower exciton contributions are involved.

The consistent answer obtained from the comparison of total and partial spectra, seems to suggest a wrong exciton dependence at the adopted p-h level density. (Really all statistical assumptions underlying Williams' formula breakdown at low exciton numbers, where more appropriately combinatorial calculations should be used).

In fig.11 we show the results of the angular distribution of the neutrons with energy E = 2-3 MeV (where equilibrium emissions dominate) and of the neutrons with energy E=8-9 MeV (where preequilibrium emissions dominate). Here a level density from combinatorial calculations has been used.

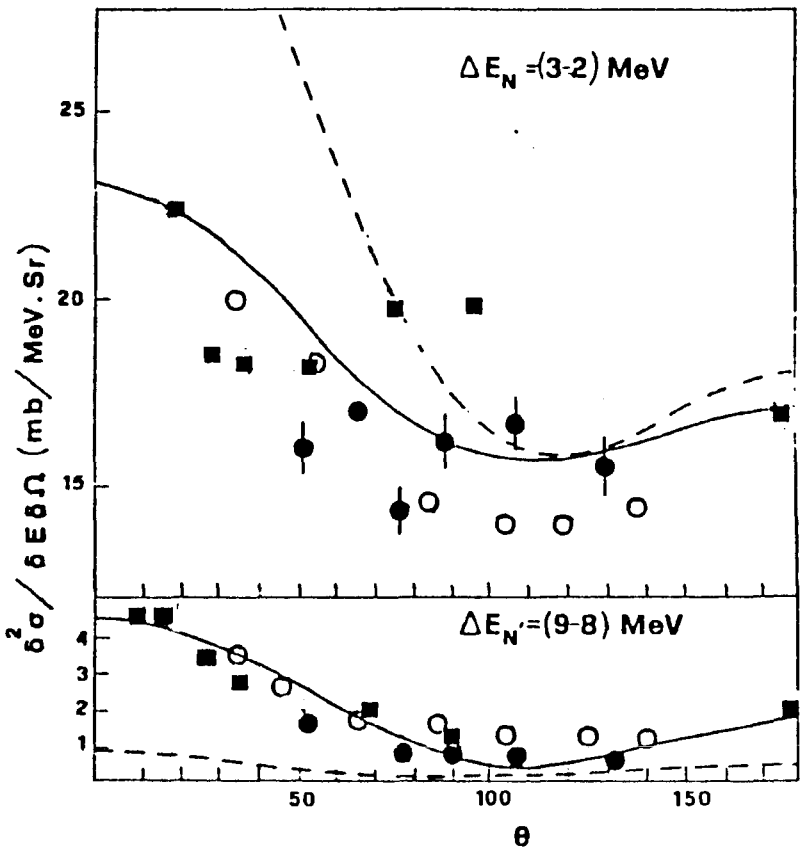

Fig. 11

■ = Zfk-277 INDC(gdr)-2/L
● = SovietJ. N.P.34(299)(1981)

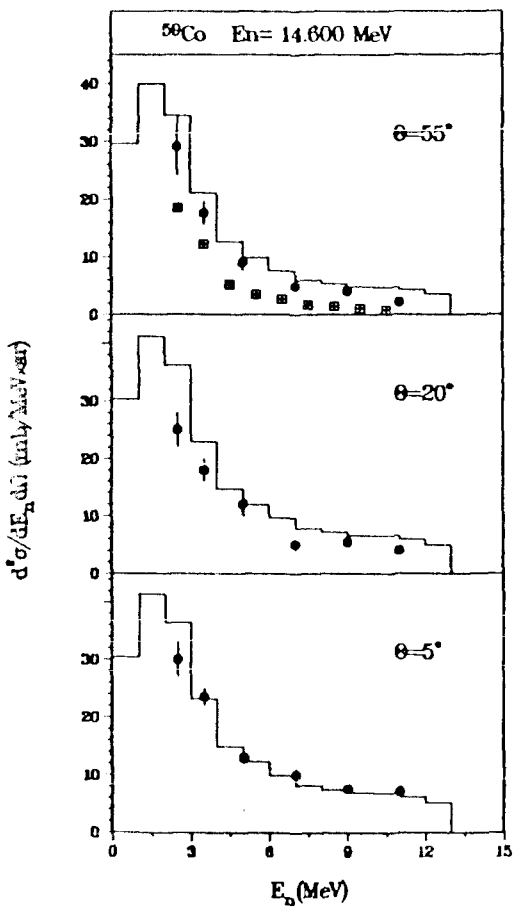

Fig. 12

■ = Zfk-277 INDC(gdr)-2/L
● = SovietJ. N.P.34(299)(1981)

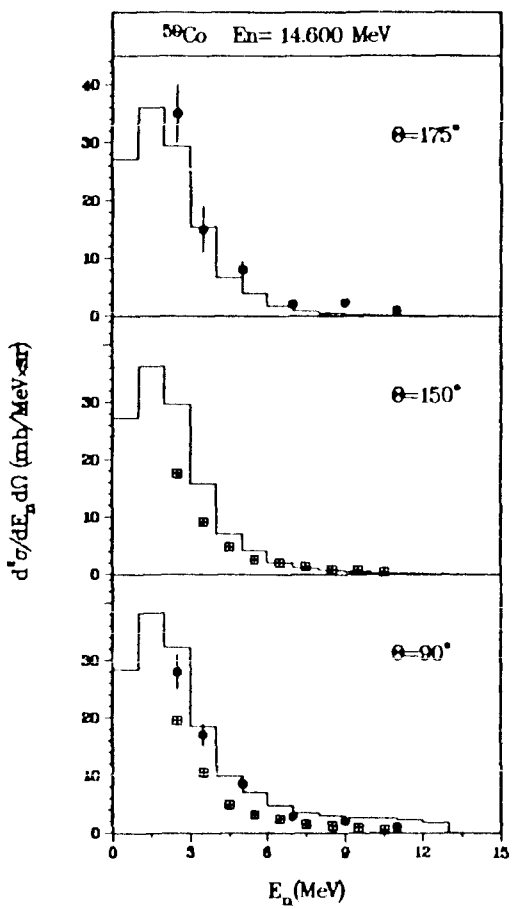

Fig. 13

■ = Zfk-277 INDC(gdr)-2/L
● = SovietJ. N.P.34(299)(1981)

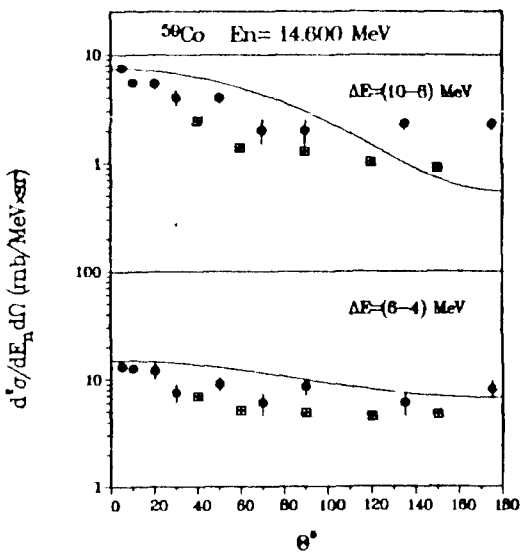

Fig. 14

■ = Zfk-277 INDC(gdr)-2/L
● = SovietJ. N.P.34(299)(1981)

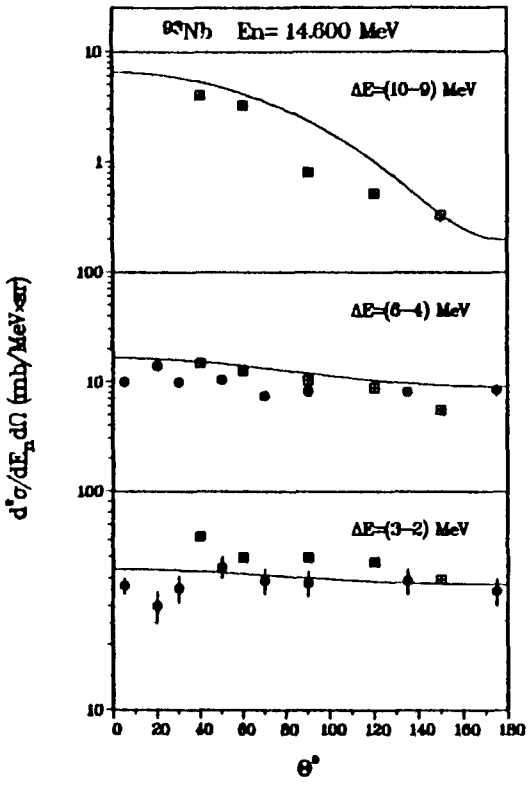

Fig. 15

■ = Zfk-277 INDC(gdr)-2/L
● = SovietJ. N.P.34(299)(1981)

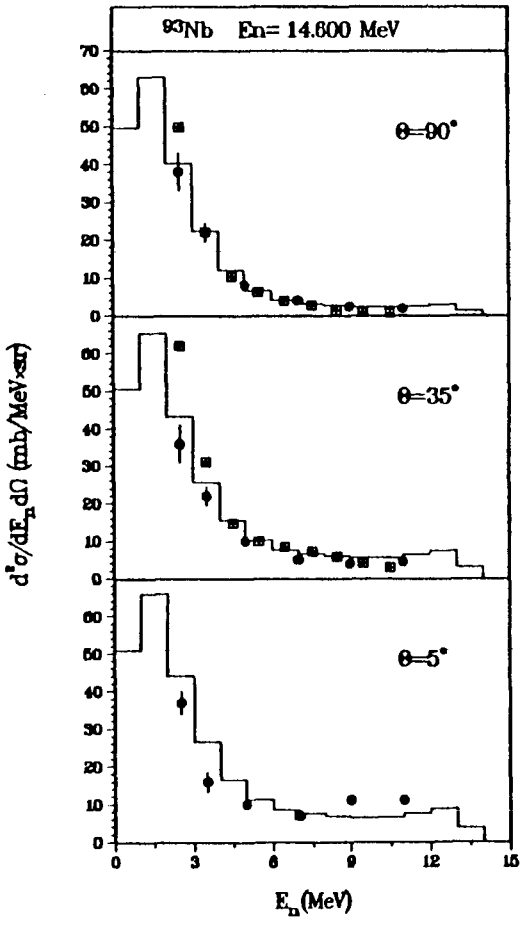

Fig. 16

■ = Marcikowski N.S.E. 83,13 (1983)

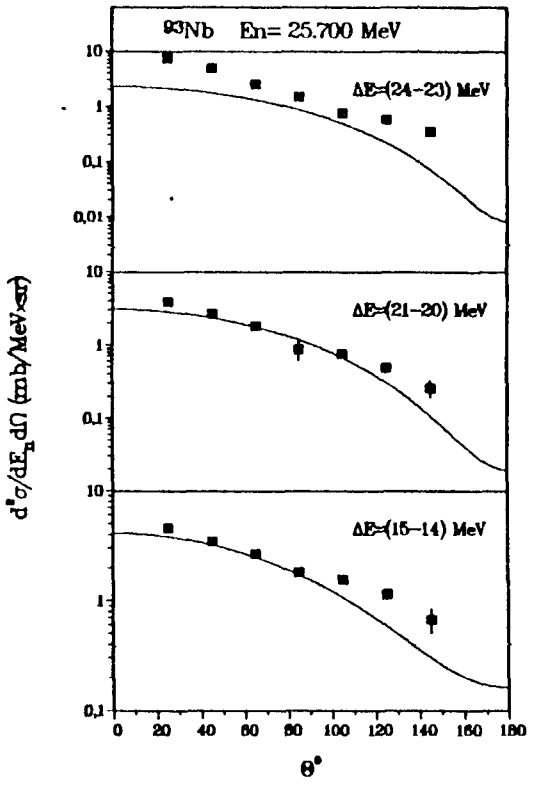

Fig. 17

■ = Marcikowski N.S.E. 83,13 (1983)

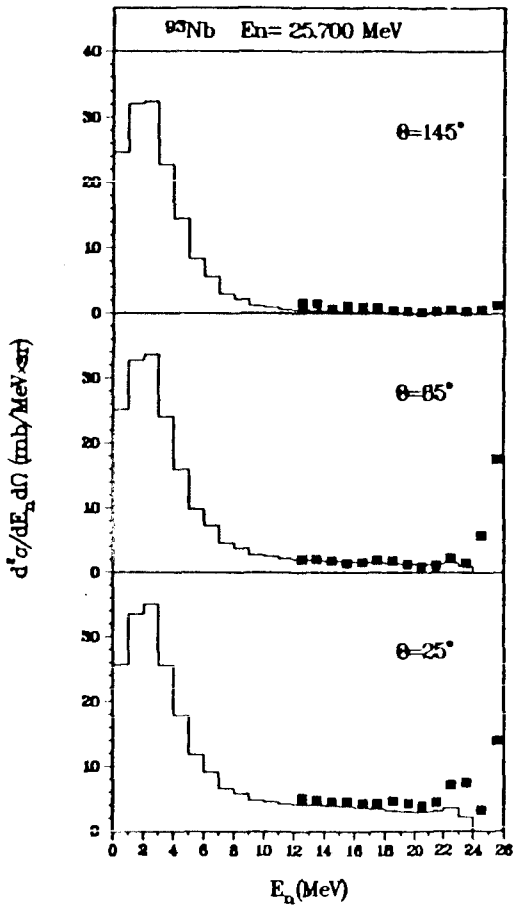

Fig. 18

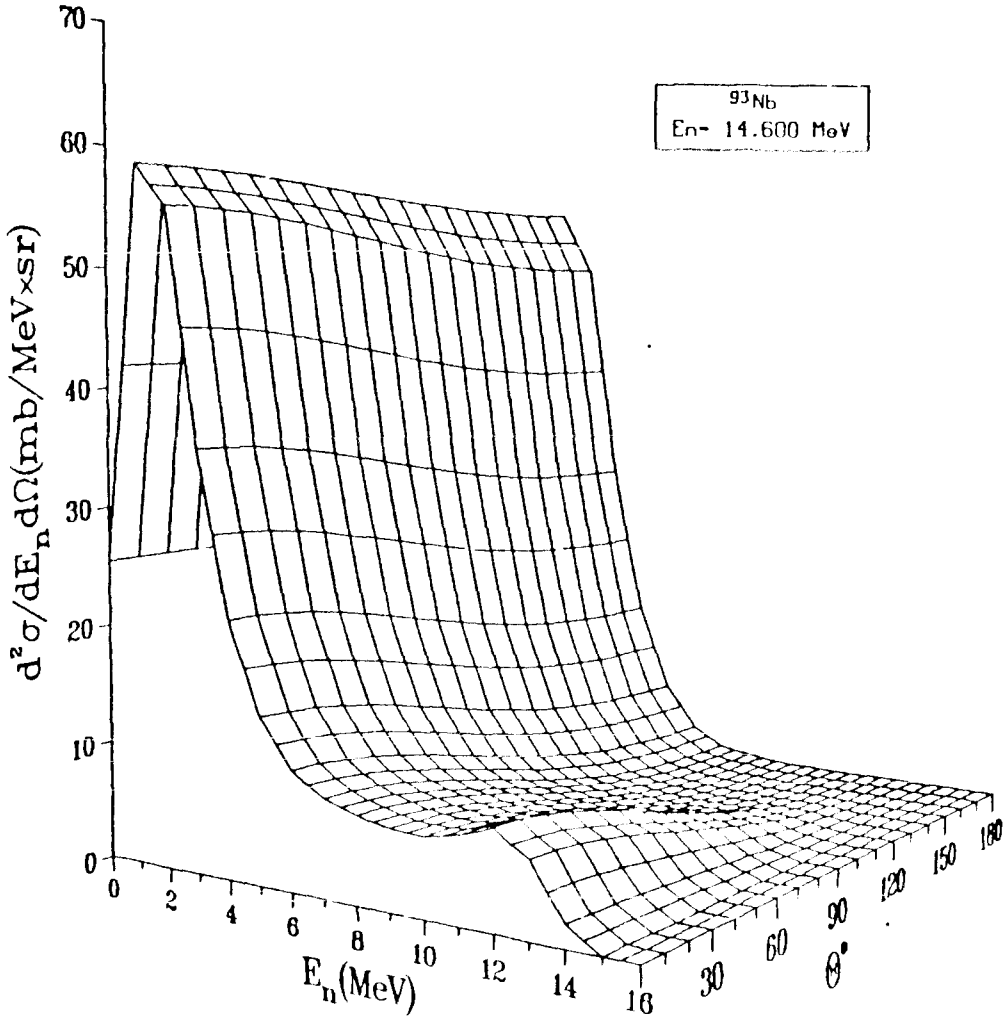

Fig. 19

Dots and open circles are the meausurements of ref. 33 and ref. 34 respectively. In the lower part of fig.11, to be consistent with previous results, one would expect that the spectrum calculated at forward angles be higher than the corresponding experimental one. This, however, is not the case for open circle data, neither for the data of ref. 35 (squares). This fact and the spread of points in the upper part of the figure rise questions on a possibile rôle of experimental uncertainties in the discrepancies found. In figs. 12 to 14 we show the results of the calculations for ^{59}Co at 14.5 MeV obtained using the input[36] fixed in the frame of the international intercomparison of codes for compound nucleus calculations, sponsored by the NEA DATA BANK. In figs. 15 and 16 we show the results of the calculations for ^{93}Nb at 14.5 MeV obtained using the input[37] fixed in the frame of the international intercomparison of codes for prequilibrium calculations, sponsored by NEA DATA BANK.

In figs. 17 and 18 the results of calculations in ^{93}Nb at 25.6 MeV are also shown, using the same input.

From all the cases here illustrated one can see that calculations compare to experimental data substantially good and always the same way. At 14.5 MeV we repeated the calculations after replacement of the free nucleon scattering assumed in ref. 27 by the scattering of nucleons bound in a square well and after introduction of the refraction term of nucleons beams at the nuclear surfaces.

The calculations with inclusion of the latter refinements did not show any substantial improvement with respect to the previous one. In particular the two effects considered showed evidence for a reciprocal cancellation.

In fig. 19 one can see very well the physical features of the two reaction mechanisms involved. Namely at low emitted neutron energies one has the bulk of the spectrum with a symmetric angular distribution carachteristic of equilibrium emissions (dominant process) while at high emitted neutron energies one finds forward peacked emissions carachteristic of a dominant preequilibrium process.

Conclusions

Spectra and IR calculations are valuable in view of the need for them in a number of applications and of the measurement diffuculty.

Recently, spectra calculations offered appreciable help in correcting systematic errors of relative neutron radiative capture measurements made with Moxon-Rae detectors[1),(2),(5)].

A number of recent experiments proves the validity of basic assumptions adopted for the energy dependence of γ-ray intensities.

A weak point of these calculations remains however the determination of reliable level schemes and inherent γ-ray branchings when these are not measured. In fact, the consi-

derable theoretical efforts in this direction proved very useful in understanding nuclear structure, but cannot yet replace all cases where experimental information is missing. A possible improvement of present calculations may be obtained by the introduction of considerations of rotational bands in order to fill the gaps in level schemes and introducing K-selection rules in the γ-ray transitions.

In view of these difficulties, stress should be laid on the need for experts to provide cross section evaluators with appropriate level schemes, at least for the cases of recognized interest.

Frome the model calculations illustrated one can realize that M1 contributions cannot be neglected in the theoretical estimate of any of the quantities here discussed, where a nuclear structure which favours M1 transitions (via the play of $J\pi$ selection rules) couples to M1 transition strength comparable to that of E1 transitions.

From the example illustrated, one may conclude that even if valence mechanism do not contribute appreciably to neutron capture cross section nevertheless, in specific nuclei, it may be of great help in explaining apparently ambiguous situations and in determining the appropriate model parameterization.

The case considered also gives additional evidence for the validity of the adopted models for radiative decay of compound nucleus and capture cross section calculations.

For the particle emissions at 14.5 Mev, one has to say that a considerably better result is obtained with the improvements illustrated and introduced into the previous version[27] of the unified exciton model. This is mainly achieved becouse

i) the unified model allows for a consistent treatment of both equilibrium and prequilibrium contributions.

ii) Introduction of the principle of conservation of total angular momentum allows for a proper weighting of all reaction channels, according to the spin distribution of the p-h level density.
(Out of curiosity, in fig. 9 the results of calculations are shown too, dashed curve, with no angular momentum conservation).

iii) Introduction of the appropriate distribution of p-h levels, according to spin, allowed for the most meaningful extension mentioned in ii) above.

From the sample calculations illustrated some conclusions may be derived.

It appears very likely that the moderate discrepancies observed are due more to the very rough total level density adopted (expecially for lower excition numbers), than to conceptual inadequacy of the model.

In particular to achieve the best results, the necessity appears of a consistent tratment of equilibrium and preequi-

librium contributions like the unified model can provide us with.

One may say that the model, even as it is, is reliable in giving an overall picture of total and partial emission spectra as well as of angular distributions. In addition, becouse no free parameters were used, these results may be regarded as a model test proving a wide prediction capability valid also if no experimental information is available.

In general, one may conclude that considerable results have been achieved in the calculation of total and partial particle and γ-ray emission cross sections. Namely calculations are now possible even if no experimental information is available, becouse the degree of accuracy is, more or less known, and may be estimated pretty close to usual experimental uncertatainties for the quantities inherent to γ-ray emission and, at worse, <100% for particle spectra emission calculations in the higher energy tails.

REFERENCES

(1) Wisshak K., Wicknehauser J., Käppeler F., Reffo G., Fabbri F., Nucl.Sc.Eng. 81 (1982) 396.

(2) Reffo G., Fabbri F., Wisshak K., Käppeler F., Nucl. Sc. Eng. 80 (1982) 630.

(3) Gilbert A., Cameron A.G.W., Can.Journ. of Phys., 43 (1965) 1446.

(4) Reffo G., IAEA Report SMR-43 (1980) p.205. Lecture held at the "Winter Course on Nuclear Physics and Reactors" at ITCP Trieste, 17 Jan. - 10 Mar. 1978.

(5) Reffo G., Fabbri F., Wisshak K., Käppeler F., Nucl. Sc.Eng. 23 (1983) 401.

(6) KOPECKI J., Proc. of the 4th (n,) Int. Symp., Grenoble 7-11 Sept. 1981, pag. 423. Inst. of Phys. Conf. Series n. 62. Bristol and London.

(7) Reffo G., Fabbri F., IDA modular System Not torino 13 E.

(8) Reffo G., "Limits and Validity of the phenomenological Gilbert-cameron level density approach, Inviated paper at the IAEA advisory group meeting on "Basic and applied Problems of Nuclear Level Densities". Brookhaven Not. Lab. (USA) April 11-15 1983.

(9) Dover C.B., LEMMER R.H., HALME F.J.W., Ann. Phys. (N.Y.) 70 (1972) 458.

(10) Arenhovel H., Grainer W., Danos M., Phys. Rev. 157 (1967) 109.

(11) Gardner D.G., Gardner M.A., Dietrich F.S., Report UCID--18759, August 7, 1980 and in Nuclear Cross Sections for Technology, edited by J.L. Fowler, C.H. Johnson and C.D. Bownman (NBS (Special Publication No. 594), Washington D.C. 1980).

(12) McCullagh C.M., Stelts M.L., Chrien R.E., Phys. Rev. 23, 1394 (1981).

(13) Raman S., invited paper at IV Int. Symposium on Neutron Capture Gamma-Ray Spectroscopy and Related Topics, Sept. 7-11, 1981, Grenoble.

(14) Morgan G., Newman E., Report ORNL-TM-4973, August 1975.

(15) Benzi V., Reffo G., Vaccari M., Contributed paper to the IAEA "Fission Product Nuclear Data Meeting", Bologna 26-30 Nov. 1973. Report IAEA 169, pag. 123 (1974).

(17) Lederer C.M. and Shirley V.S., Tables of isotopes, 7th ed., John Wiley & Sons, Inc. New York (1978).

(18) Perey C.M., Harvey J.A., Macklin R.L., Winters R.R. and Perey F.G., "Neutron transmission and capture meausurements and analysis of ^{60}Ni from 1 to KeV, ORNL-5893, ENDF- 330, Oak Ridge National Laboratory, November 1982.

(19) Corvi F., Brusegan A., Buyl R., Rohr G., Shelley R. and Van der Veen T., Proc. Int. Conf. on Nuclear Data for Science and Technology, Antwerp 6-10 September 1982.

(20) Wisshak K., Käppeler F., Reffo G., Fabbri F., Neutron Capture in s-wave resonances of ^{56}Fe, ^{58}Ni and ^{60}Ni, KfK report 3516, July 1983.

(21) Beer H., Spencer R.R. and Käppeler F., Zeitschrift für Physik A 284, 173 (1978).

(22) Lane A.M., Mughabghab S.F., Phys. Rev. C 10 (1974), 412.

(23) Mengoni A., Reffo G., International Conf. on Nuclear Data for Science and Technology, pag. 755, Antwerp 1982, K.H. Böckhoff (ed.).

(24) Walter G., Käppeler F., Bao Z.Y., p.c. 1982.

(25) Walter G., Beer H., Käppeler F., Penzhorn R.E., p.c. 1982.

(26) Raman S., Fögelberg B., Harvey J.I., Macklin R.L., Stelson P.H., Schröder H., Kratz K.L. to appear in Phys. Rev. C 1983.

(27) Akkermans J.M., Gruppelaar H., Reffo G., Phys.Rev. C 22, 73 (1980).

(28) Gruppalaar H. contribution to this meeting.

(29) Williams F.C., Jr., Nucl. Phys. A116, 231 (1971).

(30) Costa C., "La conservazione del Momento angolare nei processi multistep compound". University of Bologna thesis. Relatore G.Reffo. Academic year 1980-81)

(31) Reffo G., Herman M., Nuovo Cimento Lett., 34, 261 (1982)

(32) Becchetti F.D., Greenless G.W., Phys. Rev. 182, (1969) 1190.

(33) Hermsdorf D., Meister A., Sassonoff S., Sceliger D., Seidel K., Shalvin F., Zentralinstitut für Kernforschung, Rossendorf bei Dresden, ZfK-277(U) (1979).

(34) Kamerdienen Y.L., report UCRL-51232 (1972).

(35) D.Procopet et al. Soviet J.N.P. 34 (1981) 299.

(36) A.Prince, G.Reffo, E.Sartori, "Spherical optical and Statistical Model Study" Report NEANDC-152 "A", INDC (NEA)4, 1983.

(37) Gruppelaar H., p.c. 1983.

Translated from Russian

RE-EVALUATION OF THE NEUTRON CROSS-SECTION FILE FOR CHROMIUM

T.S. Belanova, A.I. Blokhin, N.N. Buleeva, V.V. Vozyakov, A.V. Ignatyuk, V.N. Manokhin, V.P. Lunev, A.B. Pashchenko and V.I. Popov

All the experimental and evaluated data available are analysed with a view to drawing up a new version of the neutron cross-section file for chromium.

The previous evaluation of neutron cross-sections for chromium was prepared at the Centre for Nuclear Data (TsYaD) in 1977 [1]. That evaluation was taken as the basis for group-averaged constants of chromium recommended for reactor and radiation protection calculations [2]. In the last few years, in addition to new experimental data, more up-to-date evaluations of neutron cross-sections have appeared (JENDL-1 [3] and ENDF/B-V [4]). In view of the important part played by chromium as a structural material in fast reactors, we have analysed the discrepancies found between the results of different evaluations and have drawn up a revised version of the chromium file.

In this paper we discuss the main differences in the new evaluation.

In all the evaluations the neutron energy region up to ~ 600 keV is represented in the form of isolated resolved resonances with the addition of a backing. However, the resonance parameters have been measured with sufficient reliability only for the strongest s-resonances, whereas for p-resonances the values found for neutron and radiative widths are subject to considerable errors and relate only to the energy range up to 100 keV [5]. All uncertainties in parametrization of the resonance structure of neutron cross-sections above 100 keV are in effect transferred to the backing, and as the upper limit of the resonance region is approached the backing accounts for between 50 and 80% of the total cross-sections, and up to 100% of the capture cross-sections [1,3,4]. Although in this case the backing has a relatively complex and non-monotonic dependence, given this parametrization, the thin resonance structure is completely lost. The defects of this method of representing cross-sections become apparent when calculating the self-shielding factors of cross sections [2]. In order to overcome these defects, for p-neutrons we have used a method of representing isolated unresolved resonances. The energy dependence of the average neutron

and radiative widths was determined from a statistical description of averaged neutron capture cross-sections in the energy region above 30 keV. On the basis of an analysis of all the experimental data available, preference was given to Ref. [6], the results of which agree relatively well with each other. In the group-averaged representation the results of this average cross-section evaluation do not differ from our previous evaluation [1], but the discrepancies between other evaluations for capture cross-sections in the energy region above 10 keV are relatively large (see Fig. 1). These discrepancies are caused by the fact that the authors drew on different experimental data, and new reliable measurements of average neutron capture cross-sections will presumably be needed for the differences in evaluations to be eliminated.

The discrepancies in evaluated total neutron cross-sections at energies above 650 keV are due to the selection of different reference experiments: in Ref. [1] the data of Cierjaks [7] are used, in ENDF/B-V those of Perey [8] and in JENDL-1 the optical calculations of total cross-sections with a set of parameters obtained for neutrons with energies above 5 MeV. Obviously, in optical calculations the fluctuations in cross-sections are smoothed out, and this distorts the self-shielding factors; since the measurements of Ref. [8] were made with a somewhat better resolution than those of Ref. [7] and in the energy region 2-6 MeV they agree better with the results of other authors, in re-examining total cross-sections we took the ENDF/B-IV evaluation in the whole range of neutron energies from 650 keV to 20 MeV.

When comparing existing evaluations of angular distributions of elastically scattered neutrons [3,4,9], we also gave preference to the evaluation of ENDF/B-IV for neutron energies below 1 MeV and above 14 MeV. In the energy region between 1 and 14 MeV our evaluation of angular distributions was obtained in the context of the phenomenological approach, whereby cross-sections calculated in accordance with the optical model were later corrected on the basis of experimental data. By virtue of this correction, a better approximation of the angular distributions observed was achieved than those calculated by the optical model with a single set of parameters [3,4]. The differences in the evaluated angular distributions can easily be seen if the average cosines of the scattering angle are compared (Fig. 2), but on the whole all evaluations meet the practical requirements of reactor calculations.

There are also significant differences in the evaluations of neutron inelastic scattering cross-sections at isolated levels. These are particularly marked for the first 2^+ level of the isotope ^{52}Cr (see Fig. 3). In the ENDF/B-V evaluation, the approximation of near-threshold sectors of the excitation functions for isolated levels was obtained on the basis of data measured on a $(n,n'\gamma)$ spectrometer [10]. These data contradict the measurements of excitation functions of levels on time-of-flight spectrometers [11]. In our evaluation of inelastic scattering cross-sections we relied mainly on the results of the latest experiments [11] and on a theoretical description of excitation functions matched with resonance values of neutron force functions [12]. We also took into account contributions from direct transitions to excitation functions of levels, which are found to be particularly marked with neutron energies above 7 MeV (Fig. 3). Inclusion of direct transitions is also important for a correct approximation of neutron inelastic scattering spectra.

From a comparison of the evaluations of threshold reaction cross-sections the following conclusions can be drawn:

(a) There are no significant discrepancies in the evaluations of (n,2n) reaction cross-sections, since all evaluations are based on the experimental data of Ref. [13];

(b) Evaluations of (n,p) reaction cross-sections agree relatively well at a neutron energy of 14 MeV, but differ considerably at energies below 10 MeV (Fig. 4). Publication of the data of Smith et al. [14] makes it possible for the evaluation to be rendered more accurate in the threshold region;

(c) The differences between evaluations of the (n,α) reaction cross-sections are also significant, since they are all based on purely theoretical calculations. Recent data on integral cross-sections of proton, deuteron and alpha-particle yields at a neutron energy of 15 MeV [15] make it possible to correct the evaluations for the (n,xp), (n,xd) and (n,xt) reactions.

We used the relationships of the statistical theory of nuclear reactions (modified STAPRE program [16]) for a simultaneous, matched approximation of the threshold reaction cross-sections mentioned above and the neutron inelastic scattering spectra observed [17]. The approximation of experimental data was

obtained by variation of level density parameters and of contributions from pre-equilibrium particle evaporation. Calculated neutron spectra were taken as those recommended for the whole incident neutron energy range between 4 and 20 MeV.

On the basis of the evaluations examined above at the Centre for Nuclear Data, a new version of the neutron cross-section file for chromium was drawn up in ENDF/B format. Testing and verification of the consistency of the evaluations adopted are to have been completed by the end of 1983.

REFERENCES

[1] BYCHKOV, V.M., et al., in Nejtronnaya fizika (Neutron Physics), TsNIIAtominform, part 4 Moscow (1977) 91.

[2] ABAGYAN, L.P., et al., Gruppovye konstanty dlya rascheta reaktorov i zashchity (Group-Averaged Constants for Reactors and Radiation Protection Calculations), Ehnergoizdat, Moscow (1981).

[3] Igarasi et al. JAERI-1261, 1979.

[4] Prince A., Burrows T.W. Evaluation of natural chromium neutron cross-sections for ENDF/B-V. ENDF-286, 1979.

[5] Mughabghab S. et al. Neutron Cross-Sections. N.Y., Academic Press, 1981, vol.1.

[6] Spencer R.R., Beer H. KfK-2046, 1973
Rigolenr C., Arnand A. Proc. Conf. on Neutron Cross-Sections and Technology, Washington, 1975, vol.1, p.367
Allen B.J. et al. Spec.Meet. on Neutron Data, Geel,1977, p.447.

[7] Cierjaks S. et al. EXFOR-20010.007, 1971

[8] Perey F.G., Kinney W.E. EXFOR-10342, 1973

[9] NIKOLAEV, M.N., BAZAZYANTS, N.O., Anizotropiya uprugogo rasseyaniya nejtronov (Anisotropy of Neutron Elastic Scattering), Atomizdat, Moscow (1972).

[10] Karatzas P.T. et al. Nucl.Sci.Eng., 1978, vol.67, p.34

[11] KORZH, I.A., et al., Yad. Fiz. 35 (1982) 1097; GUENTHER, P.T., et al., Nucl. Sci. Eng. 82 (1982) 408.

[12] VOZYAKOV, V.V., et al., Voprosy atomnoj nauki i tekhniki. Ser. "Yadernye konstanty" 4 (48) (1982) 44.

[13] Frehaut J., Moshinski G. Proc. V-Symp. on Interaction of Fast Neutron with Nuclei. ZfK-296, Dresden, 1976

[14] Smith D., Meedows A. Nucl.Sci.Eng., 1980, vol.76, p.43

[15] Barshall H.H. In: Neutron Induced Reactions. Bratislava,1982,p.279

[16] Uhl m., Strohmaier B. Report IRK-76/01, Vienna, 1976

[17] SAL'NIKOV, O.A., et al., Voprosy atomnoj nauki i tekhniki. Ser. "Yadernye konstanty" 7 (1971) 134; PLYASKIN, V.I., TRYKOVA, V.I.; ibid. 21 (1976) 62.

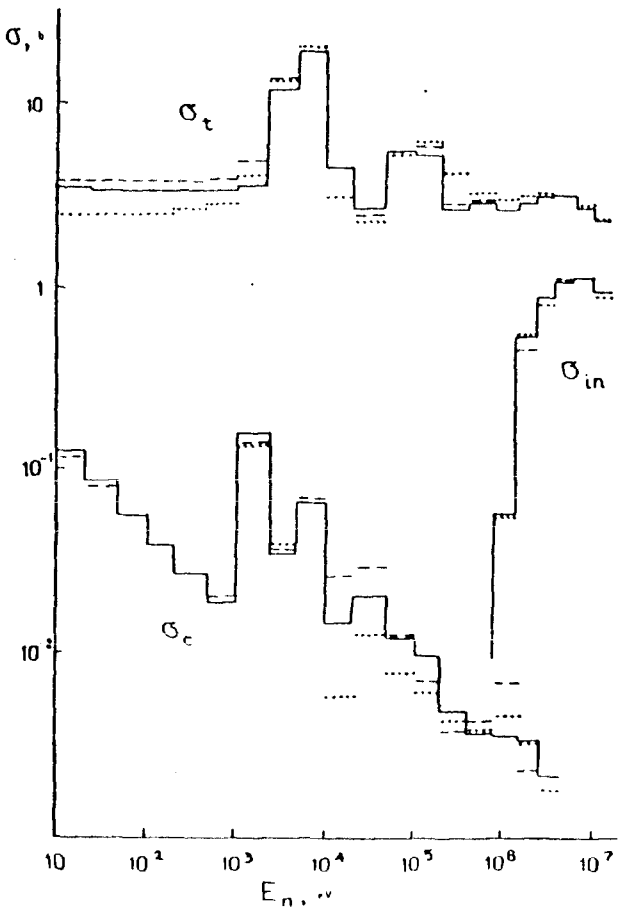

Fig. 1. 28-group averaged representation of capture, inelastic scattering and total neutron cross-sections. Dotted line: ENDL-1 evaluation; dashed line: B-5; solid line: IsYaD 2.

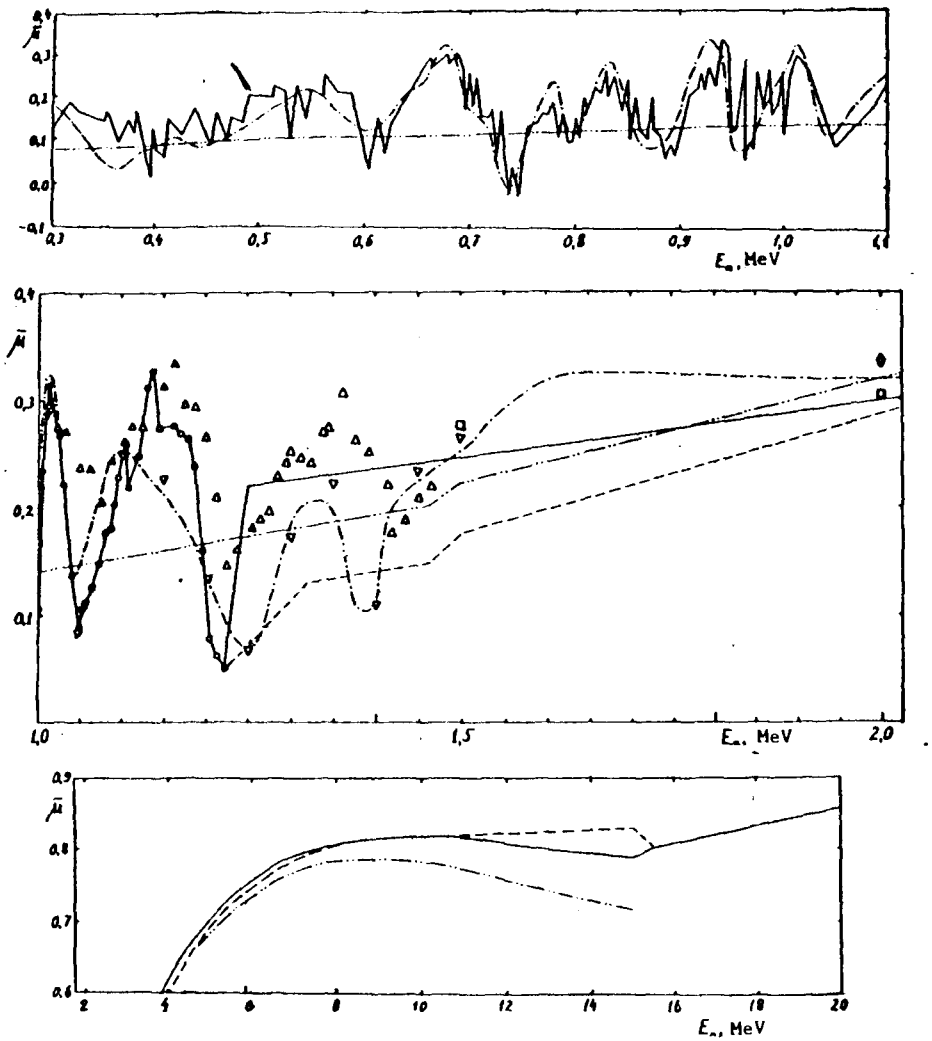

Fig. 2. Energy dependence of average cosine of neutron elastic scattering angle.
Solid line: TsYaD-2
Dashed line: B-5
Dashed-dotted line: Ref. [9]
Double dashed line: JENDL-1

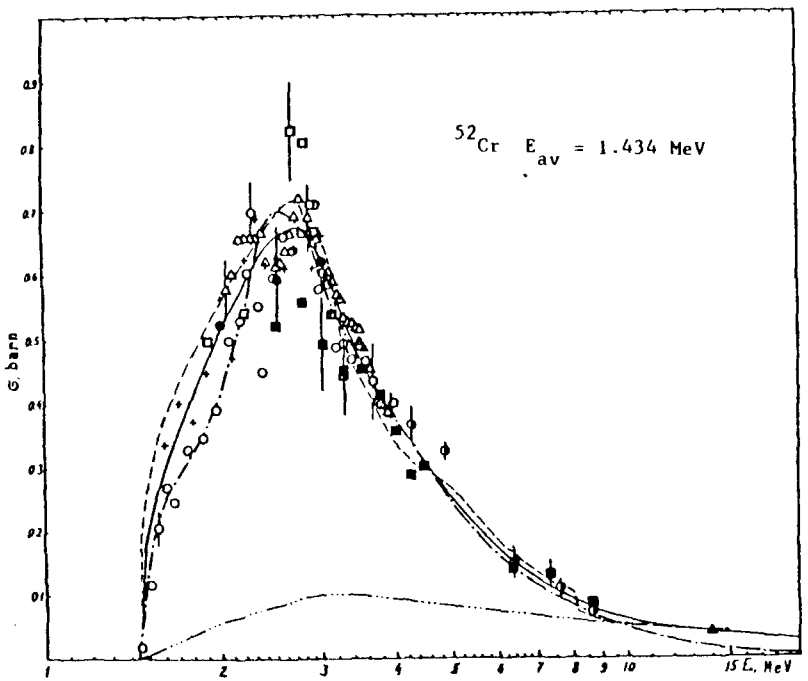

Fig. 3. Neutron inelastic scattering cross-sectionsat the first 2^+ level of the isotope ^{52}Cr.
Dashed-dotted line: B-5 evaluation
Solid line: TsYaD-2
Triple dashed-dotted line: Contribution from direct transitions

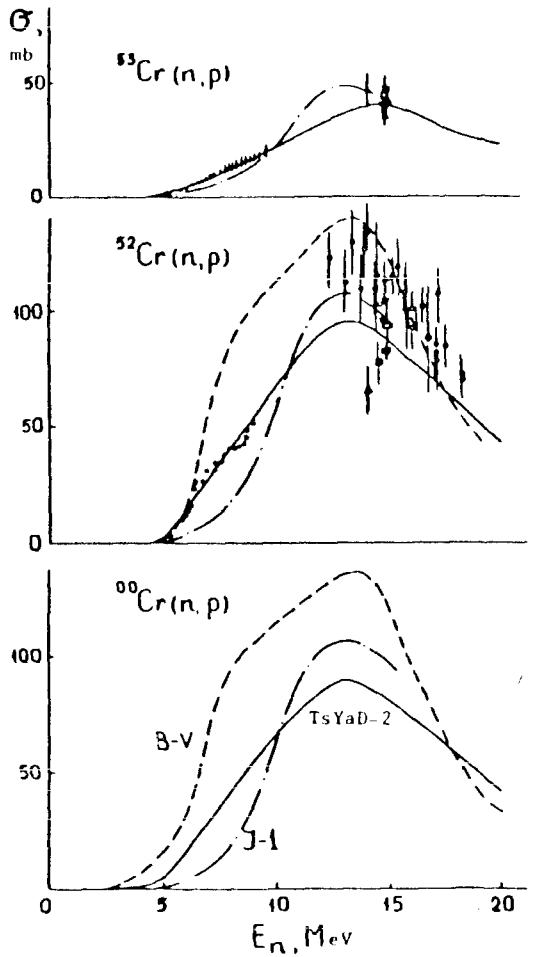

Fig. 4. Evaluations of the (n,p) reaction cross-sections for isotopes of chromium
Solid line: TsYaD-2
Dotted line: B-5
Dashed-dotted line: JENDL-1

Revised nuclear model calculations of neutron induced cross sections for ^{93}Nb

Brigitte Strohmaier, Institut für Radiumforschung und Kernphysik der Universität Wien, Vienna, Austria

1. Introduction

The present work is a continuation of two former cross section evaluations by means of nuclear model calculations, one of which concerned the dosimetry reaction ^{93}Nb(n,n')^{93m}Nb /1/, while the other comprised all important neutron induced reactions which are possible at incident energies up to 20 MeV /2/ and was based on experimental data existing in April 1981. New measurements of neutron induced proton production /3,4/ necessitated a modification of the preequilibrium (PE) model parameters. As a consequence, various other model parameters had to be adjusted in order to maintain the reproduction of the other experimental data. The physical meaning of the parameter changes is discussed together with a comparison of calculations and measurements.

2. The models

The computer codes which were used for this cross section evaluation employ on one hand the spherical optical model, on the other the statistical model, comprising the exciton model for PE decay and the Hauser Feshbach (HF) model for equilibrium decay of the composite system formed by projectile and target nucleus, and the evaporation model for the decay of the further compound nuclei /5/. Whereas in the HF and the evaporation formula there is full consideration of angular momentum and parity conservation, the exciton model is independent of spin and parity. Therefore, in order to distribute the PE contribution to the population of the 2nd compound nucleus over

its spins and parities, an additional assumption is necessary which in the used program STAPRE /5/ consists in attributing each spin and parity the same weight it has in the HF part.

The description of excited states in the PE model is by means of a particle-hole state density formula, while for the equilibrium decay calculation the back-shifted Fermi gas level density formula is applied above a region of individually considered discrete levels. In competition to each particle emission gamma ray cascades are considered including the multipolarities up to L = 3.

3. Options and parameters chosen for the previous Nb evaluations

The experimental data base which served for the determination of the model parameters is compiled in ref. 2.
Due to its good reproduction of the total and non-elastic cross section the optical potential by Delaroche et al. /6/ for neutrons was chosen. For charged particles, global potentials /7,8/ were used.

The level schemes for all relevant nuclei were taken from "Table of Isotopes" /9/ except the one for ^{93}Nb which had been derived from the work of van Heerden et al. /10/ as described in ref. 1. The Fermi gas level density parameters were chosen according to the Dilg compilation /11/ and in some cases slightly modified for better reproduction of the cross section data.

Regarding the exciton model,a value of 230 MeV^3 was used for the constant determining the internal transition matrix element. For the exciton state densities, the single particle state densities g were derived from the Fermi gas a-parameters and no energy shifts were used.

With these parameters, a very satisfactory over-all reproduction of the experimental data could be achieved with the exception of proton production at 15 MeV incident neutron energy, where the calculation resulted in a much harder spectrum than the experiment, indicating too high a PE portion. As also the low-energy end could not be reproduced with reasonable parameters, the measurement was suspected to be in error.

4. Parameter changes with respect to the previous calculations and their effect on the resulting cross sections

The revision of the previous evaluation was motivated by the measurement of neutron induced proton production at 14 MeV incident energy at the IRK, Vienna /4/. At the same time, also a Japanese group published a 14 MeV neutron induced proton emission spectrum /3/. These data clearly necessitated a reduction of the PE fraction and a shift of the high energy end of the calculated spectrum to lower energies. Both these requirements were satisfied by introducing an energy shift in the particle-hole state densities which roughly accounts for pairing; an option which in the used code STAPRE /5/ goes along with the choice of a value of $\frac{6}{\pi^2}\frac{A}{8}$ for the single particle state density g. How the introduction of the pairing correction affects the proton emission spectrum at 14 MeV is compared in fig. 1 to the effect of a simple increase of the internal transition matrix element to 400 MeV^3. A comparison of the calculation with the measured proton production at 14 and 15 MeV incident neutron energy is displayed in figs. 2 and 3. Of course, PE neutron emission is also decreased; nevertheless there is still consistency with the 14 MeV neutron production spectra (fig. 4) as well as with the measurement at 25.7 MeV (figs. 5 and 6) by Marcinkowski et al. /12/. Since α-particle emission leads to an odd-odd nucleus α-particles compete much more favourably with nucleons in the PE stage when pairing is accounted for. The resulting increase in the α-particle emission could not be counteracted by the use of another optical potential for creating the α-particle transmission coefficients; the fact experienced in the A ∿ 50 region, that the McFadden & Satchler potential /13/ reduces α-particle widths with respect to the Huizenga & Igo /7/ potential, does not hold true in the A ∿ 90 region.

Therefore, in order to reproduce the experimental α-spectra (figs. 7, 8), a smaller α-cluster preformation factor ψ (0.11 instead of 0.18) had to be used.

Once the emission data had been refit, there were still problems with the reproduction of the activation cross sections. In particular, the reduction of PE neutron emission had caused a decrease of the $(n,n')^m$ cross section of 20% at 14 MeV. A contribution of inelastic scattering to a collective state does not seem to be likely, because the 30 keV isomer of ^{93}Nb is explained as a coupling of a proton hole to a ^{94}Mo core in its ground state. The desired increase in the isomeric cross section was achieved by employing a more realistic assumption for the spin distribution of PE emission, i.e. by shifting the population resulting from PE decay to lower spins. This was accomplished by calculating the weights for the population of the various spins (cf. sec.2) by a HF calculation using for the moments of inertia I_{eff} one half of the rigid body value I_{rigid}, while for the actual HF contribution $I_{eff} = I_{rigid}$ was maintained. The spin cutoff parameters corresponding to $I_{eff} = 0.5 * I_{rigid}$ roughly agree with the exciton number dependent spin cutoff parameters as given by Reffo /14/ for low exciton numbers. While the shift of the population of ^{93}Nb to lower spins brought the $(n,n')^m$ excitation function back to its magnitude as displayed in ref. 2, it also caused a reduction of γ-competition in ^{93}Nb and a shift of the population of ^{92}Nb to lower spins and thus increased the $(n,2n)^{g+m}$ and $(n,2n)^m$ excitation functions by 5-7% (figs. 9,10).

Finally, the decrease of the $(n,\alpha)^{m+g}$ and $(n,\alpha)^m$ cross sections at higher energies where the more favourable competition due to the consideration of pairing is overcome by the reduction of ψ, was partly canceled by chosing $I_{eff} = 0.7 * I_{rigid}$ for PE α-particle emission. This seems to be justified because α-particle emission populates more complex residual states than nucleon emission does. The resulting excitation functions are shown on figs. 11 and 12.

5. Conclusion

The parameter modifications which had been necessary in order to describe new proton emission data could be performed in such a way that finally the whole body of data has been reproduced again in the frame of the optical model, the exciton PE model and the compound nucleus model with a unique set of parameters. A pragmatic way of using different spin distributions for PE and equilibrium particle emission has been found. The remaining discrepancies between calculations and experiment are not inherent to a certain reaction, but can be transferred between the reactions by small parameters changes, e.g. a reduction of the two body matrix element would improve the fit to the (n,2n) data, but deteriorate the reproduction of α-emission.

Finally, it should be mentioned that the charged particle emission data taken at the IRK, Vienna, also contain angular distribution information which had not been taken advantage of. In order to do so, they will be analyzed /15/ in the frame of the multi-step direct reaction model by Tamura et al. /16/.

References

/1/ B. Strohmaier, S. Tagesen, H. Vonach, Physics Data 13-2 (1980)

/2/ B. Strohmaier, Ann. Nucl. Energy 9 (1982) 397

/3/ N. Koori, to be published
Data displayed in M. Hanita et al., NEANDC(J)-83/U, p. 59, JAERI Progr. Rept. July 81-June 82

/4/ G. Traxler, Thesis Univ. Vienna (1983)

/5/ M. Uhl and B. Strohmaier, Rept. IRK 76/01 and addenda to this rept., and
B. Strohmaier and M. Uhl, Proc. Course Nucl. Theory for Applications, Trieste, 1978, IAEA-SMR-43 (1980) 313

/6/ J.P. Delaroche, Ch. Lagrange and J. Salvy, Proc. IAEA Consultants' Meeting on the Use of Nuclear Theory in Neutron Nuclear Data Evaluation, Trieste, 1975, IAEA-190(1976) 251

/7/ J.R. Huizenga and G. Igo, Rept. ANL-6373 (1961)

/8/ G.S. Mani, M.A. Melkanoff and I. Iori, Rept. CEA-2379 (1963)

/9/ C.M. Lederer and V.S. Shirley (eds.), Table of Isotopes, 7th ed., Wiley, N.Y., 1978

/10/ I.J. van Heerden and W.R. McMurray, Z. Physik 260 (1973) 9

/11/ W. Dilg, W. Schantl, H. Vonach and M. Uhl, Nucl. Phys. A217 (1973) 269

/12/ A. Marcinkowski, R.W. Finlay, G. Randers-Pehrson, C.E. Brient and J.E. O'Donnell, Nucl. Phys. A402(1983) 200

/13/ L. McFadden and G.R. Satchler, Nucl. Phys. 84 (1966) 177

/14/ G. Reffo, Proc. IAEA Advisory Group Meeting on Basic and Applied Problems of Nuclear Level Densities, Brookhaven, 1983, in press

/15/ M. Uhl, priv. comm.

/16/ T. Udagawa, K.S. Low and T. Tamura, Phys. Rev. C28 (1983) 1033

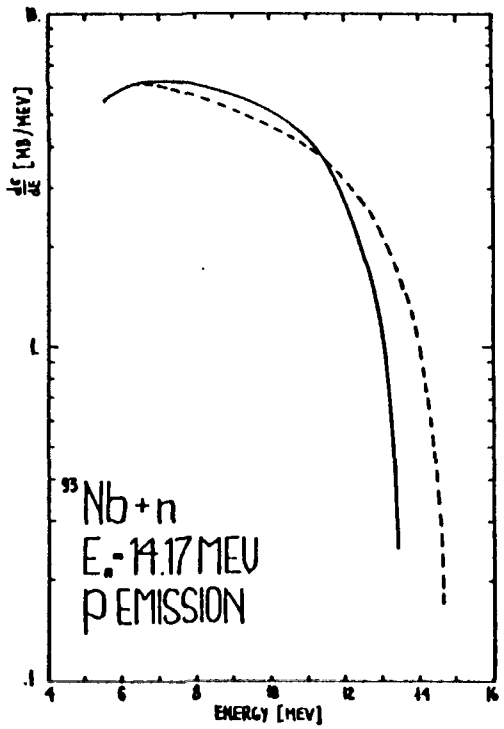

Fig. 1. Calculated proton production (CM system) from ^{93}Nb+n at 14.17 MeV incident neutron energy. Solid line: FM = 230 MeV^3, with pairing; dotted line: FM = 400 MeV^3, without pairing.

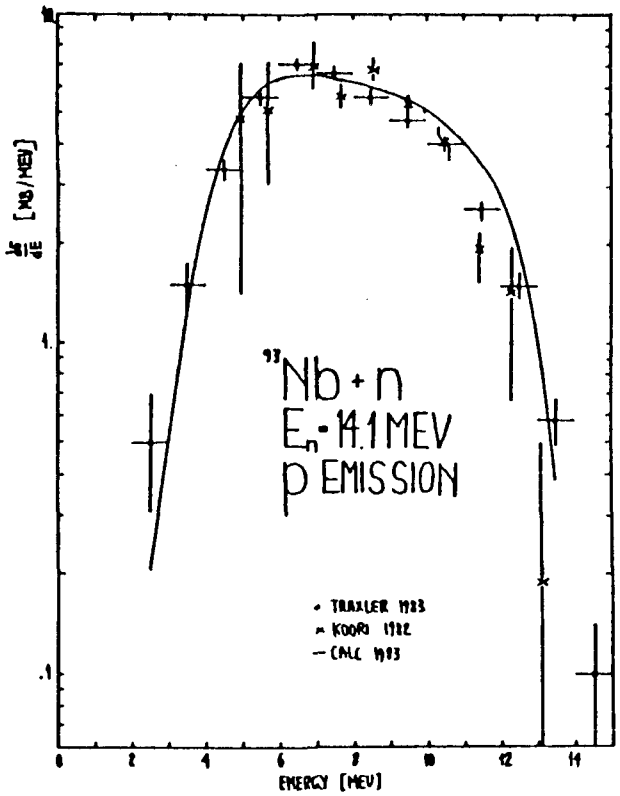

Fig. 2. Proton production (CM system) from ^{93}Nb+n at 14.1 MeV incident neutron energy. The calculation comprises the contributions of (n,p) and (n,n'p).

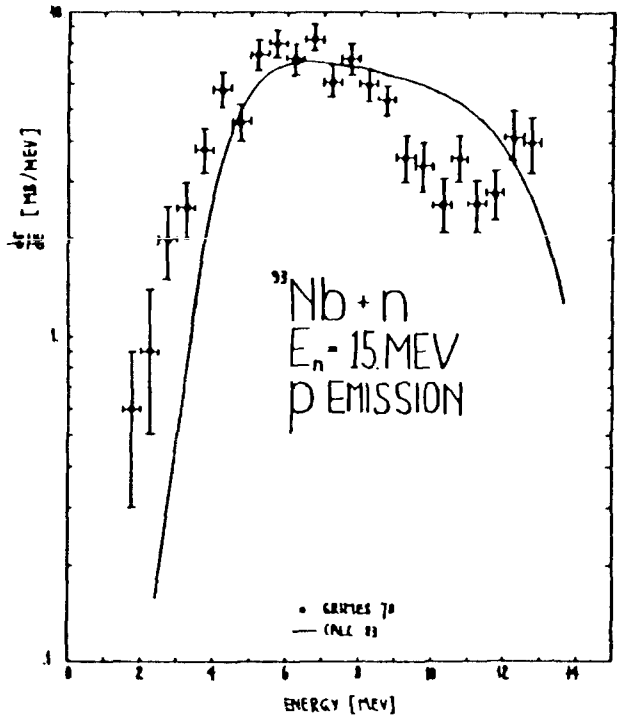

Fig. 3. Same as Fig. 2 for 15 MeV incident neutron energy.

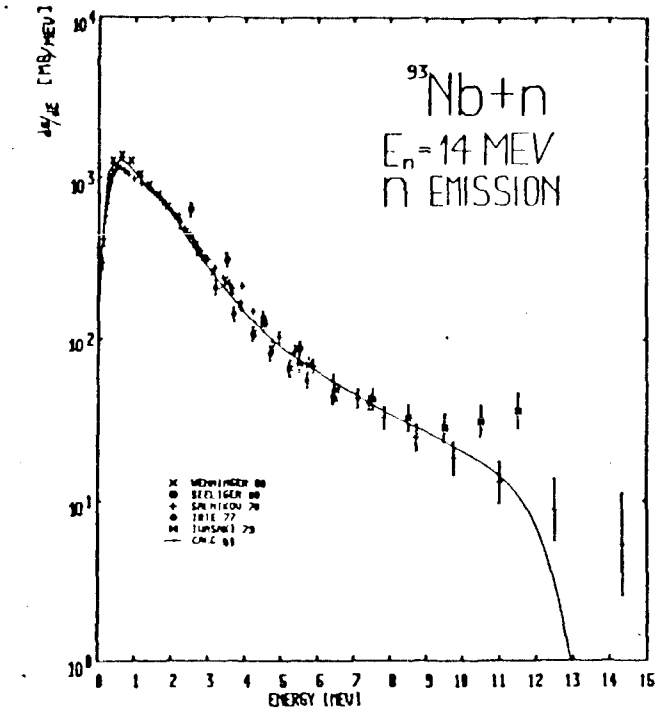

Fig. 4. Neutron production (CM system) from ^{93}Nb+n at 14 MeV incident neutron energy. The calculation comprises the contributions of (n,n') and (n,2n).

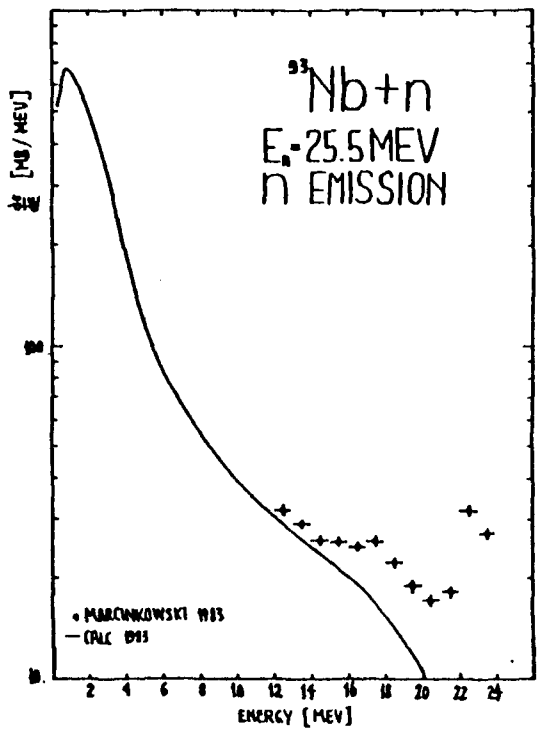

Fig. 5. Same as Fig. 4 for 25.5 MeV incident neutron energy.

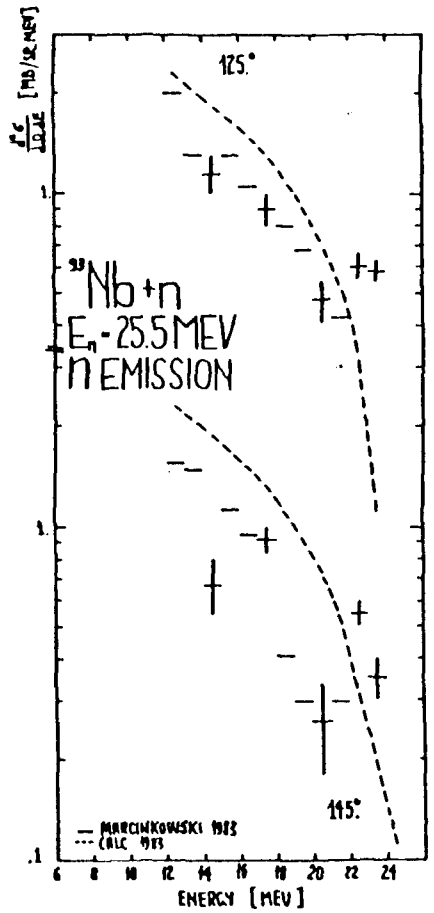

Fig. 6. Same as Fig. 5 for two angles.

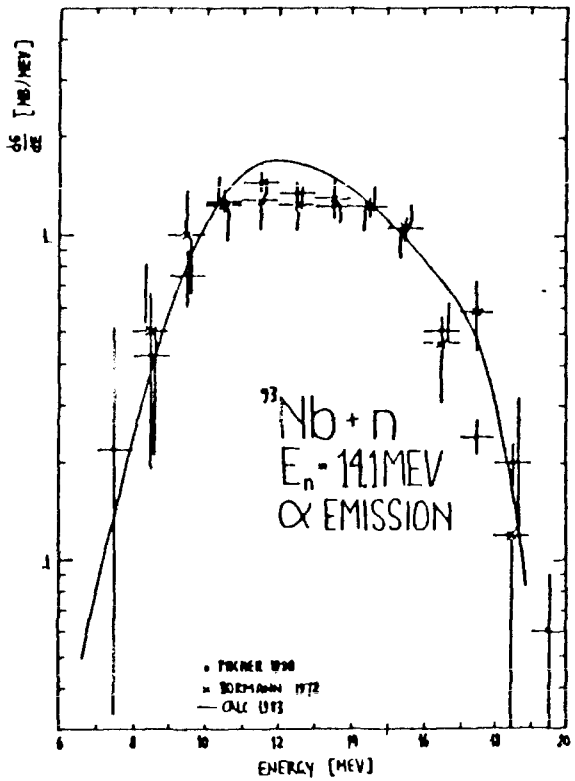

Fig. 7. Alpha-particle production (CM system) from ^{93}Nb+n at 14 MeV incident neutron energy. The calculation comprises the contributions of (n,α) and (n,n'α).

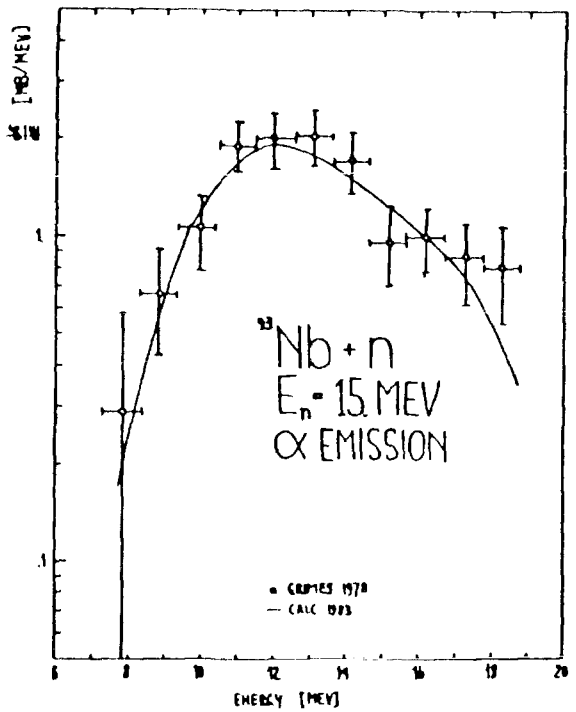

Fig. 8. Same as Fig. 7 for 15 MeV incident neutron energy.

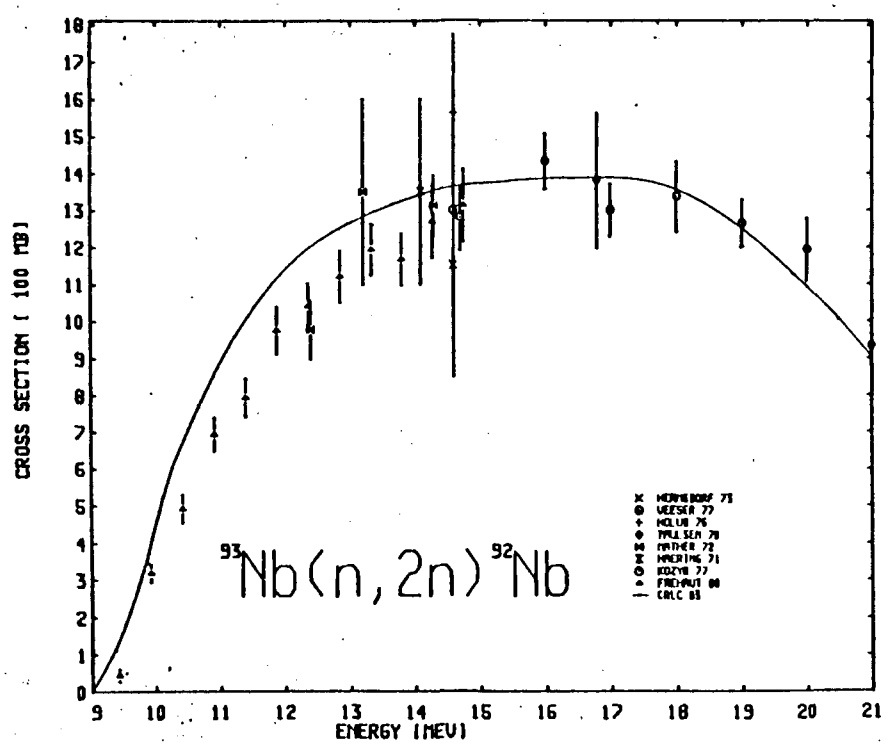

Fig. 9. Cross section for the reaction $^{93}Nb(n,2n)^{92}Nb$ versus incident neutron energy (lab. system).

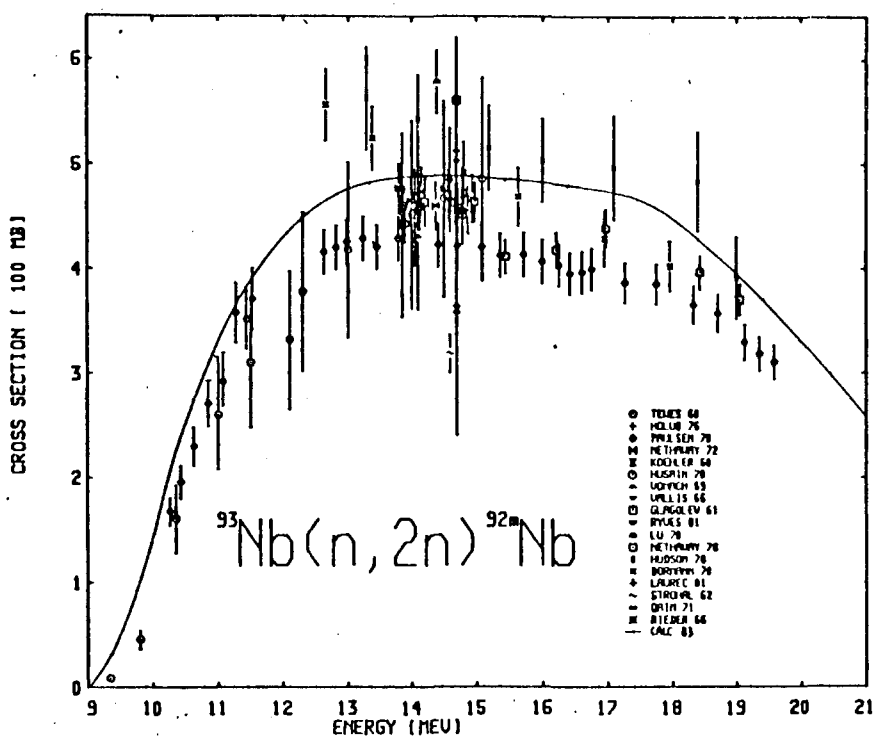

Fig. 10. Cross section for the reaction $^{93}Nb(n,2n)^{92m}Nb$ versus incident neutron energy (lab. system).

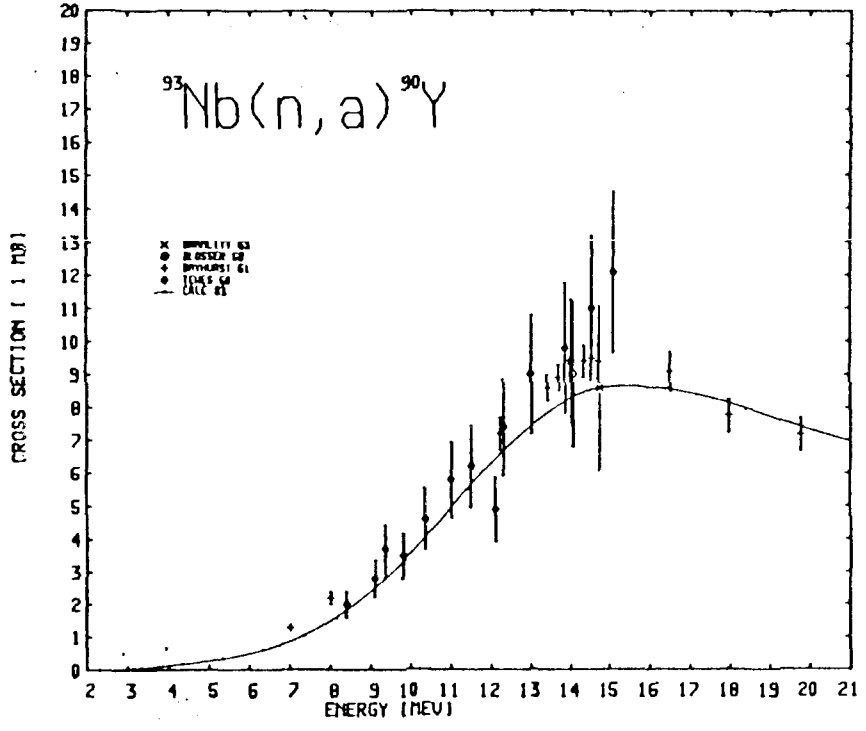

Fig. 11. Cross section for the reaction $^{93}Nb(n,\alpha)^{90}Y$ versus incident neutron energy (lab. system).

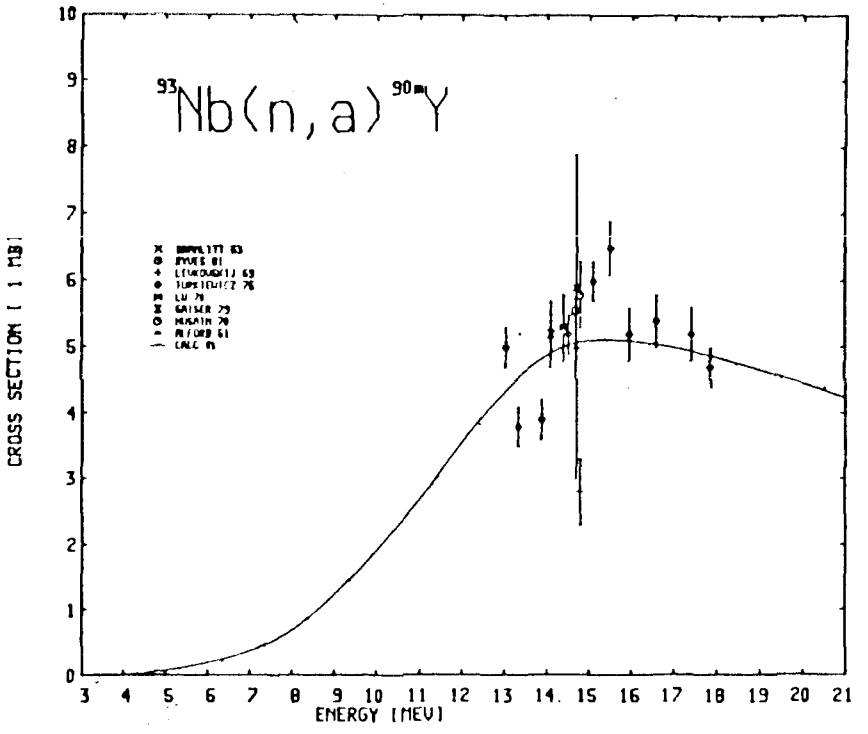

Fig. 12. Cross section for the reaction $^{93}Nb(n,\alpha)^{90m}Y$ versus incident neutron energy (lab. system).

Status of JENDL-2 Evaluated Data for Structural Materials

Tetsuo ASAMI

Nuclear Data Center
Japan Atomic Energy Research Institute
Tokai-mura, Naka-gun, Ibaraki-ken 319-11
JAPAN

Abstract

Status of the evaluated nuclear data for structural materials is outlined with emphasis on JENDL-2. The evaluated data in JENDL-2 are reviewed mainly for Fe, Ni and Cr which are the main constituents of stainless steel. The discussion is focussed on the cross-section data of interest in fast breeder reactor, fusion reactor and other application fields of atomic energy. The problems associated with the data evaluation and the requirements for the data format are also noted.

I. Introduction

The requirement for nuclear data of structural materials has extended over various items as the application fields in atomic energy have spread, and the requirement for their accuracy tends to become severer. The data for structural materials are needed not only for the development of fast breeder reactor (FBR) and fusion reactor but also operation, maintenance and decommissioning of reactors. These data include the cross sections for estimating induced-activities and the hydrogen- and helium-production cross sections for damage evaluation. In this paper, these evaluated data in JENDL-2 are reviewed mainly for Fe, Ni and Cr which are the main constituents of stainless steel. The discussion is focussed on the evaluated data for the resolved resonance parameters and for the inelastic scattering and threshold-reaction cross sections.

The measured and evaluated data on the neutron cross sections of structural materials for fast reactors were widely discussed at the 1977 Geel meeting[1]. At that meeting Smith et al.[2] reported the status of the experimental data for structural materials in relation to FBR. Froehner[3] discussed on the neutron resonance cross sections for structural materials at the 1978 Harwell Conference. The discussion for the neutron capture data was given at the 1982 ANL meeting[4]. The topical discussion was held for the nuclear data of structural materials at the 21st NEANDC meeting in 1979. Rowlands et al.[5] reviewed the status of the neutron cross- section data for structural materials at the 1982 Antwerp Conference. The present review will be given so as to avoid overlap with the discussions described above. Some problems in data evaluation are also described.

The first version[6] of Japanese Evaluated Nuclear Data Library (JENDL) was released in 1977 with the aim of being used mainly in design calculation of fast breeder reactor. The benchmark tests[7] for JENDL-1 have pointed out various problems although the tests have showed good results as a whole. Besides, addition of some important nuclides to JENDL has been required for use in wider fields of applications, i.e. fusion research, radiation shielding, nuclear fuel cycle etc.

The second version (JENDL-2) has been compiled to meet most of these requirements. The number of nuclides in JENDL-2 was increased from 72 (including 28 FP nuclides) in JENDL-1 to about 170 (including

about 90 FP nuclides). The upper limit of neutron energy was extended up to 20 MeV from 15 MeV. An outline of the data evaluation for JENDL-2 has already been described elsewhere[8]. The benchmark tests have been performed[9] on the JENDL-2 data for some selected nuclides, and have showed that JENDL-2 gives satisfactory results for fast reactor calculations. JENDL-2 contains the evaluated data for ^{51}V, Cr(^{50}Cr, ^{52}Cr, ^{53}Cr and ^{54}Cr), ^{55}Mn, Fe(^{54}Fe, ^{56}Fe, ^{57}Fe and ^{58}Fe), Ni(^{58}Ni, ^{60}Ni, ^{61}Ni, ^{62}Ni and ^{64}Ni), Cu(^{63}Cu and ^{65}Cu), ^{93}Nb and Mo(^{92}Mo, ^{94}Mo, ^{95}Mo, ^{96}Mo, ^{97}Mo, ^{98}Mo and ^{100}Mo) as structural materials. The whole reevaluation of the JENDL-1 data was made for most of these nuclides.

The status of the JENDL-2 data for structural materials is discussed in comparing mainly with the data in ENDF/B-IV and KEDAK-4 for the topical items described above. As ENDF/B-V is not generally available except the special purpose files, we examine the old ENDF/B-IV data which have been still used widely in Japan. We have not yet examined the ENDL82 file, the SOKRATOR file, the RCN-2 file and JEF (Joint Evaluated File), and have no information about the recent situation of the UKNDL file.

II. Status of Evaluated Data for Structural Materials

1. Neutron resonance parameters and low-energy neutron cross sections

JENDL-2 and ENDF/B-IV give the resolved neutron resonance parameters, instead of pointwise data, except for light nuclides. In JENDL-2 the resonance parameter sets were obtained from the experiments before 1980. For the Fe data of ENDF/B-V a new evaluation for the resonance parameters has been made[10], while the resonance parameters of Cr[11] and Ni[12] in ENDF/B-V have been left as they were in ENDF/B-IV.

Since the Geel meeting in 1977, the measurements on the neutron resonances of iron have been performed in Geel and KFK. However, these data were not considered in the above data files.

Figures 1 to 3 show the comparisons of the evaluated average capture cross-sections for Fe, Ni and Cr, respectively, in the neutron-energy range between 1 keV and 500 keV which is important for FBR. For the capture data of Fe and Ni there was generally no large discrepancy among the evaluated data files. As shown in Fig.3, however, the Cr data of ENDF/B-IV deviate largely from the other evaluated data in the energies from 10 keV to 60 keV, in spite of having the resonance parameters similar to those of JENDL-2. It is found that the Cr data of ENDF/B-IV have a large "background" cross section for neutron capture. As we pointed out elsewhere[13], this might cause the overestimation of the central reactivity worth observed in the benchmark tests[7].

As important data for structural materials there is the well-known "window" cross sections of ^{56}Fe around 24 keV. This "window" cross section was not able to be reproduced with the resonance parameters of the multi-level Breit-Wigner(MLBW) formula without background cross section, in both ENDF/B-IV and JENDL-1[13]. Froehner[3] showed that the Reich-Moore formalism was adequate to calculate these "window" cross sections without any "background" cross section. However, the Reich-Moore formalism have been excluded in the recent ENDF/B-V format rules[15]. In JENDL-2 the "window" cross sections was reproduced with the MLBW formula by truncating the contribution from higher distant levels. This was made by using the subsection structure in File 2 of the ENDF/B format. The subsection structure in the resolved resonance region is not allowed in the ENDF/B format. In the final JENDL-2 file,

therefore, the data in this structure was altered into the ordinary one with the "background" correction.

The shape of off-resonance cross section as well as the "window" one is very sensitive to the effective scattering radius R'. In general, however, the values of R' have not yet been investigated in detail and older data have often been used. Table 1 lists the values of R' used in JNEDL-2 and ENDF/B-IV and the recommended values of BNL-325 3rd ed.[16] and 4th ed.[17]. The R' values in the evaluated data file have often been taken from the recommended ones of BNL-325. For some nuclides in JENDL-2, however, the R' values were determined so as to provide a good fitting to the experimental data.

Unfortunately, few experimenters on neutron resonance have generally given the R' values used (or fitted) in a shape analysis of resonance in their literature. On the other hand, almost all the resonance analyses have provided a single values of R' in rather wide neutron energies, although the R' value is essentially dependent on neutron energy. As a matter of fact the energy-dependent R' values needed for the evaluations of the Ni isotope data[18] in JENDL-2 and of ^{56}Fe data[10] in ENDF/B-V. However, the energy-dependent R' is not allowed in the present format of ENDF/B.

2. Inelastic scattering cross sections

The inelastic scattering data for structural materials are most important for both FBR and fusion development. Although many measurements on the inelastic scattering have been performed recently the status of experimental data for structural materials is yet unsatisfactory and the main part of the data evaluation for inelastic scattering has to rely on theoretical estimation.

In JENDL-2, the evaluation of the excitation cross sections for some low-lying levels was made based on measured data. For example, the excitation cross section for the 845-keV of ^{56}Fe were estimated from the measurement on $(n,n'\gamma)$. The high-energy part of the inelastic scattering cross sections for some levels of Cr and Ni was estimated using the measured data. However, the inelastic scattering cross sections for most of the discrete levels were generally estimated from the statistical model calculations with the CASTHY code[19]. In order to make these calculations on a common base, the parameters for the optical model and the level density have been studied systematically. Kawai[20] has determined the spherical-optical model parameters for structural materials to reproduce the experimental values of the average total cross section in rather wide energy range of a few tens of keV to 20 MeV (SPRT method[22]). Figure 4 shows an example for some structure materials. Kawai's parameters also explain well the angular distributions for the elastic scattering over wider energy range as shown in an example for chromium (Fig.5). The level density parameters have been determined systematically by Yoshida[21] for the composite formula of Gilbert-Cameron[23], which was corrected for the spin cut-off factor, using recent data of the level spacing and low-lying levels.

The evaluated inelastic scattering cross sections for some major levels are shown in Figs.6, 7 and 8 for Fe, Ni and Cr, respectively, in comparing with the experimental data. These evaluated data of the inelastic scattering cross sections are in good greement with the experimental data below several MeV.

The sensitivity analyses have been carried out to examine the role of the partial inelastic scattering cross sections for the Fe data of

both JENDL-1 and ENDF/B-IV from the viewpoint of shielding application[24], and it was pointed out that even the contribution from minor discrete levels should not be disregarded in the data evaluation of the inelastic scattering cross section. In ENDF/B-IV the contributions from ^{57}Fe and ^{58}Fe on the inelastic scattering cross sections of element Fe are neglected while these are taken account of in JENDL-1 and -2. However, all the Fe stable isotopes except ^{57}Fe are even nuclides with large level-spacing compared to that of ^{57}Fe, and all the contribution from the levels below the first 845-keV level of ^{56}Fe results in the low-lying levels of ^{57}Fe. The senaitivity test indicated that a neutron flux below 10 keV increased about 60 % at 30 cm from the central 0.65-MeV source when the cross sections for inelastic sacttering to the low-lying levels of ^{57}Fe and ^{58}Fe were added in the ENDF/B-IV data. It also showed that the neutron flux increased by about 20 % even for a 14-MeV neutrons. On the basis of these tests the Fe data of ENDF/B-V have been revised in 1982[25].

The analysis of the trasmitted neutron spectra below a few MeV also indicates some features of the inelastic scattering cross section for structural materials. Kimura et al.[26] have tested the evaualted data of Fe, Ni, Cr, Ti, Nb and Mo in JENDL-2/JENDL-1 and ENDF/B-IV through transmitted neutron spectra, and have showed that the inelastic scattering cross sections to discrete levels often are very important in the prediction of spectrum.

Although JENDL-2 gave rather good results in the benchmark tests[9] for the fast reactor systems as described above, some problems have been pointed out in analyses of fusion neutronics, particularly on the inelastic scattering cross section for higher-energy neutrons. The benchmark test[27] of the Fe data in JENDL-2 has been performed for the experiments on trasmitted spectra of the 14-MeV neutrons by Hansen et al[28]. Figure 9 shows the comparison of the experimental neutron leakage spectrum with the calculated ones from the evaluated data. The spectrum calculated with the JENDL-2 data deviates markedly from the experimental one in the neutron energies of a few MeV to about 12 MeV, whereas the calcualted one from the ENDF/B-IV data are in good agreement with the experimental data. This resulted from the fact that the first-level cross section of Fe in JENDL-2 was underestimated by several 10 mb above a few MeV because of neglecting direct process in the data evaluation, as shown in Fig. 6. As the JENDL-2 data for structural materials aimed originally to be used mainly for fast reactor calculations the direct process was igonored. This drawback is very severe for the fusion reactor applications and will be revised before the compilation of JENDL-3.

Takahashi et al.[29] have also measured the secondary neutron spectra scattered inelastically from structural materials using the 14-MeV neutrons, and have compared the measured spectra with the calcualted ones from the ENDF/B-IV data. They have showed that the measured spectra have strong anisotropy in the neutron energies of 5 to 14 MeV and the anisotropy should be considered correctly in the evaluated data of the inelastic scattering cross sections for discrete levels.

3. Threshold reaction cross sections

As for the threshold reaction cross sections, the evaluated data have to be given accurately for each stable isotope. In some cases, the threshold cross section of element is not usually determined by that of

major isotope. For the reactions whose experimental data were abundant, the evaluated data of JENDL-2 were obtained by a least-squares fitting to the measured values. For the other threshold reactiona the cross sections were estimated from theoretical calculationa combined with experimental data. In the theoretical calculationa the multi-step Hauser-Feshbach evaporation codes, GROGI[30] and GNASH[31] were often used and the calculated values were usually normalized to the so-called 14-MeV values. The parameters for the optical model and the level density described above were used.

The (n,p) cross sections of element Fe above 10 MeV are governed by the contribution from ^{56}Fe of the major isotope. Below 6 MeV, on the contrary, are determined by the (n,p) cross section for ^{54}Fe with minor abundance. The (n,p) cross section of ^{56}Fe is as well known as it has been utilized as a standard for dosimetry. In Fig. 10, the ^{54}Fe (n,p) cross section of JENDL-2 are compared with both the other evaluated data and the experimental ones. The evaluated data of the ^{54}Fe (n,p) cross section is also satisfactory below 6 MeV, while the data between 6 and 14 MeV are still uncertain. Hence, it is considered that the (n,p) data of element Fe have been established. The (n,p) cross sections of element Ni and Cr are determined mainly by ^{58}Ni and ^{52}Cr of the major isotopes, respectively. The (n,p) cross section of ^{58}Ni is well known as dosimetry reaction and the evaluated data are sufficient. Those of ^{52}Cr, on the other hand, are still unstisfactory as illustrated in Fig.11.

The measured data on the (n,n'p) cross sections* for structural materials are generally scarce and moreover are limited around 14 MeV.

* The (n,n'p) cross section meana the sum of the (n,n'p) and (n,pn') cross sections. The (n,n'a) cross section means also like this.

The (n,n'p) cross sections for structural materials have a general trend to be in the same order of magnitude as that of the (n,p) cross section around 14 MeV and to increase abruptly with decreasing the (n,p) cross section. Hence the (n,n'p) reaction significantly contributes to hydrogen production in fusion reactors in spite of the minor effect in FBR systems. The other hydrogen production reactions of (n,d), (n,t), (n,2p) etc. are generally less important for structural materials in these energies. Therefore the evaluated data file should contain accurate data of the (n,n'p) reaction for structural materials. As the data evaluation for the (n,n'p) reaction has to rely fully on the theoretical estimation in the present, a series of the recent measurements on the charged-partice-producing reactions for structural materials at Lawrence Livermore Laboratory[32)~34)] is very valuable for evaluating the gas production data. Figures 12 and 13 show the comparison of the hydrogen production [(n,p) + (n,n'p)] cross-section for element Cr and Ni between the evaluated and experimental data. Although the JENDL-2 data on the hydrogen production cross section for both Cr and Ni are in good agreement with the experimental data by Grimes et al.[32] at 15 MeV, the evaluated ones at higher energies remain uncertain. On the other hand, the hydrogen production cross sections for Fe in ENDF/B-IV agree with the experimental data as shown in Fig. 14. The Fe data in JENDL-2 and KEDAK-4 are insufficient for the hydrogen production because of no data of the (n,n'p) cross section.

In general, the (n,α) and (n,n'α) cross sections for structural materials are not well known and the requirements even for the (n,α) cross sections have generally not been met. The status of the experimental data on the (n,α) and (n,n'α) cross sections has not

changed since the review by Smith et al.[2] at the 1977 Geel meeting.

The iron (n,α) cross sections are largely governed by the contribution from ^{56}Fe. However, the (n,α) cross section of ^{56}Fe cannot be measured with activation techniques and then has to be estimated from theoretical calculations. On the other hand, the ^{54}Fe (n,α) cross section is rather well known, as shown in Fig.15. The evaluated data for the helium-production cross section of element Fe are compared with the experimental data in Fig. 16. Although the Fe data of ENDF/B-IV for the helium-producing cross section is in a good agreement with the experimental data of Grimes et al.[32] and Kneff et al.[35], the JENDL-2 and KEDAK-4 data are largely overestimated. This might be due to the overestimation of the ^{56}Fe (n,α) cross section.

In the (n,α) cross section of element Ni the contribution from ^{58}Ni of the major isotope is dominant. The measurements on the (n,α) cross section of ^{58}Ni are limited around 14 MeV, and the measurement of the (n,n'α) cross-section has not been made. Figure 17 shows the compariaon of the evaluated data for the helium-production cross section of element Ni. Both the (n,n'α) cross-section data of JENDL-2 and the (n,α) ones of ENDF/B-IV seem to be overestimated. Thus the requirements for the helium-production cross section of element Ni are not met.

The measured data on the (n,α) cross section for stable isotopes of Cr are available only around 14 MeV. In JENDL-2, therefore, the evaluated data of the (n,α) reaction cross sections for the Cr isotopes were obtained from the theoretical calculations. In Fig.18 the evaluated (n,α) and helium-production cross sections of element Cr are compared with the experimental data. The agreement between them is fairly good as compared to the cases for Fe and Ni. The evaluated (n,α) cross section of JENDL-2 are in good agreement with both the measured data by Grimes et al.[32] and the ENDF/B-IV data of the helium production cross section at 15 MeV . This fact suggests that the (n,n'α) cross sections of element Cr are less prominent for helium production, at least below 15 MeV. The helium production cross sections for other structural materials would be in the situation similar to this.

The evaluated (n,2n) cross sections of JENDL-2 for Fe, Ni and Cr are compared with the other evaluated dats and the experimental ones in Figs. 19 to 21, respectively. No structural material except ^{93}Nb and Mo acts as neutron multiplier for fast breeder reactor and fusion reactor. However, some (n,2n) cross sections are of considerable interest in production of activity as described below.

4. Activation cross sections

Among the reactions described above, all the reactions conducted towards induced activity are treated as activation ones. The various types of the activation cross sections are needed for estimating induced activities for some structural materials. In the present the large evaluated nuclear data files do not treat the data relevant to activation reactions, except the special purpose files for fission products, dosimetry etc. and some files have been compiled to estimate the induced activity in connection with computer-code system (for example, THIDA library [36),37)]). Most of these files are tentative and the data contained in these files are restricted in a small number. The needs for such data file have increased gradually. Fortunately the format for the isomer-production cross section has been newly defined in ENDF/B-V. Therefore, it would be desirable that the general purpose

file contains isotopic data as in JENDL and KEDAK, not only elemental data, and gives the activation cross section for many nuclides.

III Further Problems in Data Evaluation

The following problems are pointed out through the above discussions on evaluated data for structural materials.

(1) Systematic study on parameters for optical model and level density

As described above, a considerable part of data evaluation has to rely on theoretical calculations. In the calculation, plenty of parameters, especially the parameter sets for optical model and for level density are needed. For individual data files, it is necessary that these parameter sets are determined systematically in data evaluation. For the optical-model parameters, it is also desirable that a single data-set can cover a wide energy range. Although the Gilbert-Cameron's parameters[23] for level density have been widely used, these parameters remain as they were obtained based on rather old data. Therefore a whole revison for these data is required. Another approach for level density has often employed the back-shifted Fermi- gas model[38-40] in which Lang-Le Couteur formulation[41] was used. Dilg et al.[42] have given the parameters for this model in the mass range from 40 to 250. Hence, it is desirable that nuclear model codes can accept these two types of the parameters for level density.

(2) Consistent nuclear model calculations

The evaluated data above about 10 MeV for structural materials are generally insufficient except the total cross sections of elements. For applications to fusion reactor development the improvement on the accuracy of these data is required especially for the inelastic scattering cross section. In the theoretical estimations for this data, the direct process and the pre-equilibrium process have to be taken into account at higher energies. The coupled-channel calculation is required for the low-lying levels with collective states. Especially these processes should be estimated in a consistent way with the statistical-model calculations. The parametrization for the coupled-channel calculation is also required.

(3) Variety of evaluated data in general purpose file

Generally the data evaluation for general purpose file should not be directed towards specific engineering objectives and should be done for all the significant reactions and for all the stable isotopes existing in element.

For gas-production estimates the data evaluations for both the (n,n'p) and (n,n'α) reactions are essential. Especially the data on the (n,n'p) reaction are indispensable for hydrogen-production estimation.

Recently the evaluated data on photon production (cross section, angular distributions and spectra of photon) are needed for the applications to shielding calculation, gamma-heating estimations and so on. Nevertheless only the ENDF/B file and the ENDL file have the evaluated data on photon production for restricted nuclides. Moreover these photon-production data are not always enough both for accuracies and for the number of nuclides. Some photon-production data in ENDF/B-IV are lacking in energy balance. This is because the data evaluations for photon production (files 12 to 15) would have been made independently of that for the other reactions. In the ENDF/B-V data this point might have been fully improved, but these ENDF/B-V data are not available outside U.S.A. and Canada. JENDL-3 aims to have the

photon production data for some prominent nuclides including structural materials. The large evaluted data files should have these data for many nuclides.

(4) "Background" cross section

An artificial "background" (or "smooth") cross section has often been used unavoidably in the evaluation for the resonance cross section. Since the background cross sections affect the calculations of Doppler broadened cross section and of self-shielding factor, the backgrounds should be given in small amount and in smooth curve without structures. However, in the case that the evaluated parameter set is obtained by the formula which is not permitted for data file, the background cross sections have sometimes large positive or negative values and show complex structures. In this reason it is desirable that various resonance formula are permitted for data evaluation, as described below.

VI. Requirement for data format

In the present the ENDF/B format has been widely used in the world and the number of data file which adopts the ENDF/B format has gradually increased. The JENDL-2 data have been compiled in the ENDF/B-IV format and JENDL-3 intends to adopt the ENDF/B-V one. From this standpoint, we would address some requirements for the ENDF/B-V format and its format rules.

Experimenters for the neutron resonances have often used the Reich-Moore formalism in their analysis of the resonance parameters for medium-weight nuclides. As described above, the Reich-Moore resonance parameter representation is no longer permitted in the ENDF/B-V format[15]. This causes the adoption of unreasonable "background" cross section to use the formalism different from that of the resonance parameters obtained originally. Therefore, the ENDF/B-V format would be better to treat the Reich-Moore representation of the resonance parameters at least in the manner similar to ENDF/B-IV.

The data evaluation for the accurate resonance cross sections requires the energy-dependent effective scattering radius. The ENDF/B-V format has not accepted the energy-dependent scattering radius in File 2. Therefore, we expect a partial revision of the format rule in ENDF/B-V for this respect.

V. Conclusions

The JENDL-2 data for Fe, Ni and Cr are reviewed in comparing with that those of ENDF/B-IV and KEDAK-4. The cross sections for the resolved resonance, neutron capture, inelastic scattering and threshold reactions are disccused. Although these evaluated data for structural materials are satisfactory for fast reactor calculations some drawbacks are observed for application to the fusion research. The further problems on the data evaluation are pointed out through these discussions. The requirements for ENDF/B-V format and its format rule are also presented.

Acknowledgment

The author wishs to express his sincere thanks to Drs. S. Igarasi, Y. Kikuchi, T. Nakagawa and K. Shibata of JAERI nuclear Data Center for their valuable discussion on the structural material data and the data evaluation. The author also wishs to thank the members of Japanese Nuclear Data Committee (JNDC), especially Drs. S. Iijima, H. Yamakoshi,

M. Kawai and M. Hatchya for many helpful comments. This work was supported by JNDC.

References

1) K.H. Boeckhoff (ed.): Neutron Data on Structural Materials for Fast Reactors, Proceedings of a Specialists' Meeting held at the Central Bureau for Nuclear Measurements, Geel, Belgium, 5-8 December 1977 (Pergamon Press, 1979).

2) A. Smith, R. McKnight and D. Smith: Energy-Averaged Cross Sections of Fast-Reactor Structural Materials, Ref(1) p.374.

3) F.H. Froehner: Resonance Cross Sections for Structural Materials, Proc. of Intern. Conf. on Neutron Physics and Nuclear Data for Reactors and Other Applied Purposes, Harwell 1978, p.268.

4) A. B. Smith and W.P. Poenitz (ed.): Proceedings of the NEANDC/NEACRP Specialist's Meeting on Fast-Neutron Capture Cross Sections ,April 20-23, 1982, NEANDC(US)-214/L (1983).

5) J. L. Rawlands, R. W. Smith, J. M. Stevenson and W. H. Taylor : Convergence of Integral and Differential Cross-Section Data for Structural Materials, Proceedings of the International Conference on Nuclear Data for Science and Technology, Antwerp, 6-10 Sept. 1982, (D. Reidel Pub. Comp., 1983) p.85.

6) S. Igarasi, T. Nakagawa, Y. Kikuchi, T. Asami and T. Narita: Japanese Evaluated Nuclear Data Library, Version-1 --- JENDL-1 ---, JAERI 1261 (1978).

7) Y. Kikuchi, A. Hasegawa, H. Takano, T. Kamei, Y. Hojuyama, M. Sasaki, Y. Seki, A. Zukeran and I. Otake : Benchmark Tests of JENDL-1, JAERI - 1275 (1982).

8) Y. Kikuchi and Members of JNDC : Present Status and Benchmark Tests of JENDL-2, Proceedings of the International Conference on Nuclear Data for Science and Technology, Antwerp, 6-10 Sept. 1982, (D. Reidel Pub. Comp., 1983) p.615.

9) Y. Kikuchi, T. Narita and H. Takano: J. Nucl. Sci. Tech. 17, 85 (1980).

10) C.Y. Fu and F.G. Perey: Evaluation of Neutron and Gamma-Ray-Production Cross Sections for Natural Iron (ENDF/B-V MAT 1326), ORNL/TM-7523 (1980).

11) A. Prince and T.W. Burrows: Evaluation of Natural Chromium Neutron Cross Sections for ENDF/B-V, BNL-NCS-51152, ENDF-286 (1979).

12) M. Divadeenam: Ni Elemental Neutron Induced Reaction Cross-Section Evaluation, BNL-NCS-51346, ENDF-294 (1979).

13) T. Asami, Y.Kikuchi, T. Nakagawa and S. Igarasi: Structural Material Data Evaluation for JENDL-1, Ref(1) p.118.

14) H. Yamakoshi and S. Iijima: J. Nucl. Sci. Tech. 17, 81 (1980).

15) R. Kinsey (rev.): Data Fromats and Procedures for the Evaluated Nuclear Data File, ENDF, BNL-NCS-50496 (ENDF-102), 2nd Edition (ENDF/B-V) (1979).

16) S.F. Mughabghab and D.L. Garber: Neutron Cross Sections, Resonance Parameters, BNL-325,3rd ed. Vol.1 (1973).

17) S.F. Mughabghab, M. Divadeenam and N.E. Holden: Neutron Cross Sections, Vol.1, Neutron Resonance Parameters and Thermal Cross Sections, Part A, Z = 1 - 60, (Academic Press, 1981).

18) Y. Kikuchi: private communication (1982) and this meeting(1983).

19) S. Igarasi: J. Nucl. Sci. Tech. 12, 67 (1975).

20) M. Kawai: Determination of Spherical Optical Model Parameters for Structural Materials, JNDC Progress Report, NEANDC(J)-61/U, INDC(JAP)-47/U (1979) p.18 (unpublished).

21) T. Yoshida: Systematic Determination of Level Density Parameters for Structural Materials (Cr, Fe, and Ni), ibid. p.16 (1979) (unpublished).

22) J.P. Delaroche, Ch. Lagrange, and J. Salvy: The Optical Model with Particular Consideration of the Coupled-Channel Optical Model, IAEA-190 (1975) p.251.

23) A. Gilbert and A.G.W. Cameron: Can. J. Phys. 43, 1446 (1965).

24) M. Kawai, N. Yamano and K. Koyama: Request to Evaluating Neutron Cross Section of Structural Material for Shielding Application, Proc. of Intern. Conf. on Nuclear Cross Sections for Technology, Knoxville, Oct. 1979, NBS Special Pub. 594 (1980) p.586.

25) C.Y. Fu: Summary of ENDF/B-V Evaluations for Carbon, Calcium, Iron, Copper, and Lead and ENDF/B-V Revision 2 for Calcium and Iron, ORNL/TM-8283, ENDF-325 (1982).

26) I. Kimura, S.A. Hayashi, K. Kobayashi, S. Yamamoto, H. Nishihara, T. Mori and M. Nakagawa: The Integral Check of Neutron Cross Section Data for Reactor Structural Materials by Measurement and Analysis of Neutron Spctra, Proc. of the Intern. Conf. on Nuclear Data for Science and Technology , Antwerp,6-10 Sept. 1982,(D. Reidel Publishing Comp.,1983) p.98.

27) N. Yamano: Problems in Evaluation on Inelastic scattering Cross Section of Iron , JAERI-M 9523 (1981) p.50 (in Japanese).

28) L.F. Hansen: Nucl. Sci. Eng. 60, 27 (1976).

29) A. Takahashi, J. Yamamoto, T. Murakami, K. Oshima, H. Oda, K. Fujimoto and K. Sumita: Measurement of Double Differential Neutron Emission Cross Sections with 14 MeV Source for D, Li, Be, C, O, Al, Cr, Fe, Ni, Mo, Cu, Nb and Pb, ibid. p.360.

30) J. Gilat: GROGI2--A Nuclear Evaporation Computer Code, Description and User's Manual, BNL-50246(T-580) (1970).

31) P.G. Young and E.D. Arthur: GNASH-- A Preequilibrium, Statistical Nuclear-Model Code for Calculation of Cross Sections and Emission Spectra, LA-6947 (1977).

32) S.M. Grimes and R.C. Haight: Phys. Rev. C19, 2127 (1979).

33) S.M. Grimes, R.C. Haight and J.D. Anderson: Phys. Rev. C17, 508 (1978).

34) R.C. Haight, S.M. Grimes and R.G. Johnson: Phys. Rev. C23, 700 (1981).

35) D.W. Kneff, B.M. Oliver, M.M. Nakata and Harry Farrar IV: Helium Generation Cross Sections for Fast Neutrons, BNL-NCS-51245 (1980) p.289.

36) H. Iida and M. Igarashi: THIDA --- Code System for Calculation of the Exposure Dose Rate around a Fusion Device, JAERI-M 8019 (1978) (in Japanese).

37) Y. Seki, H. Iida and H. Kawasaki: Graphical Representation of Transmutation and Decay Chain Data, Transmutation Cross Section and Delayed Gamma Ray Emission Data, JAERI 1280 (1982).

38) E. Gadioli and L. Zetta: Phys. Rev. 167, 1016 (1968).

39) J.R. Huizenga, H.K. Vonach, A.A. Katsanos, A.J. Gorski and C.J. Stephan: Phys. Rev. 182, 1149 (1969).

40) H. Vonach and M. Hille: Nucl. Phys. A127, 289 (1969).

41) D.W. Lang and K.J. Le Couteur: Nucl. Phys. 14, 21 (1959).

42) W. Dilg, W. Schantl, H. Vonach and M. Uhl: Nucl. Phys. A217, 269 (1973).

Table 1 Recommended and Evaluated Values of Effective Scattering Radius, R'(fm)

	BNL-325 3rd ed[16]	BNL-325 4th ed[17]	ENDF/B-IV	JENDL-2
^{51}V	6.9 ± 0.2	6.9 ± 0.2	6.308	5.0
^{50}Cr	5.4 ± 0.4	5.0 ± 0.3	4.95	5.4
^{52}Cr	5.7 ± 0.3	5.2 ± 0.4	5.9	5.1
^{53}Cr	6.9 ± 0.3	5.4 ± 0.3	6.9	6.9
^{54}Cr	4.8 ± 0.2	5.3 ± 0.3	6.5	4.8
^{55}Mn	3.6 ± 0.4	———	4.54	5.3
^{54}Fe	5.6 ± 0.6	5.0 ± 0.3	4.6	5.6
^{56}Fe	6.1 ± 0.7	6.1 ± 0.3	4.6	5.4
^{57}Fe	6.5 ± 0.7	5.9 ± 0.3	4.6	6.5
^{58}Fe	———	———	——	5.9
^{59}Co	5.3 ± 0.4	6.80 ± 0.70	6.8	6.8
^{58}Ni	7.3 ± 0.4	8.0 ± 0.5	7.5	7.5
^{60}Ni	6.7 ± 0.3	6.7 ± 0.3	6.5	6.5
^{61}Ni	6.4 ± 0.3	6.5 ± 0.3		6.4
^{62}Ni	6.2 ± 0.3	6.2 ± 0.3	6.9	6.2
^{64}Ni	6.4 ± 0.1	7.55 ± 0.3	7.5	6.4
^{63}Cu	7.1 ± 0.2	6.7 ± 0.3	7.302	6.7
^{65}Cu	7.1 ± 0.2	6.7 ± 0.3	7.302	6.56
^{93}Nb	7.0 ± 0.2	6.9 ± 0.1	7.024	7.1
^{92}Mo	6.4 ± 0.8	7.0 ± 0.2	6.0944	7.0
^{94}Mo	6.5 ± 1.3	7.2 ± 0.2	6.1382	7.2
^{95}Mo	7.1 ± 1.4	7.0 ± 0.2	6.1599	7.0
^{96}Mo	6.6 ± 1.3	7.0 ± 0.2	6.1815	7.0
^{97}Mo	6.6 ± 1.3	6.9 ± 0.2	6.2028	6.9
^{98}Mo	7.0 ± 1.4	6.9 ± 0.2	6.2240	6.9
^{100}Mo	6.5 ± 1.3	6.9 ± 0.2	6.2662	6.9

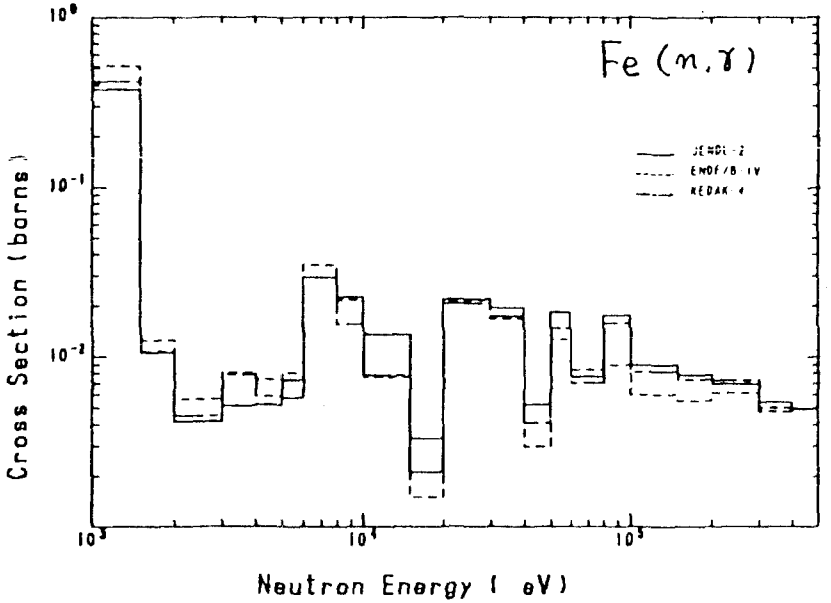

1. Comparison of the evaluated average capture cross section of JENDL-2 for Fe with those of ENDF/B-IV and KEDAK-4.

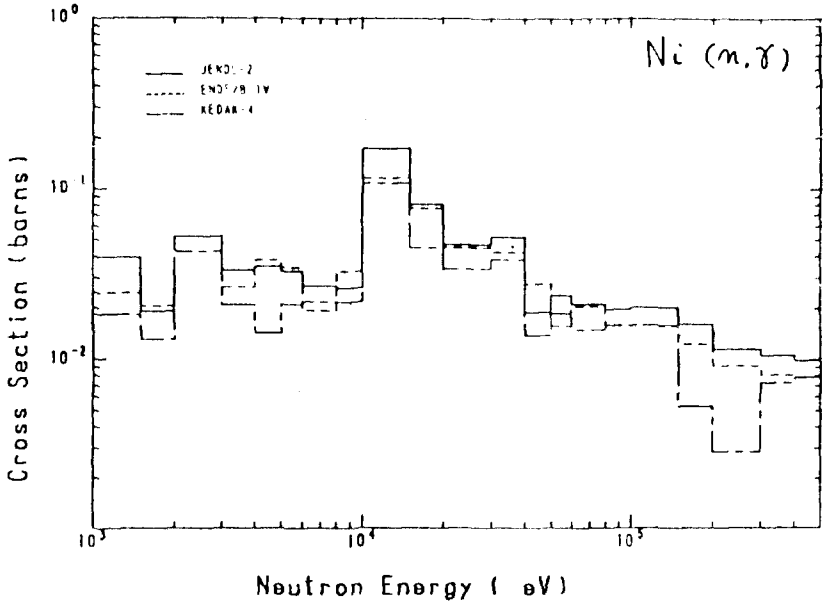

2. Comparison of the evaluated average capture cross section of JENDL-2 for Ni with those of ENDF.B-IV and KEDAK-4.

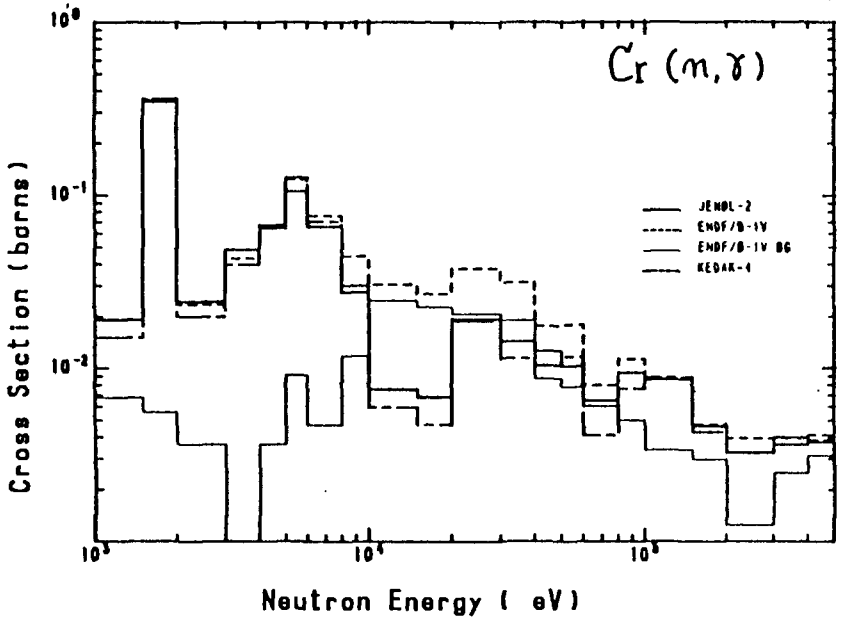

3. Comparison of the evaluated average capture cross section of JENDL-2 for Cr with those of ENDF/B-IV and KEDAK-4.

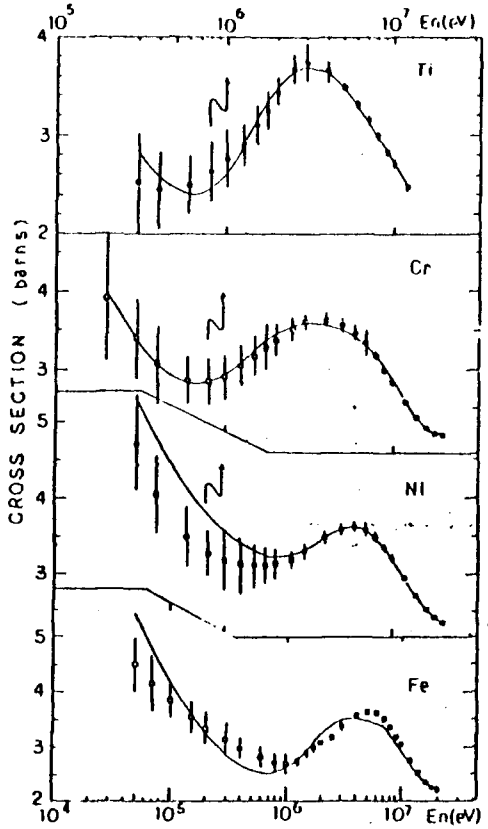

4. The calculated total cross sections for some structural materials compared with the experimental data. Ref(20)

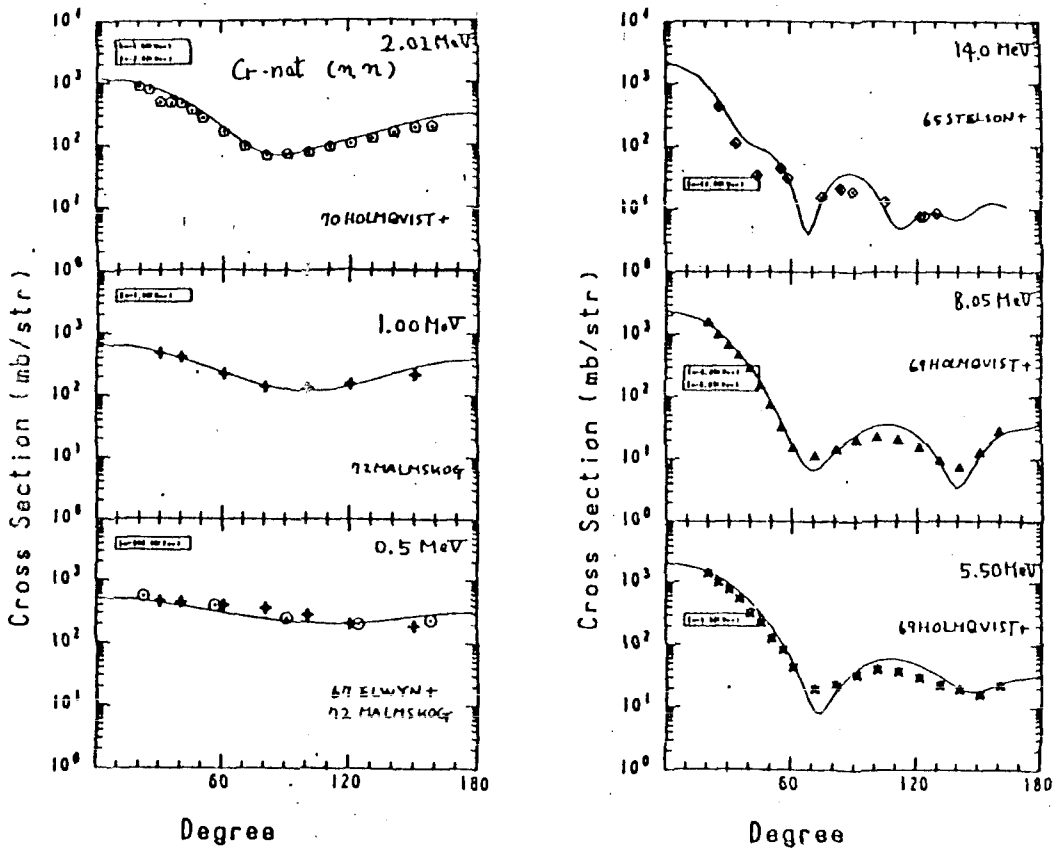

5. The calculated angular distributions for Cr.

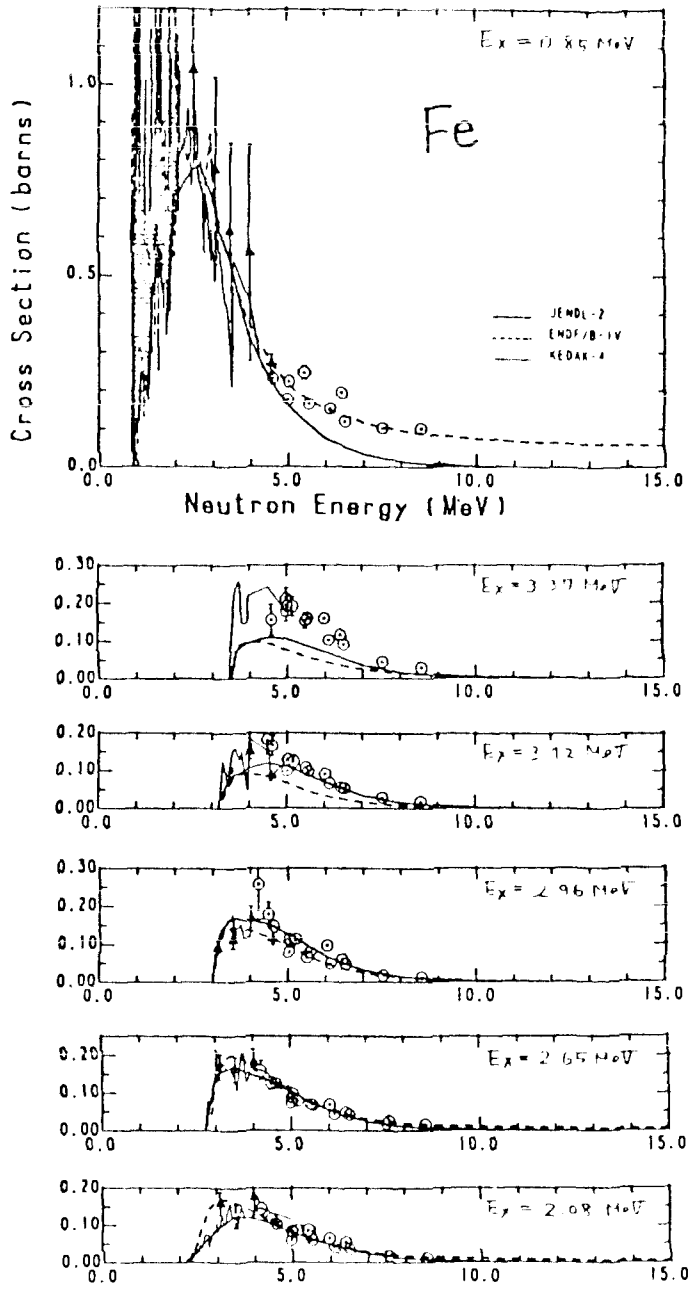

6. Inelastic scattering cross sections of Fe for the low-lying discrete levels. The evaluated data of JENDL-2 are compared with those of ENDF/B-IV and KEDAK 4 and with the experimental data.

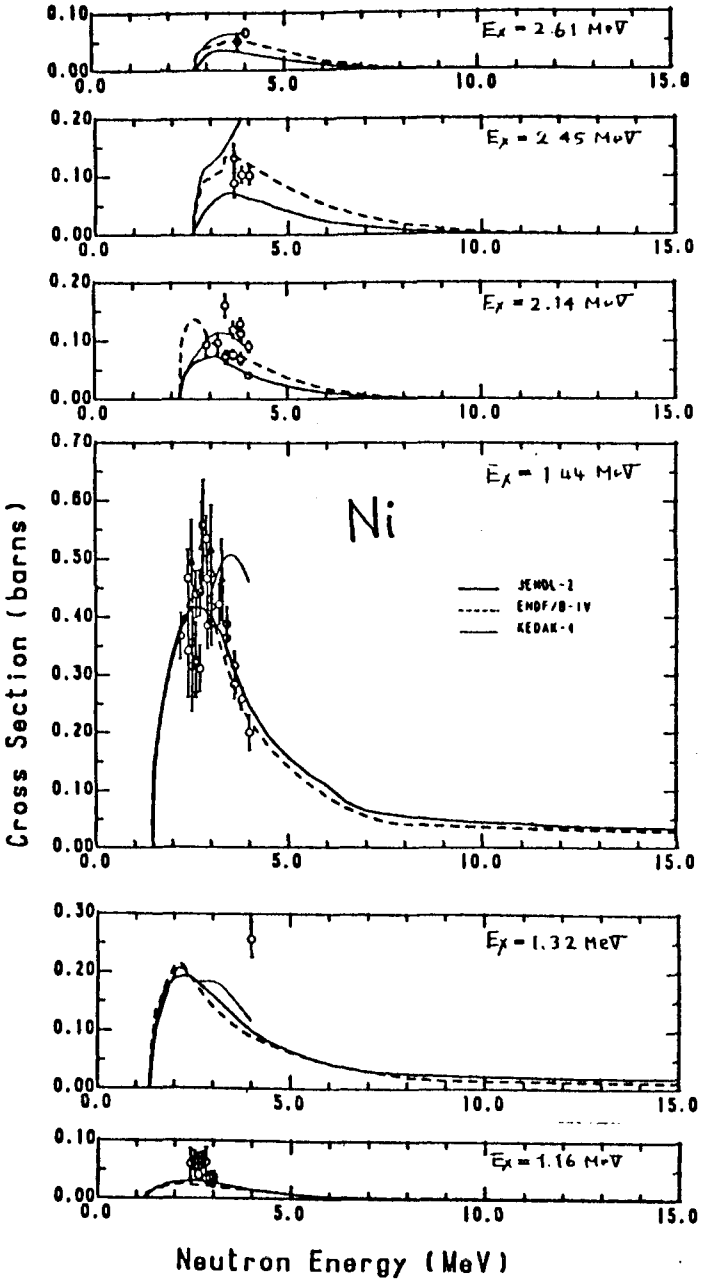

7. Inelastic scattering cross sections of Ni for the low-lying discrete levels. The evaluated data of JENDL-2 are compared with those of ENDF/B-IV and KEDAK-4 and with the experimental data.

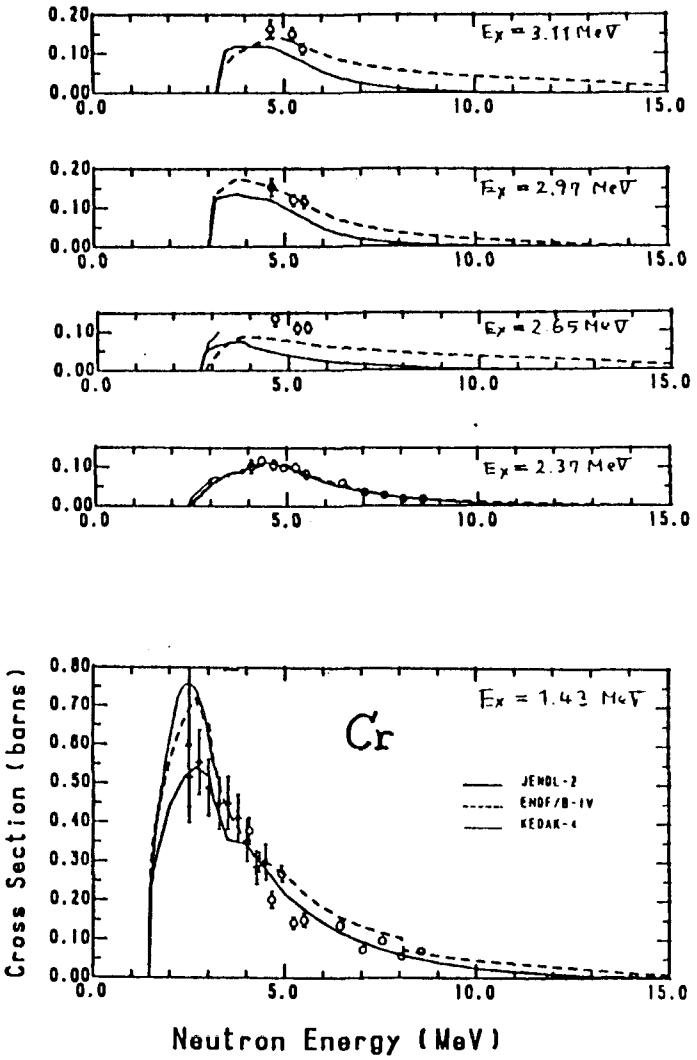

8. Inelastic scattering cross sections of Cr for the low-lying discrete levels. The evaluated data of JENDL-2 are compared with those of ENDF/B-IV and KEDAK-4 and with the experimental data.

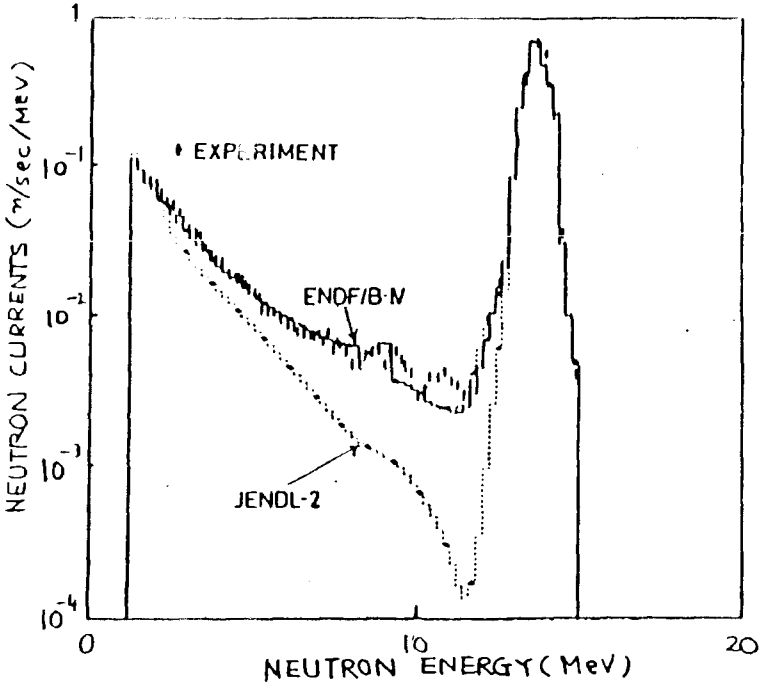

9. Neutron leakage spectra at 120 deg. for iron. The calculated spectra[27] from the evaluated data of JENDL-2 and ENDF/B-IV are compared with the experimental spectrum obtained by Hansen et al.[28].

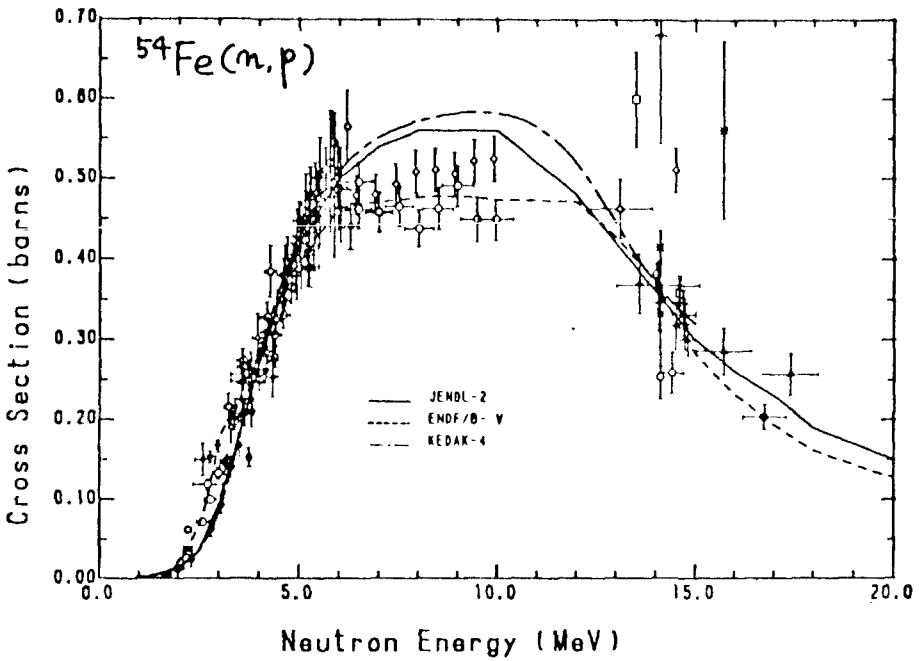

10. The (n,p) cross section of ^{54}Fe.

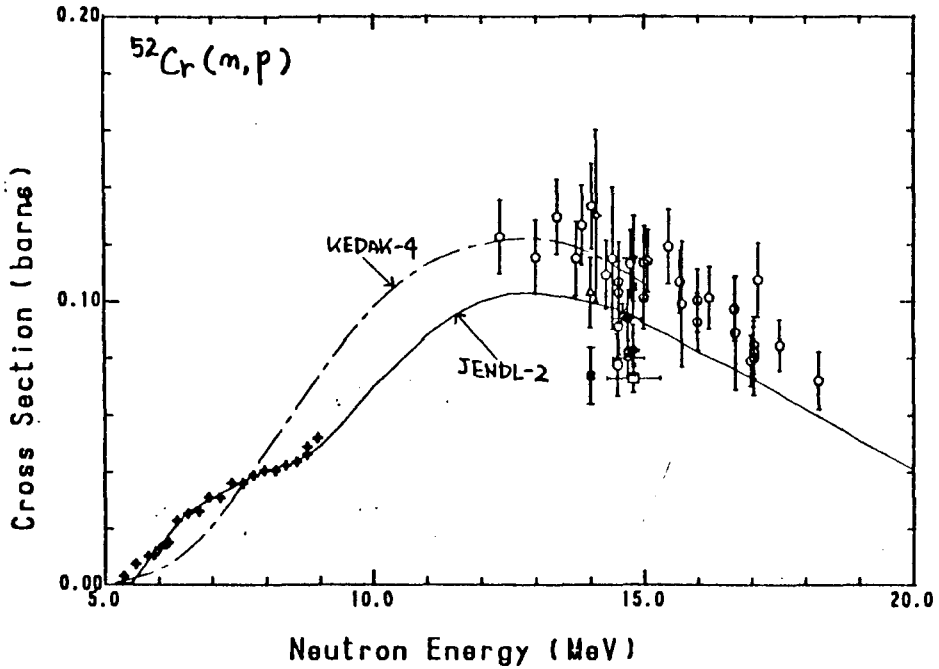

11. The (n,p) cross section of ^{52}Cr.

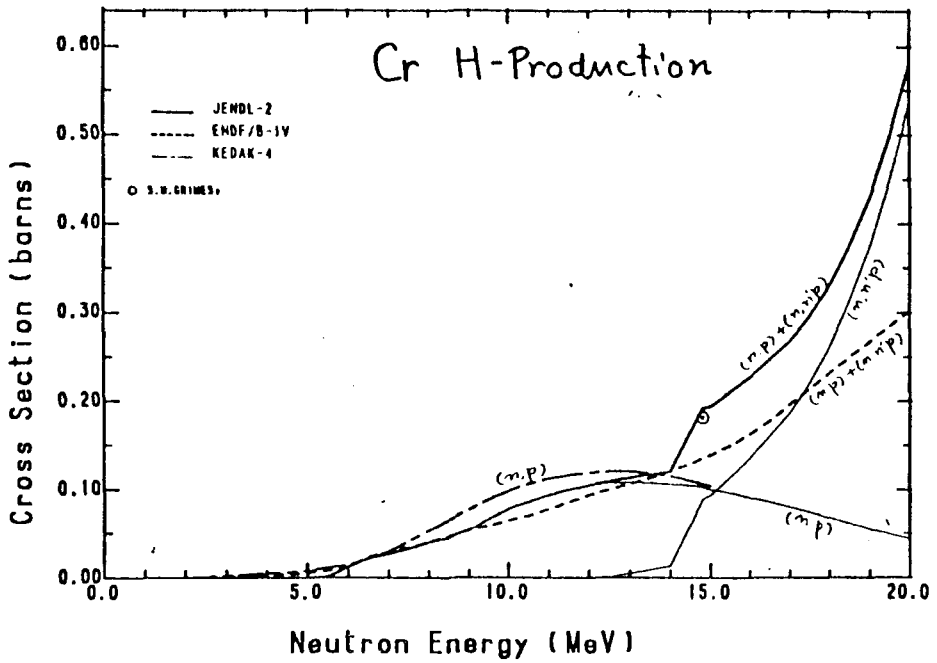

12. The hydrogen-production cross section of Cr.

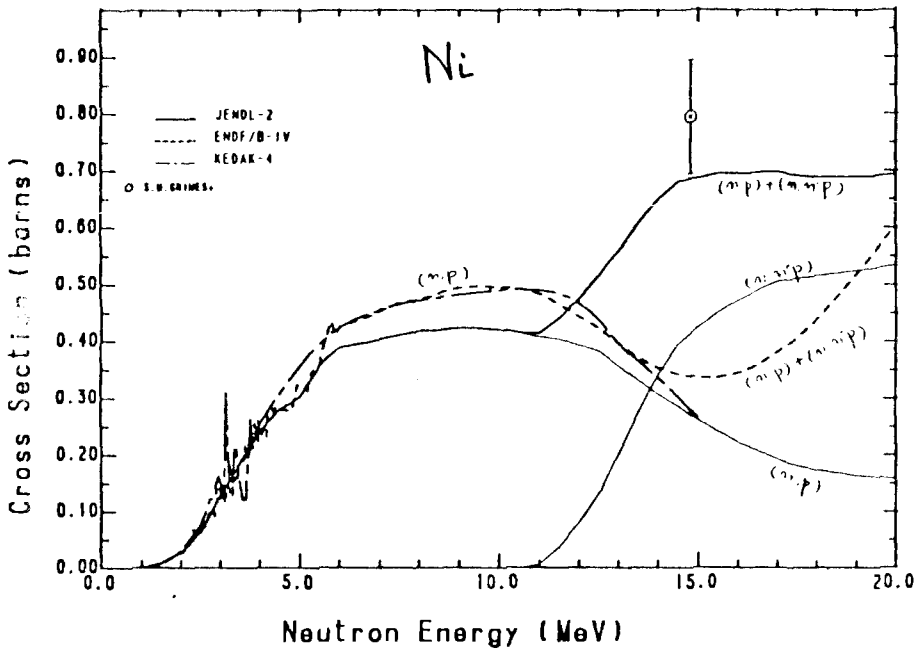

13. The hydrogen-production cross section of Ni.

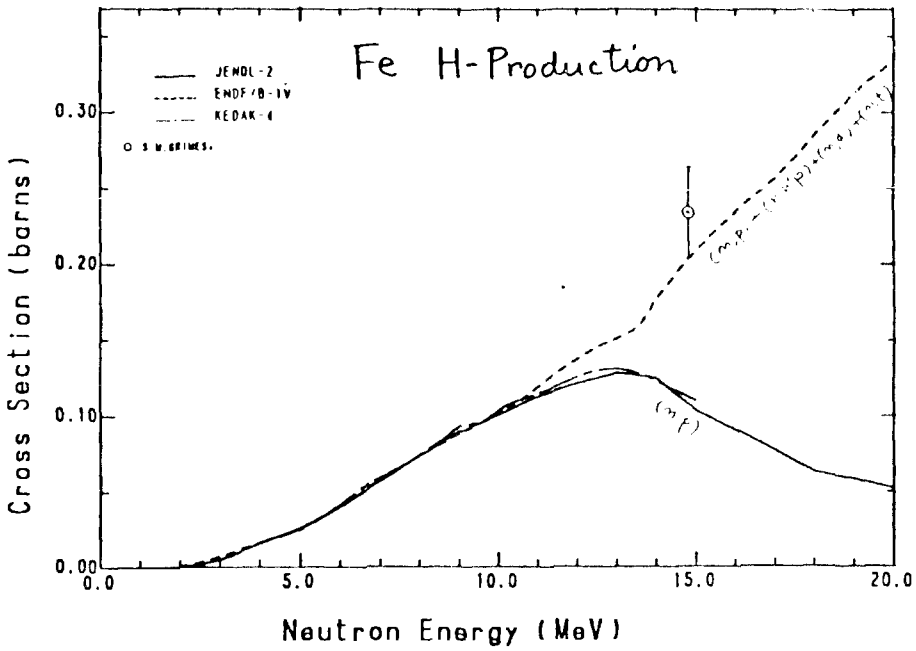

14. the hydrogen -production cross section of Fe.

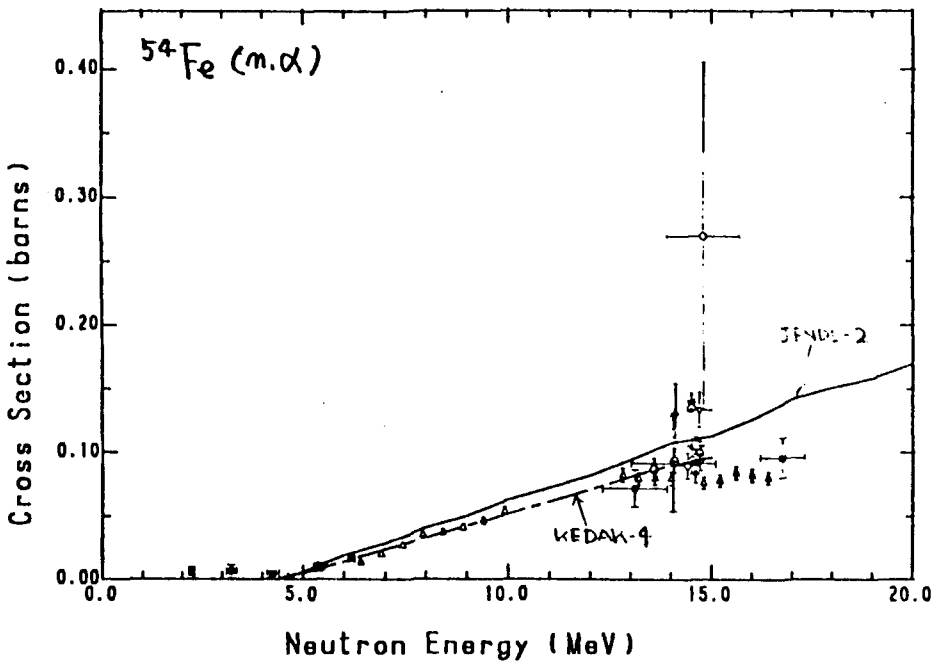

15. The (n,α) cross section of ^{54}Fe.

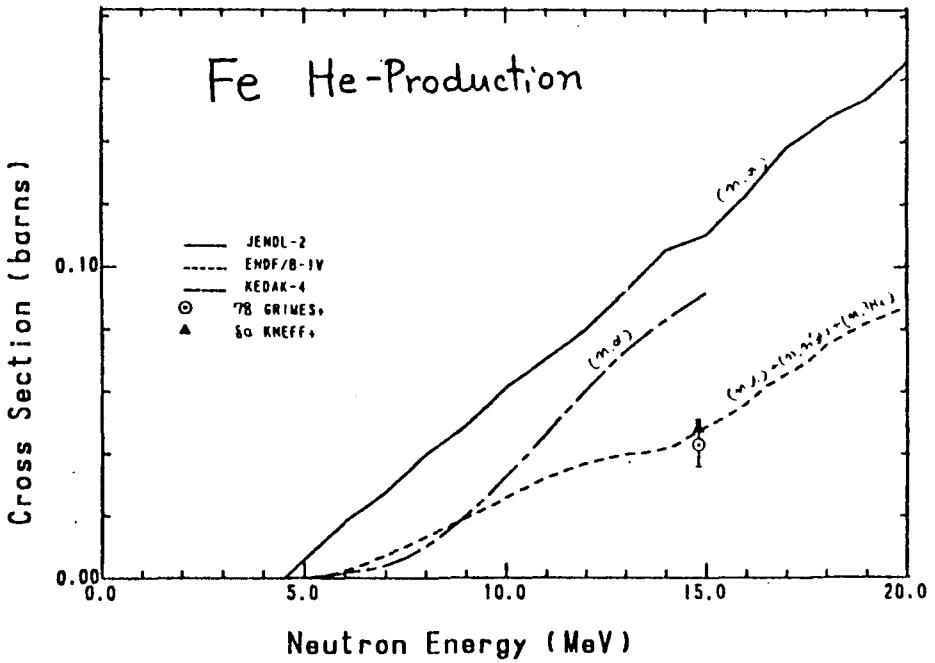

16. The helium-production cross section of Fe.

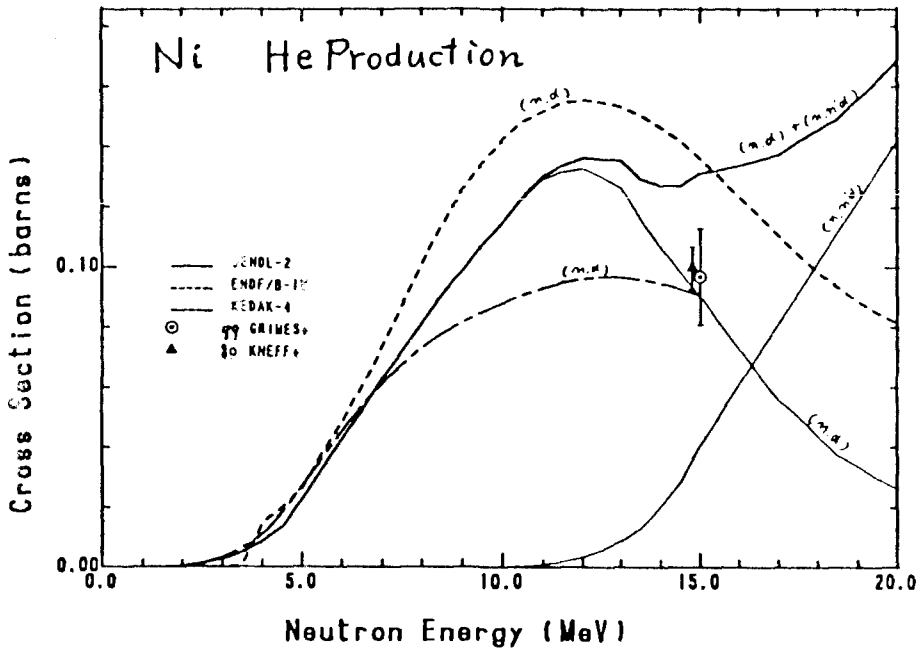

17. The helium-production cross section of Ni.

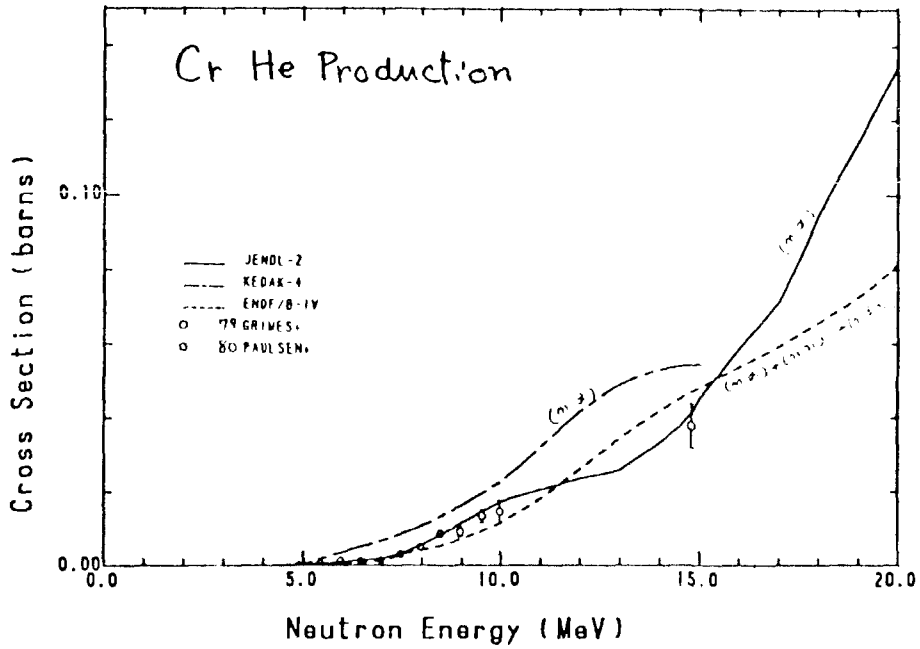

18. The (n,α) cross section of Cr.

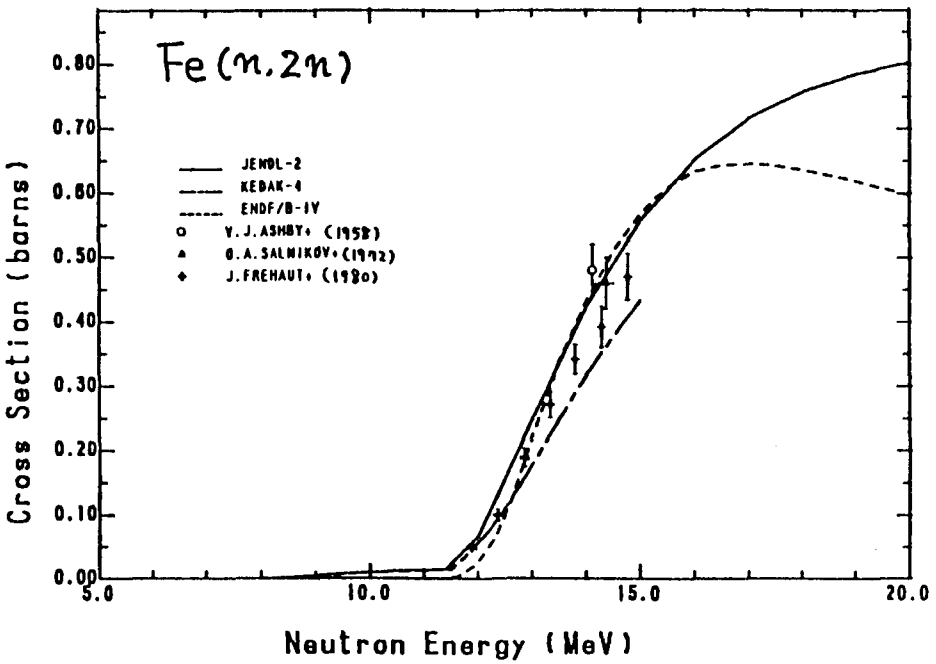

19. The (n,2n) cross section of Fe.

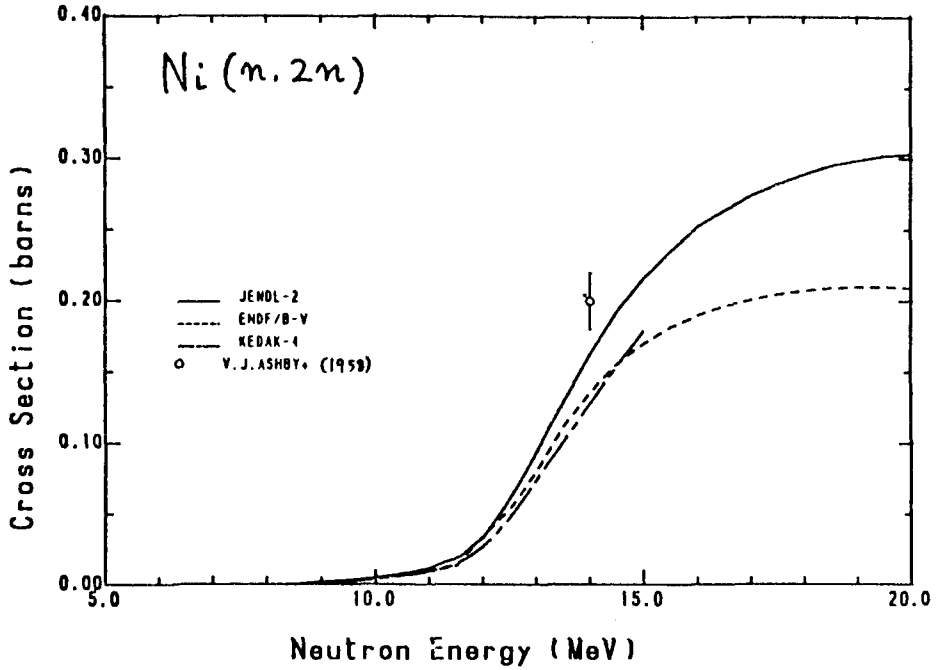

20. The (n,2n) cross section of Ni.

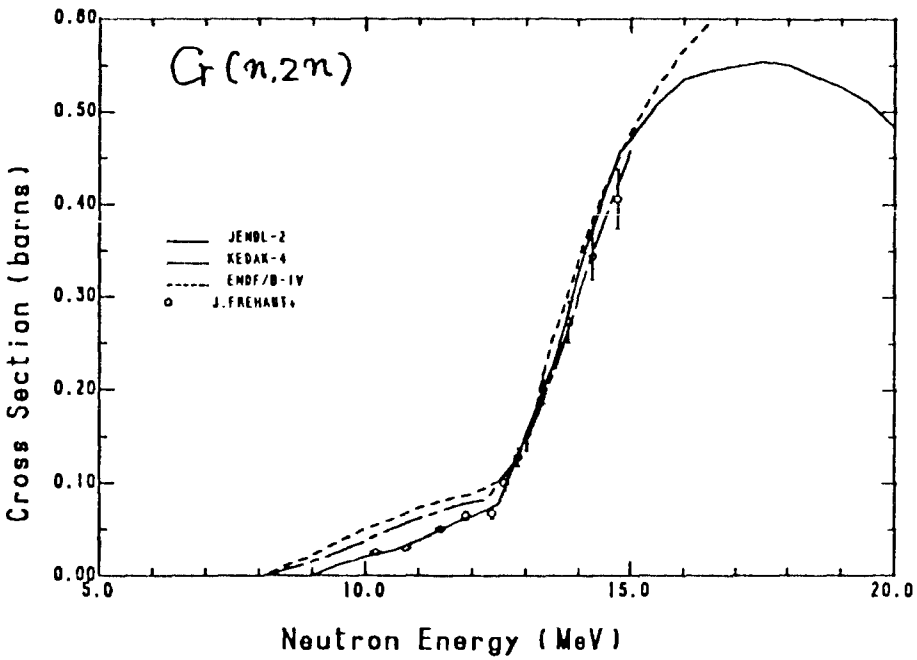

21. The (n,2n) cross section of Cr.

APPLICATION OF THE DEFORMABLE NONAXIAL ROTATOR MODEL TO THE NEUTRON CROSS-SECTION EVALUATION

E.S. Sukhovitskij, V.A. Konshin, A.B. Klepatskij

The Institute of Nuclear Power Engineering,
BSSR Academy of Sciences, Minsk, U.S.S.R.

ABSTRACT

The attempt to apply the dynamic model of the deformable rotator for nonaxial nuclei to the neutron cross-section calculations has been made. The parameters of nuclear softness and nonaxiality are determined from the experimental data according to the level schemes; then the coupled-channel method is used. The channel coupling strengthening leads to the direct excitation growth of inelastic levels.

The purpose of further development of theoretical models is to minimize the disagreements between theory and experiment, and in particular to obtain the detailed description of fast neutron scattering processes. In this context the application of dynamic theoretical nuclear models for the evaluation and theoretical prediction of neutron cross-sections is of interest.

Davydov and Filippov /1/ postulated the existence of nonaxial nuclei. They calculated the energy spectra and E2-transition probabilities using the asymmetric rotator concept. Asymmetric rotator model generalization made by Davydov and Chaban /2/,

enabled to take into account the nuclear extension effect while rotating and to link nuclear deformability properties relative to longitudinal vibrations with the energy of β-vibration spinless excitations. According to this theory the longitudinal γ-vibrations of nuclear surface are taken into account only by the introduction of the effective parameter, γ_{eff} (nonaxiality parameter). The second parameter of the theoretical model, μ, is determined by the relation of the zero-point vibration amplitude of the nuclear surface in its ground state to the value of nuclear shape equilibrium deviation from the spherical state. The value $\mu = 0$ corresponds to the complete excitation expansion into rotations and vibrations (adiabatic approximation); hence, the parameter μ can be termed as a nonadiabatic parameter. The more μ is, the larger corrections to adiabatic approximation are. The parameter μ describes the nuclear shape in relation to longitudinal vibrations and is referred as a nuclear softness parameter. The nuclei with neutron and proton numbers far from the magic ones are the most rigid towards the longitudinal vibrations. As fast as neutrons and protons approaching the magic numbers one can observe the cosiderable increase in nuclear deformability relative to the longitudinal vibrations.

For the nuclei with $50 < N < 82$ the value of γ is near to 0.4. In this connection there is no pronounced rotational state in this nuclear region. The excitations of nuclei with μ and γ-values less than 0.2 are characterized by rotational bands. It is just these nuclei that are attributed to the non-spherical ones ($A = 19 \div 28$; $A = 150 \div 190$; $A \geqslant 222$).

The nuclear shape deviation from the rotating ellipsoid causes to the violation in the main rotational band of the interval rule. Moreover taking into account the effective nonaxiality one can observe that it leads to the appearance of new anomalous bands that are the composite excitations of a rotational-vibrational type. Within the framework of the nonaxial asymmetric rotator model the nucleus ^{56}Fe, for example, has the value of $\mu \geqslant 0.5$ and that is why it shows more deformability relative to the longitudinal extensions and compressions (soft nucleus). The excited states are of a very complicated nature in the soft nuclei and therefore their division into rotational and vibrational excitations is rather relative.

The model of the asymmetric rotator gives the same energy level behaviour both in qualitative and quantitative respect as the vibrational and rotational model /3/. For nuclei - soft vibrators (structural materials) the predictions of the rotational-vibrational model and of the asymmetric rotator model are similar and in a good agreement with the experimental. Both models are equivalent in taking account of rotation and vibration interaction at least for the lowest rotational bands.

The asymmetric rotator model proposed by Davydov and Chaban /2/ makes use of the parameters μ and γ, which should be determined from the experimental data on energy levels. The model permits to describe the nuclear level schemes by their fitting using two, parameters - the parameter of softness μ and the parameter of nonaxiality γ. It means that the type of Hamiltonian which is used for the calculation of the nuclear

levels is correct enough and for that reason it can be used for neutron cross-section calculations by the coupled-channel method. The attractiveness of the model is that it allows to take into account the fact that sometimes the energy nuclear levels are the mixture of different bands that is, certainly, essential while calculating matrix coupling elements. Thus, for instance, for ^{238}U 43 KeV 2^+ level, that is regarded as being belonged to the band of K=0 according to the traditional coupled-channel method, is a mixture of two states with K=0 ($\sim$ 99 per cent) and K=2 ($\sim$ 1 per cent) in the nonaxial rotator model. Naturally, it results in greater state coupling strengthening. Similar examples can be given for nuclei of structural materials.

The asymmetric rotator model can be used for the neutron cross-section calculation using coupled-channel method. In this case one needs to calculate the matrix coupling element for different states. It can be shown that in comparison with the traditional coupled-channel method the matrix elements in the asymmetric rotator model acquire one more factor, associated with shape vibrations. This factor is always more or equal to unit. For ^{48}Ti it is equal on an average to 1.5 for different states; for chromium - $\sim$ 1.2. These values are the functions of the nuclear softness and nonaxiality which are determined by the fitting of a theoretical level scheme to experimental data. The channel coupling strengthening leads to the direct excitation of inelastic levels by the same order value. The fact that the model takes into account the nuclear shape (nonaxiality) more accurately enables to the more correct account of angular distributions of neutron scattering on nuclear levels.

The respective computer programme was written that permits to carry out the neutron cross-sections calculations.

Fig. 1 shows the experimental data in comparison with the theoretical values of the energy levels for ^{56}Fe and ^{48}Ti calculated according to the asymmetric rotator model /2, 4/. One can see the satisfactory agreement of the compared values. The values of $\int^{(1)}$ and γ - parameters and the strengthening coefficients of $I_\rho^{(1)}$ matrix elements for nuclei of ^{56}Fe, ^{48}Ti, ^{76}Se obtained within the framework of the model under consideration are given in Table 1. Undoubtedly that for the application of the deformable nonaxial rotator model within the framework of the coupled-channel method there is the necessity of the thorough determination of nuclear potential parameters as it is being generally done in the traditional coupled-channel method. This kind of work is carried out in our laboratory, however we haven't yet managed to obtain optimum potential parameters and to carry out the calculations for the number of nuclei, that, certainly, doesn't allow to draw the final conclusions concerning the place of the model considered among the other available models. Fig.2 and 3 illustrate the calculation results of angular distributions of elastic and inelastic neutron scattering for ^{48}Ti at E_n=3.9MeV and their comparison with the experimental data /5/. The Hauser-Feshbach formalism was used for the calculation of the compound-nucleus cross-sections; the direct process cross-sections were calculated by the strong coupled-channel method with the asymmetric rotator model.

At this stage it would be premature to draw the definite conclusions of asymmetric rotator model possibilities for nuclear

data evaluation purposes. However, one can hope that the use of more correct ideas of the type of nuclear Hamiltonian with the possibility of its parameter determination through the experimental data on nuclear level schemes enhances the reliability of the results being received by the coupled-channel method.

Table 1. Values of softness parameter μ, nonaxiality parameter γ and matrix element strengthening coefficients $I_\beta^{(1)}$ for ^{56}Fe, ^{48}Ti, ^{76}Se

Nucleus	μ	γ	$I_\beta^{(1)}$	The type of transitions
^{56}Fe	0.689	23°44' (0.414)	1.146	(+2-0-1 → 0^+-0-1) I_i^π-n_i-τ_i → I_f^π-n_f-τ_f
			1.224	(2-0-1 → 2-0-1)
			1.279	(2-0-1 → 2-0-1)
^{48}Ti	0.903	21°30' (0.375)	1.421	(2-0-1 → 0-0-1)
			1.556	(2-0-1 → 2-0-1)
			1.636	(2-0-1 → 2-0-2)
^{76}Se	0.4395	24°36' (0.429)	1.086	(2-0-1 → 2-0-1)
			1.041	(2-0-1 → 0-0-1)
			1.116	(2-0-1 → 2-0-2)
			1.165	(2-0-2 → 2-0-2)

References

1. Davydov A.S., Filippov G.F. Nucl. Phys., 1958, v. 8, p. 237.
2. Davydov A.S., Chaban A.A. Nucl. Phys., 1960, v. 20, p. 499.
3. Faessler A., Greiner W., Sheline R. Nucl. Phys., 1965, v. 80, p. 417.
4. Kashuba I.Ya., Kotishevskaja Eh.Yu. Izv. AN SSSR, 1975, v. 39, p. 617.
5. Smith A. et al. Nucl. Phys., 1978, v. A307, p. 224.

Figure captions

Fig.1. The comparison of the theoretical and experimental energy level values for ^{56}Fe and ^{48}Ti

Fig.2. The comparison of the calculation results of elastic neutron scattering angular distributions for ^{48}Ti with the experimental data /5/ at E_n= 3.9 MeV

Fig.3. The comparison of the calculation results of inelastic neutron scattering angular distributions for ^{48}Ti with the experimental data /5/ at 3.9 MeV (1 - present calculations, 2 - spherical optical model, 3 - traditional coupled-channel model)

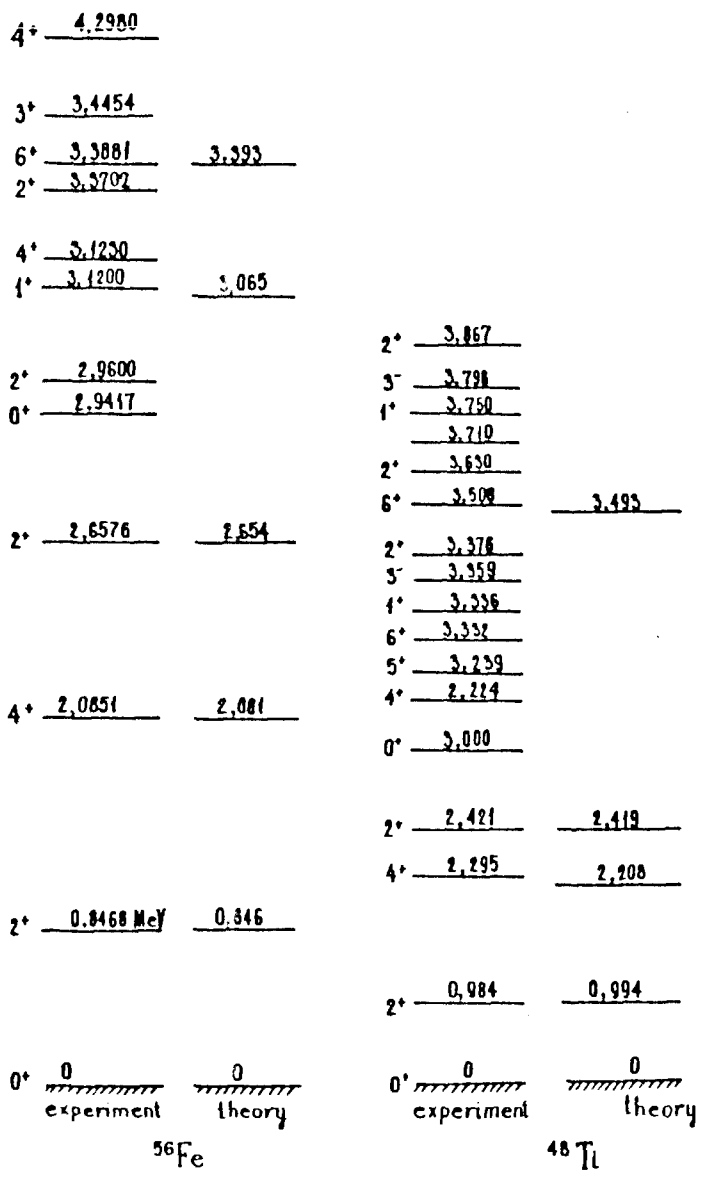
4+ 4,2980
3+ 3,4454
6+ 3,3881
2+ 3,3702
4+ 3,1230
1+ 3,1200
2+ 2,9600
0+ 2,9417
2+ 2,6576
4+ 2,0851
2+ 0,8468 MeV
0+ 0
experiment
theory
56Fe
3,393
3,065
2,654
2,081
0,846
2+ 3,867
3- 3,798
1+ 3,750
3,710
2+ 3,630
6+ 3,508
2+ 3,378
3- 3,359
1+ 3,336
6+ 3,332
5+ 3,239
4+ 2,224
0+ 3,000
2+ 2,421
4+ 2,295
2+ 0,984
0+ 0
experiment
theory
48Ti
3,495
2,419
2,208
0,994

Fig. 1

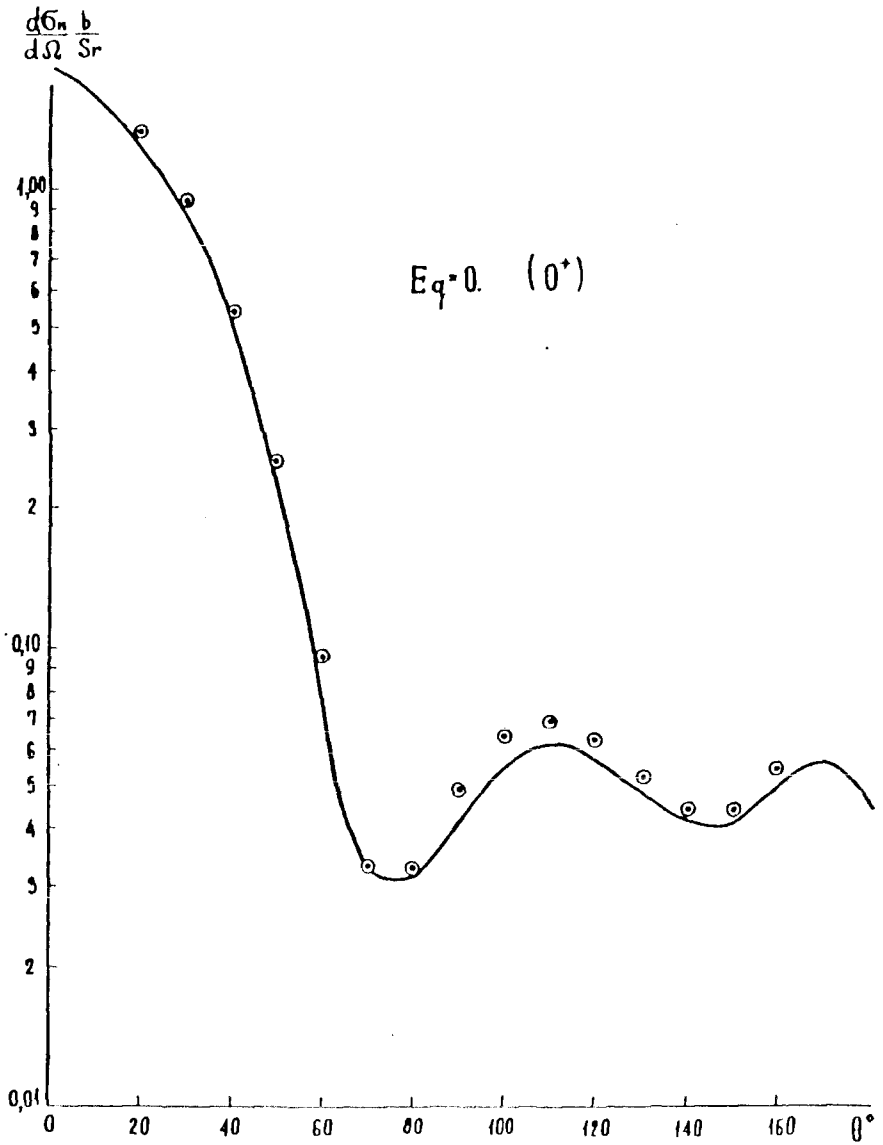
dσn/dΩ b/Sr
Eq=0. (0+)
1,00
0,10
0,01
0
20
40
60
80
100
120
140
160
θ°

Fig 2

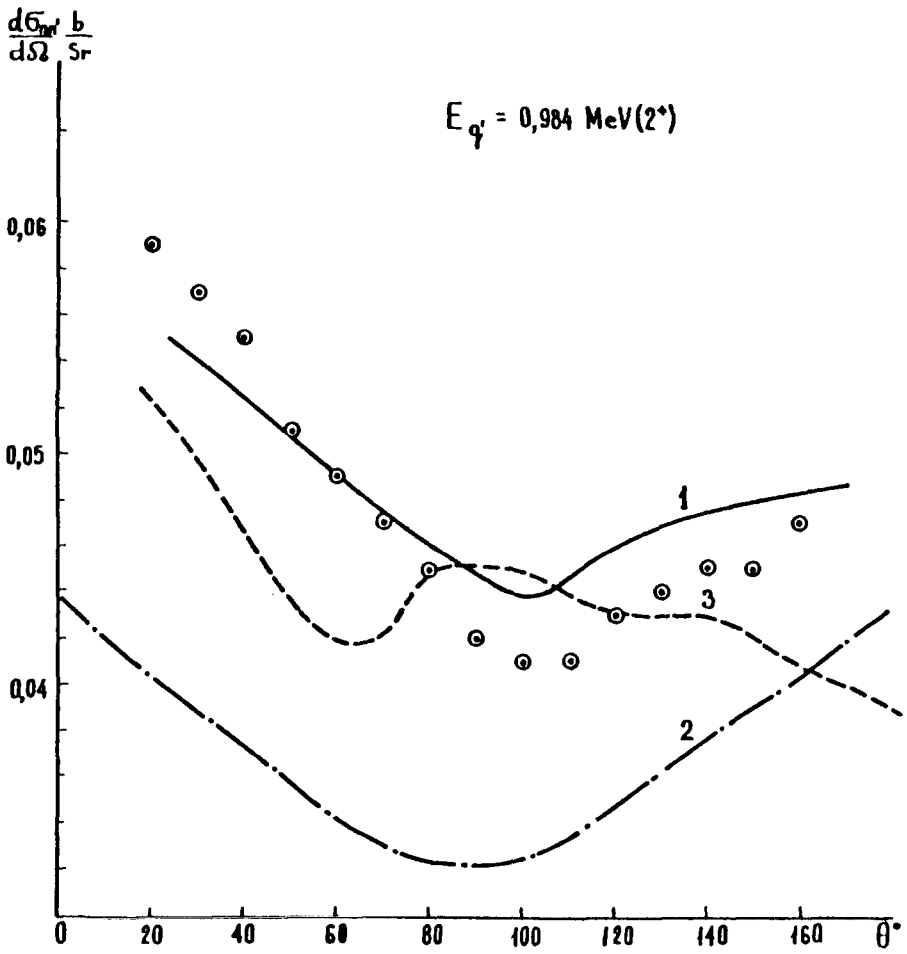

Fig.3

NEUTRON RADIATIVE CAPTURE AND INELASTIC SCATTERING IN CHROMIUM AND THEIR INFLUENCE ON THE CALCULATED CHARACTERISTICS OF A REACTOR WITH DISSOCIATING COOLANT

V.P. Korennoy, O.V. Khatkevich, Yu.G. Fokov, N.M. Grusha, B.I. Popov

The Institute of Nuclear Power Engineering, BSSR Academy of Sciences, Minsk, U.S.S.R.

V.V. Vozjakov

The Institute of Physics and Energetics, Obninsk, U.S.S.R.

ABSTRACT

The analysis of (n,γ) reaction chromium cross sections in different libraries, the calculation of average capture cross sections and the comparison with the experimental data,obtained on critical assemblies, have been carried out in this paper. The derivation of the calculated values from the experimental ones exceeds measurement errors. The best agreement with the experimental data has been received for the library JENDL-1. Inelastic scattering matrix for Cr with taking into account of the last experiments and ENDF/B-V library is obtained too. The possibility of data corrections for σ_a and σ_{in} in the library ABBN-78 and their influence on the parameters of fast neutron reactor with dissociating coolant are being considered.

The cross section investigation of fast neutron interaction with chromium nuclei is of great interest as this material is widely used in reactor construction for the radiation stability and chemical resistance of stainless steels and alloys. In some variants of the fast reactors with dissociating coolant [1] chromium content in an active core reaches 30 vol.%. One should consider the element as not only a pure absorber but take into account its active influence on a neutron spectrum formation when chromium high concentrations are being used in the reactor and this requres higher accuracy of all neutron interaction cross sections with this matter.

The representative average estimation error of the cross sections of neutron capture by natural chromium isotope mixture is assumed to be equal to 20% in the neutron energy range of 1-400 keV in the last version of the home group constant library (ABBN-78) for reactor design and protection [2]. As it is noted in this work, the authors have considered insufficiently reliable data, indicating on nesessity fall of neutron capture cross sections of construction materials.

The inelastic scattering data in ABBN-78 are taken from Prince estimation [3] for the ENDF/B-IV microconstant library. The appearance of new experimental data [4] wastaken into account in Prince estimation for the fifth ENDF/B version [5] and in Nuclear Data Center estimation (NDC-2) [6].

One of the main conclusions that could be drawn from the results [4] is a considerable difference between the measured inelastic scattering cross sections at levels close to the threshold and the statistical theory predictions. The results of the model calculations, fitted for the reasonable description of data at energies higher than the threshold exceed the cross sections in a nearly threshold region.

In general inelastic scattering on natural chromium is determined by the scattering at 2^+level of ^{52}Cr with energy of 1434 keV that makes a contribution of about 75% at 2 MeV neutron energy, 65% - at 3 MeV and 30% - at 4 MeV in total inelastic scattering cross section $\sigma_{tot\ in}$. Fig. 1 shows experimental measurement results and estimated curves for this level. Prince estimation [5] was completely rested on the data obtained in [4] that resulted in $\sigma_{tot\ in}$ lowering in nearly threshold region up to 30% in comparison with ENDF/B-IV. In the estimation of NDC-2 the gap in this cross section in the neutron energy region of 1.8-2.2 MeV is not described.

The comparison of the calculated relations according to different constant libraries and measured ones in the Central Institute for Nuclear Research at the SEG-4(PO-2) assembly [23] on the spectrum given in table 1 (forth column) shows that the deviation of calculated values from the experimental ones exceeds the measurement errors (see fig.2). It being known that the earlier libraries such as ABBN-70, JAERI-70, KEDAK-75 give the absorption cross sections smaller than the experimental ones, whereas the tendency of chromium absorption cross section increase has lead to the essential overestimation α (ranging from 25% for ABBN-78 to 60% in BARC-77)[2] recently. The use of the JENDL-1 library constants gives the best agreement with the experimentally obtained data.

The 26-group cross sections of chromium neutron absorption, including the reaction cross sections such as (n,p) and (n,α) for the ABBN-78 and JENDI-1 are given in table 1. Especially

Table 1. Group capture cross sections according to the ABBN-78 and JENDL-1 estimations and neutron spectrum in SEG-4(PO-2) critical assembly

Energy group number	ABBN-78 $\langle\sigma_c\rangle$, barn	JENDL-1 $\langle\sigma_c\rangle$, barn	Neutron spectrum, relative units
1	0.0550	0.0338	0.002
2	0.0140	0.0041	0.014
3	0.0060	0.0021	0.032
4	0.0040	0.0034	0.080
5	0.0037	0.0050	0.095
6	0.0037	0.0043	0.132
7	0.0043	0.0045	0.113
8	0.0065	0.0061	0.102
9	0.0130	0.0073	0.100
10	0.0220	0.0136	0.083
11	0.0160	0.0081	0.075
12	0.0730	0.0728	0.057
13	0.0360	0.0418	0.042
14	0.1840	0.1400	0.029
15	0.0200	0.0219	0.019
16	0.0290	0.0295	0.011
17	0.0420	0.0414	0.006
18	0.0620	0.0605	0.003
19	0.0960	0.0883	0.002
20	0.1400	0.1275	0.001
21	0.1960	0.1890	-
22	0.2880	0.2775	-
23	0.4230	0.4023	-
24	0.6200	0.5971	-
25	0.9110	0.8770	-
T	3.2000	-	-

strong difference is observed in the 14th energy group with the boundaries of 1-2.15 keV. In this group in the capture cross section $\langle\sigma_c\rangle_{14}$ the main contribution is produced by the strong ^{52}Cr P-resonance at E_o=1.626 keV for which the following parameters are accepted in the ENDF/B-IV microconstant library: J^{π} = $3/2^-$, Γ_γ=0.600 eV ($g\Gamma_n\Gamma_\gamma/\Gamma$ =0.0767). This value contribution of 0.135 barn is being summed up with the smooth part (0.06 barn) and if we consider the contributions of the resonances, occuring above 2.15 keV we obtain $\langle\sigma_c\rangle_{14}$=0.154 barn, that is by 16% lower than the value of 0.184 barn, given by ABBN-78. It should be noted that while estimating, the JENDL-1 library presents the accepted parameters of J^{π} =$3/2^-$, Γ_n=0.040 eV, Γ_γ =0.444 eV, which give the lower value of $\langle\sigma_c\rangle_{14}$=0.140 barn and $g\Gamma_n\Gamma_\gamma/\Gamma$ = 0.0734, being correlated with that of measured by Stieglitz et al within the error (0.080±0.012) [18].

In this paper the group inelastic neutron scattering cross section and intergroup transition matrixes have been obtained on the base of ENDF/B-V and NDC-2 estimations by the technique in [19]. The total cross section of inelastic scattering is assumed as the sum of discrete levels contributions in the

resonance region ranging from the threshold to 2 MeV. The scheme of chromium isotopes levels that was made use while obtaining inelastic transition matrix in accordance with ENDF/B-V estimation is given in table 2. The first ^{50}Cr level, the first ^{54}Cr level and the five of each fist levels of $^{52,53}Cr$ are taken into account in NDC-2 estimation. In the region higher 2 MeV $\sigma_{tot\ in}$ was calculated as the difference between total non-elastic cross sections and the sum of neutron capture reaction cross sections.

While comparing the estimated data an inelasting neutron scattering cross section an important criterion is the magnitude of a fission neutrons removal cross section under the fission threshold of ^{238}U, which is determined by the following equation:

$$\sigma_{rem} = \frac{\int_{\cdot} dE' \phi(E') \sigma_f^{238}(E') \int_{\cdot} dE \sigma_{in}(E' \to E) \left[1 - \frac{\sigma_f^{238}(E)}{\sigma_f^{238}(E')}\right]}{\int_{\cdot} dE' \phi(E') \sigma_f^{238}(E')}$$

The removal cross section for isotopes natural mixture turned out to be 0.53 barn in accordance with ABBN-78 estimation . According to our calculations ENDF/B-V and NDC-2 estimations give the value of σ_{rem} lower by 11 and 10 percents, respectively. Unfortunately, there are no experimental data on this magnitude.

The intergroup transition matrixes due to inelastic scat - tering and reaction (n, 2n) for ENDF/B- V (upper line) and NDC-2 (middle line) estimations in comparison with ABBN-78 matrix (lower line) are presented in table 3. As it's seen from the table the matrixes, obtained on the data from [5,6], predict lower neutron energy dumping owing to inelastic scattering.

The influence of variation accounting in inelastic scattering cross section according to ENDF/B-V and NDC-2 estimations and in radiative capture cross sections in the ABBN-78 system of group

Table 2. Energy level schemes of chromium isotopes

Isotope and its natural abundance	^{50}Cr 4.35%		^{52}Cr 83.79%		^{53}Cr 9.50%		^{54}Cr 2.36%	
	E_{lev} (MeV)	J^π	E_{lev} (MeV)	J^π	E_{lev} (MeV)	J^π	E_{lev} (MeV)	J^π
	0.000	0^+	0.000	0^+	0.000	$3/2^-$	0.000	0^+
	0.783	2^+	1.434	2^+	0.564	$1/2^-$	0.8349	2^+
			2.370	4^+	1.006	$5/2^-$		
			2.647	0^+	1.287	$7/2^-$		
			2.758	4^+	1.539	$7/2^-$		
			2.965	2^+	1.573	$9/2^-$		
			3.114	0^+	2.321	$3/2^-$		
			3.152	2^+				
			3.344	4^+				
			3.471	3^+				
			3.771	2^+				
Binding energy of last neutron in compound nucleus	9.262 (MeV)		7.940 (MeV)		9.72 (MeV)		6.246 (MeV)	

neutron constant upon an integral reactor characteristics had been investigated for a breeder reactor version as an example with dissociating N_2O_4 gas as a coolant.[1,7]. The changes in $\sigma_{tot\ in}$ and σ_c were compensated by according changes of elastic scattering group cross sections so that total cross

Table 3. Intergroup transition matrixes due to inelastic scattering and reaction (n,2n) according to ENDF/B-V, NDC-2 and ABBN-78 estimations

j \ k	0	1	2	3	4	5	6	7	8	9	Sum
	0.038	0.363	0.449	0.3000	0.102	0.056	0.019	0.005	0.001	-	1.333
1	0.038	0.250	0.290	0.347	0.223	0.126	0.046	0.012	0.002	0.001	1.335
	0.011	0.231	0.272	0.341	0.238	0.140	0.049	0.015	0.005	0.002	1.304
	0.056	0.398	0.443	0.287	0.104	0.032	0.009	0.002	0.001	-	1.332
2	0.063	0.385	0.452	0.274	0.109	0.036	0.010	0.002	0.001	-	1.332
	0.040	0.386	0.422	0.237	0.109	0.040	0.012	0.003	0.001	-	1.250
	0.027	0.441	0.354	0.119	0.050	0.019	0.006	0.002	0.001	-	1.013
3	0.022	0.419	0.367	0.116	0.044	0.020	0.006	0.002	0.001	-	0.997
	0.021	0.441	0.397	0.124	0.052	0.018	0.005	0.002	-	-	1.060
	0.021	0.172	0.211	0.076	0.043	0.013	0.004	0.002	-	-	0.542
4	0.020	0.172	0.231	0.090	0.041	0.014	0.004	0.001	-	-	0.572
	0.020	0.182	0.256	0.104	0.044	0.016	0.008	-	-	-	0.630
	-	0.021	0.020	0.008	0.003	0.001	-	-	-	-	0.053
5	-	0.022	0.023	0.008	0.003	0.001	-	-	-	-	0.057
	-	0.022	0.024	0.009	0.004	0.001	-	-	-	-	0.060

section of neutron-chromium nuclei interaction remained constant in ABBN-78 library. The calculation of neutron spectrum, breeding coefficient (K_{eff}), reactor reproduction coefficient (RC) and other characteristics was carried out by DRZM program from NF-6 program complex [20]. Multigroup neutron transfer equations in DRZM are solved in diffusion approximation. The iterative net-point method of variable directions in two-dimensional cylindrical geometry is ised for difference equation solution. The 26-group micro-sections were calculated by MIM program [21] in which resonance effect consideration is being carred out appling the formalism of resonance cross section self-shilding factors. The typical neutron spectrum of such a reactor active core has the maximum within of 5 to 10 energy groups (21.5 keV - 1.4 MeV). At the same time in spite of the small member of neutrons with 1-

20 keV energy , the strong capture on chromium resonances in this range leads to the 11-14th group capture fraction ammounting to about 50%, the half of which accounts for the 14th group. The resonance self-shielding accounting of the 14th group capture cross section (the dilution cross section σ_o=10) decreases this value slightly without changing general conclusions. The ABBN-78 constant system was used as a basic one in the design of a rector. The variations associated with the correction of resonance parameters at E_o=1.626 keV result in RC increase by 0.05 in comparison with the basic calculation. The variations attributed to the substitution of the ABBN-78 capture cross sections by the group ones of the JENDL-1 library increase RC by 0.027.

Transition to the matrix obtained from ENDF/B-V estimation as calculation show has led to the additional rise of K_{eff} by 0.4% and RC by 0.013. The use of NDC-2 estimation has given the rise of K_{eff} by 0.2 % and RC by 0.006, respectively.

In conclusion it should be noted that the JENDL-1 library with a lower capture cross section in chromium gives the better description of the integral experiments[22] with the average deviation of 1.4 % for the relative reactivity coefficent of chromium samples ($\rho_{Cr}/\rho_{^{239}Pu}$) that is indicative of the possibility to use this library data for the prediction of high content chromium reactor characteristics.

In order to make the final choice of evaluated data system on inelastic neutron scattering cross sections for chromium it's necessary to carry out the additional measurements of σ_{in} in the region near threshold and the measurements of sphere transmission on chromium samples by a fission chamber with ^{238}U for σ_{rem} determination.

References

1. Kukhaev A.I., Naumov V.A., Popov B.I. VANT, ser. fizika i tekhnika reaktorov, 1982, No 7(29), p. 51.
2. Abagjan L.P., et al. Group Constants for Nuclear Reactor Calculations, Moskow, 1981, 231 p.
3. Prince A. Evaluator, ENDF/B-IV (MAT 1191), National Neutron Cross Section Center, BNL, 1974.
4. Karatzas P.T., et al. Nucl. Sci. Eng., 1978, v. 67, No 1, p.34.
5. Prince A., Burrows T.W. BNL-NCS-52152 (ENDF-246), 1979, 86 p.
6. Vozjakov V.V., et al. VANT, ser. jadernye konstanty, 1982, No 4(48), p. 44.
7. Degtjarev Yu.G. & Protopopov V.N. Sov. J. At. Energy, 1967, v. 23, p. 1350.
8. Winkler G.,& Hansjakov K. Int'l Conf. on Nucl. Cross Sections for Technology, Washington, 1980, p. 150.
9. Korg I.A., Kashuba I.E., Golubova A.A. 3rd All-Union Conf. on Neutron Physics, Kiev, june 1975, Moskow, 1976, v. 4, p. 203.
10. Fedorov M.B. & Jakovenko T.I. 2nd Nat'l Sov. Conf. on Neutron Physics, Kiev, june 1973, proc. publ. by F.E.I. Obninsk, 1974, v. 3, p. 56.
11. Almen-Ramström E.A. AE-503, Studvik, Sweden, 1975, 70 p.
12. Kinney W.E. & Perey F.G. ORNL-4806(ENDF-198), 1974, 45 p.
13. Van Patter D.N., et al. Phys. Rev., 1962, v.128, No 3, p.1246.
14. Broder D.L., et al. Sov. J. At. Energy, 1964, v. 16, p. 113.

15. Igarasi S., et al. Japanese Evaluated Nuclear Data Library, Version-1, JENDL-1, JAERI 1261, NEANDC(J)-59/L, INDC(JAP)-45/L, 1979, 206 p.

16. Goel B., Küsters H., Weller F. Proc. of Conf. on Nuclear Cross Sections and Technology, Washington D.S., 1975(1975), p. 313.

17. Garg S.B. BARC-892, INDC(IND)-21/G+Spesial, 1977, 69 p.

18. Stieglitz R.C., et al. Nucl. Phys., 1971, A163, p. 592.

19. Levis R.C. & O'Relly B.D. NAA-SR-11530, 1960, 56 p.

20. Zizin M.N., Savochkin O.A., Chukhlov O.P. Preprint SRIAR-49 P-481334, Dimitrovgrad, 1977.

21. Bashmachnikov A.I. Preprint SRIAR-49(408), Dimitrovgrad, 1974.

22. Hojuyame Y., et al. JAERI 1275, NEANDC(J)-78/U, INDC(JAP)-65/L, 1982, 80 p.

23. Bemer V., Ditze K., Fermann K., et al. 6th All-Union Conf. on Neutron Physics, Kiev, oct. 1983.

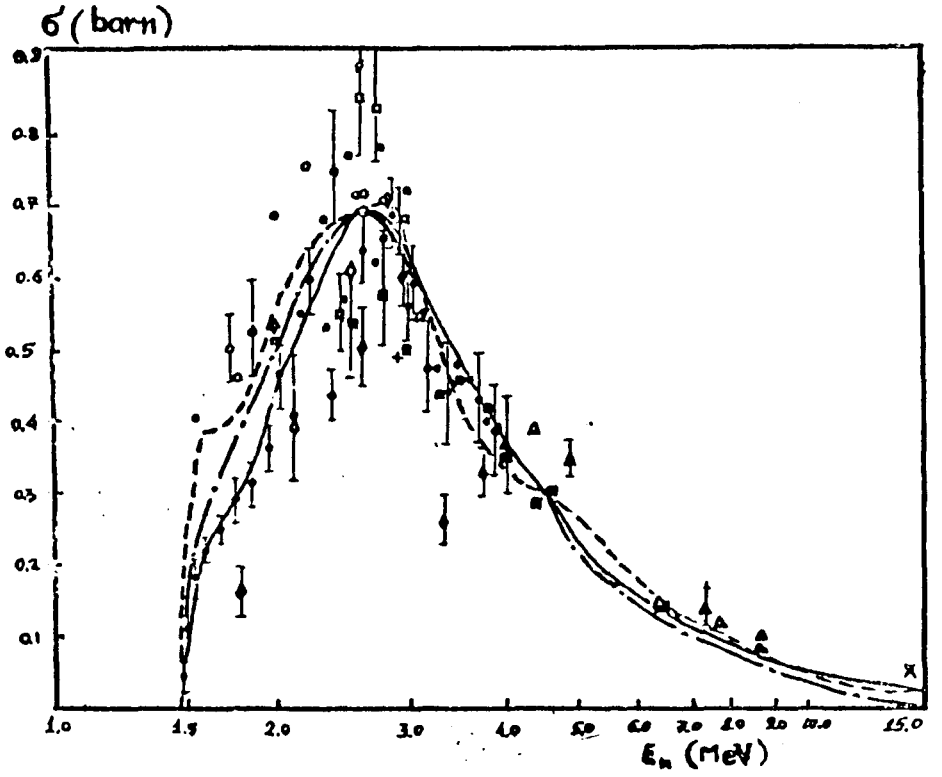

Fig. 1. The excitation cross section of ^{52}Cr 1434 keV level (brought into accord with isotope content in a natural mixture).

Estimations: —— - ENDF/B-V, —·— - NDC-2, — — — - ENDF/B-IV.

Experimental data: • - [4], ♦ - [7], × - [8], ◇ - [9], + - [10], ■ - [11], ▲△ - [12], □ - [13], ○ - [14].

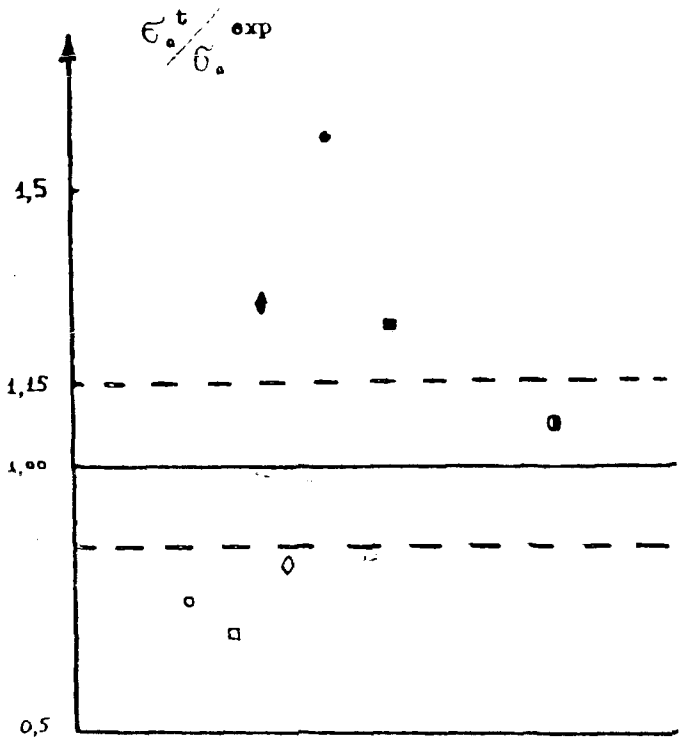

Fig. 2. The relations of the average neutron absorption cross sections on chromium calculated according to different constant libraries [2,3,15,16,17] and the measured ones on the SEG-4(PO-2) critical assembly of CINR(GDR) which are arranged in a chronological order:
grapfic symbols: o - ABBN-64, □ - JAERI -70,
♦ - ENDF/B -IV (1974), ◊ - KEDAK-75,
● - BARC-77, ■ - ABBN-78, ◐ - JENDL-1 (1979).
The error corridor of experimental data estimated by 15% is shown by a dash line.

Revised Proposal for a Co-ordinated Research Programme (CRP) on "Methods for the Calculation of Fast Neutron Nuclear Data for Structural Materials"

J.J. Schmidt, D.E. Cullen, H.D. Lemmel, V.G. Pronyaev
IAEA Nuclear Data Section

This is a working paper for use at the IAEA/NDS Consultants' Meeting on Nuclear Data for Structural Materials, Vienna, 2-4 November 1983. It should be considered as a proposal to be discussed and amended during the meeting. The conclusions and recommendations of this meeting in regard to this CRP will be submitted by IAEA/NDS to the INDC for approval, before submitting it for internal IAEA approval.

1. Background

Fast neutron reaction data for structural materials (Fe, Ni, Cr and some others) including the energy and angular distributions of secondary emitted neutrons, charged particles and γ-rays are of high importance in neutron economy and shielding calculations and for the assessment of nuclear safety and radiation damage in fission as well as fusion reactors.

With regard to structural materials, apart from improvements in evaluated data for a few selected reactions in special purpose files, the internationally available more comprehensive evaluated neutron data files used in fission and fusion neutronics calculations are quite old and generally no longer reflect the present state of knowledge. Many of these evaluations, at least partially, date back as far as 1975; since then many new experimental data have become available, as illustrated, e.g. by the many new results reported at the *NEANDC Specialists' Meeting on Fast Neutron Capture Cross Sections* held at Argonne National Laboratory in April 1982. Also in the field of nuclear models and computer codes, significant improvements have been made in recent years in the prediction and interpretation of non-compound contributions in fast neutron-nuclear reactions as reflected, e.g. in the remarkable improvements achieved in recent years in the description of the energy and angular distributions of secondary emitted particles including consideration of direct and pre-compound emissions.

These new developments have led to the necessity to improve the existing evaluations and perform re-evaluations with due consideration of more recent experimental data and nuclear model descriptions. As a consequence, new evaluations have been started or are planned in several countries, and, as part of this overall effort,

a co-ordination of the current developments and uses of calculational methods for the computation of these neutron cross sections appears to be timely and desirable.

2. Scientific scope and proposed programme goals

The materials to be covered by this CRP should be the elements and isotopes of the most common structural materials of fission and fusion reactors such as Fe, Cr, Ni, which are the main constituents of steel, inconel and other structural alloys; in additon some other important materials will be included. The energies covered should range from resolved resonances to 20 MeV; in this energy range all neutron reactions should be dealt with, with an emphasis on neutron elastic and inelastic scattering and partial reaction cross sections and secondary particle energy and angular distributions.

Currently recognized problem areas to whose solution this CRP could contribute, are:

- calculational methods for the interpretation of experimental resolved resonance data;
- consistency problems between fluctuating cross sections of different neutron reactions in the unresolved resonance region;
- treatment of elastic scattering angular distributions for resolved resonances and in the unresolved resonance region (e.g. intermediate structure);
- treatment of energy distributions of inelastically scattered neutrons in the transition from discrete to "continuously" distributed rest nucleus levels;
- problems and methods in the calculation of (n,xn) reactions;
- problems and methods in the calculation of (n,p) and (n,α) reactions and in the separation of (n,np), (n,pn), (n,nα) and (n,αn) reactions;
- problems and methods in the calculation of "small yield" neutron cross sections for the (n,d), (n,t) and (n,He^3) reactions;
- problems and methods in the calculation of secondary particle energy and angular distributions (treatment of level densities; transmission coefficients for the various reaction exit channels; compound, pre-compound and direct contributions).

3. Programme objectives

The objectives of the CRP are visualized to be as follows:

(1) discussion and intercomparison of the various calculational methods used and/or developed by the CRP participants in dealing with the problem areas mentioned under point 2 above;

(2) summary of the results of these intercomparisons and, if possible, identification of the most appropriate methods recommended for use in calculations of neutron cross sections of the structural materials considered under this CRP, (final goal).

4. Benefits

Exchange of experience and developments in methodologies of calculation neutron cross sections for structural materials will be of benefit to

(1) developed countries, since it will accelerate the development of improved evaluated neutron data files for structural materials needed for their nuclear power programmes, and to

(2) developing countries, since it will provide an opportunity for training and gaining experience in methods of nuclear cross-section calculations and thus help in the development of scientific infrastructure for nuclear technology.

5. Connection with other programmes

The proposed CRP will partly complement, partly have a natural interconnection with other IAEA/NDS programes, i.e. with

- the Workshop on Nuclear Model Computer Codes organized jointly by IAEA-NDS and the ICTP in Trieste in January/February 1984;
- the ongoing CRP on the measurement and analysis of 14 MeV neutron nuclear data needed for fission and fusion reactor technology;
- the development of an international radiation damage neutron cross section file; and
- the activity in the field of nuclear level densities (IAEA Advisory Group Meeting in Brookhaven in April 1983).

6. Participation

Many laboratories from different parts of the world are or may be interested to participate in the proposed CRP:

ANL (Argonne), BNL (Brookhaven) and LLNL (Livermore) from the USA;
FEI (Obninsk) and INE (Minsk) from the USSR;
TUD (Dresden) from the GDR;
KFK (Karlsruhe) from the FRG;
ENEA (Bologna) from Italy;
CEN (Saclay, Cadarache, Bruyeres-le-Chatel) from France;
IRK (Vienna) from Austria;

ANEB (Sofia) from Bulgaria;
PFU (Bratislava) from Czechoslovakia;
BARC (Bombay) from India;
JAERI (Tokyo) from Japan;
ECN (Petten) from the Netherlands
IBJ (Warsaw) from Poland
IFIN and IRNE (Bucharest) from Romania
AERE (Harwell) from the United Kingdom
CTA/IEA Nuclear Data Centre (São José dos Campos) from Brazil.

Of course, in view of budgetary limitations, only a limited, carefully selected number of these institutes could participate in the CRP.

7. CRP start and duration

Subject to INDC and internal IAEA approval, the CRP could be started in the course of 1984 by concluding research agreements or contracts with several institutes for the first year of the CRP with the possibility of renewal after the first year. In order to accomplish the goals of this CRP as tentatively outlined under point 2 above, a total duration of three years, in line with the normal duration of IAEA CRPs, is deemed necessary. The funds will be provided from the NDS' part of the Agency's Research Contract Programme Budget.

8. INDC recommendation

The comments of INDC on this suggested CRP are appended for information.

Comments of the INDC on this CRP

13th INDC Meeting

Rio de Janeiro, 16-20 May 1983

Proposed new CRP on methods for the calculation of fast neutron nuclear data for structural materials

The subcommittee supported this proposal in principle. Proposed objectives should be defined by participants during the planned Consultants Meeting. These should be limited to the most important structural materials (e.g. Fe, Cr, Ni) and the neutron cross sections of highest importance (inelastic scattering, elastic scattering anisotropy, (n,p) and (n,α) reactions). The proposed objectives should then be distributed by NDS to INDC participants who should reply saying whether they support the proposals before the end of the year.

V. Contributed Papers

Comparison of Fe, Na and Cr Evaluated Nuclear Data

by

D.E. Cullen
Nuclear Data Section
IAEA

Introduction

One approach toward identifying problem areas in evaluated data is to compare a number of currently used evaluations for the same materials. By determining where these evaluations differ (i.e. in which reactions and energy ranges) it is possible to identify where the evaluators felt that the experimental data and nuclear models available at the time of the evaluation could be interpreted to yield different cross sections. As such these comparisons indicate where there is uncertainty in the evaluated data and at least in a relative sense the order of magnitude of the uncertainty. However, this approach does not necessarily indicate which of the evaluation is the "best", nor does it give an absolute estimate of the uncertainty in the evaluations. But, if the various evaluations were performed during different time periods by comparing them it is possible to see the effects of the more recently available experimental data and nuclear models and to identify deficiences in some of the currently used evaluations.

Comparisons

Evaluations from four evaluated data libraries have been compared: ENDF/B-IV, ENDL82, SOKRATOR and JENDL2. Many different reactions and types of data (e.g. angular and energy distributions) have been compared. However, herein only a few results are presented in a compact form in an attempt to identify the magnitude of differencea over broad ranges.

The following tables present a comparison of evaluations for natural Fe, Na and Cr, total, capture and total-inelastic cross sections in a broad group structure (the ABBN structure). In addition to group averaged cross sections, in an attempt to clearly indicate the areas and magnitude of differences, in each group the average value of the four evaluations has been calculated and results are presented to indicate the per-cent deviation of each evaluation from this average. These per-cent differences should only be used as an indication of the magnitude of the disagreement between evaluations; in particular it must not be interpreted as indicating the uncertainty in any given evaluation.

Comments on differeces

Even for these broad group cross sections there are surprising ditferences even in the total cross section. For all materials differences in excess of 10% in the total cross section were found in one of more groups.

For the capture cross sections we see large differences over most of the energy range and increasing differences toward higher energies. However we can see that more recent evaluations have a more reasonable high energy variation.

For the total inelastic cross sections we generally see smaller differences. The major difference that we see is that more recent evalutions are using low lying inelastic levels to account for direct and pre-compound effects.

NATURAL IRON - GROUP AVERAGES (BARNS)

GROUP	TOTAL				CAPTURE				INELASTIC			
	ENDF/B-IV 1974	ENDL82 1976	SOKRATOR 1975	JENDL2 1979	ENDF/B-IV 1974	ENDL82 1976	SOKRATOR 1975	JENDL2 1979	ENDF/B-IV 1974	ENDL82 1976	SOKRATOR 1975	JENDL2 1979
THERMAL	13.96	13.36	13.950	14.96	2.560	2.554	2.552	2.521				
0.215 EV	12.13	11.42	12.135	13.09	0.711	0.705	0.709	0.670				
0.465	11.90	11.21	11.886	12.90	0.484	0.479	0.485	0.461				
1.0	11.74	11.03	11.738	12.72	0.330	0.327	0.331	0.334				
2.15	11.63	10.86	11.631	12.60	0.225	0.223	0.225	0.218				
4.65	11.56	10.82	11.554	12.50	0.153	0.151	0.153	0.153				
10.0	11.51	10.79	11.504	12.40	0.104	0.106	0.104	0.104				
21.5	11.48	10.73	11.474	12.26	0.0711	0.0000	0.0695	0.0745				
46.5	11.45	10.61	11.435	12.00	0.0484	0.0511	0.0459	0.0543				
100	11.36	10.56	11.156	11.53	0.0330	0.0526	0.0293	0.0364				
215	10.92	10.22	10.601	10.65	0.0225	0.0437	0.0175	0.0217				
465	9.802	8.273	9.594	9.231	0.0152	0.0333	0.00957	0.0119				
1 KEV	8.730	8.155	7.003	7.542	0.2308	0.0125	0.1163	0.1604				
2.15	6.757	6.519	6.853	5.971	0.00700	0.0146	0.0111	0.00470				
4.65	10.50	10.94	10.456	10.873	0.0230	0.0523	0.0235	0.0209				
10.0	2.559	3.633	3.301	3.655	0.00459	0.0193	0.00374	0.00738				0.01079
21.5	13.14	11.36	12.366	11.916	0.0162	0.0318	0.0171	0.0183				0.1104
46.5	5.492	5.320	5.190	4.749	0.00893	0.0199	0.0111	0.0130				0.0201
100	4.303	4.092	4.334	4.231	0.00570	0.00575	0.00729	0.00833				0.0269
200	3.356	2.943	2.925	3.108	0.00559	0.00508	0.00527	0.00619				0.0164
400	3.299	3.426	3.116	3.015	0.00502	0.00440	0.00498	0.00502				0.0211
800	2.686	2.750	2.730	2.628	0.00206	0.00203	0.00343	0.00307	0.3564	0.4401	0.3251	0.4987
1.4 MEV	3.006	3.000	3.139	3.102	0.00144	0.00147	0.00182	0.00252	0.8150	0.0124	0.7531	0.7912
2.5	3.456	3.445	3.531	3.453	0.000820	0.000850	0.000970	0.00242	1.172	1.159	1.167	1.105
4.0	3.679	3.600	3.650	3.624	0.000511	0.000610	0.000556	0.00161	1.514	1.440	1.417	1.371
6.5	3.352	3.307	3.354	3.272	0.000318	0.000297	0.000339	0.000704	1.421	1.429	1.372	1.317
10.5	2.719	2.756	2.758	2.673	0.000327	0.000085	0.000695	0.000254	1.031	1.110	0.9793	0.007
15.0												

NATIRN. IRON - DEVIATION FROM MEAN (%)

GROUP	TOTAL				CAPTURE				INELASTIC			
	ENDF/B-IV 1974	ENDL82 1976	SORRATOR 1975	JENDL2 1979	ENDF/B-IV 1974	ENDL82 1976	SORRATOR 1975	JENDL2 1979	ENDF/B-IV 1974	ENDL82 1976	SORRATOR 1975	JENDL2 1979
THERMAL	-0.69	-4.96	-0.76	6.42	0.52	0.20	0.21	-1.01				
0.215 EV	-0.52	-6.35	-0.40	7.35	1.75	0.89	1.47	-4.11				
0.465	-0.58	-6.34	-0.69	7.61	1.41	0.37	1.62	-3.40				
1.0	-0.57	-6.58	-0.58	7.73	-0.15	-1.06	0.15	1.06				
2.15	-0.43	-7.02	-0.42	7.87	1.01	0.11	1.01	-2.13				
4.65	-0.42	-6.79	-0.47	7.68	0.33	-0.98	0.33	0.33				
10.0	-0.35	-6.59	-0.41	7.35	-0.48	1.44	-0.48	-0.48				
21.5	-0.05	-6.50	-0.10	6.74	-3.63	0.44	-5.79	0.98				
44.5	0.67	-6.72	0.54	5.51	-3.05	2.35	-8.06	8.76				
100	1.87	-5.30	0.04	3.39	-12.76	39.06	-22.54	-3.77				
215	3.04	-3.56	0.03	0.49	-28.23	103.19	-44.18	-30.78				
465	6.25	-10.32	4.00	0.07	-13.11	90.37	-45.29	-31.97				
1 KEV	11.10	3.79	-10.87	-4.02	74.85	-90.53	-11.89	27.58				
2.15	3.56	-0.09	5.03	-8.49	-25.13	56.15	18.72	-49.73				
4.65	-1.80	2.32	-2.21	1.69	-23.14	74.77	-21.47	-30.16				
10.0	-22.62	9.86	2.24	10.52	-47.56	120.51	-57.27	-15.68				
21.5	7.74	-6.85	1.40	-2.29	-22.30	52.52	-17.99	-12.23				
44.5	5.84	2.55	0.04	-8.46	-32.51	50.39	-16.12	-1.76				
100	1.49	-3.49	2.22	-0.21	-14.84	-15.29	7.40	22.73				
200	8.86	-4.54	-5.12	0.81	1.04	-8.18	-4.74	11.88				
400	2.64	6.60	-3.05	-6.19	-0.67	-12.96	-1.48	15.13				
800	-0.61	2.05	1.31	-2.76	-6.15	-7.14	12.55	0.74	-6.05	15.02	-15.03	6.87
1.4 MEV	-0.51	-0.70	1.20	0.01	-20.55	-10.90	0.41	39.03	2.70	2.46	-5.02	-0.22
2.5	-0.44	-0.76	1.72	-0.53	-35.18	-32.01	-23.32	91.30	1.85	0.72	1.41	-3.96
4.0	1.06	-0.87	0.27	-0.45	-37.82	-25.77	-32.34	95.92	5.47	0.31	-1.29	-4.47
6.5	0.32	1.37	0.38	-2.07	-27.23	-32.04	-20.14	79.41	2.62	3.20	-0.92	-4.89
10.5	-0.28	1.00	1.16	-1.96	-27.97	-73.04	120.46	-19.43	2.91	10.00	-2.25	-11.46
15.0												

NATURAL NICKEL - GROUP AVERAGES (BARNS)

GROUP	TOTAL				CAPTURE				INELASTIC			
	ENDF/B-IV 1973	ENDL02 1976	SOKRATOR 1977	JENDL2 1979	ENDF/B-IV 1973	ENDL02 1976	SOKRATOR 1977	JENDL2 1979	ENDF/B-IV 1973	ENDL02 1976	SOKRATOR 1977	JENDL2 1979
THERMAL	22.45	21.11	21.70	21.21	4.574	4.600	4.400	4.436				
0.215 EV	19.15	17.77	18.81	18.01	1.270	1.275	1.230	1.234				
0.465	18.74	17.37	18.16	17.61	0.865	0.868	0.839	0.841				
1.0	18.47	17.09	17.88	17.35	0.590	0.593	0.572	0.574				
2.15	18.28	16.90	17.70	17.16	0.402	0.403	0.389	0.391				
4.65	18.14	16.77	17.57	17.03	0.274	0.274	0.265	0.266				
10.0	18.04	16.69	17.49	16.94	0.187	0.191	0.181	0.181				
21.5	17.96	16.63	17.43	16.87	0.127	0.133	0.123	0.124				
46.5	17.85	16.59	17.38	16.81	0.0868	0.0898	0.0839	0.0842				
100	17.71	16.56	17.37	16.58	0.0595	0.0604	0.0568	0.0575				
215	17.43	16.54	17.34	16.21	0.0409	0.0420	0.0386	0.0393				
465	16.90	16.53	17.19	15.62	0.0286	0.0289	0.0264	0.0272				
1 KEV	16.00	16.52	16.34	15.02	0.0231	0.0230	0.0187	0.0279				
2.15	21.17	22.35	20.00	20.83	0.0403	0.0604	0.0289	0.0424				
4.65	13.66	14.05	13.18	13.05	0.0203	0.0863	0.0126	0.0282				
10.0	44.48	46.86	41.87	46.69	0.0947	0.1705	0.0804	0.1242				
21.5	10.57	13.61	10.46	11.00	0.0347	0.0778	0.0234	0.0363				
46.5	7.698	11.06	7.840	9.178	0.0194	0.0407	0.0206	0.0220				0.00166
100	5.844	5.430	5.629	5.962	0.0140	0.0105	0.0140	0.0181			0.00033	0.00545
200	5.471	5.042	5.006	5.441	0.00865	0.0116	0.0101	0.0110			0.00260	0.00637
400	3.302	3.573	3.548	3.626	0.00764	0.00895	0.00789	0.00956			0.00735	0.00651
800	2.932	3.260	3.253	3.245	0.00749	0.00762	0.00720	0.0106	0.0062	0.0062	0.0153	0.0155
1.4 MEV	3.001	3.173	3.174	3.166	0.00400	0.00535	0.00437	0.00734	0.5207	0.4984	0.4343	0.4643
2.5	3.314	3.393	3.397	3.389	0.00207	0.00247	0.00218	0.00407	1.117	1.052	0.9469	0.9765
4.0	3.664	3.500	3.500	3.529	0.00114	0.00105	0.000943	0.00177	1.162	1.157	1.062	1.117
6.5	3.441	3.422	3.425	3.422	0.000381	0.000450	0.000730	0.000740	0.862	0.844	0.0847	0.9018
10.5	2.073	2.074	2.073	2.073	0.000025	0.000301	0.000912	0.000215	0.764	0.517	0.5124	0.5648
15.0												

NATURAL NICKEL - DEVIATION FROM MEAN (%)

GROUP	TOTAL				CAPTURE				INELASTIC			
	ENDF/B-IV 1973	ENDL82 1976	SOKRATOR 1977	JENDL2 1979	ENDF/B-IV 1973	ENDL82 1976	SOKRATOR 1977	JENDL2 1979	ENDF/B-IV 1973	ENDL82 1976	SOKRATOR 1977	JENDL2 1979
THERMAL	3.85	-2.35	0.30	-1.69	1.54	2.30	-2.32	-1.52				
0.215 EV	3.80	-3.61	2.03	-2.31	1.42	1.02	-1.78	-1.46				
0.465	4.28	-3.34	1.06	-2.00	1.30	1.73	-1.67	-1.44				
1.0	4.37	-3.43	1.03	-1.96	1.33	1.05	-1.76	-1.42				
2.15	4.40	-3.48	1.09	-2.00	1.45	1.70	-1.03	-1.32				
4.65	4.39	-3.50	1.11	-2.00	1.50	1.50	-1.76	-1.39				
10.0	4.34	-3.47	1.16	-2.02	1.08	3.24	-2.16	-2.14				
21.5	4.28	-3.44	1.20	-2.05	0.20	4.93	-2.96	-2.17				
46.5	4.04	-3.31	1.30	-2.03	0.73	4.21	-2.64	-2.29				
100	3.84	-2.90	1.05	-3.79	1.62	3.16	-2.99	-1.79				
215	3.26	-2.01	2.73	-3.97	1.74	4.40	-3.98	-2.24				
465	2.03	-0.18	3.00	-5.68	2.97	4.05	-4.95	-2.07				
1 KEV	0.56	3.31	2.19	-6.07	-3.60	0.33	-18.43	21.70				
2.15	-0.55	4.99	-2.29	-2.15	-6.28	40.47	-32.79	-1.40				
4.65	1.30	4.19	-2.26	-3.23	-27.16	122.14	-67.57	-27.41				
10.0	-1.10	4.19	-6.90	3.81	-19.37	45.17	-31.55	5.75				
21.5	-7.36	19.28	-8.33	-3.59	-19.40	80.72	-45.64	-15.68				
46.5	-13.45	33.35	-11.85	-9.05	-24.44	58.52	-19.77	-14.31				
100	2.23	-5.01	-1.53	4.30	-14.37	13.15	-9.48	10.70			-88.60	88.60
200	4.41	-3.70	-4.47	3.84	-16.32	12.21	-2.30	6.41			-42.16	42.16
400	-5.99	1.73	1.02	3.24	-10.22	5.17	-7.29	12.34			-7.31	7.31
800	-7.58	2.76	2.54	2.29	-8.96	-7.30	-12.49	28.84	-42.33	-42.33	42.33	42.33
1.4 MEV	-4.08	1.42	1.45	1.20	-11.03	-2.46	-20.33	33.82	6.40	1.04	-11.26	3.02
2.5	-1.76	0.59	0.70	0.47	-17.38	-10.10	-20.66	48.13	9.12	2.77	-7.49	-4.41
4.0	1.76	-0.58	-0.58	-0.60	-7.00	-14.34	-23.07	44.40	3.33	2.89	-5.56	-0.67
4.5	0.39	-0.16	-0.07	-0.16	-33.77	-21.77	26.90	20.64	-1.27	-3.33	1.33	3.27
10.5	-0.01	0.03	-0.01	-0.01	-93.12	-17.14	151.07	-40.81	29.59	-12.31	-13.09	-4.20
15.0												

NATURAL CHROMIUM - GROUP AVERAGES (BARNS)

GROUP	TOTAL				CAPTURE				INELASTIC			
	ENDF/B-IV 1974	ENDL82 1973	SOKRATOR 1977	JENDL2 1979	ENDF/B-IV 1974	ENDL82 1973	SOKRATOR 1977	JENDL2 1979	ENDF/B-IV 1974	ENDL82 1973	SOKRATOR 1977	JENDL2 1979
THERMAL	7.444	7.201	7.100	6.904	3.101	3.102	3.200	3.074				
0.215 EV	5.208	4.952	4.819	4.690	0.861	0.857	0.903	0.856				
0.465	4.932	4.639	4.523	4.418	0.587	0.581	0.606	0.583				
1.0	4.746	4.540	4.325	4.233	0.400	0.408	0.413	0.397				
2.15	4.620	4.476	4.186	4.104	0.273	0.272	0.278	0.271				
4.65	4.534	4.372	4.100	4.020	0.186	0.184	0.189	0.184				
10.0	4.478	4.372	4.040	3.966	0.127	0.129	0.130	0.126				
21.5	4.444	4.347	4.000	3.936	0.0867	0.0852	0.0930	0.0861				
46.5	4.432	4.321	3.962	3.931	0.0594	0.0580	0.0606	0.0591				
100	4.448	4.320	3.942	3.964	0.0412	0.0406	0.0413	0.0409				
215	4.517	4.313	3.930	4.076	0.0291	0.0277	0.0283	0.0289				
465	4.752	4.303	3.921	4.406	0.0216	0.0220	0.0192	0.0216				
1 KEV	5.960	4.395	4.352	5.875	0.1651	0.0596	0.2603	0.1618				
2.15	18.45	12.41	16.527	18.972	0.0429	0.0371	0.0400	0.0450				
4.65	22.39	16.49	23.116	23.573	0.0726	0.0355	0.0690	0.0591				
10.0	4.043	4.218	3.070	3.235	0.0281	0.00911	0.0159	0.00718				
21.5	2.799	3.097	3.045	2.424	0.0295	0.00365	0.0220	0.0139				
46.5	6.354	5.100	8.244	6.116	0.0124	0.00455	0.0132	0.00982				
100	6.675	6.160	6.080	6.603	0.00693	0.00396	0.00972	0.00664				
200	3.186	2.769	3.110	3.042	0.00395	0.00367	0.00484	0.00363				
400	3.356	3.060	3.103	3.019	0.00484	0.00411	0.00374	0.00374	0.00701	0.00847	0.00393	0.00503
800	3.099	2.945	2.923	2.919	0.00740	0.00327	0.00372	0.00403	0.0792	0.0845	0.0373	0.0345
1.4 MEV	3.406	3.412	3.084	3.278	0.00410	0.00198	0.00208	0.00185	0.6726	0.6675	0.6286	0.5075
2.5	3.730	3.694	3.590	3.571	0.00227	0.00156	0.00118	0.00194	1.0673	1.049	1.054	0.0762
4.0	3.693	3.621	3.507	3.427	0.000937	0.00130	0.000763	0.00136	1.4103	1.252	1.330	1.256
6.5	3.174	3.183	3.097	3.107	0.000154	0.00109	0.000562	0.000575	1.3120	1.133	1.288	1.246
10.5	2.559	2.609	2.502	2.497	0.000671	0.00100	0.000717	0.000165	0.9705	0.0746	0.9990	0.0736
15.0												

NATURAL CHROMIUM - DEVIATION FROM MEAN (%)

GROUP	TOTAL				CAPTURE				INELASTIC			
	ENDF/B-IV 1974	ENDL82 1973	SOKRATOR 1977	JENDL2 1979	ENDF/B-IV 1974	ENDL82 1973	SOKRATOR 1977	JENDL2 1979	ENDF/B-IV 1974	ENDL82 1973	SOKRATOR 1977	JENDL2 1979
THERMAL	3.93	0.34	-0.87	-3.61	-0.59	-0.55	2.59	-1.45				
0.215 EV	5.91	0.71	-2.00	-4.62	-0.95	-1.41	3.08	-1.52				
0.465	6.45	0.56	-2.37	-4.64	-0.30	-1.40	2.84	-1.06				
1.0	6.39	1.77	-3.05	-5.11	-1.11	0.07	2.10	-1.85				
2.15	6.29	2.98	-3.69	-5.58	-0.10	-0.55	1.63	-0.91				
4.65	6.39	3.06	-3.79	-5.67	0.13	-0.94	1.75	-0.94				
10.0	6.26	3.75	-4.13	-5.89	-2.31	-0.77	6.15	-3.08				
21.5	6.27	3.95	-4.35	-5.88	-1.40	-2.05	5.68	-2.16				
46.5	6.50	3.83	-4.79	-5.54	0.21	-2.15	2.24	-0.30				
100	6.71	3.63	-5.43	-4.91	0.49	-0.98	0.73	-0.24				
215	7.32	2.47	-6.63	-3.16	2.11	-2.81	-0.70	1.40				
465	9.35	-0.98	-9.77	1.39	1.41	7.04	-9.06	1.41				
1 KEV	15.94	-14.62	-15.45	14.13	0.82	-63.60	63.97	-1.19				
2.15	11.21	-25.19	-0.38	14.36	3.50	-10.49	-3.50	10.49				
4.65	4.66	-22.92	8.06	10.19	22.95	-39.00	16.85	0.08				
10.0	-2.38	1.85	22.42	-21.89	86.43	-39.56	5.49	-52.36				
21.5	-1.49	9.00	7.17	-14.69	70.23	-78.79	27.81	-19.24				
46.5	-1.57	-20.87	27.71	-5.26	24.09	-54.47	32.10	-1.73				
100	4.60	-3.35	-4.72	3.47	1.72	-41.87	42.68	-2.53				
200	5.26	-8.52	2.75	0.50	-1.80	-8.76	20.32	-9.76				
400	7.07	-2.38	-1.00	-3.60	17.83	0.06	-8.95	-8.95	-60.30	67.31	-21.98	14.96
800	4.29	-0.87	-1.63	-1.77	60.70	-28.99	-19.22	-12.49	24.58	31.34	-41.33	-14.59
1.4 MEV	1.82	2.00	-1.82	-2.00	50.77	-20.50	-24.98	2.80	8.57	7.75	1.47	-17.77
2.5	2.30	1.31	-1.54	-2.06	30.65	-10.22	-32.09	11.65	5.56	3.75	4.24	-13.54
4.0	3.17	1.16	-2.03	-2.30	-13.64	17.97	-29.68	25.35	7.92	-5.96	1.77	-3.74
6.5	1.07	1.36	-1.30	-1.06	-44.87	68.00	-12.97	-10.96	5.40	-8.90	3.47	0.10
10.5	0.60	2.65	-1.56	-1.76	5.13	56.60	12.34	-74.15	6.00	-6.41	6.90	-6.47
15.0												

International Nuclear Model and Code Comparison

on Pre-Equilibrium Effects

H. Gruppelaar, H.A.J. van der Kamp
Netherlands Energy Research Fondation,
ECN, Petten, The Netherlands

and

P. Nagel
NEA Data Bank, Gif-sur-Yvette, France

1. Introduction

This paper gives the specification of an intercomparison of statistical nuclear models and codes with emphasis on pre-equilibrium effects. It is partly based upon the conclusions of a meeting of an ad-hoc working group on this subject (see document NEANDC-A-137), on some criticism by Prof. M. Blann, communicated to the NEA Data Bank by Dr. M. Uhl, and on some suggestions of the present authors. We are very grateful to Drs. Betak, Blann, Fu, Gardner, Gmuca, Gupta, Herman, Mann, Ribansky, Seeliger, Sarg, Uhl and Young for their comments on the draft version of this document. Most of the remarks have been included in the updated specifications given in this paper. The present proposal deviates from the previous one mainly in the choice of a somewhat heavier nucleus : ^{93}Nb instead of ^{59}Co. Using ^{93}Nb has several advantages:

1. The pre-compound part of the neutron emission spectrum is more pronounced than that of ^{59}Co.

2. This nucleus is quite well studied with respect to pre-equilibrium aspects, both experimentally and theoretically; it is often used as a "sample problem" in nuclear model calculations to illustrate pre-equilibrium effects.

3. There are experimental data for neutron emission spectra and angular distributions not only at 14.6 MeV, but also at 25.7 MeV(1). Furthermore, there are experimental data for σ_{n2n} and σ_{n3n} from 14.6 to 24 MeV(2). Proton-emission data including angular distributions are also available at 15 MeV (13, 14).

It is realised that the previous nucleus ^{59}Co is well studied in the statistical-model exercise and that it requires some additional effort by the participants to change to another nucleus. However, we think that the above-mentioned arguments are convincing, in particular point 3.

The character of this exercise differs from the equilibrium exercise in that the pre-equilibrium models currently in use are quite different. Therefore it is more correct to speak about a model intercomparison rather than a code intercomparison. Since the models differ in the modelling of pre-equilibrium aspects, we cannot specify all the parameters.

Therefore we restrict these to:

1. Masses, Q-values,
2. level-scheme data (discrete levels),
3. Optical-model parameters (global spherical potential),
4. γ-ray competition parameters,
5. total level-density specification.

The parameters, specific for the precompound emission are not prescribed. Instead it is required to fit the 14.6 MeV total neutron emission spectrum $\frac{d\sigma}{d\epsilon}$ at ϵ = 6 to 9 MeV, where precompound emission dominates. The participants should therefore specify their model and the parameters used. To facilitate this task, a questionnaire has been included (Appendix A).

The main quantity to be calculated is the total neutron emission spectrum $\frac{d\sigma}{d\epsilon}$ as a function of incoming energy E and outgoing energy ϵ. These angle-integrated spectra should be calculated at E = 10, 14.6, 20 and 25.7 MeV. Comparison with experimental data will be performed at the NEA Data Bank. If possible, also the reduced Legendre coefficients of the angular distributions should be calculated. Other important quantities to be calculated are: $\sigma_{nn'\gamma}$, σ_{n2n}, $\sigma_{np\gamma}$, $\sigma_{n\alpha\gamma}$ and their energy spectra (angle-integrated).

Finally, for the more sophisticated model codes, it is requested to calculate the total energy-integrated particle-production cross sections, the isomeric state population from the (n,n') and (n,2n) reactions and the total photon production cross section (at 14.6 MeV).

It is not necessary to include width-fluctuation corrections in the calculations. There is also no need to calculate $\sigma_{n\gamma}$ in this exercise. However, γ-ray competition should be included (if possible) to calculate the multi-particle emission cross sections (and isomeric-state populations).

2. Masses, Q-values, etc.

The masses and Q-values should be taken from a recent nuclear mass table. Some values are provided in Table 3a(10).

3. Level scheme data (discrete levels)

The level schemes of most of the residual nuclei are specified in Table 1. These data are usually based upon recent issues of the Nuclear Data Sheets. The first energy of the continuum calculation, E_c, is indicated in Table 3a.

Notes: 1. For codes that calculate only continuum emission, these data are not relevant.
2. For other residual nuclei, the participants should perform a continuum calculation only, assuming E_c = 0.1 MeV.
3. For ^{92}Nb and ^{93}Nb γ-ray branchings are given for discrete levels.

4. Optical model

In this exercise, a spherical optical model is used, of which the definition of the parameters is given in Table 2a. The selected global optical-model parameters are given in Table 2b.

For neutrons and protons, parametrisation close to those of F.G. Percy (e.g. (3)) have been selected. These parametrisations should work well at energies from 0.9 to 22 MeV. Please indicate when the channel-spin dependence of the transmission coefficients has been neglected (T_l instead of $T_{l,j}$).

For neutrons, we have checked that the potential is in reasonably good agreement with available experimental ^{93}Nb data for σ_t and σ_{el} from 1 to 15 MeV.

For α-particles, the potential of Igo and Huizenga(4) has been selected.

5. Gamma-ray parameters

For the calculation of γ-ray competition the Brink-Axel giant-dipole model should be used to describe E1 transitions. For all residual nuclides, the same data are prescribed, i.e.

$$E_r = 16.5 \text{ MeV},$$
$$\Gamma_r = 5.0 \text{ MeV},$$
$$\sigma_r = 0.162 \text{ b}.$$

Using these parameters, the following value of the total s-wave radiation width is obtained for the reaction ^{93}Nb(n,γ) ^{94}Nb at the neutron binding energy:

$$\langle\Gamma_\gamma(I=0)\rangle = 165 \text{ meV}.$$

The value $\langle\Gamma_\gamma\rangle$/Dobs amounts to 0.156 x 10^{-4}. If necessary, a normalisation constant in the Brink-Axel formula should be used to obtain this value (the same normalisation constant should be used in each residual nucleus). The authors should specify their formalism used.

Note: If no γ-ray competition is used, the participants should clearly indicate this.

For γ-ray cascade calculations (isomeric state population), the M1 and E2 electromagnetic transitions should be allowed with the strengths of M1 and E2 set to: strength (E1/M1) = strength (M1/E2) = .10, relative to the total E_1 radiation width for s-wave resonances of the reaction ^{93}Nb(n,γ) ^{94}Nb at the neutron binding energy (Γ_γ= 165 meV) (the same normalisation constants should be used for each residual nucleus). For the energy dependences of the M1 and E2 transitions the Weisskopf formula should be used.

The branching ratios for ^{92}Nb and ^{93}Nb levels are given in Table 1. Use theory to obtain branchings for other residual nuclides (only needed for calculation of total photon production).

The participant should specify the Yrast line used in the calculation of the gamma-ray emission data.

6. Total level-density parameters

For the calculation of the equilibrium part - or in the unified codes, the combined pre-equilibrium and equilibrium parts - it is requested to fit the total level density (i.e. summed over all possible particle-hole combinations) at two energies, so that:

1. the total number of levels equals N_c at E=E_c;

2. the level spacing of s-wave levels equals Dobs at the neutron binding energy B.

With these conditions, the participant should preferably use the composite Gilbert-Cameron formula(5). When this formula is not programmed, the Fermi-gas formula of Dilg et al(6) or another representation could be used (other formulas could be important in unified models, where it is required that the sum of all particle-hole components equals the total level density).

In Table 3a, the values of the parameters required to calculate N_c and Dobs are specified. When the Gilbert-Cameron formula is used, the pairing energies P of ref. (5) are also prescribed (see Table 3a). Table 3b gives the parameters a, U_x and Δ for three possible representations:

1. Gilbert-Cameron formula with improved definition of the spin cut-off parameter(7):

$$\sigma^2 = 0.146 \sqrt{aU}\, A^{2/3}.$$

2. Gilbert-Cameron formula with original definition of the spin cut-off parameter(5):

$$\sigma^2 = 0.0888 \sqrt{aU}\, A^{2/3}.$$

3. Back-shifted Fermi gas model(6) with:

$$I_{eff} = I_{rigid}.$$

The parameter a follows from the quantity a by means of the relation:

$$a = \frac{\pi^2}{6} g.$$

Notes:

1. The participant should clearly specify the formula used. The preferred representation is formula 1.

2. At low energies the definition of σ^2 is not clear in the case of Gilbert-Cameron. It is suggested to use a linear interpolation between σ^2_{exp} at $E = E_c$ and $\sigma^2(E_x)$ at the dividing energy $E_x = U_x+P$. The value of σ^2_{exp} is given in Table 3a.

3. From some preliminary calculations with the Gilbert-Cameron formula and the back-shifted Fermi gas formula, it follows that the differences in the cross sections due to the use of different level density formulas cannot be neglected, particularly at energies above 10 MeV. This has to be regretted, but it is a basic uncertainty in our model calculations, as long as these simple level-density formulas are used. In some codes, different level-density formulas could be used. The participants are invited to use these options to study the effect of the different approaches. Our preference for the Gilbert-Cameron formula is only based upon the fact that this formula is probably the most widely used.

7. Particle-hole state density

In most cases it is expected that the particle-hole state densities are based upon the expression of Williams(8), possibly with corrections. The exact formula used should be specified, both for the initial and final state densities. When the calculations of precompound parts and compound parts are unified, the sum over all particle-hole level densities should satisfy the conditions given in the previous section. When the precompound calculation is used as a correction to the compound model, one could use the same parameters as used in the equilibrium calculation, including energy shifts or pairing energy corrections. This would facilitate the intercomparison of the results. However, as it is noticed that another parametrisation could be more realistic for pre-equilibrium calculations, deviations are allowed, provided that they are indicated clearly. In many codes only the option $g = A/13\ MeV^{-1}$ and P=0 is allowed. This should be specified.

When angular momentum is conserved in the calculation, the adopted expression for the p-h spin cut-off parameter should be specified.

8. Precompound parameters

In some codes there are some "free" parameters to fit the emission spectra, such as K occurring in the expression for the average transition matrix elements, e.g.

$$\left| M^2 \right| = \frac{K}{A^3 E}.$$

This, or a similar expression, should be indicated, together with the value of the parameter(s). The value(s) of the free parameter(s) should be adjusted in order to obtain agreement with the (angle-integrated) total neutron emission spectrum at E = 14.6 MeV and ϵ = 6 to 9 MeV:

$$\frac{d\sigma}{d\epsilon}\ (6\text{-}7\ MeV) = 56.0 \pm 6\ mb/MeV,$$

$$\frac{d\sigma}{d\epsilon}\ (7\text{-}8\ MeV) = 46.9 \pm 5\ mb/MeV,$$

$$\frac{d\sigma}{d\epsilon}\ (8\text{-}9\ MeV) = 36.5 \pm 4\ mb/MeV.$$

These data are obtained from an analysis of the experimental data of Hermsdorf et al(9), performed at ECN, Petten*. At ϵ = 6-9 MeV, most of the emission is due to pre-equilibrium; at higher energies the experimental data are quite uncertain due to direct effects or uncertainties in the subtraction of the elastic scattering peak.

Other parameters, such as R or D factors(10,15) should also be specified. Gadioli et al.(11) have proposed $R = \frac{n^+}{n^-}$, where the "+" and "-" signs refer to neutron and proton emission, n^+, n^- respectively, to account for charge conservation. For "unified" models it is desired that these parameters approach unity at equilibrium.

The treatment of the α-channel has also to be described, e.g. according to ref. (12). When fit-parameters are used, such as form-factors, they should be specified.

Parameters for the description of angular distribution are not prescribed. The user should specify the formalism used.

9. Requested calculations

The incident energies for the calculations are E=10, 14.6, 20 and 25.7 MeV. For the outgoing centre-of-mass energies ϵ the energy mesh should be appropriate to describe the data (indicate when the spectra are stored in a histogram form). It is suggested to use at least 1 MeV bins up to 14 MeV, if possible smaller bins up to 2 MeV and 2 MeV bins above 16 MeV. The following quantities need to be calculated.

9.1 Integrated cross sections at 5 incident energies:

a) σ_t, σ_{el}, σ_r (composite-formation cross section),

b) σ_{nnx}, σ_{npx}, $\sigma_{n\alpha x}$ (first emission of n, p, and α respectively),

c) $\sigma_{nn'}$ (inelastic scattering cross section), σ_{n2n}, σ_{n3n}, σ_{nnp}, σ_{np}, σ_{npn}, $\sigma_{n\alpha n}$ (other cross sections are relatively small),

d) total particle (and gas-) production cross sections σ_{nnem}, σ_{npem}, $\sigma_{n\alpha em}$.

* This analysis was performed by fitting the coefficients of the function $A_0+A_1P_1(\cos\theta)+A_2P_2(\cos\theta)$ through the original data of Hermsdorf et al. (9). The results are in agreement with a similar analysis of Kammerdiener's data (16) and those of Seliakov et al. (17).

Notes: 1) In cases b) to d) it is of interest to indicate the equilibrium component separately; also the full equilibrium calculation (with pre-equilibrium turned off) should be performed (specify equilibrium definition).

2) As intermediate results the transmission coefficients T_ℓ (averaged over j) and/or the inverse reaction cross sections should be given at each incident energy and for each outgoing particle.

9.2 Angle-integrated spectra at 14.6 and 25.7 meV

a) $\frac{d\sigma_{nnx}}{d\epsilon}$, $\frac{d\sigma_{npx}}{d\epsilon}$, $\frac{d\sigma_{n\alpha x}}{d\epsilon}$ (first emission of n, p and α, respectively).

b) Total neutron emission spectra (excluding elastic scattering) $\frac{d\sigma_{nnem}}{d\epsilon}$ (summed over all outgoing neutrons).

9.3 Angular distributions of (total) neutron emission spectra at 14.6 and 25.7 MeV

The preferred representation is given by reduced centre-of-mass Legendre coefficients f_ℓ (ℓ=1, 2, 3) where

$$\frac{d^2\sigma}{d\epsilon d\Omega} = \frac{1}{4\pi}\frac{d\sigma}{d\epsilon}\sum_\ell (2\ell+1)\, f_\ell\, P_\ell\,(\cos\theta);$$

f_ℓ should be tabulated as a function of ϵ (in c.o.m.).

9.4 γ-ray emission at 14.6 MeV

a) Reaction cross section for the population of the isomeric states ^{93m}Nb and ^{92m}Nb.

b) Total photon-production cross section.

c) γ-ray emission spectrum $\frac{d\sigma}{d\epsilon}$.

The participants are kindly asked to send all information on their codes and to answer the questions in the questionnaire (Appendix A).

Please send your contribution and direct any questions of interpretation related to the specifications, to :

Dr. Pierre Nagel
NEA Data Bank
91191 Gif-sur-Yvette CEDEX
France

The deadline for the solutions to reach the above address is 1st November 1983.

10. References

(1) A. Marcinowski et al., Nucl. Science and Eng., 83 (1983), p. 13.

(2) L.R. Veeser, E.D. Arthur and P.G. Young, Phys. Rev., C16 (1977), 1792.

(3) F.G. Percy, Phys. Rev., 131 (1963), 745.

(4) J.R. Huizenga and G. Igo, Nucl. Phys., 29 (1962), 462.

(5) A. Gilbert and A.G.W. Cameron, Can. J. of Phys., 43 (1965), 1446.

(6) W. Dilg et al., Nucl. Phys. A217 (1973), 269.

(7) U.E. Facchini and E. Saetta-Menichella, Energ. Nucl., 15 (1968), 54.

(8) F.C. Williams, Nucl. Phys., A166 (1971), 231.

(9) D. Hermsdorf et al., ZfK-277 (1974), Zentralinstitut für Kernforschung, Rossendorf bei Dresden Report.

(10) C. Kalbach, Z. für Physik A283 (1977), 401.

(11) E. Gadioli, E. Gadioli-Erba and P.G. Sona, Nucl-Phys. A217 (1973), p. 589.

(12) L. Milazzo-Colli and G.M. Braga-Marcazzan, Nucl-Phys. A210 (1973), p. 297.

(13) S.M. Grimes et al., Phys.Rev. C17 (1978) 508.

(14) H.K. Vonach, private communication (1983).

(15) S.K. Gupta, Z.Phys. A303 (1981) 329.

(16) J.L. Kammerdiener, UCRL-51232 (1972).

(17) O.A. Salnikov et al., Yad. Konstanty 7 (1971) 134.

(18) A.H. Wapstra and K. Bos, Atomic Data and Nuclear Data Tables, 19 (1977) 177.

Table 1

Level scheme data

LEVELS FOR 86RB

1	0.0	-2.0
2	0.4881	+1.0
3	0.5560	-6.0
4	0.5569	-3.0
5	0.7795	-7.0
6	0.8732	-3.0
7	0.9705	-4.0
8	1.0271	+1.0
9	1.0327	-3.0
10	1.0925	-4.0
11	1.1059	+2.0
12	1.1220	+1.0
13	1.1560	+0.0
14	1.1962	-3.0
15	1.2472	-4.0
16	1.3050	+3.0

LEVELS FOR 89SR

1	0.0	+2.5
2	1.0320	+0.5
3	1.4734	+3.5
4	1.9402	+2.5
5	2.0076	+1.5
6	2.0574	-1.5
7	2.0613	+4.5
8	2.0790	-5.5
9	2.2801	+0.5
10	2.4516	+1.5
11	2.5701	-1.5
12	2.6710	+3.5

LEVELS FOR 93ZR

1	0.0	+2.5
2	0.2669	+1.5
3	0.9471	+0.5
4	1.018	+0.5
5	1.151	+0.5
6	1.222	+0.5
7	1.4255	+1.5
8	1.4356	+0.5
9	1.4504	+1.5
10	1.4702	+2.5
11	1.477	+3.5
12	1.597	+2.5
13	1.640	+1.5

LEVELS FOR 90Y

1	0.0	-2.0
2	0.2025	-3.0
3	0.6820	+7.0
4	0.7768	+2.0
5	0.9537	+3.0
6	1.0474	+5.0
7	1.1895	+4.0
8	1.2147	-0.0
9	1.2982	+6.0
10	1.3710	-1.0

LEVELS FOR 92Y

1	0.0	-2.0
2	0.2415	+0.0
3	0.3100	-2.0
4	0.4306	+1.0
5	0.4403	-3.0
6	0.7801	-0.0
7	0.8924	+1.0
8	0.9534	-4.0

LEVELS FOR 92ZR

1	0.0	+0.0
2	0.9345	+2.0
3	1.3828	+0.0
4	1.4954	+4.0
5	1.8473	+2.0
6	2.0667	+2.0
7	2.1500	+4.0
8	2.3397	-3.0
9	2.3983	+4.0

LEVELS FOR 89Y

1	0.0	-0.5
2	0.9092	+4.5
3	1.5074	-1.5

LEVELS FOR 91NB

1	0.0	+4.5
2	0.1045	-0.5
3	1.1868	-2.5
4	1.3126	-1.5
5	1.5010	+3.5
6	1.6125	-1.5
7	1.6370	+4.5
8	1.7904	-4.5
9	1.8448	-2.5
10	1.8850	+0.5
11	1.9631	+2.5
12	1.9844	-6.5
13	2.0345	-8.5

LEVELS FOR 92NB

1	0.0	+7.0
2	0.1355	+2.0
3	0.2259	-2.0
4	0.2956	+3.0
5	0.3574	+5.0
6	0.3898	-3.0
7	0.4802	+4.0

LEVELS FOR 94NB

1	0.0	+6.0
2	0.0410	+3.0
3	0.0587	+4.0
4	0.0787	+7.0
5	0.1184	+5.0
6	0.1404	-2.0
7	0.3119	+5.0
8	0.3342	+2.0

LEVELS FOR 93MB (updated)

1	0.0	+4.5
2	0.0304	-0.5
3	0.686	-1.5
4	0.7440	+3.5
5	0.8087	+2.5
6	0.8101	-1.5
7	0.9499	+6.5
8	0.9791	+5.5
9	1.0026	+4.5
10	1.127	+2.5
11	1.29	-1.5
12	1.2974	+4.5
13	1.3156	-1.5
14	1.3351	+0.5

γ-RAY BRANCHINGS

GAMMA: TO LEVEL	2	(1.0)
	2	(1.0)
	1	(1.0)
	2	(0.03)
	3	(0.96)
	4	(0.01)
	4	(0.76)
	5	(0.24)

γ-RAY BRANCHINGS

GAMMA: TO LEVEL	2	(1.0)
	1	(1.0)
	1	(0.9877)
	4	(0.0123)
	2	(1.0)
	2	(1.0)
	1	(1.0)
	1	(0.265)
	4	(0.663)
	8	(0.072)
	5	(1.0)
	3	(1.0) ?
	1	(0.53)
	4	(0.3)
	8	(0.17)
	4	(1.0)
	7	(1.0)

Table 2a

Definition of Optical Potential

(according to Becchetti and Greenlees, Phys. Rev. 182, 1190 (1969)

	expression	validity range	explanation
$U_{opt}(r)$ =	$-V_R f_R$		central real
	$+(\frac{\hbar}{m_\pi c})^2 \frac{V_{SO}}{r}(\frac{d}{dr} f_{SO})\ \vec{l}\cdot\vec{\sigma}$		spin orbit
	$+\begin{cases}\frac{Zze^2}{2R_c}[3-(\frac{r}{R_c})^2] \\ \frac{Zze^2}{r}\end{cases}$	for $r \leqslant R_c$ for $r \geqslant R_c$	Coulomb
	$- iW_v f_I$		imaginary volume
	$+ 4ia_I W_{SF}(\frac{d}{dr} f_I)$		imaginary surface

where $f_x = f(r,R_x,a_x) = [1+\exp(r-R_x)/a_x]^{-1}$

$Rx = r_x A^{1/3}$

$R_x = r'_x A^{1/3} + r''$ for heavier projectiles (such as alphas)

r_c = Coloumb Radius

Note: Whenever a parameter is omitted, it is assumed that the corresponding potential is not considered.

Table 2b

Optical Model Parameters

Neutron Parameters

V_R = 48.0 - 0.29$\Im$E (E in MeV-Lab)

r_R = 1.27 fm a_R = 0.66 fm

W_{SF} = 9.6 MeV

r_I = 1.27 fm a_I = 0.47 fm

V_{SO} = 7.2 MeV

r_{SO} = 1.27 fm a_{SO} = 0.66 fm

Proton Parameters (ref. 3)

V_R = 53.3 - 0.55E + 0.4 Z/$A^{1/3}$ + 27.0 (N-Z)/A (E in MeV-Lab)

r_R = 1.25 fm a_R = 0.65 fm

W_{SF} = 13.5 MeV

r_I = 1.25 fm a_I = 0.47 fm

V_{SO} = 7.50 MeV

r_{SO} = 1.25 fm a_{SO} = 0.65 fm

r_c (coulomb radius) = 1.25 fm

Alpha Parameters (ref. 4)

V_R = 50.0 MeV

r_R' = 1.17 fm a_R = 0.576 fm r_R'' = 1.77 fm

W_V = 13.74 MeV

r_I' = 1.17 fm a_I = 0.576 fm r_I'' = 1.77 fm

r_c = 1.17 fm

Note: If the code does not allow for the second form of the radius expression in Table 2a, an effective radius parameter has to be calculated for each mass number (i.e. r_x = 1.56 for A = 93).

Table 3a

Calculation of level-density parameters[a)]

Nucleus (compo-site nucleus)	Mass (amu)	B (MeV)	J^π (target)	σ^2_{exp} [b)]	pc) (MeV)	E_C [d)] (MeV)	N_C [e)]	Dobs (eV)
86Rb	85.911	8.650	5/2-	7.24	0	1.309	15.5	201.4
89Sr	88.907	6.364	0+	5.31	1.24	2.707	11.5	37430
89Y	88.906	11.469	4-	6.47	0.93	1.745	7.5	140.0
90Y	89.907	6.857	1/2-	9.49	0	1.417	9.5	4414
92Y	91.909	6.544	1/2-	3.12	0	1.030	7.5	869.5
92Zr	91.905	8.635	5/2+	6.12	1.92	2.486	8.5	336.6
93Zr	92.907	6.732	0+	2.46	1.20	1.735	12.5	3678
91Nb	90.907	12.055	8+	9.36	0.93	2.065	12.5	51.2
92Nb	91.907	7.883	9/2+	11.6	0	0.501	6.5	267.3
93Nb	92.906	8.832	7+	6.70	0.72	1.364	13.5	41.5
94Nb	93.907	7.230	9/2+	12.0	0	0.396	7.5	99.6

a) The level density is characterised by the total number of levels N_C at energy E_C and the s-wave level spacing Dobs at the neutron binding energy B.

b) Spin cut-off parameter σ^2, derived from experimental spin distribution of levels up to $E=E_C$.

c) Pairing energy correction for Gilbert-Cameron formula, from (5).

d) E_C = first energy of continuum calculation.

e) "Average" number of levels at energy E_C.

Table 3b

Level-density parameters[a)]

Nucleus	Gilbert-Cameron 1 [b)]		Gilbert-Cameron 2 [c)]		Dilg et al.[d)]	
	a (MeV^{-1})	U_x (MeV)	a (MeV^{-1})	U_x (MeV)	a (MeV^{-1})	Δ(MeV)
86Rb	10.01	4.998	9.278	5.060	9.214	-1.069
89Sr	9.501	3.477	8.375	3.883	8.924	0.4802
89Y	8.600	2.213	8.112	1.537	8.460	0.3116
90Y	9.318	3.792	8.390	4.066	8.914	-0.7409
92Y	12.10	2.628	11.02	2.705	11.30	-0.5117
92Zr	11.83	4.047	10.92	3.995	10.43	0.7695
93Zr	12.69	4.607	11.46	4.774	10.63	-0.1563
91Nb	9.400	5.132	9.415	4.407	8.725	-0.2954
92Nb	10.30	6.400	9.762	6.259	8.923	-1.747
93Nb	12.58	4.678	12.39	4.270	11.24	-0.4636
94Nb	12.51	5.707	11.86	5.603	10.65	-1.553

a) Level-density parameters calculated from the data given in Table 3a.

b) Improved Gilbert-Cameron formula, with $\sigma^2 = 0.146 \sqrt{aU}\, A^{2/3}$ (5).

c) Original Gilbert-Cameron formula, with $\sigma^2 = 0.0888 \sqrt{aU}\, A^{2/3}$ (7).

d) Back-shifted Fermi gas formula of Dilg et al.(6).

Appendix A

Questionnaire on Pre-equilibrium/Equilibrium Model Codes

1. Participant

2. Code name and references, availability (give date):

3. Equilibrium-model part

- ☐ 3.1 Weisskopf-Ewing type (no conservation of angular momentum; no discrete levels)
- ☐ 3.2 Hauser-Feshbach (H.F.) type
- ☐ 3.3 Else, or comment:

4. Pre-equilibrium-model part

- ☐ 4.1 Full master equation approach ($n_0=3$) ☐ with or ☐ without quantum mechanical conservation of angular momentum (and parity).
- ☐ 4.2 Never-come back assumption (only λ^+-transitions starting from $n_0=3$)
- ☐ 4.3 (Geometry-dependent) hybrid-model, indicate $n_0=$ ☐
- ☐ 4.4 Two-component model (protons and neutrons are explicitly distinguished as in Ref (1)).
- ☐ 4.5 Else, or comment:

5. Relation of equilibrium to pre-equilibrium parts

- ☐ 5.1 Unified model of pre-equilibrium and equilibrium emission with conservation of angular momentum and ☐ with or ☐ without treatment of discrete levels.
- ☐ 5.2 Pre-equilibrium is treated as a correction to the statistical model (indicate relation below)
- ☐ 5.3 Else, or comment (give definition of equilibrium and/or pre-equilibrium, if this is useful):

6. Options

☐ 6.1 Cross sections (angle and energy integrated).

☐ 6.2 Particle spectra (angle—integrated).

☐ 6.3 Angular distributions.

☐ 6,4 Multi-particle emission up to ☐ outgoing particles with ☐ or without ☐ multiple precompound decay treatment.

☐ 6.5 Else, or comment:

7. Total level density in equilibrium part

☐ 7.1 Gilbert-Cameron(1) ($\sigma^2=0.0888\sqrt{aU}\,A^{2/3}$ ☐). ($\sigma^2=0.146\sqrt{aU}\,A^{2/3}$ ☐).

☐ 7.2 Back-shifted Fermi-gas model of Dilg et al.(2).

☐ 7.3 Modifications or comments (e.g. σ^2 at low E):

8. Particle-hole level density

☐ 8.1 Williams state density(3) ☐ with or ☐ without an energy shift or pairing energy correction (if there is an n-dependent energy shift, indicate expression below).

☐ 8.2 g = A/13 MeV^{-1} and no pairing energy correction.

☐ 8.3 Williams' level density with n-dependent spin distribution, indicate σ_n^2 below.

☐ 8.4 Else, or comment:

9. Discrete levels

☐ 9.1 Included in equilibrium calculation only.

☐ 9.2 Not considered, E_c=0.1 MeV.

☐ 9.3 Else, or comment (e.g. when direct models are used or included in the model):

10. Internal transition rates

10.1 Average transition probability $\lambda^{\pm}=\frac{2\pi}{\hbar}\langle M^2\rangle\ \omega_f^{\pm}$ with $\omega_f^{\pm}$ according to:

☐ Williams(3)

☐ Oblozinsky et al.(4)

☐ else, or modifications:

and $\langle M^2\rangle$ according to

☐ $\langle M^2\rangle=cA^{-3}E^{-1}$ with c = ☐

☐ Kalbach(5), indicate fit parameters below.

☐ else, or comment:

☐ 10.2 Else, or comment:

11. Emission rates

11.1 Use of R- or Q-factors:

☐ Cline (without renormalisation to 1 at high values of n(6)).

☐ Kalbach's Q-factor, normalised to 1 at high values of n(7).

☐ Gadioli, et al.(8).

☐ Else, or comment:

11.2 Treatment of α-emission

☐ α-particle emission rate according to ref. (10).

☐ Form factor used P_α = ☐.

☐ Else, or comment (give reference):

11.3 Transmission coefficients

☐ Inverse reaction cross sections used in precompound part.

☐ Transmission coefficients used in compound and precompound part, with ☐ or without ☐ j-dependence.

☐ Else, or comment:

12. Spectrum calculations

12.1 Complexity

☐ Only first-emitted particles calculated.

☐ Total particle production spectra calculated.

☐ Emission spectra are calculated for every reaction, and every outgoing particle (e.g. two spectra for n,2n).

☐ γ-ray cascade calculation possible.

☐ Else, or comment:

12.2 Representation

☐ Spectrum is represented in energy bins of ☐ equal or ☐ variable width.

☐ Spectrum is given by point data at ☐ equidistant or ☐ non-equidistant energies.

12.3 Else, or comment:

13. Angular distribution calculation

☐ 13.1 Only in H.F.-part, for (in)elastic neutron scattering to discrete levels.

☐ 13.2 Systematics of Kalbach and Mann for angular distributions in precompound part.

☐ 13.3 Model of Mantzouranis et al.(10), specify version below.

☐ 13.4 DWBA-type of calculation for emission from $n=n_0$ only.

☐ 13.5 Other model, specify below, give reference.

14. Gamma-Ray emission

☐ 14.1 No gamma-ray competition included.

☐ 14.2 No gamma-ray spectrum calculation or isomeric-state population calculation.

☐ 14.3 Specify Brink-Axel formula below.
E1-normalisation constant used for all nuclei = .

☐ 14.4 Specify Weisskopf formula for M1 and E2 below.
M1 - normalisation constant used for all nuclei = .
E2 - normalisation constant used for all nuclei = .

☐ 14.5 Specify expression for Yrast line below,

e.g. $\hbar^2 J^2_{max} = 2 I (E-\delta) \geq \hbar^2 J^2_{min.}$ (12)

or the Augustyniak et al.(13) prescription.

15. Additional comments:

References to Appendix

(1) A. Gilbert and A.G.W. Cameron, Can. J. of Phys. 43 (1965), 1446.

(2) W. Dilg et al., Nucl. Phys. A217 (1973), 269.

(3) F.C. Williams, Nucl. Phys. A166 (1971), 231

(4) P. Oblozinsky, I. Ribansky and E. Betak, Nucl. Phys. A226 (1974), 347.

(5) C. Kalbach, Z. für Physik, A287 (1978), 319.

(6) C.K. Cline, Nucl. Phys. A193 (1972), 417.

(7) C. Kalbach, Z. für Physik A283 (1977), 401.

(8) E. Gadioli, E. Gadioli-Erba and P.G. Sona, Nucl. Phys. A217 (1973), p.589.

(9) L. Millazzo-Colli and G.M. Braga-Marcazzan, Nucl. Phys. A210 (1973), p.297.

(10) G. Mantzouranis et al., Phys. Lett., 57B (1975), 220.

(11) S.K. Gupta, Z.Phys. A303 (1981) 329.

(12) D.G. Gardner, Proc. of NEANDC/NEACRP Specialists' meeting on fast neutron capture cross sections, Argonne, 1982; NEANDC(US)-214/L; ANL-83-4 (1983) p.67; UCRL-87438 (1982).

(13) W. Augustyniak and A. Marcinkowski, Acta Physica Polonica 4 (1979) 357.

Proposal of Energy Dependent Effective Scattering Radius in the Resonance Region of Structural Materials

Yasuyuki KIKUCHI

Nuclear Data Center
Japan Atomic Energy Research Institute
Tokai, Ibaraki 319-11, JAPAN

ABSTRACT

Considerable overestimation is observed in the total and elastic scattering cross sections in the higher resonance energy region, when they are calculated from the resonance parameters. This comes from the following two reasons : (1) The present calculation does not consider the energy dependence of the effective scattering radius and (2) the truncation of distant resonance level causes unbalanced contribution of the interference effects. These two effects could be compensated, if the effective scattering radius is allowed to have a simple energy dependence. In order to avoid the troublesome background correction, we propose that the ENDF/B format should be modified so as to allow the energy dependent effective scattering radius.

1. Introduction

The resonance structure remains up to a few MeV in the neutron cross sections of structural materials. This resonance structure has an important role in the resonance self-shielding effects for reactor calculation. Hence it is desirable to give the resonance parameters up to the energy as high as possible. It is pointed out, however, that cross sections calculated from the resonance parameters often fail to reproduce the measured data in the high energy region. In this note, this problem is discussed in the case of nickel isotopes for JENDL-2 as an example.

2. Disagreement between Calculation and Experiment in the Resonance Region

The resonance parameters are given in the energy region up to 600 keV for Ni-isotopes except ^{61}Ni in JENDL-2. The parameters were evaluated on the basis of various transmission and capture measurements as shown in Table 1.

The capture cross sections calculated from these resonance parameters are lower than the measured data in the energy range above 100 ∿ 200 keV. This underestimation comes from the level missing of the p-wave resonances, which is obvious in the staircase plotting of resonance levels as shown in Fig.1 as an example. We corrected this underestimation by applying a slight smooth positive background cross section.

On the other hand, the total and elastic scattering cross sections calculated from the present parameters are underestimated slightly in the lower energy region and overestimated considerably in the higher energy region above a few hundred keV. Hence we have investigated why this anomalous behavior of the total and elastic scattering cross sections occurs and we have found the two reasons as will be described in the next section.

3. Reason of Disagreement

3.1 Energy Dependence of Effective Scattering Radius

In the ENDF/B format, the effective scattering radius R is required to be constant through the resolved resonance region. For a wide energy range such as up to 600 keV, however, the effective scattering radius is not constant but energy dependent. The optical model calculation shows that the radius of Ni isotopes decreases considerably with increase of the neutron energy as shown in Fig.2. The radius decreases down to factor of 0.7 at 600 keV. It is therefore evident that the constant radius approximation causes considerable overestimate in the higher energy region.

However, the energy dependence of the effective scattering radius calculated with the optical model is not sufficient to explain the overestimate in the higher energy region.

3.2 Truncation Effect of Finite Resonances

The resonance shape of the elastic scattering cross section is asymmetric as shown in Fig.3 because of the interference between the resonance and potential scattering. Hence its contribution is positive in the higher off-resonance energy region and negative in the lower energy region. Consider an energy point. If there are many resonances both in higher and lower energy region as in the case of actual nuclei, the positive and negative contributions cancel out.

In the evaluated data file, however, we take a finite number of resonances. Hence all the contributions of distant resonance levels are positive near the upper boundary of the resonance region, and are negative near the lower boundary. This situation is schematically shown in Fig.3.

In order to know how much this effect is, the cross section of ^{58}Ni was calculated by removing the resonances below 400 keV. The results are compared with those without removal of resonances in Fig.4. The cross section value is reduced more than 20% at the off-resonance energy region. It is found that the truncation effect is as much as the effect of the energy dependence of the effective scattering radius described in the previous section.

4. Adoption of Energy Dependent Effective Scattering Radius

It is revealed from the present study that the overestimation of the total and elastic scattering cross sections in the higher energy region is inevitable with the constant scattering radius. How should this overestimation be corrected? Applying the background cross section is a common way. In the present case, however, the background correction is a very difficult problem from the following reasons:

1) The overestimation becomes more than 3 barns at the off-resonance regions above 400 keV.
2) On the other hand, the cross section minimum due to the interference often becomes as low as 0.5 barns.
3) Therefore a smooth negative background correction causes a negative cross section at the energy of the cross section minimum.

Consequently the background cross section must have strong energy dependence. It is a hard job to determine the energy dependent background cross section, as so many resonance levels exist in the energy region considered.

To avoid this difficulty, we adopted the energy dependent effective scattering radius by modifying the ENDF/B format for internal use. We found that the overestimation could disappear with the following energy dependent radius:

$$R\ (fm) = 8.11 - 5.9 \times E\ (MeV) \quad \text{for } {}^{58}Ni,$$
$$= 7.0 - 5.0 \times E\ (MeV) \quad \text{for } {}^{60}Ni,$$
$$= 6.4 - 8.3 \times E\ (MeV) \quad \text{for } {}^{61}Ni,$$
$$= 7.66 - 4.29 \times E\ (MeV) \quad \text{for } {}^{62}Ni,$$
$$= 7.37 - 3.7 \times E\ (MeV) \quad \text{for } {}^{64}Ni.$$

The present radius is also shown in Fig.2. The solid line in Fig.4 shows the cross section calculated with the energy dependent radius.

As the energy dependent radius is not allowed in the current ENDF/B format, we took the difference between the energy dependent and constant radius calculations as the background cross section. Consequently, the background cross section has a resonance-like structure as seen in Fig.5. Such a strongly energy-dependent background cross section might cause other problems, however, if the Doppler broadened cross section is calculated directly from the resonance parameters and the background cross section.

5. Concluding Remarks

It was proved that the overestimation observed in the total and elastic scattering cross sections in the higher energy region for the structural materials came from the two reasons:

1) The effective scattering radius is not constant through such a wide energy range, but decreases considerably with increase of the neutron energy.

2) The truncation of resonance levels outside the defined resonance region causes the unbalanced contribution of the interference effects, resulting in the overestimate in the upper energy region and the underestimate in the lower energy region.

We found that these two effects could be compensated, if the effective scattering radius had a simple energy dependence; linear to the neutron energy. However, the energy dependent radius is not allowed in the current ENDF/B format. Therefore we must correct this overestimation by applying the background cross section with a resonance-like structure. Such a background cross section might cause other problems in the reactor calculation.

Hence as a conclusion, we would like to propose that the ENDF/B format should be modified in future so as to allow the energy dependent effective scattering radius.

References

1) Perey F.G., Chapman G.T., Kinney W.E. and Perey C.M.: "Neutron Data of Structural Materials for Fast Reactors", Proc. Specialists' Meeting, Geel, 5-8 Dec. 1977, p.503, Pergamon Press (1979).

2) Syme D.B., Bowen P.H. and Gadd A.D.: ibid, p.703.

3) Farrell J.A., Bilpuch E.G. and Newson H.W.: Ann. Phys. US, 37, 367 (1966).

4) Fröhner F.: "Neutron Data of Structural Materials for Fast Reactors", Proc. Specialists' Meeting, Geel, 5-8 Dec. 1977, p.138, Pergamon Press (1979).

5) Hockenbury R.W., Bartolome Z.M., Tatarczuk J.R., Moyer W.R. and Block R.C.: Phys. Rev., 178, 1746 (1969).

6) Stieglitz R.G., Hockenbury R.W. and Block R.C.: Nucl. Phys., A163, 592 (1971).

7) Cho M., Fröhner F.H., Kazerouni M., Müller K.N. and Rohr G.: "Nuclear Data for Reactors", Conf. Proc., Helsinki, 15-19 June 1970, p.619, IAEA (1970).

8) Beer H. and Spencer R.R.: Nucl. Phys., A240, 29 (1975).

Table 1 Measured data on the basis of which the evaluation of resonance parameters was made for JENDL-2

Isotopes	Type*	Measured Data
^{58}Ni	T	Perey et al.[1], Symme and Bowen[2], Farrell et al.[3]
	C	Perey et al.[1], Fröhner[4], Hockenbury et al.[5]
^{60}Ni	T	Symme and Bowen[2], Stieglitz et al.[6], Farrell et al.[3]
	C	Fröhner[4], Stieglitz et al.[6], Hockenbury et al.[5]
^{61}Ni	T	Cho et al.[7]
	C	Fröhner[4], Hockenbury et al.[5]
^{62}Ni	T	Beer and Spencer[8], Farrell et al.[3]
	C	Beer and Spencer[8]
^{64}Ni	T	Beer and Spencer[8], Farrell et al.[3]
	C	Beer and Spencer[8]

* T denotes transmission measurements, and C capture measurements

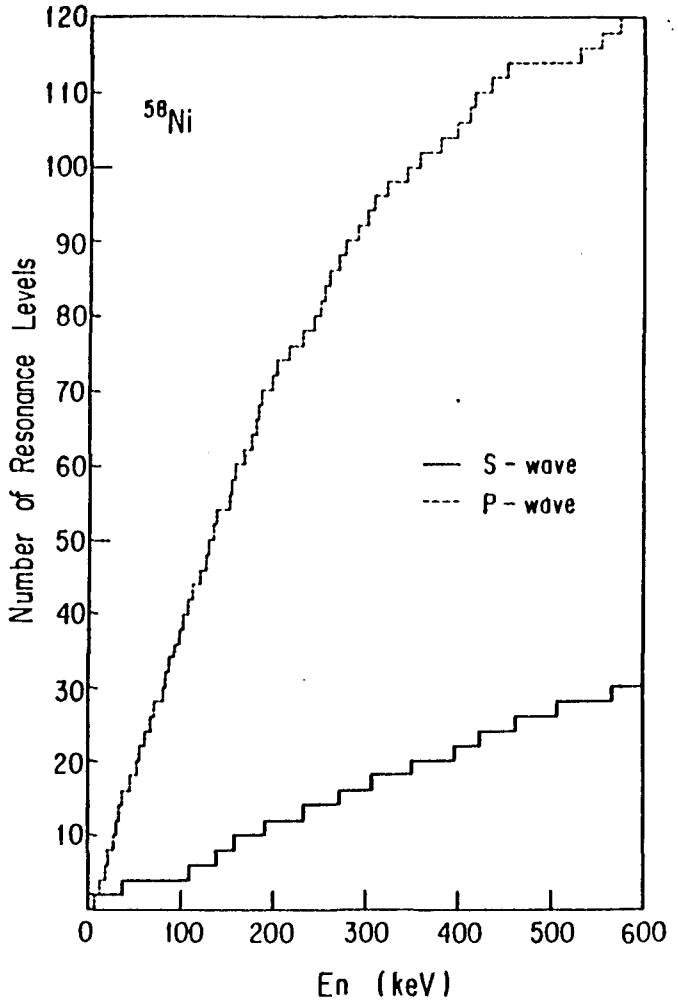

1. Staircase plotting of resonance levels of ^{58}Ni

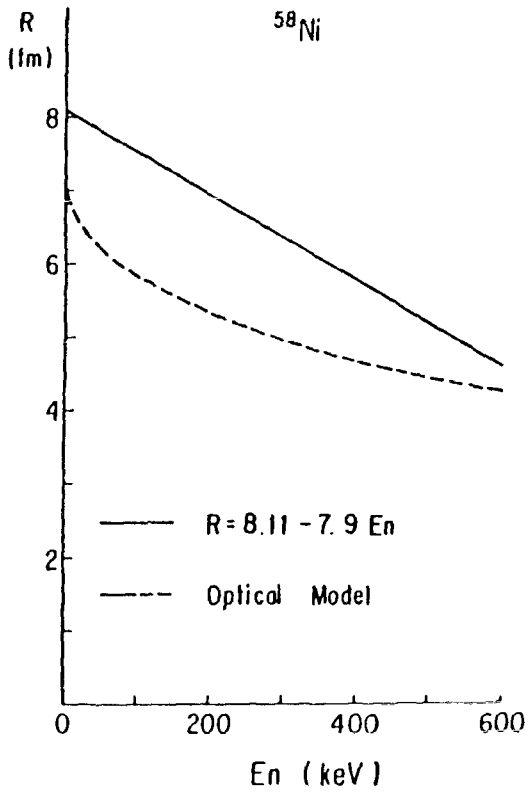

2. Energy dependence of the effective scattering radius of ^{58}Ni. The solid line is the adopted value in JENDL-2. The dashed line is calculated with the optical model.

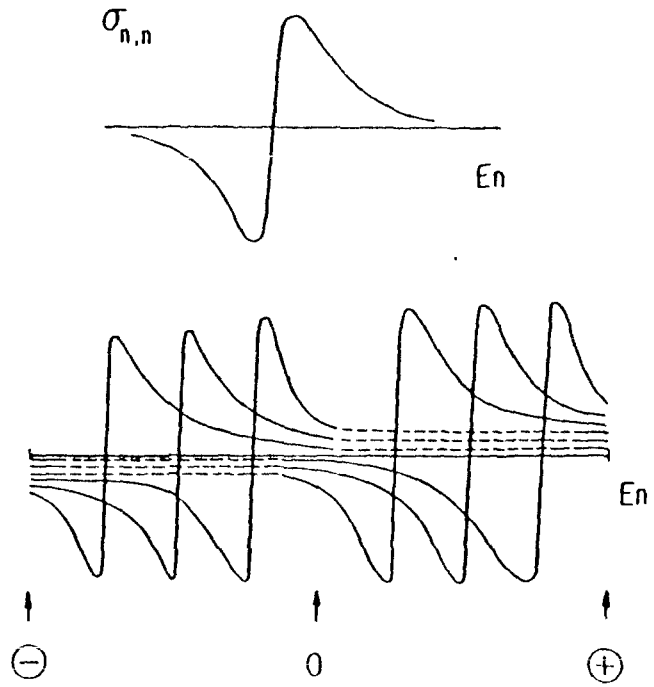

3. Shape of elastic scattering cross section (upper) and schematic view of the contribution from distant levels (lower).

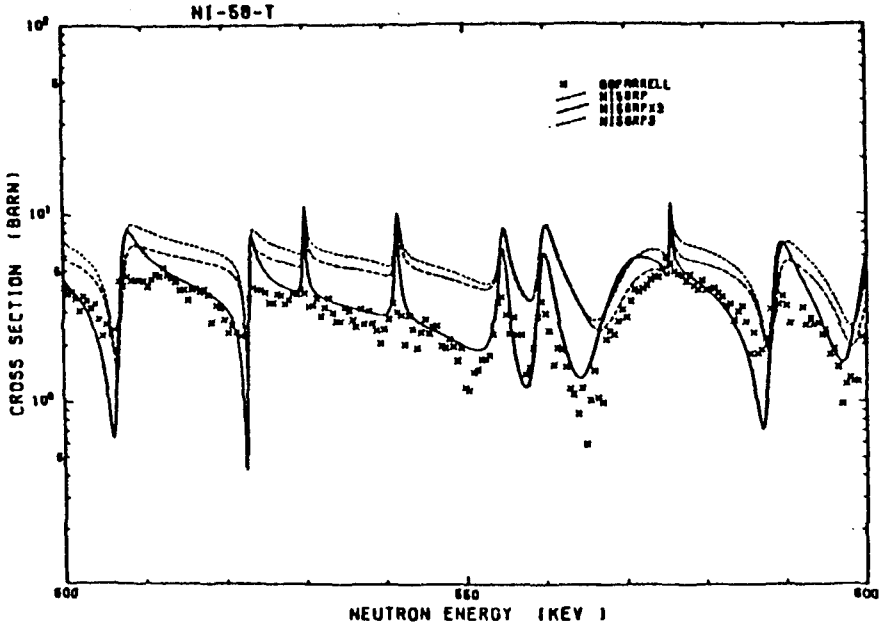

4. Total cross sections of ^{58}Ni.

The solid line is calculated with the energy dependent effective scattering radius and the dotted line with the constant radius. The dashed line is calculated with the constant radius by removing the resonances below 400 KeV in order to know the truncation effect.

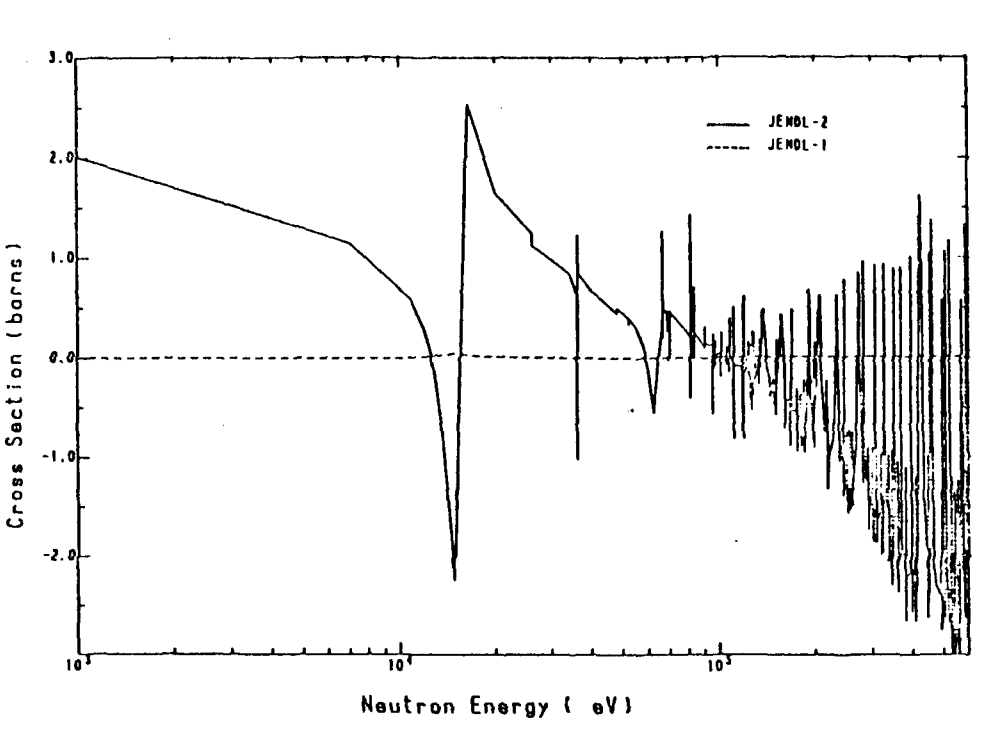

5. Background cross section of ^{58}Ni for elastic scattering.